Pipeline Circumferential Cracking in Near-Neutral pH Environment Under the Influence of Residual Stress

by

Hamed Shirazi

A thesis submitted in partial fulfillment of the requirements for the degree of

Doctor of Philosophy

in
Materials Engineering

Department of Chemical and Materials Engineering
University of Alberta

Abstract

In recent years, pipeline failures attributed to circumferential corrosion fatigue in near-neutral pH environments were reported. Despite the implementation of protective coatings and cathodic protection in buried pipeline steels, the occurrence of Near-Neutral pH Corrosion Fatigue (NNpH-CF) remains a critical pipeline integrity management challenge. (Note that this mechanism has previously been termed near-neutral pH stress corrosion cracking.) This form of corrosion fatigue can occur when the pipeline's protective coating is damaged, exposing the pipe to corrosion conditions. Circumferential near-neutral pH corrosion fatigue (C-NNpH-CF), where residual and axial stresses play a pivotal role in service failures, is less understood than the more common axial form. C-NNpH-CF failure involves several stages, including crack initiation and early growth (Stage I), sustainable crack growth (Stage II), and rapid crack propagation leading to failure (Stage III). Most cracks initiated from external pipeline corrosion pits cease growing when they reach a depth of about 1 mm and enter the dormant stage since the dissolution rate decreases as crack depth increases. Most crack-like features in NNpH-CF colonies remain dormant, and only a few can grow deeper. Using the digital image correlation (DIC) method, this research attempts to examine the effects of bending residual stress (as a source of axial stress) and cyclic loading (simulating pipeline pressure fluctuations) on these stages. The evaluation includes crack re-initiation from dormant cracks, crack growth, and failure mechanisms, considering various parameters such as applied cyclic loading, initial notch depth/position, and bending angle/direction. Fractography analysis, Crack Mouth Opening Displacement (CMOD), and Electron Backscatter Diffraction (EBSD) techniques were employed to gain deeper insights into the C-NNpH-CF failure mechanism.

The study determined the threshold conditions for crack initiation, highlighting the intricate factors influencing this phase. The analysis of crack initiation in cross-section and fractography images revealed that different factors, such as applied loading, initial notch depth/ position, and bending parameters, contribute to crack initiation by influencing the stress distribution, stress cells, stress concentration factor (exclusively in the depth direction) and hydrogen diffusion into the notched region. In addition, there are time-dependent mechanisms governing crack initiation at the bottom of the pit, including dissolution rate and hydrogen-enhanced corrosion fatigue.

Since integrity management measures should be implemented before Stage III (rapid crack propagation to rupture), crack growth rates at Stage II under various parameters were investigated and then compared with those from earlier works on longitudinally oriented NNpH-CF, providing a comprehensive understanding of the circumferential near-neutral pH corrosion fatigue process. Under the influence of maximum bending angle and axial cyclic loading, the highest crack growth rate was obtained at the bend centerline in the inward direction, where maximum tensile stress is concentrated on the external surface. Stage III crack fracture was primarily governed by a high stress intensity factor, contrasting with Stage II, which was influenced by a medium stress intensity factor and hydrogen-enhanced fatigue. The stress gradient in the depth direction of a bent pipeline emerged as a significant factor affecting crack growth rates at different stages.

A deeper understanding of these mechanisms can improve knowledge of Circumferential Near-Neutral pH Corrosion Fatigue (C-NNpH-CF), which plays a significant role in pipeline integrity management. In addition to enhancing the accuracy of C-NNpH-CF predictions, gathering this knowledge can reduce the risks, costs, and environmental consequences of these failures.

Preface

This thesis is an original work by Hamed Shirazi. Chapter 2 has been published under the title "*A Review on Current Understanding of Pipeline Circumferential Stress Corrosion Cracking in Near-Neutral pH Environment*" in the Journal of Engineering Failure Analysis, Volume 148 (2023), page 107215, authored by H. Shirazi, R. Eadie, and W. Chen. It is acknowledged that at this point, the term used for this phenomenon was still Near-Neutral pH Stress Corrosion Cracking (NNpHSCC). Additionally, Chapter 5, titled *"Pipeline Circumferential Cracking in NNpH Environment Under the Influence of Residual Stress: Dormancy and Crack Initiation"* is under review in Journal of Metallurgical and Materials Transactions A, authored by H. Shirazi, S. Wang, R. Eadie, and W. Chen. Chapter 6, titled *"Pipeline Circumferential Cracking in NNpH Environment Under the Influence of Residual Stress: Crack Growth,"* has been submitted to Acta Materialia with the same authors. Furthermore, Chapter 7, titled *"Pipeline Circumferential Corrosion Fatigue Failure Under the Influence of Bending Residual Stress in the Near-Neutral pH Environment,"* is under review in journal of Corrosion Science, authored by H. Shirazi, Sh. Wang, W. Chen, and R. Eadie.

I was responsible for data collection and analysis, as well as the manuscript composition, with supervision provided by Prof. Weixing Chen and Prof. Reg Eadie.

DEDICATION

This endeavor is dedicated to three individuals who have profoundly influenced my growth and development. Foremost, I dedicate this work to my parents, whose tireless support has driven me toward my aspirations throughout my educational journey. In addition, I extend my deepest gratitude to my wife, whose immeasurable impact surpasses the limits of words.

Acknowledgement

I extend my sincere gratitude to my esteemed supervisor, Dr. Weixing Chen, whose unwavering support, invaluable guidance, and scholarly wisdom have been instrumental in shaping this Ph.D. journey. Your mentorship has not only enriched my academic experience but also fostered my growth as a researcher and a critical thinker.

I would like to express my appreciation to Dr. Reg Eadie. Your insightful feedback and constructive criticism have significantly contributed to the refinement and depth of this thesis. I am grateful for the time and expertise you dedicated to evaluating and shaping my research.

To my esteemed supervisory committee and examiners, Dr. Jing Liu, Dr. Leijun Li, Dr. Sheng-Hui Wang, Dr. Liuyin Xia, I extend my heartfelt thanks for your thorough examination of this thesis. The scholarly quality of my work has undoubtedly been enhanced by your critiques and recommendations.

I am indebted to my colleagues and fellow researchers at the University of Alberta: Christine Vu, Hiroyuki Tanaka, Dr. Shidong Wang, Dr. Zhezhu Xu, and Greg Nelson, whose collaborative spirit and intellectual exchanges have enriched my academic journey. Additional thanks to the technical staff of the nanoFAB, Civil & Environmental Engineering (DIC lab), Department of Mechanical Engineering Machine Shop exclusively Eng. Brent Martin, thank you for all your assistance.

I extend my heartfelt appreciation to all my friends, exclusively Vanda Milani and Ali Chaboki, for the support they provided during this research. In particular, I would like to express my gratitude to Dr. Hamid Niazi for the exceptional contributions he made anytime, anywhere, before I started my Ph.D. until the end. In addition to providing support and friendship, you have always helped me put things in perspective.

A special note of appreciation goes to my family for their consistent support throughout my life. Your encouragement, understanding, and patience during the challenging moments have been my pillars of strength.

Lastly, to my beloved wife, Lawyer Minoo Ramezani, your boundless love, patience, and encouragement have been the cornerstone of my resilience. Your unwavering support has sustained me through the highs and lows of this academic journey. I am profoundly grateful for your presence in my life.

This thesis stands as a testament to the collective efforts and support of each of you. Thank you for being an integral part of this academic odyssey.

Sincerely,

Hamed Shirazi

Table of Contents

List of Tables

List of Figures

Chapter 1 Introduction

1. 1 Introduction

In today's world economy, the significance of pipeline transportation cannot be overstated, given its superior safety, reliability, and economic efficiency compared to alternative modes such as railways and tankers. However, the safety and integrity of pipelines face a potential threat from the external corrosion of steel pipelines. Stress Corrosion Cracking (SCC) and corrosion fatigue (CF), pose substantial economic and environmental risks for pipeline companies [1] [2]. For buried pipeline steels, despite the implementation of protective coating and cathodic protection, the emergence of near-neutral pH corrosion fatigue (NNpH-CF) raises significant integrity concerns. This concern stems from the likelihood of coating damage and the subsequent presence of corrosion conditions, especially in older pipelines equipped with tape coatings [3] [4]. The environment responsible for the initiation of transgranular cracking in a near-neutral pH environment is a dilute carbonic acid solution (with a pH ranging between 5.5 and 7.5). This solution forms when CO_2, originating from the decomposition of organic matter in the soil, dissolves in groundwater. This sets the stage for external surface corrosion on pipelines, creating optimal conditions for NNpH-CF [5]–[7].

While Environmentally Assisted Cracking (EAC) in near-neutral pH solutions is commonly known as Near Neutral pH Stress Corrosion Cracking (NNpHSCC), recent research [8], [9] suggests that normal crack growth rates, particularly in oil pipelines under monotonic tensile stress, do not raise significant concerns, even with considerable stress intensity factors (K). In essence, crack growth has not been observed under static loading conditions, except for very low rates in the initiation stage, whereas crack propagation requires cyclic loading [10], [6]. Consequently, corrosion fatigue

mechanisms of crack growth are attributed to cyclic loading induced by pipeline internal pressure fluctuations [8] and diffusible hydrogen (a by-product of corrosion) [9]. Henceforth, the term Near-neutral pH Corrosion Fatigue (NNpH-CF) will be used to denote what is commonly known as NNpHSCC.

While the majority of Near-neutral pH Corrosion Fatigue (NNpH-CF) cases on gas and liquid pipelines have manifested axially (aligned with the pipeline axis), a portion of failures has originated and progressed circumferentially (perpendicular to the axial direction) [1]. According to a 1995 report from the NEB [11], approximately one-third of service failures during that period were directly associated with the Circumferential Near-Neutral pH Corrosion Fatigue (C-NNpH-CF) mechanism, often leading to pipeline leakage.

Crack propagation typically occurs perpendicular to the maximum principal stress, especially under mode I loading conditions. In the context of Circumferential Near-Neutral pH Corrosion Fatigue (C-NNpH-CF), it's crucial to consider the stresses applied by internal pressure (resulting in tensile stresses in the axial direction) and axial residual stresses arising from factors like field bends, soil movement, *etc*. Additionally, the interaction between axial residual stresses and applied stresses due to cyclic loading results in a new stress distribution pattern along the length and depth of the pipeline steel. It's important to highlight that for a pipe to fail in C-NNpH-CF, the driving force for cracking in this direction must surpass that for axial NNpH-CF, meaning the total axial stress must exceed the total hoop stress. Therefore, a comprehensive assessment of high axial stresses from diverse sources, including pipe bending, hydrodynamic stresses, *etc.*, is necessary [12]–[15].

The progression of Circumferential Near-Neutral pH Corrosion Fatigue (C-NNpH-CF) failure unfolds through distinct stages: an incubation stage involving coating deterioration and failure,

Stage I (involving crack initiation and early-stage growth), Stage II (characterized by sustained crack growth due to mechanical driving forces), and Stage III (marked by rapid crack propagation leading to rupture) [10], [16]. While the initial stages may be primarily driven by environmental factors, mechanical forces become the dominant influence as cracks deepen [8]. To ensure pipeline integrity, it is crucial to focus on Stage II, as Stage III exhibits extremely rapid crack growth. Implementing integrity management measures before Stage III is essential, with a particular emphasis on Stage II, where crack growth is steadier. Periodic inspections play a key role in detecting cracks and managing their growth once identified above threshold conditions [10], [16]. Predicting the time it takes for a crack to reach a critical size involves considering factors like stress levels, hydrogen diffusion near the crack tip, and time and location dependencies [17]–[20].

While there is a comprehensive understanding of longitudinally oriented corrosion fatigue among pipeline operators, the knowledge regarding Circumferential Near-Neutral pH Corrosion Fatigue (C-NNpH-CF) is limited, leading to constraints in monitoring and mitigation techniques [14]. Existing in-line inspection (ILI) tools also face challenges in detecting circumferentially oriented cracks [21]. It is noteworthy that C-NNpH-CF has been identified as a contributing factor or direct cause of failures in some instances [14]. Enhancing the comprehension of this corrosion fatigue mechanism is vital for effective pipeline integrity management. A more profound understanding of C-NNpH-CF has the potential to enhance prediction accuracy, thereby reducing the risks, costs, and environmental repercussions associated with such failures.

1. 2 Thesis Outline

Based on the preceding introduction, there exists limited literature addressing the interaction between axial residual stresses arising from pipe manufacturing, installation, and field operation, and the applied stresses resulting from cyclic loading due to pressure fluctuations. Consequently,

additional insights into Circumferential Near-Neutral pH Corrosion Fatigue (C-NNpH-CF) are imperative for the development of predictive models that can enhance crack management capabilities. The occurrence of C-NNpH-CF has predominantly been observed in proximity to areas prone to bending [12]–[15], making bending a crucial factor contributing to axial residual stresses in the field and subsequent C-NNpH-CF. Crack propagation in a bent section is characterized by the presence of residual stress gradients in the thickness direction of the pipe, influencing the various stages leading up to rupture. This study aims to explore the interaction between diverse sources of residual and axial stresses, presenting novel insights into how the resulting stress distribution can impact distinct stages of the cracking mechanism. These stages encompass dormancy, reactivation of dormant cracks, and overall crack propagation and final fracture. The report is structured into seven chapters, each briefly outlined in the following paragraphs.

Chapter 2, titled "*A Review on Current Understanding of Pipeline Circumferential Stress Corrosion Cracking in Near-Neutral pH Environment*," conducts a thorough literature review examining the interaction between various sources of residual and axial stresses. The objective is to introduce fresh perspectives on how emerging stress distributions may impact distinct phases of the cracking mechanism. These phases encompass surface corrosion during crack initiation, early-stage growth, dormancy, reactivation of dormant cracks, and overall crack propagation. The chapter concludes by proposing remedial measures to diminish the likelihood of C-NNpH-CF occurring in both new and existing pipelines. Furthermore, it outlines the necessary research steps to address knowledge gaps in this domain.

Chapter 5, titled "*Pipeline Circumferential Cracking in NNpH Environment Under the Influence of Residual Stress, Part I: Dormancy and Crack Initiation*," presents findings on stress

distributions, as determined by the digital image correlation (DIC) method, within the length and depth dimensions of pipelines. The study investigates how the interaction of residual bending stress and cyclic loading influences stress distribution and the depth of initial dormant notches, subsequently impacting crack initiation. The chapter establishes the threshold condition for crack initiation by examining various types and magnitudes of residual bending stress and their interactions with axial cyclic loading.

Chapter 6, titled "*Pipeline Circumferential Cracking in NNpH Environment Under the Influence of Residual Stress, Part II: Crack Growth*," delves into the impact of bending residual stress (a significant source of axial residual stress) and cyclic loading (simulating pressure fluctuations in pipelines) on crack growth during Stage II. The chapter utilizes the final stress distribution to analyze crack growth under various test parameters, including applied loading, initial notch depth/position, and bending angle/direction. Additionally, it compares the obtained crack growth rates resulting from different combined factors with previous research on longitudinally oriented NNpH-CF, aiming to elucidate the crack growth mechanism in C-NNpH-CF.

Chapter 7, titled "*Pipeline Circumferential Corrosion Fatigue Failure Under the Influence of Bending Residual Stress in the Near-Neutral pH Environment*," details the collective impact of bending residual stress and cyclic loading on C-NNpH-CF failure. The chapter utilizes fractography images to offer insights into the stages of crack propagation leading to failure, considering various test parameters such as applied loading, initial notch depth/position, and bending angle/direction. To gain a deeper understanding of the C-NNpH-CF failure mechanism, the chapter employs striation analysis, Crack Mouth Opening Displacement (CMOD), and Electron Backscatter Diffraction (EBSD) investigations.

Chapter 8 provides a comprehensive summary of the findings and puts forth suggestions for future research. Additionally, the references cited in this thesis are presented in alphabetical order.

References

[1] Canadian Energy Pipeline Association (CEPA), Stress Corrosion Cracking Recommended Practices, 2nd Edition, an industry leading document detailing the management of transgranular SCC, December 2007.

[2] R. R. Fessler, M. Sen, Characteristics, cause, and management of circumferential stress-corrosion cracking, Proceedings of the 2004 International Pipeline Conference. Calgary, Alberta, Canada. IPC2014-33059. https://doi.org/10.1115/IPC2014-33059.

[3] "CEPA recommended practices for managing Near-neutral pH Stress Corrosion Cracking 3rd edition," 2015.

[4] J. A. Beavers, Integrity management of natural gas and petroleum pipelines subject to stress corrosion cracking, Corrosion 70 (2014) 3–18. https://doi.org/10.5006/0998

[5] M. Elboujdaini and M. T. Shehata, "Stress corrosion cracking: A Canadian prospective for oil and gas pipeline," 2005.

[6] J. A. Beavers and B. A. Harle, "Mechanisms of high-pH and near-neutral-pH SCC of underground pipelines," Journal of Offshore Mechanics and Arctic Engineering, vol. 123, no. 3, pp. 147–151, Aug. 2001, https://doi.org/10.1115/1.1376716.

[7] H. Shirazi, R. Eadie, and W. Chen, "A review on current understanding of pipeline circumferential stress corrosion cracking in near-neutral PH environment," Engineering Failure Analysis, vol. 148. Elsevier Ltd, Jun. 01, 2023. https://doi.org/10.1016/j.engfailanal.2023.107215.

[8] M. J. W. Ilm, "The role of pressure and pressure fluctuation in the growth of Stress Corrosion Cracks in line pipe steels," in Proceedings of the 1998 International Pipeline

Conference. Calgary, Alberta, Canada. IPC 1998-2049, 1998. https://doi.org/10.1115/IPC1998-2049.

[9] M. Yu, W. Chen, R. Kania, G. Van Boven, and J. Been, "Crack propagation of pipeline steel exposed to a near-neutral pH environment under variable pressure fluctuations," Int J Fatigue, vol. 82, pp. 658–666, Jan. 2016, https://doi.org/10.1016/j.ijfatigue.2015.09.024.

[10] J. Zhao, W. Chen, M. Yu, K. Chevil, R. Eadie, G. Van Boven, R. Kania, J. Been, S. Keane. Crack growth modeling and life prediction of pipeline steels exposed to near-neutral pH environments: dissolution crack growth and occurrence of crack dormancy in stage I, Metallurgical and Materials Transactions A: Physical Metallurgy and Materials Science 48 (2017) 1629–1640. https://doi.org/10.1007/s11661-016-3951-3

[11] National Energy Board (NEB), Report of the Inquiry concerning Stress Corrosion Cracking on Canadian Oil and Gas Pipelines, NEB MH-2-95, December 1996. https://publications.gc.ca/collections/Collection/NE23-58-1996E.pdf

[12] Y. B. Beauregard and C. Edwards, "Analysis of sever circumferential SCC found on an ethane pipeline," in Proceedings of the 2014 International Pipeline Conference. Calgary, Alberta, Canada., 2014.

[13] J. Babcock, D. Dewar, and J. Webster, "Deer Mountain case study: integration of pipe and ground monitoring data with historical information o develop landscape management plan," Proceedings of the 2020 International Pipeline Conference. Calgary, Alberta, Canada. IPC2020-9613. https://doi.org/10.1115/IPC2020-9613.

[14] N. Bates, M. Brimacombe, and S. Polasik, "Development and experience of a circumferential stress corrosion crack management program," in Proceedings of the 2018 International Pipeline Conference. Calgary, Alberta, Canada.IPC2018-78315.

[15] B. Johnson, B Tesfaye, C. Wargacki, T. Hennig, E. Suarez "Complex Circumferential Stress Corrosion Cracking: Identification, Sizing and Consequences for the Integrity Management Program," in Proceedings of the 2018 International Pipeline Conference. Calgary, Alberta, Canada. IPC2018-78564. https://doi.org/10.1115/IPC2018-78564.

[16] S. Wang and W. Chen, "Overview of Stage 1b Stress Corrosion Crack Initiation and Growth of Pipeline Steels," Corrosion, vol. 79, no. 3, pp. 284–303, Mar. 2023, https://doi.org/10.5006/4168.

[17] M. Hilvert, T. Penney, M. Enginering Ltd, I. Richardson, and A. Russell, "Integrity management of Stress Corrosion Cracking in pipeline a case study," in 26th World Gas conference Paris, France, 2015.

[18] W. Chen, "An overview of near-neutral pH stress corrosion cracking in pipelines and mitigation strategies for Its initiation and growth," Corrosion, vol. 72, no. 7, pp. 962–977, Jul. 2016, https://doi.org/10.5006/1967.

[19] W. Chen, R. Kania, R. Worthingham, and G. Van Boven, "Transgranular crack growth in the pipeline steels exposed to near-neutral pH soil aqueous solutions: The role of hydrogen," Acta Mater, vol. 57, no. 20, pp. 6200–6214, Dec. 2009, https://doi.org/10.1016/j.actamat.2009.08.047.

[20] J. Zhao, W. Chen, M. Yu, K. Chevil, R. Eadie, J. Been, G. Van Boven, R. Kania & S. Keane, "Crack growth modeling and life prediction of pipeline steels exposed to near-Neutral pH environments: stage II crack growth and overall life prediction," Metall Mater Trans A Phys Metall Mater Sci, vol. 48, no. 4, pp. 1641–1652, Apr. 2017.

[21] K. Zhang, R. Chune, R. Wang, and R. Kania, "Role of axial stress in pipeline integrity management," in Proceedings of the 2022 International Pipeline Conference. Calgary, Alberta, Canada. IPC2022-87327. https://doi.org/10.1115/IPC2022-87327.

Chapter 2 A Review on Current Understanding of Pipeline Circumferential Stress Corrosion Cracking in Near-Neutral pH Environment[1]

2. 1 Introduction

In today's world economy, pipeline transportation plays an important role because of its higher safety, reliability, and economic efficiency than other transportation modes like railways and tankers. However, the safety and integrity of pipelines may be endangered via the external corrosion of the steel pipeline. Stress Corrosion Cracking (SCC) (corrosion fatigue in its main cracking stage, which is stage II) represents substantial economic and environmental losses to pipeline companies [1] [2]. For buried pipeline steels, despite using protective coating and cathodic protection, near-neutral pH stress corrosion cracking (NNpHSCC) forms a major integrity concern caused by the probability of damage to the coating and the presence of corrosion conditions after that occurrence, particularly in older pipelines with tape coatings [3] [4].

Although most NNpHSCC on gas and liquid pipelines has been oriented axially (in the direction of the pipeline axis), a fraction of the failures has initiated and grown circumferentially (perpendicular to the axial direction) [1]. Based on the NEB report published in 1995 [5], the reason for about one-third of service failures at that time was related directly to the Circumferential-Stress-Corrosion-Crack (C-SCC) mechanism and resulted typically in leakage of

[1] A version of his chapter has been published: H. Shirazi, R. Eadie, W. Chen, "A Review on Current Understanding of Pipeline Circumferential Stress Corrosion Cracking in Near-Neutral pH Environment, Engineering Failure Analysis. It is acknowledged that at this point, the term used for this phenomenon was still NNpHSCC.

the pipeline. In NNpHSCC, most of the growth occurs in Stage II crack growth. This crack growth happens at preferential sites, where not only the coating has failed but also with higher tensile residual stresses and higher diffusible hydrogen content in the steel surrounding the crack tip [6]. Propagation of cracks occurs perpendicularly to the maximum principal stress (under mode I loading condition). In circumferentially oriented SCC (C-SCC), a subset of transgranular stress corrosion cracking in the NNpH environment, applied stresses from internal pressure (tensile stresses in the axial direction caused by the internal pressure), and axial residual stresses from temperature changes, field bends, soil movement, *etc*. should be considered. Also, the interaction of axial residual and applied stresses caused by cyclic loading makes a new stress distribution pattern in the length and depth of pipeline steel. Therefore, this final stress distribution affects different stages of the cracking, including surface corrosion related to initiation of the cracks, early-stage growth, dormancy, reactivation of dormant cracks, crack growth by corrosion fatigue, and final fracture [2] [7]. It should be noted that if the pipe fails in C-SCC, then the driving force for cracking in this direction must be higher than for axial SCC, *i.e.*, the total axial stress must exceed the total hoop stress. Thus, it is necessary to evaluate high axial stresses from various sources, such as pipe bending, hydrodynamic stresses, *etc*.

There is limited literature on the interaction of residual stresses from pipe manufacturing, installation, and operation in the field, and applied stresses from cyclic loading of pressure fluctuations. In addition, these limited works have focused on longitudinal cracks and considered only a limited number of parameters [8]. There has been very little research on C-SCC since it rarely causes more than a leaking pipeline [1]. Therefore, further information on C-SCC is needed to develop predictive models for the cracking stages to enhance crack management capabilities. This study aims to discuss the interaction of various sources of residual and axial stresses to present

new ideas on how new stress distribution can affect different stages of the cracking mechanism, including surface corrosion during initiation of cracks, early-stage growth, dormancy, reactivation of dormant cracks, and crack growth. The report will conclude with recommended remedial measures to decrease the chance of C-SCC occurring on new and old pipelines. In addition, the research steps necessary to bridge the knowledge gaps in this area will be discussed.

2. 2 Circumferential stress corrosion cracking (C-SCC)

In the first part of this paper, the history of circumferentially oriented SCC is briefly delineated. Some specific characteristics of C-SCC in a near-neutral pH environment will be discussed. Axial stresses as a source of discrimination with other SCC mechanisms will be the subject of the next section. Also, as C-SCC is a subset of transgranular cracking in the NNpH environment, essential features of NNpHSCC will be considered in the last section.

2. 2. 1 C-SCC history

In 1974, circumferentially oriented SCC was reported regarding a drip branch connection in the United States [9]. For the first time in 1977, CSSC failure was recorded in Canada on a Gr. 5L X65 National Gas Transportation pipeline (NPS 36, WT: 8.74, constructed in 1969) in the west of Alberta. This pipeline had a three-layer polyethylene coating, and failure occurred on an almost 30-degree slope, displaying soil movement. A leakage of sweet natural gas resulted from this failure [9][10].

Based on the NEB report published in 1995, the reason for about one-third of service failures is related directly to the Circumferential Stress Corrosion Crack (C-SCC) mechanism resulting in leakage of pipeline [1]. Fessler *et al*. [2] reported that most failures related to C-SCC have happened on gas pipelines. The locations of those pipeline failures in Canada included Alberta,

Ontario, and Saskatchewan. Besides, most failures resulted in leakage, and less than five percent caused in-service rupture.

As failures of C-SCC result in in-service leaks, repairing the pipe and removing cracks is a typical result. However, the pipe is usually taken out of service to repair any C-SCC cracks, increasing the economic losses. [3]

2. 2. 2 C-SCC characteristics (susceptible materials, susceptible environment)

In steel pipelines, external stress corrosion cracking in the NNpH environment could be divided into two major types based on the direction of crack propagation. Figure 2-1 shows a crack coalescing in circumferentially oriented SCC (C-SCC). Indeed, C-SCC is a subset of transgranular stress corrosion cracking in a near-neutral pH environment, so circumferential cracks grow perpendicularly to the axial tensile stress.

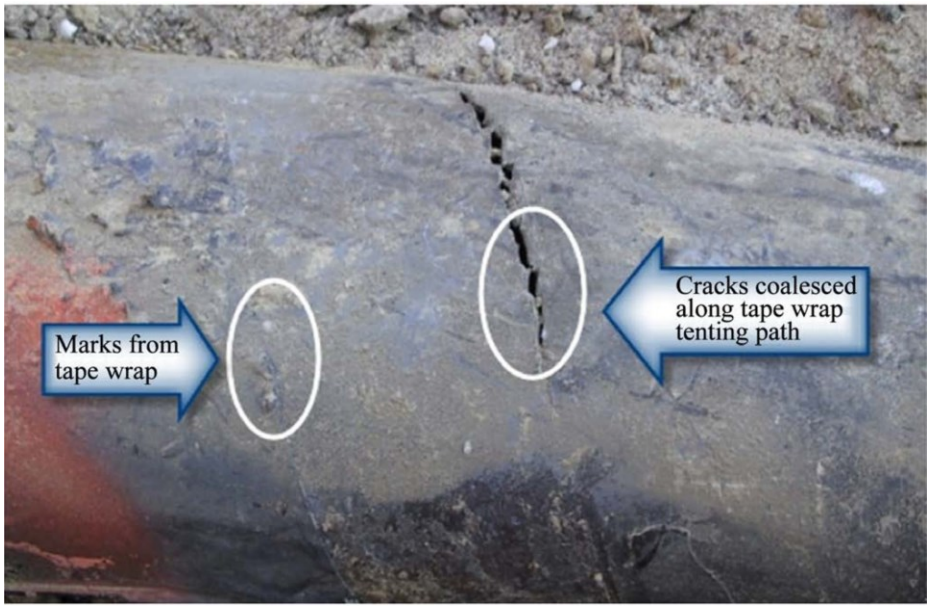

Figure 2-1 Cracks coalescing in Circumferential SCC [1]

C-SCC is a mechanism that needs susceptible material, a suitable environment, and axial tensile stress (Figure 2-2) [1] [3]. Based on the analysis done by Fessler and Batte [2] on 55 incidents of C-SCC, it is evident that C-SCC:

- Occurs on both gas and liquid pipelines
- Rarely results in rupture. (Most incidents are leakage)
- Tape, asphalt, and coal-tar coated pipelines are more susceptible to C-SCC than pipelines with Fusion Bonded Epoxy (FBE) or other high-performance coating systems
- Has occurred on a comprehensive range of grades, sizes, and wall thicknesses.

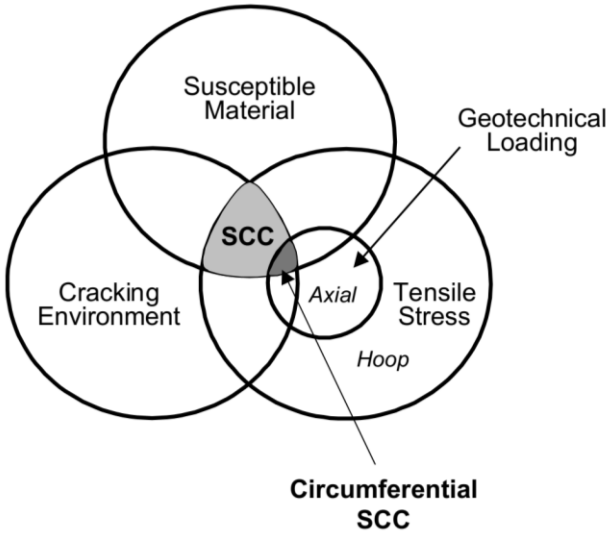

Figure 2-2 Circumferential SCC as a Subset of Pipeline SCC [1]

Coating quality and integrity are important factors affecting C-SCC occurrence. For example, C-SCC was associated with two types of tape disbondment: wrinkles and tape helix. In the first case, because of soil settlement in the trench, relative movement between pipe and soil makes some scratches on the coating, and longitudinal wrinkles are often observed towards the bottom of the pipe. In taped helically-welded-pipe cases, Figure 2-3, where damage to the coating occurs, water can enter the gap made between the edge of the previous wrap and the overlapped new one [1].

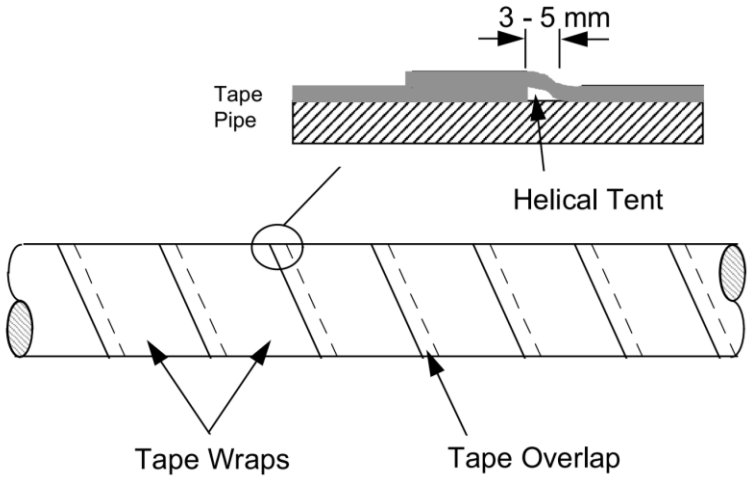

Figure 2-3 Polyethylene-Tape Helical Tent [1]

In C-SSC, the environmental conditions can act as a source of residual stress, which will be discussed in the next section. Different factors which could be investigated from an environmental susceptibility point of view are [9]:

- Topography: including topographical regions which affect annual levels of precipitation and slope of pipeline construction,
- Drainage: which defines seepage at pipe depth may increase the contact of the pipe with water,
- Soil: type of soil plays a role in soil movement on slopes. Also, the presence of rocks within the soil may result in differential settlement and exert extra force on the pipes.

Another consequence of the environment on the C-SCC mechanism is related to the corrosivity of the groundwater contacting the pipe's external surface at the disbonded coating area. Dissolved chemicals like Na^+, Cl^-, K^+, and SO_2^- in the water make a corrosive solution. Also, CO_2 gas, produced by the decay of organic matter in the soil, dissolves into the solution to form a diluted bicarbonate solution with a pH in the range of 6.5 to 7.5. Since the CP current is blocked by impermeable tape coating, the water reduction reaction is insignificant, and the solution can

maintain a near-neutral pH value. Therefore, the corrosive environment for C-SCC has these characteristics: near-neutral pH (6.5 ~ 7.5) and dilute bicarbonate solution [11]–[13]. The environment is typically anaerobic.

2. 2. 3 Sources of axial stress

Since circumferentially oriented cracks in pipelines need an unusual state of axial stress to initiate and propagate, the source of the axial stress should be considered comprehensively. Various research literature has defined a vast range of axial stress sources for C-SCC, including the movement of unstable soil on slopes, locally high axial stress from dents made by rocks in the trench, pipe bending, and thermal contraction due to temperature gradients [2] [10]. In general, the axial residual stress could be divided into five important categories [2]:

- Hydrodynamic stress at bends,
- Residual stress, from bending, welding, and other sources of plastic deformation,
- Axial stress from internal pressure,
- Axial stress from geohazards or water crossing; and
- Bourdon effect on pipe bends

To prevent the reoccurrence of C-SCC, these sources of stress should be relieved or minimized by, for instance, cutting the pipe (relaxation of residual stress) and replacing it with new pipe, readjustment of pipes to decrease bending angles, removing rocks from bottom side dents, and finally making supports limiting pipe movement on unstable slopes [2]. Since bends are often involved, this region can be redesigned or provided with extra support to reduce the stresses at these locations.

In this section, the most important sources of axial stress are discussed [2]:

Internal pressure is the source of hoop stress in the pipeline, which expands the circumferential of the pipe. [2]. As a pressurized pipeline transporting fluids typically has ends to press against, it is really a pressurized cylinder. Therefore, this stress from the internal pressure pushes on the pipe ends and makes axial stress in the pipeline, which is typically about one-half the hoop stress.

Temperature is another source of axial stress. Suppose the time of pipeline operation is different with respect to the time of installation. In that case, the pipeline will try to change dimensions through thermal expansion. Following the equation, define the axial stress caused by temperature difference [2]:

$$\sigma_t = \alpha(T_1 - T_2)E \qquad (2\text{-}1)$$

where, σ_t is the axial stress from the change in temperature, α is the coefficient of thermal expansion (6.5 x 10^{-6}/°F for steel), T_1 is the temperature of the pipeline at the time of installation, T_2 is the temperature of the pipeline in operation, and E is the elastic modulus (30 x 10^6 psi for steel) [2].

It should be noted that the pipeline reaches equilibrium with little stress from temperature over a long period of operation; however, if the operation is interrupted and the pipe cools down or heats up (depending on the depth of burial), then thermal stresses may occur. Temperatures can also vary near pumping or compression stations as a result of changing operating conditions.

For example, the axial stress of the pipeline could be increased from 21% SMYS (specified minimum yield strength) to 44% if the temperature difference between installation time in summer and operation time in winter was 45·c. See Figure 2-4.

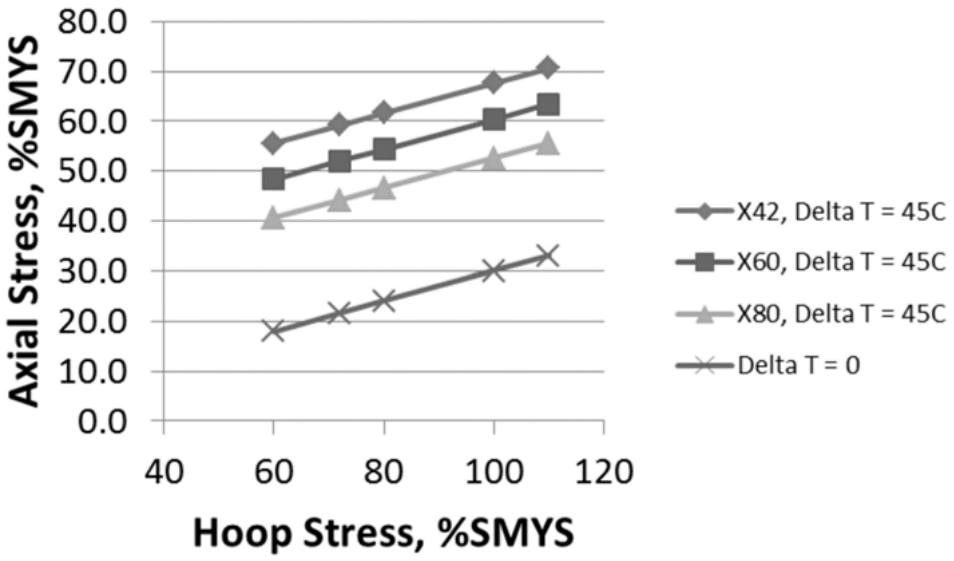

Figure 2-4 Axial Stresses Produced by Internal Pressure and Temperature [2]

Field bends should be considered to continue evaluating axial stress sources in pipelines, either residual or operating. High axial residual stress is made by bending a pipe joint at room temperature (in the installation period). The magnitude of residual stress is related to the level of spring back before final installation. The distribution of residual stress in a bent section with and without spring back is shown in Figures 2-5 and 2-6 (y is the distance from the center of the bending location on the pipe.

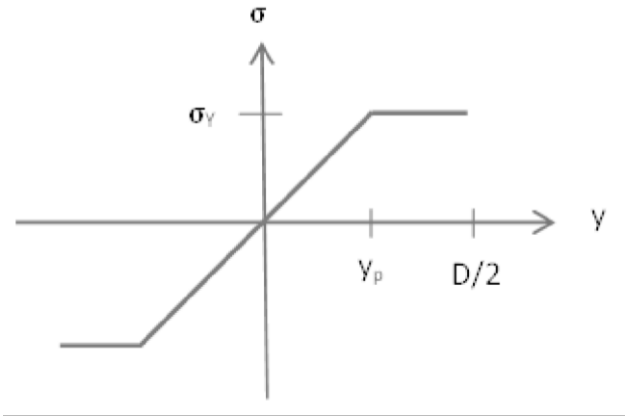

Figure 2-5 Stress profile from the concave side to the convex side for the original bend [2]

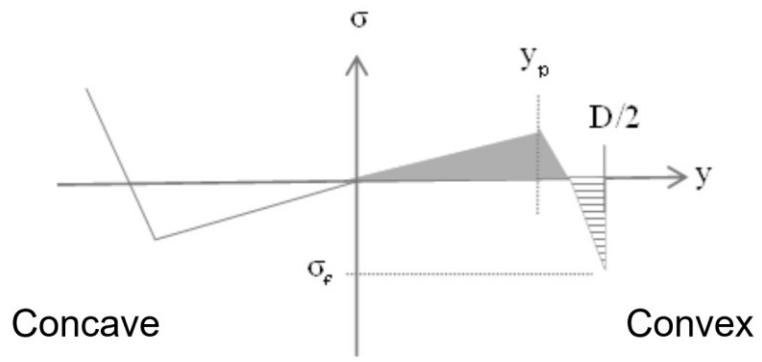

Figure 2-6 Stress distribution after the original bend is released [2]

According to Figure 2-6, if the pipe is not allowed to spring back, on the convex side of the bend, the axial strain would be D/2ρ, where ρ is the bend radius and D is the diameter of the pipe. The residual stress pattern would be changed by allowing the pipe to spring back as the convex side goes to compression and the concave side goes to tension [2]. Because of the self-equilibrating feature of residual stress, there is high tensile stress at the concave side to balance the compressive stresses throughout the wall thickness. When the axial stress from bending is added to other sources of stress, it can produce total stress approaching the yield strength of materials [2].

In addition, two important sources of stresses on a pipe bend should be considered: hydrodynamic stress and the Bourdon effect. These two separate sources of stress are considered in the sections below.

A. Bourdon Stress

An additional source of stress on the bend in pipes is related to the Bourdon effect [14], [15]. When bends are subjected to internal pressure, the pipe starts to straighten out due to the difference in surface area between intrados and extrados. A bend pipe's stiffness and surrounding constraints influence the unbalanced thrust forces caused by the internal pressure. It is known as the "Bourdon effect" when these forces also tend to cause ovalization of the cross-section, which must be considered if accurate pipe wall stresses are to be determined. Unanticipated deformations and

high stress levels may occur at the bend pipe location if these unbalanced thrust forces are not considered [14], [15]. The maximum stresses occur at intrados, and the minimum stresses at extrados for all pipe bend sizes. According to the research done by D. Abdulhameed *et al.* [14], [15] the combined stress obtained from the CSA-Z662 code was compared to the Tresca stress obtained from ABAQUS. For NPS 42 pipe elbows with a bend radius equal to the outer diameter of the cross-section, the ABAQUS simulation showed around 390 MPa for the maximum stresses, which was higher than CSA-Z662 estimates of 290 MPa for shear stresses (where the Bourdon effect was ignored). It should be noted that the level and distribution of stresses on a pipe bend are greatly affected by the internal pressure level, pipe diameter and bend angle. For instance, pipes that have a small bend angle behave more like straight pipes, and exhibit lower Bourdon-effect stresses [14], [15].

B. Hydrodynamic Stress

Fluid flowing through a bend in a pipe changes direction, resulting in a change in the momentum of the fluid. Newton's second law states that a body's momentum changes at the same rate as the net force upon it. Due to these forces, a pipeline bend can experience stresses along the bend that are called “hydrodynamic stresses.” The exact stress at any point in the pipe can be determined by the mechanics of materials, but we are not aware of accurate calculations for underground pipelines. We will, however, examine the nature of these forces to determine if they are likely to be significant. The impulse-momentum equation can be used to calculate the resultant force exerted by a flowing fluid on a pipe bend [16].

For instance, in the case of a 20-degree bend at an 8-inch crude oil pipeline with an oil density of 844 kg/m^3, pressure of 2300 kPa and flow rate of 63000 kg/h, it creates about 30 kN (6750 lbf) of force at the bend. This force would increase with the angle of the bend and with the square of the

diameter of the pipe since the change in momentum varies with the volume of the pipe fluid flowing in the pipe. For example, with a 90-degree bend on a 30" pipeline, the hydrodynamic force is estimated to be around 1500 kN (337,200 lbf). The force would be a distributed force exerted all along the side of the pipe, acting to straighten the pipe. This means, of course, that the hydrodynamic stress adds to the effect of the Bourdon stress to increase axial tensile stresses on the inside of the bend.

To see the bending moments that these forces would introduce, we need to consider the geometry of the bend. According to section 6.2.3 of the CSA-Z662 code (Canadian standard for oil and gas pipeline systems), for field cold bends, the longitudinal axis of the pipe must not be deflected more than 1.5 degrees along the axis equal to the outside diameter. It is possible to achieve a cold bend of 1.5 degrees on an 8-inch pipe with a length of 8 inches, for instance. Therefore, a 20-degree bend requires a pipe 106 inches long. Also, for a 30-inch diameter pipe with a 90° bend, the necessary length of the bend would be 1800 inches (45.72 m).

To determine the bending stresses in the pipe wall resulting from these large internal bending forces distributed along these long bends, it would be necessary to determine the support the pipe receives from the trench since there must be a counterbalancing moment to the moment created by the hydrodynamic forces. This is a significant problem, which requires looking in detail at the clearances around the pipe and the compressibility of the soil around the pipe since this is the counter bending moment to the internal bending moment from the hydrodynamic force. We intend to look in more detail at these stresses in a future paper. It is sufficient to say that the bending stresses within the pipe wall necessary to support these internal bending forces are significant relative to the SMYS of the pipe and must be considered to get a full picture of the axial stresses at bends in pipelines. This is especially so, since they are in addition to the Bourdon stresses, which

have been the subject of some recent publications. The purpose of this section was to provide a starting point for further research on the effect of different sources of axial stresses on bent pipes (both hydrostatic and hydrodynamic). It has been clearly demonstrated, we believe, that the value of this combination of axial sources at the bend is significant enough to make that location in the pipe prone to the initiation and propagation of cracks in NNpH environments.

2. 2. 4 Near-neutral-pH SCC introduction and its relation to corrosion

Near-neutral pH SCC is a type of external pipeline cracking clearly identified in Canada in the 1980s but thought to have occurred earlier. Because of some similarities to high pH SCC, it was referred to as 'near-neutral-pH SCC,' and this term is now in widespread usage, although the second stage would more correctly be termed 'corrosion fatigue.' These features could be considered for this mechanism [2], [13], [17], [18]:

- Occurs at the free corrosion potential (-760 $mV_{Cu/CuSO4}$ to -790 $mV_{Cu/CuSO4}$),
- Occurs under disbonded coatings where cathodic protection (CP) does not reach (because of the presence of a shielding coating and/ or some specific conditions (such as a very high-resistivity soil) which prevent the CP from reaching the pipe and allow the environment to remain neutral or slightly acidic,
- The cracks are transgranular as compared to high pH SCC cracks, which are intergranular,
- The electrolyte penetrates under the disbonded coating, a dilute HCO^{3-} solution with pH in the range of 5.5 to 7.5 because of the absorption of carbon dioxide into the groundwater,
- High ratios of crack length over crack depth, as compared with the ratios of high pH SCC,
- The presence of corrosion products within the cracks and
- Evidence of crack coalescence.

Propagation of cracks generally takes place in the direction perpendicular to the maximum principal stress (Under mode I loading conditions). Although cracks may propagate in a direction inclined to the maximum principal stress, they cannot continue propagation in this direction as the stress intensity factor is the largest on the main crack plane. As a result, the branched crack must return to the main crack lane, and this results in a "zig-zag" pattern on the fracture surface [19].

In general, NNpHSCC is coupled with the corrosion of the pipe's external surface, so it occurs beneath a mechanically damaged or disbonded coating when an adequate cathodic protection current cannot reach the steel surface. Different reasons, including shielding of the current via failed coating or inadequate cathodic protection current because of high soil resistivity, result in this type of corrosion [1], [2], [4].

When the coating is damaged, groundwater (as an electrolyte) reaches the pipe surface. The presence of this groundwater with pH between 5.5 and 7.5 and the dissolution of CO_2 present in the soil from the decay of organic material provides suitable conditions for pipe external surface corrosion in this dilute carbonic acid solution [4], [11]. In the presence of different pH values, carbonic acid can dissociate into bicarbonate ions (HCO_3^-) and carbonate ions (CO_3^-), although bicarbonate ions (HCO_3^-) dominate in the NNpH environment. Therefore, the corrosion of pipeline steels in near-neutral pH environments can be described by the anodic dissolution of the steel and cathodic reduction of water, respectively [20], [21], [22]:

$$Fe \leftrightarrow Fe^{2+} + 2e^- \quad (2\text{-}2)$$

$$H_2O + e^- \leftrightarrow H_{ads} + OH^- \quad (2\text{-}3)$$

$$CO_2 + H_2O \leftrightarrow H_2CO_3 \quad (2\text{-}4)$$

$$H_2CO_3 \leftrightarrow H^+ + HCO_3^- \quad (2\text{-}5)$$

The Fe^{2+} can be generated through iron dissolution or oxide reduction. In fact, pipelines are manufactured with mill scale present on the surface, and this, too, plays a role. Wang *et al.* [22], [23] reported that precipitation of $FeCO_3$ is possible at porous or cracked locations of the mill scale (the narrow region beneath the mill scales with a nearly static electrolyte) where a higher concentration of Fe^{2+} or CO_3^{2-} was achieved through increased immersion time. Otherwise, $FeCo_3$ formation may be unlikely.

$$Fe_2^{+} + CO_3^{2-} \rightarrow FeCO_3 \qquad (2\text{-}6)$$

2. 3 Residual Stress

On the condition that there is no source of external forces or thermal gradients, those stresses that remain in materials after being manufactured or processed are called residual stress [24]. Such stresses may have positive or negative effects on the machine or structure, depending on the type (compressive or tensile) and magnitude. Here, they should be considered to be important in fracture analysis as, when they are sufficient, they influence crack initiation and growth [20],[25]. As the crack grows these residual stresses are usually reduced to zero.

2. 3. 1 Residual Stress Distribution

There are many sources of axial residual stress in pipelines that could result in circumferentially oriented cracks. However, most work done up to now has considered axial residual stresses in the girth welds. T. Neeraj *et al*. [26] reported that the magnitude of axial residual stresses is about half of the hoop stresses in a girth weld of API 5L X-65 line pipe with 508 mm outside diameter (O.D.) and 25.4 mm wall thickness (WT). Also, residual stresses varied through the thickness direction, as they were compressive at the I.D of the weld centerline and reached the highest tensile stress near the O.D. surface. These stresses are shown from published measurements in Figure 2-7, the

shape of the curve is related to the self-equilibrating feature of stress distribution in a steel pipeline [26].

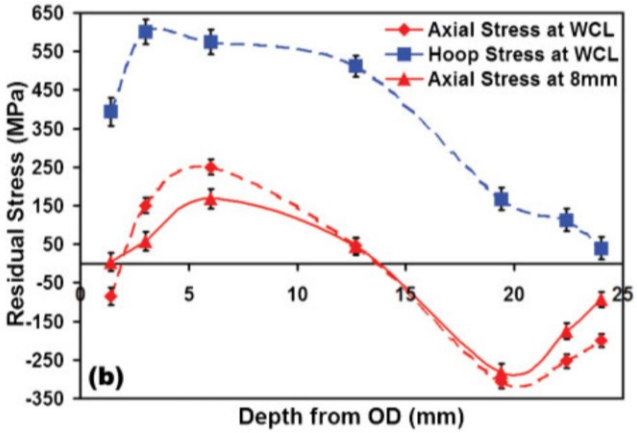

Figure 2-7 Axial and hoop residual stress profiles along weld centerline (WCL) and 8 mm from WCL [26].

Another study was done on the girth weld of API 5L- Gr. X70 line pipe with 56 inches (1422 mm) outer diameter and 19.8 mm wall thickness, and emphasized that the weld zone is under two simultaneous influences of the angular distortion and the longitudinal shrinkage during cooling of the weld [27]. The angular deformation tries to push the external surface of the weld, which is in interaction with the length contraction and tends to pull the weld inside the pipe [24]. Hence, the residual stresses are compressive on the weld centerline. Based on Figure 2-8, when distance increases from the weld centerline, axial residual stresses can increase to a maximum limit caused by more constraint near the base metal and then gradually decrease because of the inherent self-equilibrating nature of residual stresses.

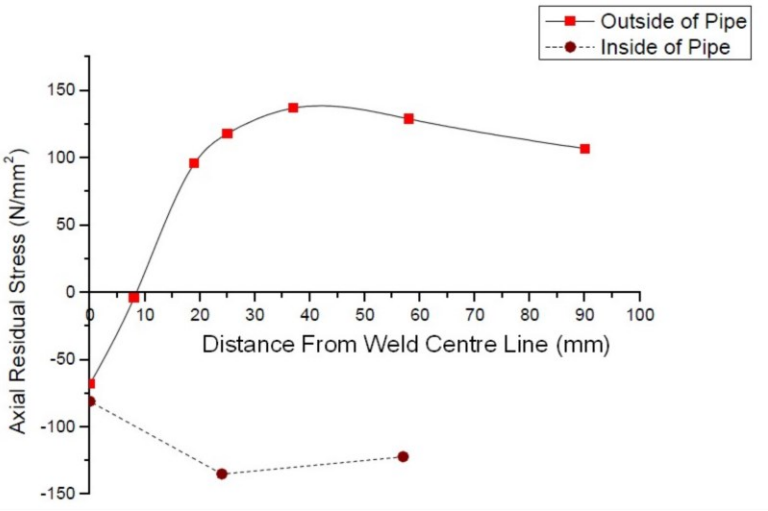

Figure 2-8 Distribution of axial residual stresses on the external and the internal surface of the pipe [27]

2. 3. 2 Residual stress relaxation

N. Hempel *et al*. [28] investigated the interaction of static bending stresses with residual welding stresses on structural steel with 7.75 mm thickness. They employed a 4-point bending machine to make a source of bending stresses (182 MPa and 337 MPa) precisely on the weld centerline. Figures 2-9a and b depict the axial residual stresses on the outer surface of the pipeline before and after applying the bending stresses. In Figure 2-9a, after applying a stress equal to 50% of the yield stress, the change of residual stress is negligible, although loading 337 MPa (About 95 % of the yield stress) on the outer surface (Figure 2-9b) results in residual stress relaxation. There is a reduction of the compressive residual stress in the heat-affected zone and base material close to the weld. A relaxation of tensile residual stress is observed at a distance far from the centerline (about 40- 50 mm).

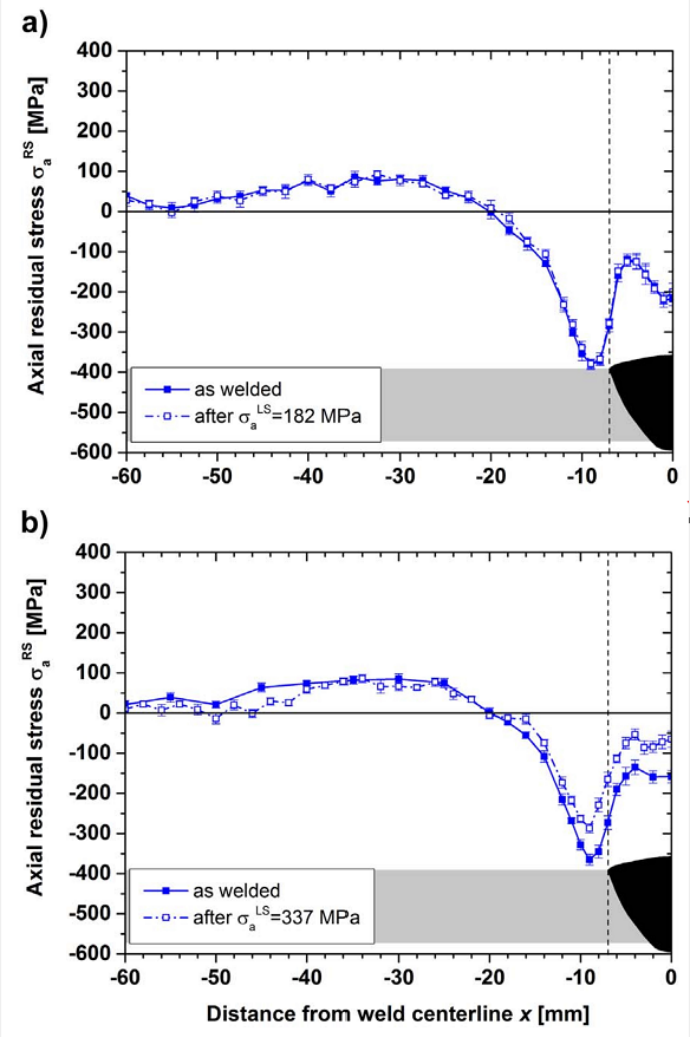

Figure 2-9 Axial residual stresses on the outer surface: a) before and after an axial load of 182 MPa, b) before and after an axial load of 337 MPa [28]

To study the effect of interaction between two sources of stress (weld residual stress and applied bending stress), the von Mises yield criterion can be used. Stress relaxation happens if elastic strains are transformed into plastic strains when the value of combined residual stress and applied stress exceeds the yield stress criterion given in equation (2-7) [28]:

$$\sigma_{vM} = \sqrt{\frac{1}{2}\left[(\sigma_r^{RS} - \sigma_\varphi^{RS})^2 + (\sigma_\varphi^{RS} - (\sigma_a^{RS} + \sigma_a^{LS}))^2 + ((\sigma_a^{RS} + \sigma_a^{LS}) - \sigma_r^{RS})^2\right]} \qquad (2\text{-}7)$$

In Equation (2-7), σ_r^{RS}, σ_φ^{RS} and σ_a^{RS} are the residual stress components in radial, hoop, and axial direction, respectively, whereas σ_a^{LS} is the axial applied load stress. Figure 2-10 shows the three

distributions: as-welded residual stress, residual stress during loading, and residual stress after unloading. In Figure 2-10 a, von Mises stress during loading of 182 MPa does not reach the yield stress, so there is no relaxation. However, load stress of 337 MPa causes an exceeding of the yield stress for a definite distance between 14 mm and 50 mm. Figure 2-10 b depicts that those residual stresses after bending are relaxed. In brief, residual stress relaxation depends on the type and magnitude of the applied bending stress [28]. Therefore, by applying an appropriate external loading source, changing residual stress distribution can possibly affect crack initiation and propagation.

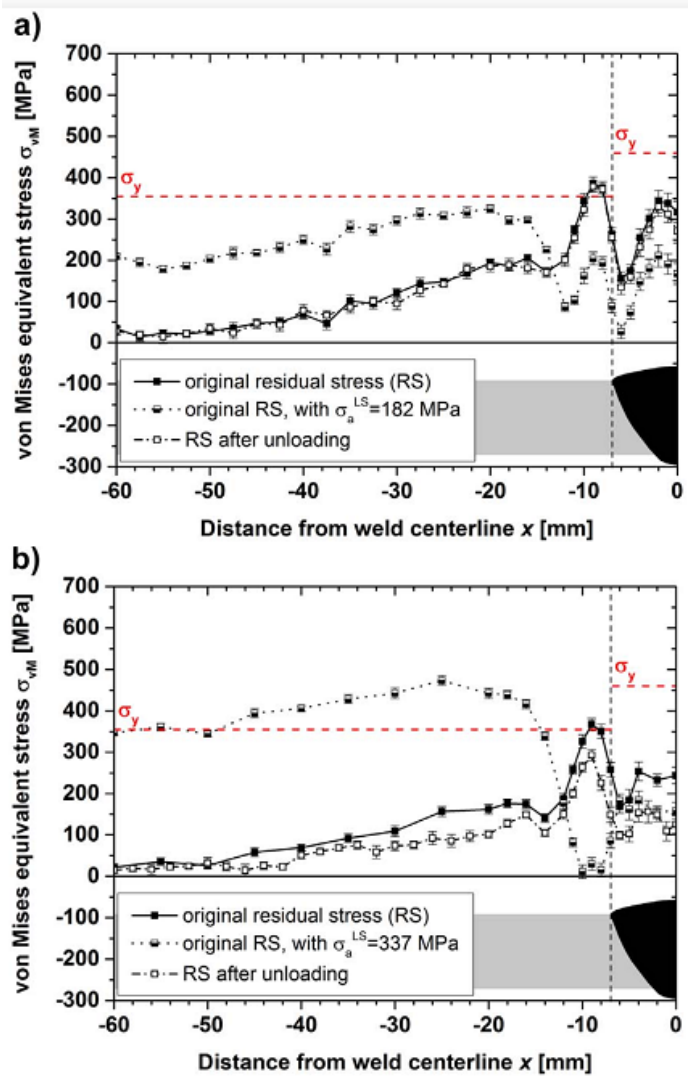

Figure 2-10 Von Mises equivalent stress on the outer surface: a) before, during and after an axial load of 182 MPa, b) before, during and after an axial load of 337 MPa [28]

2. 3. 3 Effect of residual stress on axial NNpHSCC

As mentioned in previous sections, stress is a vital parameter in causing transgranular corrosion in the NNpH environment. When the evolution of NNpHSCC in pipeline is the subject of study, the residual stresses can play an important role through acceleration or retardation regarding nucleation and growth of environmentally assisted cracking in pipeline steels subjected to cyclic loading, mainly in those situations associated with the presence of hydrogen. Indeed, residual

stresses can affect the susceptibility to stress corrosion cracking (SCC) in buried pipeline steel [7], [24]. In a near-neutral-pH environment, the residual stress can alter the stress state in the vicinity of the element surface and affect hydrogen entry and diffusion toward the fracture process zone. The residual stress also causes the deformed steel to be anodic, in comparison with the undeformed steel, due to the stress cell effect. The nature of residual stress in the pipeline is complicated because of the interaction of different sources, such as internal operating pressure, residual stress from pipe fabrication, girth welding, temperature gradient, *etc*. In other words, these stresses are sometimes undesired, although unavoidable, as a result of various external and internal sources in pipeline fabrication, pipeline construction, and processing in the field [24], [29], [30].

J. A. Beavers *et al*. [31] compared the level of residual stress at SCC colonies with adjacent SCC-free material for axial NNpH SCC. They found that SCC incidence is more probable in areas with more residual stresses. Figure 2-11 shows the correlation between residual stress for SCC and non-SCC areas in various pipe samples. These data show that the residual stress in the areas close to SCC colonies was almost twice as high as in areas far from near-neutral pH SCC colonies (Control areas) [31]. This shows that the initiation of the NNpHSCC colonies is favored by tensile residual stress.

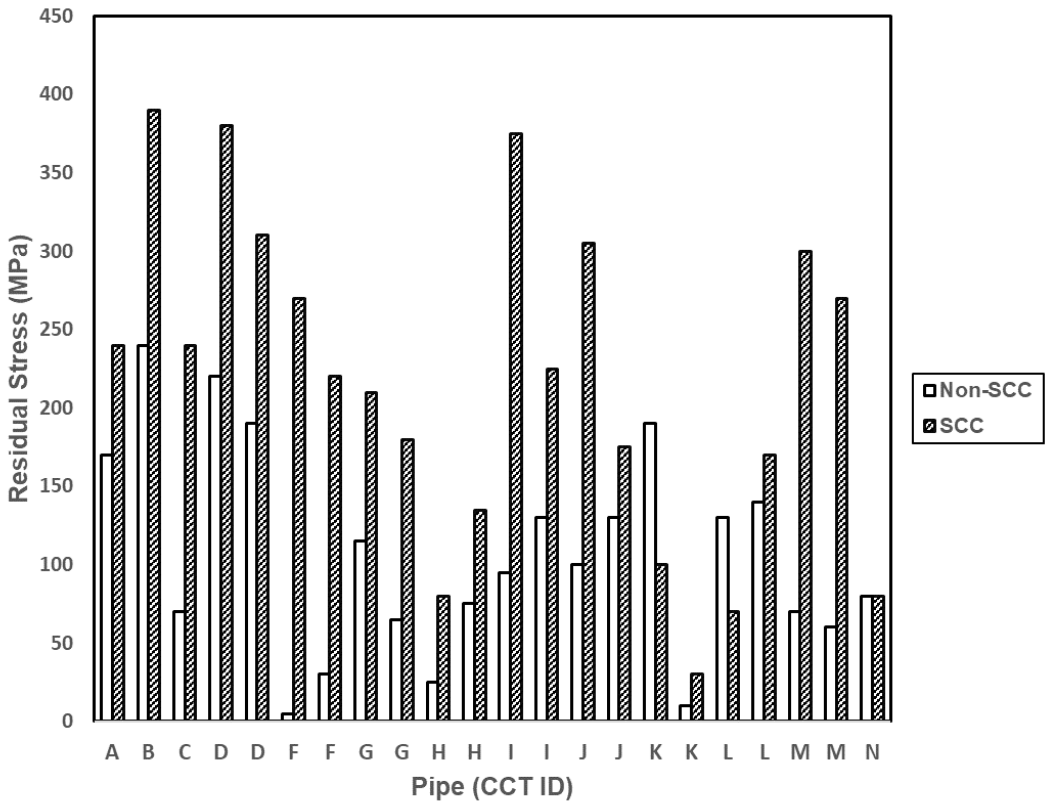

Figure 2-11 Residual stresses for SCC and non-SCC areas on pipe samples. [31].

To understand the mechanism of correlation between residual stress and SCC, residual stresses should first be categorized into three important groups based on the length scale: Type I is macro-scale residual stresses that occur over large distances (at least several grain diameters). The pipeline bending during pipe manufacturing and installation, temperature gradients, and plastic deformation during handling are significant sources of this type of residual stress. In type II, Micro-scale, residual stresses change over the grain scale, and important sources for having this type of residual stress is the presence of regions with various microstructures like pearlite colonies/ ferrite grains and banded structures in pipeline steels. Atomic scale as type III residual stress includes stresses in atomic scale caused by sources such as chemical segregation at grain boundaries [32]. It is evident that interaction type I residual stresses with other stress sources should adversely affect the NNpHSCC mechanism.

2. 3. 4 Interaction of residual stress and cyclic loading

The interaction of residual stresses and applied sources, like pressure fluctuation in pipelines, influences the fatigue life of the pipeline by altering the shape and magnitude of the mean stress distribution experienced over a fatigue cycle [8]. For example, relaxation of residual stress caused by interaction with applied cyclic loading may reduce this effect on the component's fatigue life. For instance, cracking relieves internal stresses, so they are more important for nucleation and early-stage behavior.

In the study done by G. Van Boven *et al*. [7], [8], the interaction of residual stress and cyclic loading was investigated by applying a bending force on the pipeline. In fact, in that project, they used forces to straighten the curvature of the pipeline by 3-point bending. As a result, the long axis of the specimens was cut in the hoop direction, and when it straightened, the residual stress was in the original hoop direction of the pipe. Then, after conducting an “SCC” test in the NNpH environment, they analyzed transitions in residual stress distribution. Cyclic loading had increased the residual stress at the surface of the pipeline, as illustrated in Figure 2-12, to the level at which the steel is very prone to crack initiation.

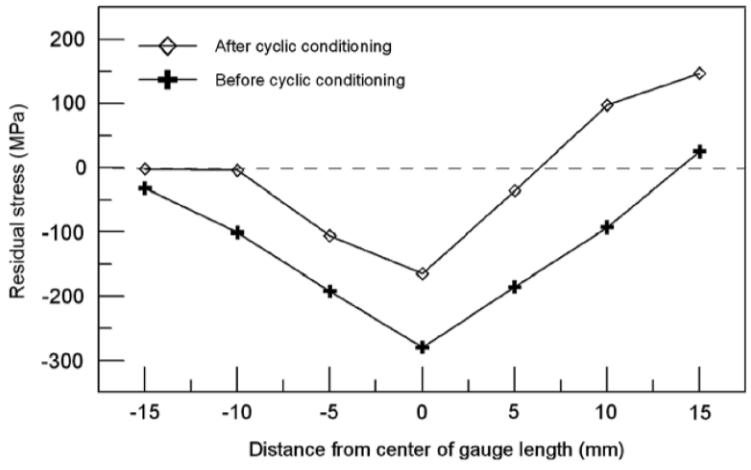

Figure 2-12 A comparison of axial residual stress as measured before and after cyclic conditioning in air [8]

G. Van Boven *et al*. [7], [8] achieved different residual stress distributions by making different bending angles. Regardless of the depth and length of residual stress measurement points, the change of nature and magnitude of residual stress caused by applying cyclic loading in the SCC test is shown in Figure 2-13. In region I of this graph, cyclic loading causes an increase in residual stress (which was utterly compressive prior to cyclic loading.) On the other hand, in the initial tensile residual stress region (region III of Figure 2-13), a stress decrease was caused by cyclic loading [7]. These changes could be attributed to the relaxation of residual stresses, discussed in section 3.2 of this literature review.

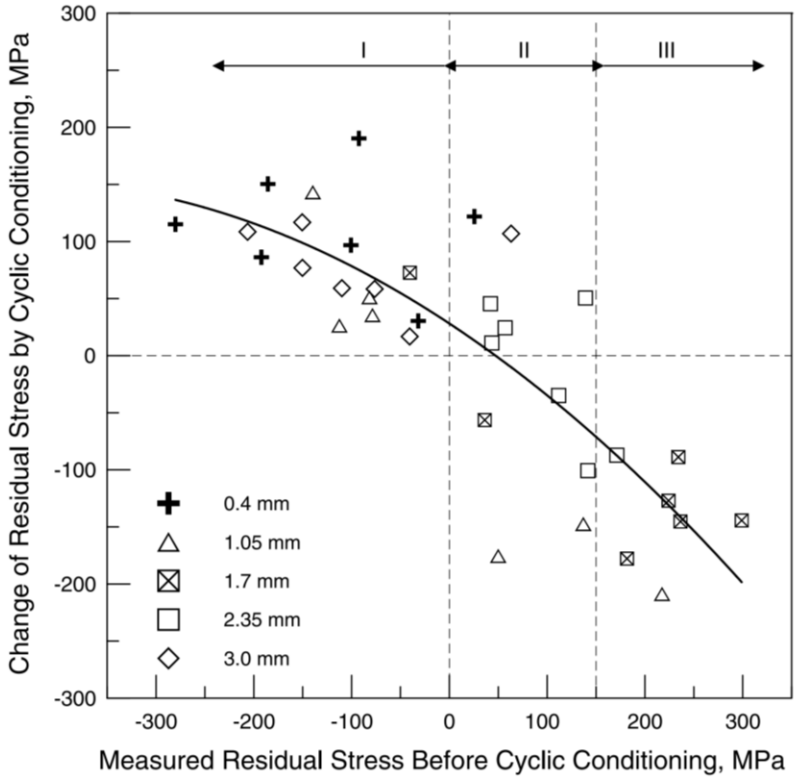

Figure 2-13 Change of residual stresses by cyclic conditioning as a function of residual stresses measured prior to cyclic conditioning in different depths (mm) [7]

2. 4 Effect of residual stress on different stages of C-SCC

In the previous section, Circumferential Stress Corrosion Cracking (C-SCC) and residual stress phenomena were discussed separately. This part focuses on how residual stresses affect cracking

failure. The failure mechanism for cracking is usually divided into three stages. Stage I, crack initiation and early-stage crack growth, Steady-state Crack growth in stage II, and rapid crack growth (fracture) in stage III [33].

2. 4. 1 Crack initiation and early-stage growth mechanism

In this stage, conditions for corrosion have been well established, like coating damage and groundwater in contact with the pipe surface. After localized corrosion on the pipe surface, crack initiation may happen. The presence of tensile residual stress, coating conditions, soil environment, and steel metallurgy are the most crucial factors in this stage [18]. Different mechanisms can result in crack initiation, including preferential dissolution at physical or metallurgical discontinuities like scratches and banded structures, corrosion at stress riser locations like corrosion pits, corrosion alongside persistent bands caused by applying cyclic loading before corrosion exposure, and finally, the presence of galvanic effects related to mill scale, microstructure, or residual stresses. When crack depth increases, the rate of dissolution decreases. As a result, most initiating cracks cease growing when they reach a depth of about 1 millimeter and enter the next stage, dormancy, which will be discussed in the next section [33], [34].

Constant loading tensile stress can cause the initiation of microstructurally short cracks (typically less than 100 μm). In other words, high residual stresses at the pipe subsurface plus operating stresses cause early-stage crack growth [6]. The cracks formed at this stage should be characterized as shallow notches caused by corrosion, not cracks since they have less than 1 mm of depth and a very small depth/length aspect ratio of around 0.1–0.2. Because of this, fracture mechanics principles do not work for these crack-shape notches [35], although their shape will influence the stress magnitude.

2. 4. 2 Effect of residual stress on crack initiation and early-stage growth

Van Boven *et al*. [8] worked on different stages of crack failure and reported that the presence of residual stress on the surface of pipeline steel can produce a galvanic cell as areas with regions of plastic deformation are anodes because of higher dislocation density. As a result, these regions corrode. As described previously, the bottom of the pit is the susceptible site for crack initiation. Figure 2-14 illustrates different cracks formed at the bottom of the pits. These cracks exhibit different morphologies, such as balloon-like or cone-like [8]. It should be emphasized that these shapes result from the particular residual stress pattern introduced in their experiment and may not be typical of pipes in the field.

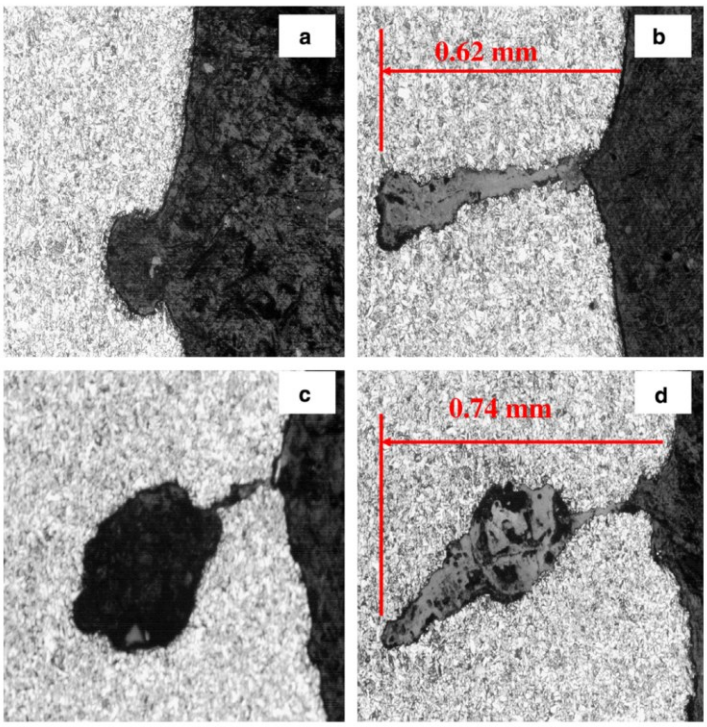

Figure 2-14 Typical cracks formed during a cyclic loading test in an aqueous environment: b) cone-like shape, c) balloon-like shape [8].

It is important to know that not only does the magnitude of residual stress play an important role in crack initiation at the bottom of the pit, but also the type of this residual stress has a crucial

effect on cracking. It should be noticed that the residual stress pattern at the bottom of the pit must be the focal point of investigations, not residual stresses on the surface. Also, these residual stress distributions, after applying cyclic loading, govern crack initiation at the bottom of pits. As discussed previously, the interaction of residual stress and cyclic loading changes the residual stress pattern close to the pit bottom. Therefore, the initiation of a pit or crack is related to the initial residual stress distribution, the pace of changing this distribution through cyclic loading, and the final distribution after cyclic loading. On the condition that appropriate stress conditions disappear because of a new residual stress pattern after cyclic loading, pits can develop instead of initiation of cracks. Returning to Figure 2-14, the increased lateral dissolution at the crack tip caused by decreased residual stress as the crack propagates leads to a cone-like shape. However, balloon-like morphology is the result of a rapid reduction of residual stress and the development of extensive lateral corrosion. It was suggested by W. Chen *et al*. [7] that the change of residual stress happens after only a few cycles. The equation developed for the long crack growth mechanism and the stress intensity factor for early-stage crack growth are needed to simplify this problem [7]:

$$\frac{da}{dN} = \alpha(\Delta K)^n = \alpha(1-R)^n K_{max}^n \qquad (2\text{-}8)$$

Where da/dN is the crack growth rate per cycle, ΔK is the stress intensity factor range, α is the material constant, R is the stress ratio ($\sigma_{min}/\sigma_{max}$) and K_{max} can be calculated by [7]:

$$K_{max} = \sigma_{tot}\sqrt{\frac{\pi a}{Q}}\, f(\frac{a}{w}) \qquad (2\text{-}9)$$

Where Q = 1 + 1.464 for a crack with a/c = 1, and f(a/w) is the geometric factor, which is estimated to be $1.04 + 0.2(a/t)^2 - 0.106(a/t)^4$ for the current situation; σ_{tot} is equal to the sum of applied stress (σ_a), the residual stress at the surface (σ_{r-o}), and the change in residual stress with depth into the

pipe (Ma). In the following formula, M is always negative since, with depth of pipe, the residual stress decreases [7]:

$$\sigma_{tot} = \sigma_a + \sigma_{r-o} + Ma \qquad (2\text{-}10)$$

Note that as cracks grow, the stress pattern changes and the residual stress is relaxed so the above-mentioned formula could be considered as the initial stress conditions, not the stress after pitting or cracking. Typically, crack growth rate decreases as crack depth increases, caused by the effect of M on decreasing the stress intensity factor. In the presence of maximum residual stress on the surface, there is a reduction in the magnitude of residual stress in the depth direction caused by the self-equilibrating feature of residual stress [7]. On the other hand, as a result of crack propagation, all the applied stresses carried by the cracked material are transferred to the remaining material. In fact, during crack formation, the residual stress is gradually removed since the crack allows the forces to relax, and the part becomes stress-free.

In conducting research on the reduction of total stress with increasing crack depth, the effect of transferring residual stress from tensile to compressive in the depth direction, as well as stress relaxation through crack formation, should be considered concurrently.

2. 4. 3 Crack dormancy mechanism

It has been estimated that over 95 percent of cracks in NNpHSCC colonies remained dormant, and only 5 percent can grow past this depth [36]. This feature is called crack dormancy. The crack depth for growing cracks should be larger than 1 mm, which corresponds to about 10% of wall thickness in large-diameter pipeline steels prone to NNpHSCC. From a pipeline integrity management point of view, these dormant cracks are not so dangerous for pipelines working with hoop stress less than 72% of SMYS [7]. Figure 2-15 shows a field dormant crack and a population of cracks with different depths found in the field.

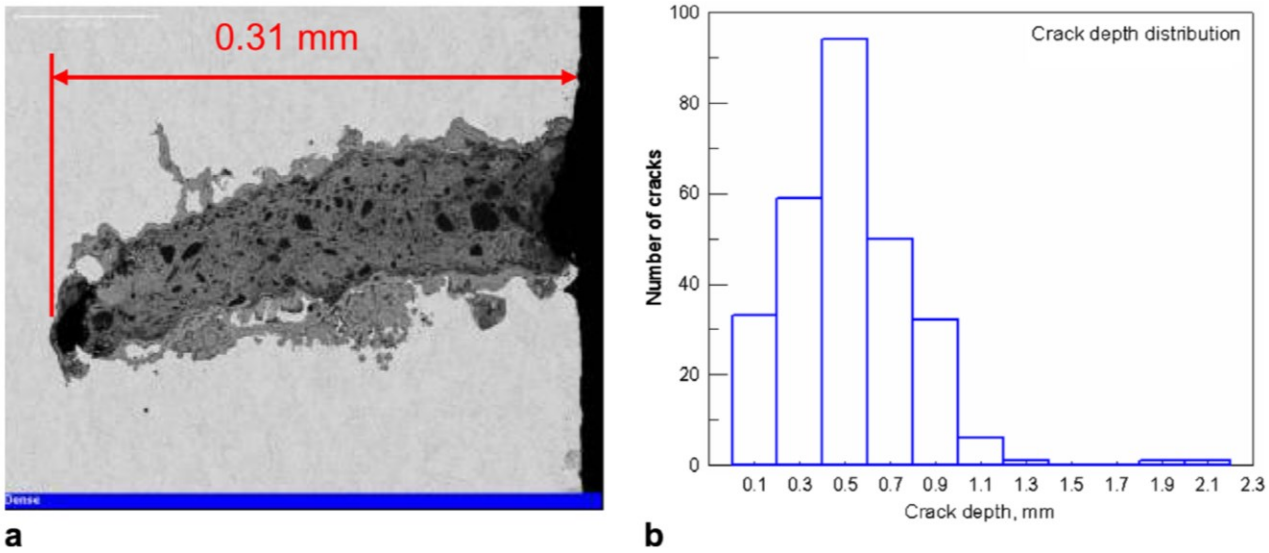

Figure 2-15 a) A typical dormant crack from the field, b) crack depth distribution in various crack colonies found on a ruptured line pipe [7]

There are some reasons for crack dormancy [1], [6], [37]–[40]:

- The rate of dissolution is reduced at the crack tip caused by complicated processes related to the gradient of dissolved CO_2 and the variation of ionic concentrations of other solutes. In the NNpH environment, corrosion occurs simultaneously on the crack tip and wall, and material passivation does not happen in this transgranular crack. Hence, a sharp crack blunts, particularly if its growth rate slows, so there is more time for corrosion.
- Tensile residual stress close to the crack tip is insufficient for crack growth. In other words, overall mechanical driving forces are lower than the threshold for crack propagation. Maximum tensile residual stresses decrease in the depth direction and even become compressive, which may impede the onset of stage II.
- The amount of diffusible hydrogen surrounding the crack tip is low. Hydrogen is produced by corrosion at the crack tip, cathodic reaction, or general corrosion (carbon dioxide (CO_2)-water reactions) on the pipe surface. However, only the hydrogen atoms which diffuse to the hydrostatic stress zone ahead of the crack tip could be considered an effective parameter

for crack growth. The value of hydrogen that could reach the crack tip depends on the diffusivity of hydrogen, temperature, and thickness of the specimen. Also, the presence of hydrostatic tensile stress at the crack tip allows hydrogen to accumulate ahead of the crack tip and make the material close to the crack tip brittle. Although crack tip corrosion and residual stress govern the onset of crack growth, hydrogen accumulation determines the ability to attain crack growth by the corrosion fatigue mechanism. The hydrogen level ahead of the crack tip will drop as the crack blunts and stresses decrease.

- Room-temperature creep may also cause crack blunting causing retardation of fatigue crack growth. In some cases related to the loading pattern, the additional deformation from this creep can increase the residual compressive stresses ahead of a crack tip and enhance the retardation effect [39]. In other words, cyclic creep retardation is related to the cyclic hardening effect. In general, the presence of sustainable strain at the crack tip can help cracks grow, so exhausting this strain via applying a stress a little more than operational stress could produce enough plastic deformation at the crack tip and produce a retardation effect [39].

2. 4. 4 Effect of residual stress on dormancy and transition from dormant state to active state

Some location-specific conditions are necessary to reactivate a dormant crack. The first is related to the magnitude and nature of residual stresses near the crack tip. The second one is related to how much diffusible hydrogen can reach the crack tip. These two are related to one another. Suppose the level of tensile residual stress is high enough. In that case, the residual stress and this hydrogen interaction can decrease the chance of crack dormancy in a specified crack colony in an NNpH environment [33], [41]. Figure 2-16 illustrates how the nature and magnitude of residual stress are related to dormancy [6]. These residual stresses add to the applied stresses and extend

the time of dormancy if they are compressive or can shorten this time if they are tensile (and high enough) [33], [41]. Also, the fact that these residual stresses are not uniformly distributed along the pipe can explain the location dependence of cracks in pipeline steels [35].

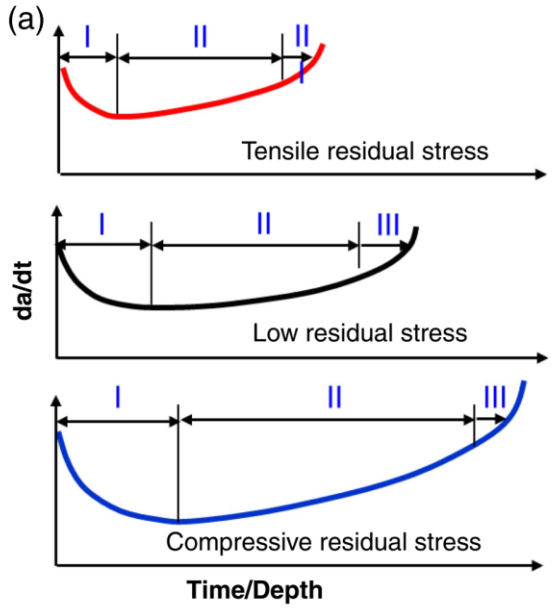

Figure 2-16 Effect of different nature and magnitude of residual stresses on crack growth [6]

As introduced previously, crack tip blunting and dormancy are intrinsic to crack growth in pipeline steels (in a NNpH environment). On the other hand, the extrinsic sources of crack sharpening are cyclic loading and the hydrogen enhancement of fatigue. The balance between these two intrinsic and extrinsic sources could define dormancy or reactivation of cracks [35]. Combining hydrostatic stresses in the plastic zone, hydrogen segregation, and the presence of weakest link sites, such as inclusions close to the crack tip, creates hydrogen-induced microcracks, which can connect to the main blunted crack and re-sharpen it. This mechanism of crack growth requires cyclic loading to occur. In fact, the synergistic interaction of cyclic loading and hydrogen-related sharpening can cause resharpening of the blunted cracks. Wherever these two conditions can act simultaneously,

the probability of growth is high. This is the reason that less than five percent of dormant cracks can grow continuously [35].

The presence of tensile stress ahead of the crack tip is a prerequisite condition for the reactivation of cracks. However, this 5 % of the total crack population that gains this condition cannot have continued growth, causing pipeline rupture. Indeed, only those cracks that experienced repeated cycles of dormancy and reactivation are a concern for the integrity of the pipeline [35]. A growing crack may repeatedly experience the process of growth, dormancy, and reactivation of blunted crack. This process is shown in Figure 2-17 [6].

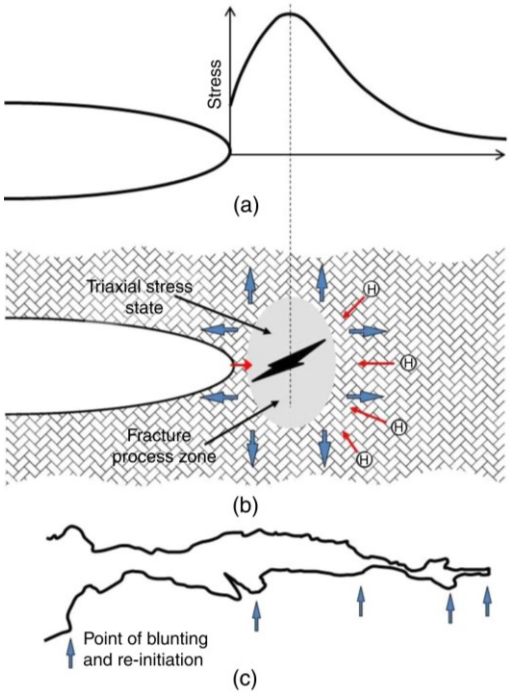

Figure 2-17 The mechanism of discontinuous crack growth: (a) stress distribution at the blunt tip, and (b) microcrack initiation at the fracture process zone. (c) cycles of crack tip blunting and microcrack initiation and growth [6]

Five residual stress patterns which could be added to stresses generated by internal pressure and the predicted crack service life (obtained by a simulation program) are shown in Figures 2-18 and 2-19 [41]. Profile II, with the highest tensile residual stress near the surface, has the minimum service life.

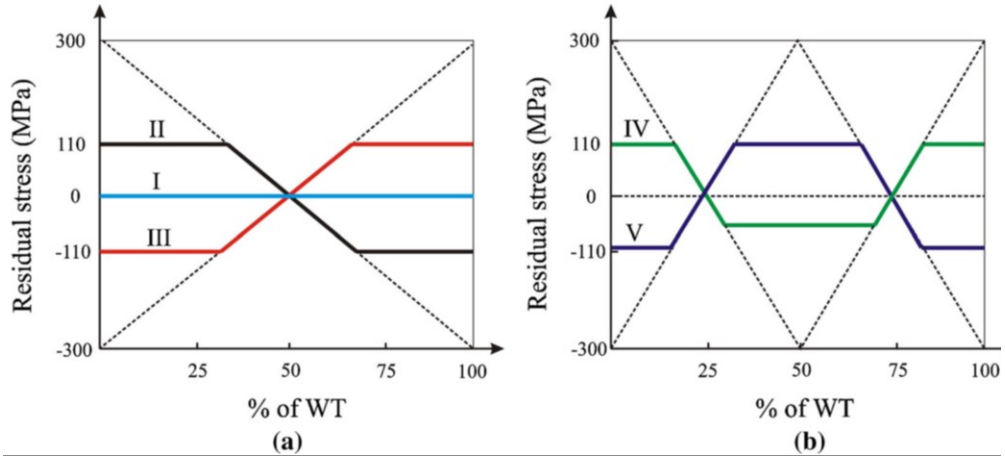

Figure 2-18 Five tracks of residual stress vs percent of wall thickness (WT): (a) track I to III, (b) track IV and V. [41]

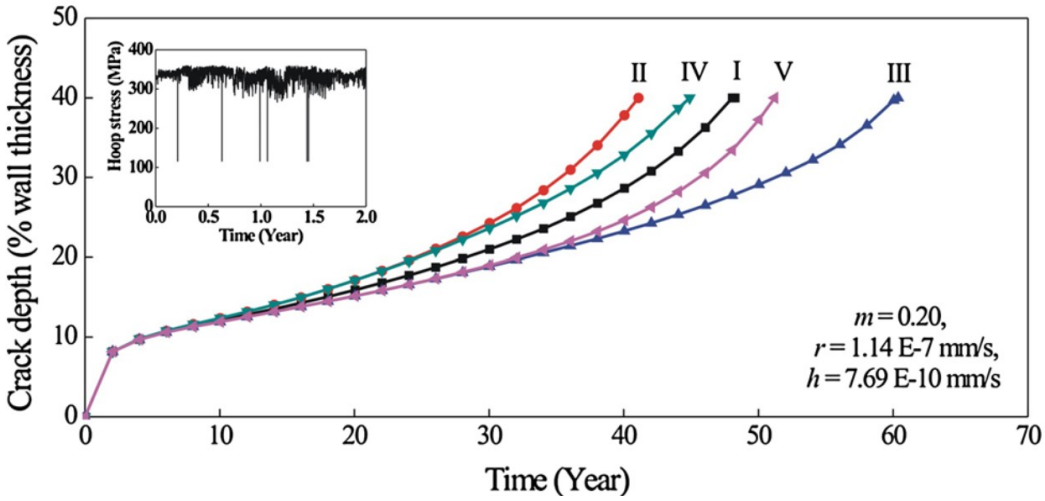

Figure 2-19 Residual stress effects on life prediction. [41]

2. 4. 5 Crack growth mechanism

The classic 'bathtub' model proposed by Parkins [42] for high pH SCC, presented in Figure 2-20a, is employed with modifications to understand SCC life. This model includes the following four stages: (Stage 0) Insufficient conditions for SCC to occur; (Stage Ia-b) Corrosion occurs, and crack-like features grow but with a decreasing rate of crack growth and a limited number of coalesced cracks; (Stage 2) Steady-state crack growth and crack coalescence; and (Stage 3) Fast crack growth rate and failure or plastic collapse [43].

As an improvement to the high pH SCC crack growth mechanism, which is related to a repeated process of crack tip passivation and rupture of the passive film [44]–[46], based on the current understanding of the crack growth mechanism in the NNpH environment, Figure 2-20b could give a better model for cracking mechanism in NNpH conditions [33], [41], [45].

As dissolution has no significant contribution to crack growth after dormancy, mechanical driving force becomes predominant in stage II crack growth, and crack growth happens at preferential sites with higher tensile residual stresses and higher diffusible hydrogen content in the material surrounding the crack tip [47].

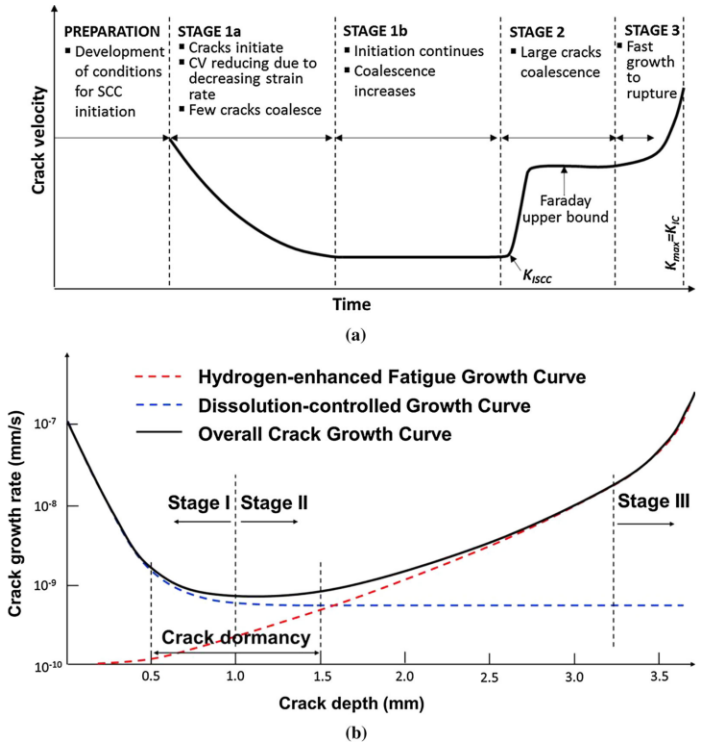

Figure 2-20 a) Parkins' Original SCC model;[4] (b) Bathtub model for NNpH stress cracking [33], [42], [48]

Another important feature related to crack growth in the NNpH environment is that crack propagation has never been observed in laboratory testing under a static loading condition. Indeed, cyclic loading is a crucial factor for having crack growth in stage II. Hence, the crack growth rate is described by a corrosion fatigue model [6], [49]:

$$\frac{da}{dN} = A(\frac{\Delta K^{\alpha} K_{max}^{\beta}}{f^{\gamma}})^{n} + h \qquad (2\text{-}11)$$

Where A, n (= 2), α (= 0.67), β (= 0.33), and γ (= 0.033) are constants, α + β = 1, and h is related to the dissolution, which makes stable crack growth rate in depth and is less important than the first term. The overall power of frequency is an indication of a corrosion environment [50] and could be considered 0.1 [6]. Also, A is defined as [6]:

$$A = \left[\frac{4\sqrt{2.476}(1+\nu)\Omega}{3\pi K_B T\sqrt{2\pi} ln\,(\frac{1}{c_0})}\right]^{2n} \qquad (2\text{-}12)$$

Where N= 0.6n, K_B is the Boltzmann constant, T is the temperature, ν is the Poisson's ratio, c_0 is the atomic ratio of H/Fe away from the crack tip, and Ω is the partial molar volume of the hydrogen atom. In this equation, the rate of hydrogen diffusion, temperature, and hydrogen concentration in the material in this constant A is connected to the cracking mechanism [41].

Based on the latter discussions [51], in the NNpH environment, the cracking mechanism of pipeline steel in stage 2 could be explained by the corrosion fatigue mechanism. This assumption and data gathered from the field coincidently showed that the combined effect of ΔK, K_{max}, and loading frequency f have a strong effect on crack growth rate. This correlation is shown in Figure 2-21. The first term ($\Delta K^2 K_{max}$) is consistent with crack growth through the Paris fatigue equation [52]: $\frac{da}{dN} = c\Delta K^{M}$ (where c and M are materials constant); and the term ($1/f^{0.1}$), reflects crack growth by corrosion. W. Chen *et al*. [51] have shown that the boundary between active and dormant cracks in Stage II for CT specimens on demarcation could be 8500 $(MPa\sqrt{m})^3/Hz^{0.1}$ for C2 solution (Synthetic field soil solution with a pH value of around 6.3, which shows the greatest corrosion cracking potential). Also, it is noted that the environmental effect at more aggressive loading conditions is minimal, and the model converges to the fatigue (Paris) line at high ΔK 's. At lower ΔK 's, the line is independent of ΔK and corresponds to crack growth divided by frequency.

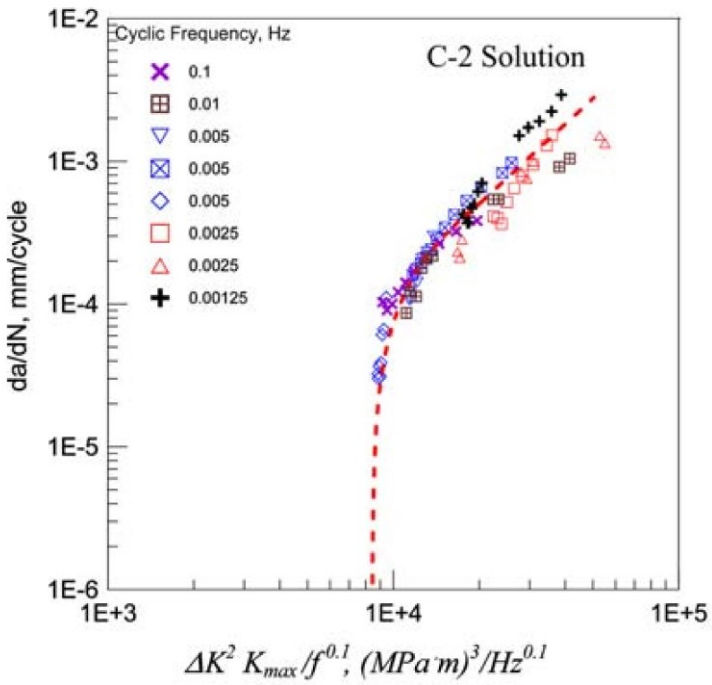

Figure 2-21 Crack growth rate da/dN as a function of $\Delta K^2 K_{max}/f^{0.1}$obtained from testing in C2 solution [51]

To characterize crack growth in pipeline steel, the effect of operation under variable amplitude fluctuation should be evaluated. Based on the so-called load-history-dependent load interaction feature of pipeline steels, a previous cyclic loading with an R- ratio can increase or decrease the crack growth rate of current and future cycles as it affects crack tip blunting, cyclic plasticity-induced residual stress around the crack tip, crack tip plasticity, and plasticity-induced crack closure. These fluctuations are divided into three types: Type I: Underload Pressure Fluctuation within 30 km downstream of a compressor station, Type II: Mean Load Pressure Fluctuations where further away from the compressor (Gas pipeline)/ Pump station (Oil pipeline), and type III: Overload Pressure Fluctuations close to a suction site where pressure spikes above the mean pressure. Among these various fluctuation patterns, Type I is the harshest in crack growth [33].

2. 4. 6 Effect of residual stress on crack growth

This section analyzes the consequence of residual stress as determined by the interaction of residual stress in the material caused by different sources with applied cyclic loading on crack growth in the NNpH environment. J. Toribio [53] has focused on the impact of cyclic and residual stresses on the maximum intensity factor (K_{max}). To achieve this point, residual stress distribution ahead of the crack tip should be known, although there are some barriers to doing this. For example, it is impossible to measure the exact residual stress distribution at the crack tip. Based on their investigations, on condition that material has been subjected to cyclic loading (which produces compressive stress close to the crack tip) before contacting with the solution in the SCC test, the final failure load in an aggressive environment can be increased by either delaying metal dissolution or hydrogen entry [53], [54]. In other research done by D. O. Harris, it is mentioned that the stress intensity factor is a function of crack size and residual stress [25]:

$$K = \sigma_{ap} a^{0.5}\, Y\left(\frac{a}{h}\right) + K_{res}(a) \qquad (13)$$

Where σ_{ap} is the applied stress, (a) is the crack size (single-edge crack or a center crack in a strip), h is the width or thickness of the body, and $K_{res}(a)$ is the stress intensity factor caused by residual stress. In general, increasing the depth of cracks results in more stress intensity factor (not considering the effect of residual stress). However, the residual stress pattern can accelerate the growth of shallow cracks but retard the growth of deeper cracks. In other words, increasing crack depth may result in decreasing the maximum stress intensity factor because the effective stress intensity factor is the result of applied stress and residual stress. Figure 2-22 illustrates the crack growth in the presence of residual stresses [8].

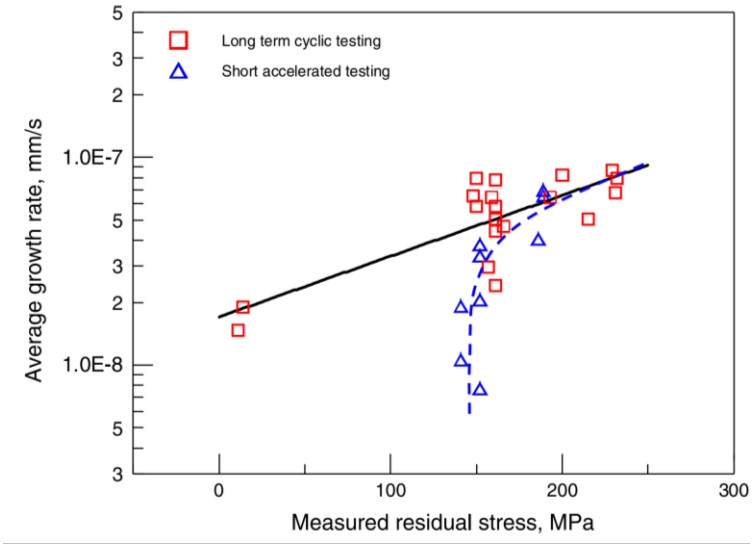

Figure 2-22 Crack growth rate as a function of residual stresses measured at the surface of the specimen [8].

2. 5 Gaps in knowledge about C-SCC in near-neutral pH environment

As discussed earlier, there is limited literature on the interaction of residual stresses from pipe manufacturing, installation, and operation in the field, and applied stresses from cyclic loading of pressure fluctuation (simulated as a stress corrosion test). In addition, these limited works focused on longitudinal cracks and considered only limited parameters. For instance, G. Van Boven *et al*. [8] have considered the combined effect of only one cyclic and residual stress on the cracking mechanism in longitudinal cracks in pipeline steels.

Clearly, further information on C-SCC is needed to develop predictive models in cracking stages to enhance management capabilities. Therefore, to accomplish the understanding of this topic, more small-scale tests should be carried out considering a wide range of important factors in the C-SCC. Also, as axial residual stress has a crucial impact on failure, parameters making various distributions of residual stresses in depth and length are required for the evaluation.

In circumferentially oriented cracks in a near-neutral pH environment, the mechanism of crack initiation and growth could be affected by various parameters, including:

- Source of axial residual stress causing circumferential crack initiation and growth
- Distribution of residual stress along the length of the target zone
- Distribution of residual stress in the depth direction close to the susceptible area for cracking (tensile or compressive and level of residual stresses)
- Interaction of residual stresses with cyclic stresses in the near-neutral pH media (increasing or decreasing of cumulative stresses based on type and magnitude of these residual and applied stresses.)
- There is a clear need to establish the applicable Bourdon and hydrodynamic axial stress at bends in pipelines since it has been shown that these can be substantial, particularly in larger-diameter pipes with higher bending angles.

The sum of the stresses from axial applied and residual stress sources strongly impacts various cracking stages, including surface corrosion and initiation of cracks, early-stage growth, dormancy, reactivation of dormant cracks, crack growth, and final fracture. To achieve this understanding, these objectives can be defined:

- Understanding the interaction of various residual stress distribution patterns (in length and depth direction) with mechanical loading, particularly the effects of cyclic loading
- Finding the relationship between accumulated stresses with reactivation of dormant cracks and crack growth
- Establishing the crack initiation and growth mechanism for circumferentially oriented cracks in the presence of residual stresses

Through finding the crack growth rate, the time needed for an initial crack to reach the threshold point where it will become unstable and cause failure could be calculated. This factor is vital in pipeline integrity management.

2. 6 Recommended remedial actions

To mitigate issues related to C-SCC in NNpH environments, acquiring a benchmark report containing all the related information from industrial pipeline construction, operation, inspection, repair, and maintenance companies is essential.

It is imperative to include the history of pipeline segments that are susceptible to C-SCC in the report:

- Stress distribution in pipelines from different sources (pipe manufacturing and pipeline construction),
- Operating parameters in areas with C-SSC, such as service pressure fluctuations and temperature,
- Types, sensitivity, and resolution of the inspection instruments used to detect circumferential cracks,
- Failure assessment,
- Repair procedures for removing or neutralizing circumferential cracks.

Mitigation strategies could be developed based on academic and industrial achievements. Fessler *et al.* [2] outline some practical strategies for existing pipelines in their article.

- Modifying operating practices to reduce future crack growth and to prevent nucleation of new cracks,
- Relieving residual stress within a pipeline,
- Locating existing cracks, assessing their severity, and
- Managing or repairing existing cracks to prevent them from becoming critical during future operations.

- Consider options such as increasing pipe walls at bends and providing support at bends during construction to reduce the Bourdon and hydrodynamic stresses.

In addition, it is recommended to consider the obvious susceptibility factors for C-SCC during pipeline design and route-planning stages. For instance, by monitoring the level of axial stress during construction and removing any potential geohazards, a pipeline system will be less likely to be affected by C-SCC. The following points should be considered for new pipelines [2]:

- Do not force-fit the pipe for connections in tie-ins
- Do not perform constrained cold bends
- Protect the pipe with high-quality coatings
- Monitor soil movement on slopes
- Design bends that minimize Bourdon and hydrodynamic stresses

There is no doubt that these recommended strategies are the first step in mitigating C-SCC. In order to fill the C-SCC knowledge gap, comprehensive studies are needed to reduce the risk of failure (pipeline rupture and leakage).

References

[1] Canadian Energy Pipeline Association (CEPA), Stress Corrosion Cracking Recommended Practices, 2nd Edition, an industry leading document detailing the management of transgranular SCC, December 2007.

[2] R. R. Fessler, M. Sen, Characteristics, cause, and management of circumferential stress-corrosion cracking, Proceedings of the 2004 International Pipeline Conference. Calgary, Alberta, Canada. IPC2014-33059. https://doi.org/10.1115/IPC2014-33059.

[3] M. Yu: Crack Growth Behavior of Pipeline Steels under Variable Pressure Fluctuations in a Near-Neutral pH Environment. PhD thesis, University of Alberta, 2015. https://era.library.ualberta.ca/items/e58655f5-77bb-4365-ac1f-706734810719

[4] J. A. Beavers, Integrity management of natural gas and petroleum pipelines subject to stress corrosion cracking, Corrosion 70 (2014) 3–18. https://doi.org/10.5006/0998

[5] National Energy Board (NEB), Report of the Inquiry concerning Stress Corrosion Cracking on Canadian Oil and Gas Pipelines, NEB MH-2-95, December 1996. https://publications.gc.ca/collections/Collection/NE23-58-1996E.pdf

[6] W. Chen, An overview of near-neutral pH stress corrosion cracking in pipelines and mitigation strategies for Its initiation and growth, Corrosion 72 (2016) 962–977. https://doi.org/10.5006/1967

[7] W. Chen, G. van Boven, and R. Rogge, The role of residual stress in neutral pH stress corrosion cracking of pipeline steels - Part II: Crack dormancy, Acta Materialia 55 (2007) 43–53. https://doi.org/10.1016/j.actamat.2006.07.021

[8] G. van Boven, W. Chen, and R. Rogge, The role of residual stress in neutral pH stress corrosion cracking of pipeline steels. Part I: Pitting and cracking occurrence, Acta Materialia 55 (2007) 29–42. https://doi.org/10.1016/j.actamat.2006.08.037

[9] R. L. Sutherby, P. Eng, The CEPA Report on Circumferential Stress Corrosion Cracking, Proceedings of the 1998 International Pipeline Conference. Calgary, Alberta, Canada. IPC1998-2057. https://doi.org/10.1115/IPC1998-2057

[10] R. Palmer-Jones, A. Young, B. Kerrigan, J. Soltis, and T. Beuker, A practical process for managing the threat of circumferential stress corrosion cracking, Proceedings of the 2017 Rio Pipeline Conference & Exhibition, Rio de Janeiro, Brazil.

[11] J. A. Beavers, B. A. Harle, Mechanisms of high-pH and near-neutral-pH SCC of underground pipelines, Journal of Offshore Mechanics and Arctic Engineering 123 (2001) 147–151. https://doi.org/10.1115/1.1376716

[12] M. Javidi, S. Bahalaou Horeh, Investigating the mechanism of stress corrosion cracking in near-neutral and high pH environments for API 5L X52 steel, Corrosion Science 80 (2014) 213–220. https://doi.org/10.1016/j.corsci.2013.11.031

[13] Sutcliffe J.M., Fessler R.R., Boyd W.K., and Parkins R.N, Stress corrosion cracking of carbon steel in carbonate solutions, Corrosion 28 (1972) 313–320. https://doi.org/10.5006/0010-9312-28.8.313

[14] D. Abdulhameed, S. Adeeb, and R. Cheng, The influence of the Bourdon effect on pipe elbow, Proceedings of the 2016 International Pipeline Conference. Calgary, Alberta, Canada, IPC2016-64659. https://doi.org/10.1115/IPC2016-64659

[15] S. Attia, M. Mohareb, M. Martens, N. Yoosef-Ghodsi, Y. Li, and S. Adeeb, Numerical assessment of elbow element response under internal pressure, Journal of Pressure Vessel Technology 143 (2021) 051302, https://doi.org/10.1115/1.4050091

[16] R. K. Bansal, A Textbook of Fluid Mechanics, and Hydraulic Machines, Laxmi Publications, Delhi, 2005.

[17] M. Pope, *C. S. Camerini, J. C. G. Teixeira, M. T. Piza, W. Baptista, B. G. de Souza, H. L. Oliver*, Circumferential SCC in pipeline due to land creeping, Proceedings of the 2002 International Pipeline Conference. Calgary, Alberta, Canada, IPC2002-27192. https://doi.org/10.1115/IPC2002-27192

[18] N. Sridhar, Transgranular stress corrosion cracking of high-pressure pipelines in contact with solutions of near neutral pH, Corrosion 50 (1994) 394–408. https://doi.org/10.5006/1.3294348

[19] R. Sutherby, W. Chen, Deflected stress corrosion cracks in the pipeline steel, Proceedings of the 2004 International Pipeline Conference. Calgary, Alberta, Canada. IPC2004-0600. https://doi.org/10.1115/IPC2004-0600

[20] L. Y. Xu and Y. F. Cheng, An experimental investigation of corrosion of X100 pipeline steel under uniaxial elastic stress in a near-neutral pH solution, Corrosion Science 59 (2012) 103–109. https://doi.org/10.1016/j.corsci.2012.02.022

[21] X. Tang and Y. F. Cheng, Quantitative characterization by micro-electrochemical measurements of the synergism of hydrogen, stress and dissolution on near-neutral pH stress corrosion cracking of pipelines, Corrosion Science 53 (2011) 2927–2933. https://doi.org/10.1016/j.corsci.2011.05.032

[22] S. Wang, L. Lamborn, K. Chevil, E. Gamboa, and W. Chen, Near-neutral pH corrosion of mill-scaled X-65 pipeline steel with paint primer, Journal of Materials Science and Technology 49 (2020) 166–178. https://doi.org/10.1016/j.jmst.2020.01.016

[23] S. Wang, L. Lamborn, and W. Chen, Near-neutral pH corrosion and stress corrosion crack initiation of a mill-scaled pipeline steel under the combined effect of oxygen and paint primer, Corrosion Science 187 (2021) 109511. https://doi.org/10.1016/j.corsci.2021.109511

[24] A. Contreras, L. Quej-Ake, R. Galvan-Martinez, O. Vega, L. Cárdenas Norte, and C. San Bartolo Atepehuacan, Residual stress assessment and its effect on SCC of pipelines steel in acidic soil environment, MRS Online Proceedings Library 1616 (2014) 122. https://doi.org/10.1557/opl.2014.235

[25] D. O. Harris, Stress Corrosion Crack Growth in the Presence of residual Stresses, in: Eric Kula, Volker Weiss, Residual Stress and Stress Relaxation (1982), Springer, New York, pp. 273–295. https://doi.org/10.1007/978-1-4899-1884-0_15

[26] T. Neeraj, T. Gnäupel-Herold, H. J. Prask, and R. Ayer, Residual stresses in girth welds of carbon steel pipes: Neutron diffraction analysis, Science and Technology of Welding and Joining 16 (2011) 249–253. https://doi.org/10.1179/1362171810Y.0000000028

[27] M. Sabokrouh, M. Farahani, Experimental study of the residual stresses in girth weld of natural gas transmission pipeline, Journal of Applied and Computational Mechanics 5b (2019) 199–206. https://doi.org/10.22055/JACM.2018.25756.1294

[28] N. Hempel, J. R. Bunn, T. Nitschke-Pagel, E. A. Payzant, and K. Dilger, Study on the residual stress relaxation in girth-welded steel pipes under bending load using diffraction methods,

Materials Science and Engineering A 688 (2017) 289–300. https://doi.org/10.1016/j.msea.2017.02.005

[29] J. Toribio, Residual stress effects in stress-corrosion cracking, Journal of Materials Engineering and Performance 7 (1998) 173–182. https://doi.org/10.1361/105994998770347891

[30] L. Niu and Y. F. Cheng, Corrosion behavior of X-70 pipe steel in near-neutral pH solution, Applied Surface Science 253 (2007) 8626–8631. https://doi.org/10.1016/j.apsusc.2007.04.066

[31] J. A. Beavers, J. T. Johnson, and R. L. Sutherby, Materials factor influencing the Initiation of Near- neutral pH SCC on Underground pipelines, Proceedings of the 2000 International Pipeline Conference. Calgary, Alberta, Canada. IPC2000-221. https://doi.org/10.1115/IPC2000-221

[32] P. J. Withers, H. K. D. H. Bhadeshia, Residual stress Part 1-Measurement techniques, Materials Science and Technology 17 (2001) 355–365. https://doi.org/10.1179/026708301101509980

[33] J. Zhao, W. Chen, M. Yu, K. Chevil, R. Eadie, G. Van Boven, R. Kania, J. Been, S. Keane. Crack growth modeling and life prediction of pipeline steels exposed to near-neutral pH environments: dissolution crack growth and occurrence of crack dormancy in stage I, Metallurgical and Materials Transactions A: Physical Metallurgy and Materials Science 48 (2017) 1629–1640. https://doi.org/10.1007/s11661-016-3951-3

[34] R. Chu, W. Chen, S.-H. Wang, F. King, T. R. Jack, and R. R. Fessler, Microstructure dependence of stress corrosion cracking initiation in X-65 pipeline steel exposed to a near-neutral pH soil environment, Corrosion Science 60 (2004) 275–283. https://doi.org/10.5006/1.3287732

[35] W. Chen, R. Kania, R. Worthingham, and G. van Boven, Transgranular crack growth in the pipeline steels exposed to near-neutral pH soil aqueous solutions: The role of hydrogen, Acta Materialia 57 (2009) 6200–6214. https://doi.org/10.1016/j.actamat.2009.08.047

[36] W. Chen and R. Sutherby, Environmental effect of crack growth rate of pipeline steel in near neutral pH soil environments, Proceedings of the 2004 International Pipeline Conference. Calgary, Alberta, Canada. IPC2004-0449. https://doi.org/10.1115/IPC2004-0449

[37] J. Zhao, T. Mo, D. F. Nie, M. F. Ren, X. L. Guo, and W. X. Chen, Acceleration, and retardation of fatigue crack growth rate due to room temperature creep at crack tip in a 304 stainless steel, Journal of Materials Science 41 (2006) 6431–6434. https://doi.org/10.1007/s10853-006-0502-0

[38] S. L. Asher and P. M. Singh, Role of stress in transgranular stress corrosion cracking of transmission pipelines in near-neutral pH environments, Corrosion Science Section 65 (2009) 79. https://doi.org/10.5006/1.3319122

[39] W. Chen and S.-H. Wang, Room temperature creep behavior of pipeline steels and its influence on stress corrosion cracking, Proceedings of the 2002 International Pipeline Conference. Calgary, Alberta, Canada. IPC2002-27273. https://doi.org/10.1115/IPC2002-27273

[40] Y. F. Cheng and L. Niu, Mechanism for hydrogen evolution reaction on pipeline steel in near-neutral pH solution, Electrochemistry Communications 9 (2007) 558–562. https://doi.org/10.1016/j.elecom.2006.10.035

[41] J. Zhao, W. Chen, M. Yu, K. Chevil, R. Eadie, J. Been, G. Van Boven, R. Kania, S. Keane. Crack growth modeling and life prediction of pipeline steels exposed to near-Neutral pH environments: stage II crack growth and overall life prediction, Metallurgical and Materials

Transactions A: Physical Metallurgy and Materials Science 48 (2017) 1641–1652. https://doi.org/10.1007/s11661-016-3939-z

[42] R. N. Parkins, Factors influencing stress corrosion crack growth kinetics, Corrosion 43 (1987) 130–139. https://doi.org/10.5006/1.3583125

[43] W. Chen, J. Zhao, J. Been, G. van Boven, S. Keane, and K. Chevil, Update of understanding of near-neutral pH SCC crack growth mechanisms and development of pipe-online software for pipeline integrity management, Proceedings of the 2016 International Pipeline Conference. Calgary, Alberta, Canada. IPC2016-64626. https://doi.org/10.1115/IPC2016-64626.

[44] H. Niazi, S. Wang, L. Lamborn, R. Eadie, W. Chen, and H. Zhang, Effects of load interactions on the onset of stage two of high pH stress corrosion cracking, Journal of Pipeline Science and Engineering 1 (2021) 122–136. https://doi.org/10.1016/j.jpse.2021.01.003

[45] H. Niazi, H. Zhang, and K. Korol, High pH Crack Growth Sensitivity to Underload-Type of Pressure Fluctuations, Proceedings of the 2018 International Pipeline Conference. Calgary, Alberta, Canada. IPC2018-78394. https://doi.org/10.1115/IPC2018-78394

[46] H. Niazi, R. Eadie, W. Chen, and H. Zhang, High pH stress corrosion cracking initiation and crack evolution in buried steel pipelines: A review, Engineering Failure Analysis 120 (2021) 105013. https://doi.org/10.1016/j.engfailanal.2020.105013

[47] B. T. Lu, J. L. Luo, P. R. Norton, and H. Y. Ma, Effects of dissolved hydrogen and elastic and plastic deformation on active dissolution of pipeline steel in anaerobic groundwater of near-neutral pH, Acta Materialia 57 (2009) 41–49. https://doi.org/10.1016/j.actamat.2008.08.035

[48] W. Chen, Modeling, and prediction of stress corrosion cracking of pipeline steels, in: A.M. El-Sherik, Trends in Oil and Gas Corrosion Research and Technologies, Elsevier, Amsterdam,

2017, pp. 707–748. https://www.sciencedirect.com/book/9780081011058/trends-in-oil-and-gas-corrosion-research-and-technologies

[49] B. Y. Fang, E. H. Han, J. Q. Wang, and W. Ke, Stress corrosion cracking of X-70 pipeline steel in near neutral pH solution subjected to constant load and cyclic load testing, Corrosion Engineering Science and Technology 42 (2007) 123–129. https://doi.org/10.1179/174327807X196843

[50] S. B. Lambert, J. A. Beavers, B. Delanty, R. Sutherby, and A. Plumtree, Mechanical factors affecting stress corrosion crack growth rates in buried pipelines. Proceedings of the 2000 International Pipeline Conference. Calgary, Alberta, Canada. IPC2000-219. https://doi.org/10.1115/IPC2000-219

[51] W. Chen and R. L. Sutherby, Crack growth behavior of pipeline steel in near-neutral pH soil environments, Metallurgical and Materials Transactions A: Physical Metallurgy and Materials Science 38 (2007) 1260–1268. https://doi.org/10.1007/s11661-007-9184-8

[52] X.-Y. Zhang, S. B. Lambert, R. Sutherby, and A. Plumtree, Transgranular stress corrosion cracking of X-60 pipeline steel in simulated ground water, Corrosion 55 (1999) 297–305. https://doi.org/10.5006/1.3283991

[53] J. Toribio, Role of crack-tip residual stresses in stress corrosion behaviour of prestressing steel, Construction and Building Materials 12 (1998) 283–287. https://doi.org/10.1016/S0950-0618(98)00010-5.

[54] C. Byoung-Ho and C. Alexander, Stress corrosion crack growth in pipe grade steels in near-neutral pH environment, International Journal of Fracture 116 (2002) 43–48. https://doi.org/10.1023/A:1022665831622.

Chapter 3 Materials and method

This chapter presents a comprehensive overview of sample preparation and parameter design procedures to establish correlations between laboratory experiments and real circumferential near-neutral pH corrosion fatigue (C-NNpH-CF). As a result of these experiments, cracking behavior will be discussed, and models will be established, which can then be used to model cracking in real pipelines.

3. 1 Material Characterization

The material investigated in this research was a 16" API-5L Gr. X52, featuring a 9.2 mm wall thickness, which was extracted from a pipeline with a documented history of near-neutral pH CF cracking. Table 3-1 provides the chemical composition of this pipeline steel. Based on the literature review of this study, some information on the presence of C-NNpH-CF in pipelines and conditions for initiation and growth has been obtained by inspecting some pipes removed from slopes [1], [2]. Notably, the majority of inspections indicated that C-NNpH-CF tends to occur in proximity to areas where bending poses challenges. Recognizing bending as a potential source of residual axial stresses leading to C-NNpH-CF in practical scenarios [3], [4], [5], [6], this study acknowledges bending as a significant contributor to axial residual stresses within the pipeline.

Table 3-1 Elemental composition of the X52 pipeline steel (Wt. %).

Elements	C	Mn	P	S	Si	Cu	Ni	Cr	Fe
Composition, wt.%	0.25	1.07	0.011	0.023	0.025	0.051	0.052	0.027	Balance

The tensile characteristics of the pipeline steels employed in this investigation were assessed following ASTM Standard E8, utilizing 9.2 mm thick rectangular sheet-type samples and a crosshead speed of 0.015 mm/mm/min. The testing procedure was conducted on an INSTRON

8516 machine. Figure 3-1 illustrates the outcomes of the tension test. The yield stress of this pipe, determined at a 0.2% offset strain, and the ultimate tensile stress were recorded as 356 MPa and 561 MPa, respectively.

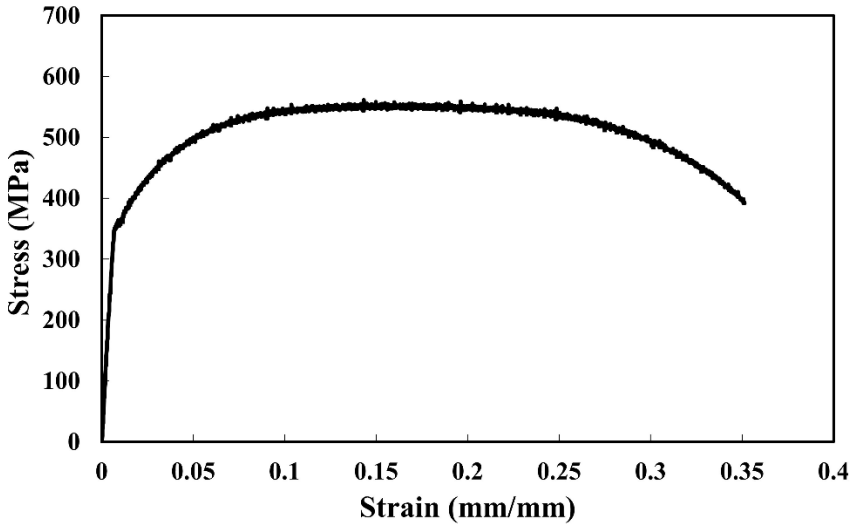

Figure 3-1 Stress-strain curve of X-52 steel used in testing

3. 2 Specimen and cell Preparation

The elongated specimens are machined with the longitudinal tensile axis aligned along the axial direction of the pipe, employing electrical discharge machining (EDM). Figure 3-2 illustrates the design and dimensions of these specimens.

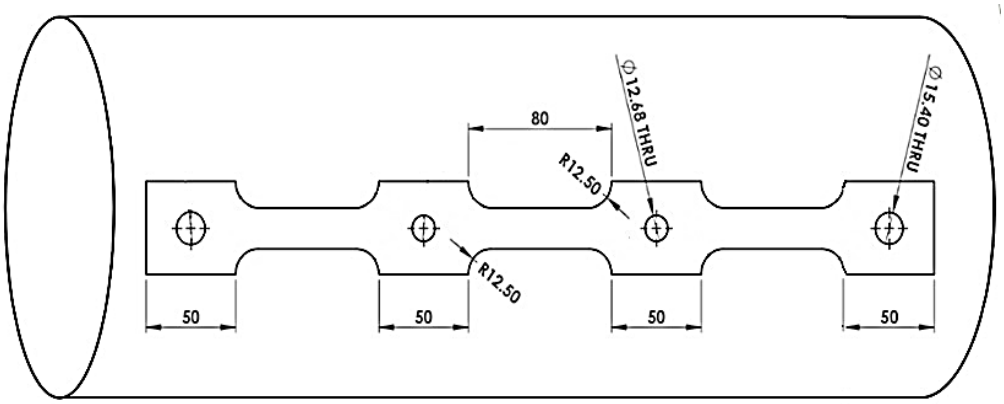

Figure 3-2 Design of long sample for C-NNpH-CF test (dimensions are in millimeters)

Three distinct reduced-gauge segments, measuring 80 mm× 20 mm× 9.2 mm and featuring artificial through-thickness notches, were intentionally configured to optimize the parameters under evaluation. These specified narrowed regions within a lengthy sample underwent bending at varying angles. It is important to emphasize that both the inner and outer surfaces of the samples were maintained in their original state to prevent alterations in the residual stress distribution profile caused by cold working processes like machining.

Residual stress exhibits a self-equilibrating characteristic, as dictated by Newton's second law, where the net force on a stationary object must be zero, resulting in a balance of forces in any cross-section. Additionally, varying bending angles lead to different residual stress alterations. This study incorporated two bending angles, 10 and 20 degrees, to simulate cold bending scenarios in the field. For example, Figure 3-3 depicts a 20-degree bent pipe (with each side at 10 degrees). This illustration underscores the existence of two distinct bending directions relative to the outer surface of the pipeline, denoted as inward and outward samples. This design simulates real-world scenarios where pipe bending, induced by factors such as slope or the need to change direction, results in two identifiable bending directions on the outer surface of pipes.

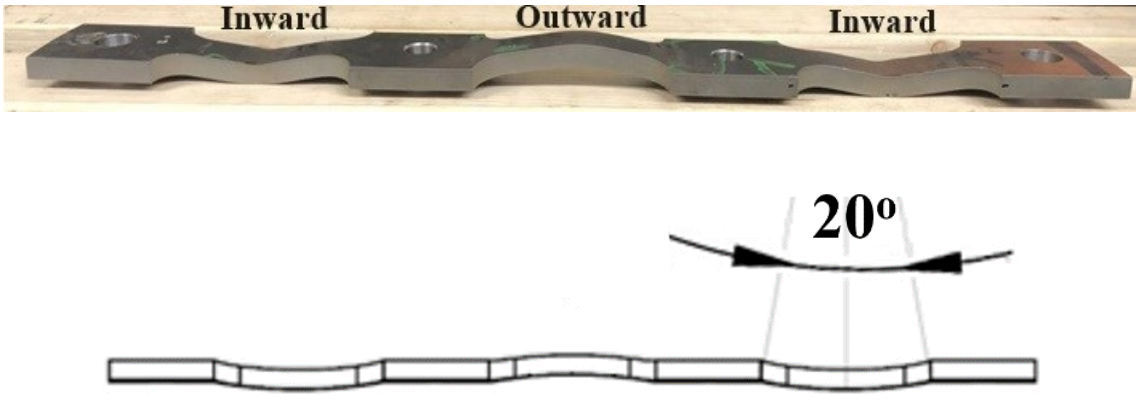

Figure 3-3 The 20-degree bent specimen; the top surface was the outer surface.

Cold bending, a contributing factor to this type of cracking (arising from pipeline construction or in-service damage related to geohazards, soil movement, *etc.*), induces axial stress throughout the entire bent section of the pipe. This stress, when combined with cyclic loading from pressure fluctuations, contributes to the occurrence of such cracking. Notably, two distinct conditions apply to a bent pipe. If the pipe is not allowed to spring back, the axial strain on the convex side of the bend is given by $D/2\rho$, where ρ is the bend radius, and D is the pipe diameter. Allowing the pipe to spring back by removing applied loads results in an altered residual stress pattern, with the convex side entering compression and the concave side experiencing tension [2]. Due to the self-equilibrating nature of residual stress, there is elevated tensile stress on the concave side to counterbalance the compressive stress on the convex side. Adding this bending axial stress to other stress sources can lead to an approach towards the material's yield strength [7], [2].

An additional origin of axial stress arises from pressure fluctuations in pipeline steel. While internal pressure generates hoop stress in the pipeline, causing the pipe circumference to expand, this pressure-induced stress also exerts force on the pipe ends, creating axial stress within the pipeline. This is particularly relevant for pressurized pipelines transporting fluids, which typically have ends against which the pressure acts. Generally, axial stress is approximately half the magnitude of hoop stress [7], [8]. Importantly, in the field where a pipe bend experiences internal pressurization, Bourdon and hydrodynamic stresses introduce complexities to the situation [7].

Based on the findings of J. Beavers *et al.* [9], pipelines operating at stress levels exceeding 60% of the specified minimum yield strength (SMYS) are more vulnerable to near-neutral pH corrosion fatigue. Consequently, stress levels of 35% SMYS (approximately half of the hoop stress) and 50% SMYS (under the consideration that additional stresses could be introduced to the hoop stress) were adopted for this study. Furthermore, it is crucial to note that this cyclic axial stress exhibits

distinct behaviours in the inward and outward bending directions of the bent pipe, assuming no residual stress from the bend (or if the bent section undergoes heat treatment and complete stress relief). To elaborate, axial loading induces tensile stress on the concave side and compressive stress on the convex side of the bend, resembling the residual stress distribution in a bent sample after springback (in the absence of axial loading).

The initial dormant crack/notch depth is a crucial parameter to consider, as it influences the evaluation of the residual stress distribution near the crack tip. A 1 mm depth was chosen for the initial notch, given that many cracks tend to cease growing once they reach this depth, entering a state of dormancy [10]. Additionally, a 0.5 mm depth for the initial notch was introduced into the study to examine the effects of varying initial notch depths on crack initiation. Subsequently, artificial notches were created on the bent sections of each long sample. Figure 3-4 illustrates the positioning of through-thickness notches on the long samples, with a 20 mm separation between notches to prevent interaction of crack tip plastic zones in close proximity. A milling machine was utilized to cut notches with a minimal width of approximately 0.2 mm and diverse depths, as depicted in Figure 3-4. This method generated rectangular-shaped notches, serving as stress concentrators at two corners. This facilitates the monitoring and assessing of crack initiation and propagation at these specific corners.

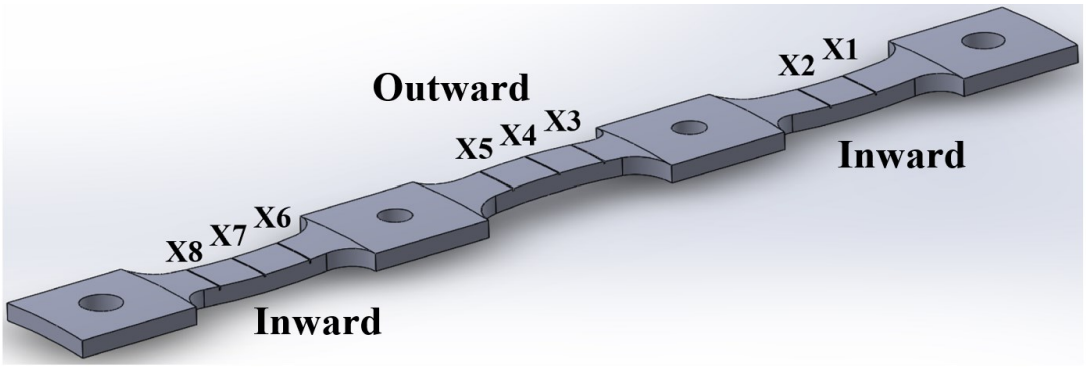

Figure 3-4 Schematic of artificial notch position on the long samples. (Width: 0.2 mm, through-thickness, distance between notches: 20 mm, notches are perpendicular to the surface of samples regardless of the bending angle and position of notches)

Moreover, a specific cell (Figure 3-5) was designed to contain C2 solution (a synthetic field soil aqueous solution with a pH value of 6.3), which exhibits the greatest corrosion cracking potential. This solution comprises 0.0274 grams of $MgSO_4.7H_2O$, 0.034 grams of $CaCl_2.2H_2O$, 0.0035 grams of KCl, 0.0195 grams of $NaHCO_3$, and 0.0606 grams of $CaCO_3$ per litre of deionized water. The solution underwent sparging with a continuous gas mixture of 5% CO_2 and 95% N_2. The resulting solution achieved a final pH of 6.3 ± 0.1, indicative of a near-neutral pH environment. Figure 3-5 illustrates the design of this specific cell and the placement of a long sample within it. Before commencing cyclic loading, the sample was introduced to the NNpH environment through gas sparging at a rate of 1 bubble per second for 12 days in a temperature-controlled laboratory set at 22°C. This process facilitated the corrosion-induced hydrogen diffusion into the samples.

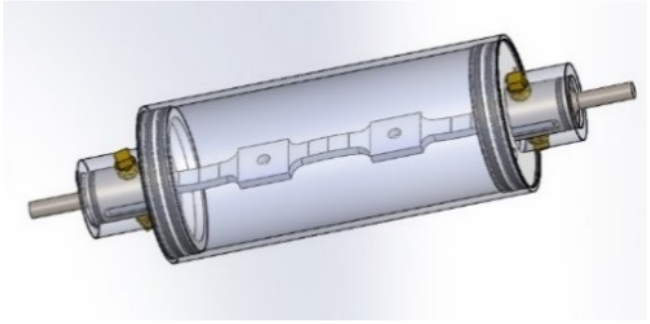

Figure 3-5 Specific cell designed for Circumferential NNpH-CF

3. 3 C-NNpH-CF testing conditions

Following the 12-day static corrosion conditioning, a C-NNpH-CF test involving cyclic loading was conducted. The test employed various axial loads, operated at a frequency of 0.001 Hz (triangle waveform), and maintained a stress ratio, R (Min stress/Max stress) of 0.1. An Instron 8516 servo-hydraulic testing machine, controlled by Wavemaker Runtime software, facilitated the testing process. The evaluation spanned 45 days unless the long sample experienced failure during the test. Continuous CO_2 sparging through the solution was maintained throughout the entire duration of the test. Table 3-2 outlines the test plan, providing insights into the assessment of the C-NNpH-CF mechanism's response to the specified parameters. Since the stress was offset from the bending position, the applied stress was increased at bends by the bending moment. In real bends, this induced bending moment can approximate Bourdon and hydrodynamic stresses.

Table 3-2 Test parameters*

Long Samples No. (X in Figure 3-4)	Radius of Bending (Degree)	Initial Notch Depth (mm)	Maximum Applied Stress (% SMYS)	Test duration (hour)
1	20	1.0	50	208
2 (Complementary)	20	1.0	50	224
3	10	1.0	50	848
4	20	1.0	35	325
5	10	1.0	35	1075
6	20	0.5	50	354
7	10	0.5	50	997
8	20	0.5	35	1283
A1	0	0.5	35	1080
A2	0	1.0	35	1080
B1	0	0.5	35% for 45 days + 50% for 45 days	2160
B2	0	1.0		2160

* Stress Ratio: 0.1, Frequency: 0.001 Hz

Notches were identified using two-digit numbers, with the first digit denoting the long sample of origin and the second indicating the notch's location on the sample (1, 2, 6-8: inward bending direction, 3-5: outward bending direction). Long sample No. 2 served as a duplicate test to long

sample No. 1, assessing data consistency. Two additional experiments involved non-bent sections with 0.5 mm and 1 mm initial notches, cyclically loaded at 35% and 50% SMYS. These tests aimed to assess the impact of cyclic loading on reference samples devoid of other axial stress sources, such as axial bending stress. Designations for these notches were simplified as follows: A1 (0.5 mm, 35%), A2 (1 mm, 35%), B1 (0.5 mm, step 1: 35% for 45 days, step 2: 50% for 45 days), and B2 (1 mm, step 1: 35% for 45 days, step 2: 50% for 45 days).

3. 4 Post-test Analysis

After each test (lasting 45 days or until fracture occurred), the long sample underwent a thorough rinse with acetone and was subsequently dried using hot air to prevent corrosion of the fracture surface, a potential issue with water exposure. Following this, a precision saw equipped with a diamond-coated wafer blade capable of 0.2 mm width cuts was employed to cut each unfailed notch into two samples. One half was allocated for cross-sectional analysis, while the other half was designated for fractographic analysis, enabling a comprehensive characterization of crack depth profiles and fractographic morphology.

The first half of each sample underwent grinding to a 1200-grit finish, followed by polishing to a mirror finish using 6 μm and 1 μm diamond oil slurry. Subsequently, the samples were etched for 5 to 10 seconds with 5% nital to facilitate the characterization of crack location, depth, and morphology through cross-sectional analysis. The remaining halves of the notches were intentionally fractured to investigate fractographic morphology and observe crack growth behaviour. To achieve this, the samples were subjected to liquid nitrogen for a maximum of four hours, then removed and fractured open by impacting the backside notch with a cold chisel. Adhering to the guidelines outlined in ASTM Standard G1-03, the fracture surface was immersed in a solution comprising 6N HCl and 3.5g/L hexamethylene tetramine to remove corrosion

products. The fracture surface and cross-sections were evaluated and photographed using a Zeiss Sigma 300-VP Field Emission Scanning Electron Microscopy (FESEM). The average crack growth rate was calculated by dividing the crack depth (measured from the bottom of the pit to the end of the quasi-cleavage region, Stage II) as depicted in the fractographic images.

Among all long samples encompassing diverse parameters, five long samples experienced failure during distinct test durations, as outlined in Table 3-3. Long sample No. 8 was securely positioned within an Instron 8516 servo-hydraulic testing machine, which featured a virtual extensometer accessible in Wavemaker Runtime software. Subsequently, it underwent cyclic loading to investigate the crack mouth opening displacement (CMOD) on notch No. 87. The specimen, under load, underwent deformation as a function of both time (t) and load cycles (N), resulting in elastic and plastic CMOD (δe and δp) and crack growth [11]–[14]. Every pertinent parameter was meticulously documented throughout testing and subsequently utilized to compute crucial data, including CMOD. Comprehensive photographic documentation was undertaken during the propagation of crack No. 87 to determine the actual crack growth rate.

Table 3-3 Failed notches testing parameters

Long Sample No. (X in Figure 3-4)	Notch No.	Radius of Bending (Degree)	Initial Notch Depth (mm)	Maximum Applied Stress (% SMYS)
1	17	20	1.0	50
2*	22	20	1.0	50
4	47	20	1.0	35
6	67	20	0.5	50
8	87	20	0.5	35

*****Except for notch No. 2, located 10 mm from the bend centerline, all failed notches were located at the bend centerline.

Electron backscatter diffraction (EBSD) analysis was employed to examine crystallographic orientations along fracture paths. EBSD specimens underwent a sequential process of grinding to

1200 grit, mechanical polishing using a diamond suspension with 6μm and 1 μm abrasive particle sizes, and final polishing with an alumina suspension featuring a particle size of 0.05 μm. The Zeiss Sigma FESEM, equipped with an Oxford Instruments Nordlys Nano detector (utilizing a step size of 1.5 μm, an accelerating voltage of 20 kV, and a tilt of 70°), and Oxford Instruments AZtec software version 2.4 were utilized for the acquisition and initial analysis of EBSD maps. Post-processing and data analysis were performed using Oxford Instruments HKL Channel 5. In addition to the inverse pole figure (IPF) maps, the strain contouring method was implemented to assess plastic deformation in the vicinity of the fracture path. This method calculates the extent of deformation, or strain, in individual grains on a map. The strain contouring component determines the maximum misorientation between any two points in a grain and then assigns a weight to the grain, based on this misorientation value. Since these maps are linked to orientation gradients in the material, they provide a qualitative assessment of small local strain gradients [15]–[21].

3. 5 Stress distribution analysis via Digital Image Correlation (DIC) and the calibration method

The identical long sample underwent C-NNpH-CF tests with 10- and 20-degree bending angles, employed for the digital image correlation (DIC) technique. A thin white layer was applied to prepare the long samples for the DIC system, and a black speckle pattern was introduced using spray paint before DIC system utilization. Subsequently, the specimens were loaded to maximum forces of 22.8 kN (35% SMYS of X52) and 32.6 kN (50% SMYS of X52), respectively. The tests were conducted on a computer-controlled MTS tensile testing machine with a maximum load capacity of 30 MN. Force and crosshead displacement were simultaneously recorded during the test. Sequential images of the gauge region in inward and outward bending directions were captured at each 100 N force increment using a high-resolution digital camera for DIC measurements. The analysis of sequential images during the test was performed using commercial

DIC software, Vic-3D 9. Initially, strain maps on external pipe surfaces and thickness surfaces were derived through DIC methods. Subsequently, the stress-stain curve was utilized to determine stress distributions along the length, width, and thickness directions of the gauge areas. The procedure to convert strain to stress involved defining a specific point, reading the strain value from DIC export data, and finally determining the equivalent stress corresponding to that strain based on the stress-strain curve (data details for Figure 3-1).

References:

[1] M. Brimacombe Senior Advisor, C. Wargacki Key Account Manager, and N. Global Leduc, "Circumferential crack detection: Challenges, solutions and results," in Proceedings of the 2016 International Pipeline Conference. Calgary, Alberta, Canada. IPC2016-64111., 2016. http://asmedigitalcollection.asme.org/IPC/proceedings-pdf/IPC2016/50251/V001T03A056/2510160/v001t03a056-ipc2016-64111.pdf

[2] R. R. S. M. Fessler, "Characteristics, cause, and management of circumferential stress-corrosion cracking," in International Pipeline Conference, ASME (IPC Conference), 2014.

[3] N. Bates, M. Brimacombe, and S. Polasik, "Development and experience of a circumferential stress corrosion crack management program," in Proceedings of the 2018 International Pipeline Conference. Calgary, Alberta, Canada.IPC2018-78315, 2018. http://asmedigitalcollection.asme.org/IPC/proceedings-pdf/IPC2018/51869/V001T03A062/2510991/v001t03a062-ipc2018-78315.pdf

[4] B. Johnson, B Tesfaye, C. Wargacki, T. Hennig, E. Suarez “Complex Circumferential Stress Corrosion Cracking: Identification, Sizing and Consequences for the Integrity Management

Program," in Proceedings of the 2018 International Pipeline Conference. Calgary, Alberta, Canada. IPC2018-78564. https://doi.org/10.1115/IPC2018-78564.

[5] Y. B. Beauregard and C. Edwards, "Analysis of sever circumferential SCC found on an ethane pipeline," in Proceedings of the 2014 International Pipeline Conference. Calgary, Alberta, Canada. , 2014.

[6] J. Babcock, D. Dewar, and J. Webster, "Deer Mountain case study: integration of pipe and ground monitoring data with historical information to develop landscape management plan," Proceedings of the 2020 International Pipeline Conference. Calgary, Alberta, Canada. IPC2020-9613, 2020. http://asmedigitalcollection.asme.org/IPC/proceedings-pdf/IPC2020/84461/V003T04A021/6620292/v003t04a021-ipc2020-9613.pdf

[7] H. Shirazi, R. Eadie, and W. Chen, "A review on current understanding of pipeline circumferential stress corrosion cracking in near-neutral PH environment," Engineering Failure Analysis, vol. 148. Elsevier Ltd, Jun. 01, 2023. https://doi.org/10.1016/j.engfailanal.2023.107215

[8] K. Zhang, R. Chune, R. Wang, and R. Kania, "Role of axial stress in pipeline integrity management," in Proceedings of the 2022 International Pipeline Conference. Calgary, Alberta, Canada. IPC2022-87327, 2022. http://asmedigitalcollection.asme.org/IPC/proceedings-pdf/IPC2022/86571/V002T03A053/6965592/v002t03a053-ipc2022-87327.pdf

[9] J. Beavers and T. A. Bubenik, "Stress corrosion cracking," in Trends in Oil and Gas Corrosion Research and Technologies: Production and Transmission, Elsevier Inc., 2017, pp. 295–314. https://doi.org/10.1016/B978-0-08-101105-8.00012-7

[10] J. Zhao, Weixing Chen, M. Yu, K. Chevil, R. Eadie, G. Van Boven, R. Kania, J. Been & S. Keane, "Crack growth modeling and life prediction of pipeline steels exposed to near-neutral

pH environments: dissolution crack growth and occurrence of crack dormancy in stage I," Metall Mater Trans A Phys Metall Mater Sci, vol. 48, no. 4, pp. 1629–1640, Apr. 2017, https://doi.org/10.1007/s11661-016-3951-3

[11] P. Malmqvist, "Monitoring of crack growth and crack mouth opening displacement in compact tension specimens at high temperatures Development and implementation of the Direct Current Potential Drop (DCPD) method."

[12] Y. Song, P. Yang, T. Xia, Z. Peng, and J. Zhang, "The crack growth rate and crack opening displacement of EH-36 steel under low-cycle fatigue loading," Ocean Engineering, vol. 280, Jul. 2023, https://doi.org/10.1016/j.oceaneng.2023.114734

[13] N. WALKER and C. J. BEEVERS, "A fatigue crack closure mechanism in titanium," Fatigue Fract Eng Mater Struct, vol. 1, no. 1, pp. 135–148, 1979, https://doi.org/10.1111/j.1460-2695.1979.tb00372.x

[14] S. Hu, Z. Mi, and J. Lu, "Effect of crack-depth ratio on double-K fracture parameter of reinforced concrete," in Applied Mechanics and Materials, 2012, pp. 937–941. https://doi.org/10.4028/www.scientific.net/AMM.226-228.937

[15] E. Entezari, J. L. Velázquez, M.A. Mohtadi-Bonab, D. Rivas López, M. Alejandro Beltrán Zúñiga, R. Khatib Zadeh Davani, J. Szpunar, "Experimental observations of nucleation and crack growth paths of hydrogen-induced cracking in pipeline steel," Eng Fail Anal, vol. 154, Dec. 2023, https://doi.org/10.1016/j.engfailanal.2023.107650

[16] D. Birenis, Y. Ogawa, H. Matsunaga, O. Takakuwa. Yamabe, Prytz, A. Thøgersen, "Interpretation of hydrogen-assisted fatigue crack propagation in BCC iron based on dislocation

structure evolution around the crack wake," Acta Mater, vol. 156, pp. 245–253, Sep. 2018, https://doi.org/10.1016/j.actamat.2018.06.041

[17] J. B. Wiskel, J. Ma, J. Valloton, D. G. Ivey, and H. Henein, "Strain aging on the yield strength to tensile strength ratio of UOE pipe," Materials Science and Technology (United Kingdom), vol. 33, no. 11, pp. 1319–1332, Jul. 2017, https://doi.org/10.1080/02670836.2017.1288776

[18] A. Smirnov, E. Smirnova, and S. Alexandrov, "A new experimental method for determining the thickness of thin surface layers of intensive plastic deformation using electron backscatter diffraction data," Symmetry (Basel), vol. 12, no. 4, Apr. 2020, https://doi.org/10.3390/SYM12040677

[19] Y. Ogawa*, D. Birenis , H. Matsunaga, A. Thøgersen, O. Takakuwa , J. Yamabe*, "Multi-scale observation of hydrogen-induced, localized plastic deformation in fatigue-crack propagation in a pure iron," Scr Mater, vol. 140, pp. 13–17, Nov. 2017, https://doi.org/10.1016/j.scriptamat.2017.06.037

[20] S. Nafisi, M. Arafin, R. Glodowski, L. Collins, and J. Szpunar, "Impact of vanadium addition on API X100 steel," ISIJ International, vol. 54, no. 10, pp. 2404–2410, 2014, https://doi.org/10.2355/isijinternational.54.2404.

[21] A. Laureys, M. Pinson, T. Depover, R. Petrov, and K. Verbeken, "EBSD characterization of hydrogen induced blisters and internal cracks in TRIP-assisted steel," Mater Charact, vol. 159, Jan. 2020, https://doi.org/10.1016/j.matchar.2019.110029.

Chapter 4 Stress Distribution Analysis via Digital Image Correlation (DIC)

4. 1 Introduction

A DIC algorithm calculates displacement and strain by comparing a series of grey-scale images of a sample at various stages of deformation, tracking pixel movement in the Region of Interest (ROI), and using a correlation algorithm [1- 4]. First, a discrete function describes the grey level of each pixel in the image, and then a correlation is calculated for each pattern. Figure 4-1 shows how a discrete function representing the sample before distortion is transformed into another discrete function after distortion, which gives the displacement of the grey spots. This principle states that the displacement of the spots accurately represents specimen deformation and strain [1], [3], [4].

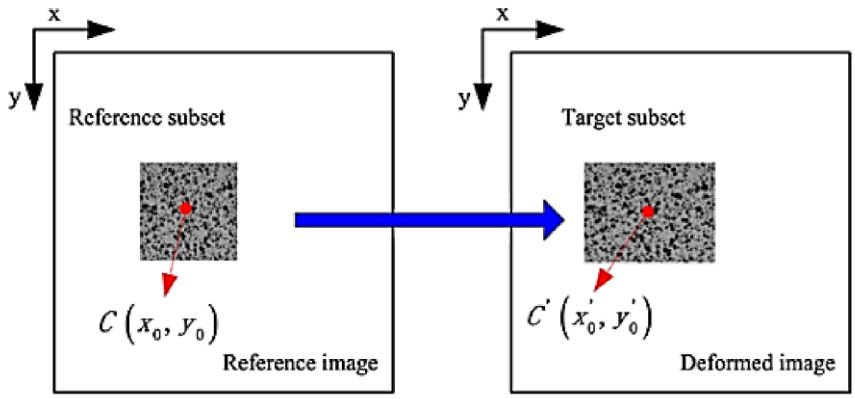

Figure 4-1 Discrete functions of C and C' showing the undeformed and deformed states of the surface post-processing of the data [2]

4. 2 Calibration method

Figure 4-2 illustrates a long sample's external surface strain map containing three 20-degree bent gauge lengths (two sides are inward, and the centre one is outward). What is required for this study

is finding stress levels at different points of interest related to the corrosion fatigue mechanisms. Therefore, the calibration method should be defined here to ensure the result of stress acquired from the mentioned procedure. To achieve this goal, the Region of Interest (ROI) should be found far from any source of plastic deformation, like edges, holes, and bent areas. Therefore, the best ROI could be in the grip region far from the central hole and edges. Based on the DIC report, the strain of the selected ROI in Figure 4-2 is 0.000393. Since the grip region is just under 50 % SMYS load, elastic modules of steel (about 210 GPa) gave us a stress value of around 82 MPa.

On the other hand, based on the grip region size (45 mm × 9.2 mm) and load applied to the sample (32.6 kN equivalent to 50% SMYS of API 5L X52 pipeline steel), the stress value was calculated around 84 MPa. As a result, this method seems to be considered a calibrated way to find stress distribution in a bent sample under the influence of two main axial sources of stress: residual stress from bending and axial loading tensile stress. This minor difference could be explained by the fact that the DIC experimental technique used for this long sample analysis provides a method with this level of accuracy. Plastic deformation sources at the selected ROI may also be responsible for these small errors.

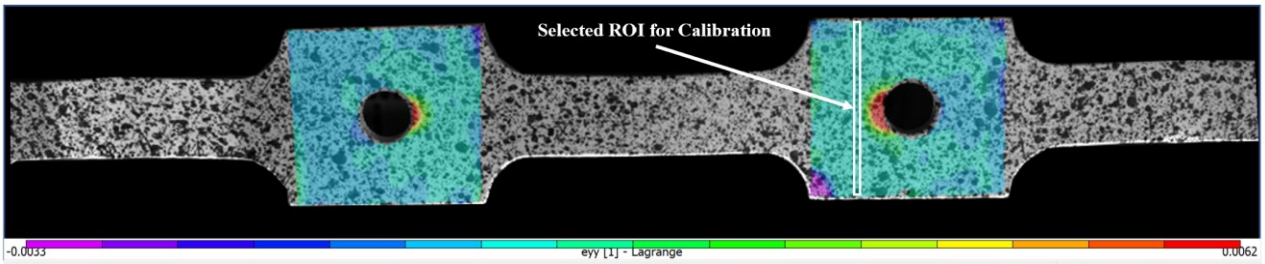

Figure 4-2 Digital image correlation (DIC) calibration method

4. 3 Stress distribution analysis

The accumulated stresses from residual bending stresses and axial cyclic stresses were comprehensively analyzed to investigate C-NNpH-CF crack growth. On the bend centerline,

inward direction bends are under maximum tensile stress (positive strain) based on Figure 4-3a. Tensile stress decreases as one moves away from the bend centerline. Similarly, the outward bend centerline is aggressively affected by maximum compressive stress (negative strain), and this decreases with distance away from the bend centerline. Comparing Figures 4-3a and 4-3b illustrates the changes in stress distribution as the final strain/ stress at 20-degree bending samples exceeds 10 degrees. Figures 4-3c and 4-3d show the strain changes in the inward and outward directions of the bend centerline over time. The DIC method uses a high-resolution camera to take a picture in each 100N increment and compare speckle patterns as loading time increases. The horizontal axis displays the number of photographs taken from zero to 50% SMYS (32.8 kN). The test started without any stress or strain in either direction. Increasing load, however, results in two different trends. Stress/strain in the inward direction goes into tension, while stress/strain in the outward direction goes into compression. As mentioned before, the inward direction is influenced by two sources of tensile stress: residual stress from bending (after the spring-back effect) and applied loading. In the field, when the pipe is not allowed to spring back (as in roping), the axial strain on the convex side of the bend is equal to $D/2\rho$, where D is the pipe diameter, and ρ is the bend radius [5]. However, as a result of the pipe springing back, the convex side will come into compression, and the concave side will turn into tension, as this investigation has confirmed. The same scenario applies to the outward direction. It should be noted that the final stress increases in both the inward and outward directions since both sources of stress are the same from a type of perspective (inward is under tension, and outward is under compression from two sources (bending and axial cyclic loading)). Due to the different bending angles, the rate of change in the 20-degree bending sample (Figure 4-3c) is greater than that in the 10-degree bending sample (Figure 4-3d).

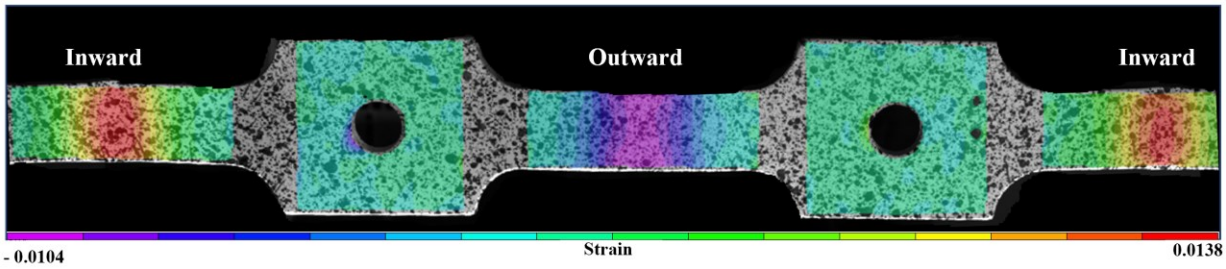

(a)

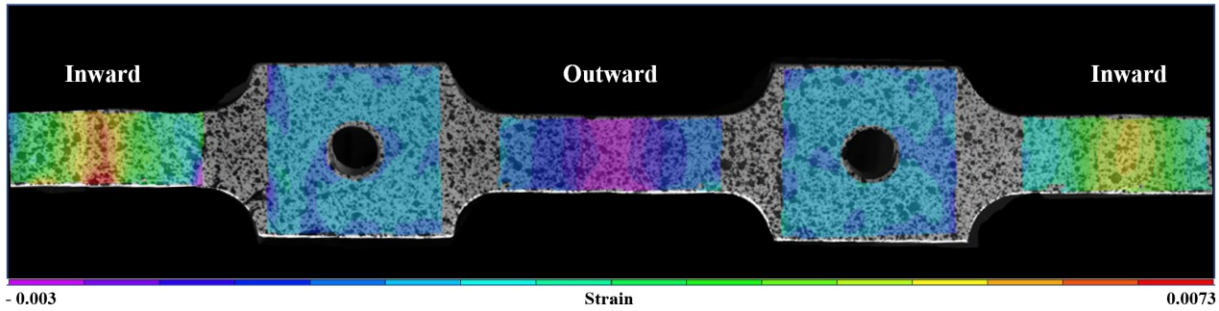

(b)

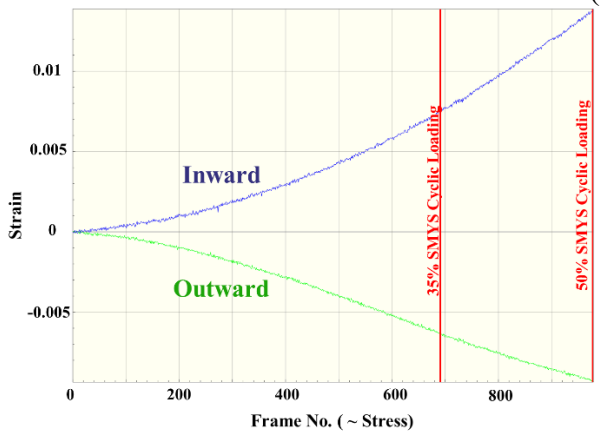

(c)

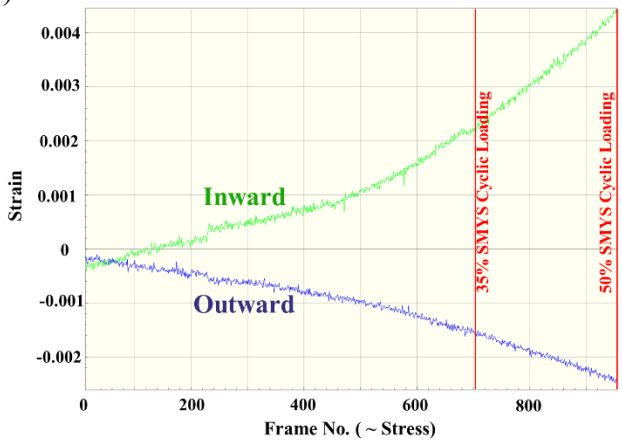

(d)

Figure 4-3 Digital image correlation pattern of the bent section under the influence of (a) 20-degree, and (b) 10-degree bending, Strain value during increasing stress (0-50% SMYS) for (c) 20-degree, and (d) 10-degree bending

References:

[1] K. Manthiramoorthy and A. Krishnaveni, “Fracture Parameter Evaluation Using Digital Image Correlation Technique,” International Journal of Engineering Technology Science and Research, Volume 4, Issue 11, 2017.

[2] B. Tasdemir and B. Taşdemir, “Determination of stress intensity factor using digital image correlation method,” Matter, vol. 2, no. 1, 2015.

[3] R. B. Á. Pradas Cristina, “Stress and strain analysis of a material with Digital Image Correlation method (DIC),” Western Norway University of Applied Sciences, 2020.

[4] L. Shi, X. Zhang, L. Zhang, C. Wang, and J. Wang, “Application of digital image correlation technique in stress and strain measurement. 15th Asia Pacific Conference for Non-Destructive Testing (APCNDT2017), Singapore.

[5] R. R. S. M. Fessler, "Characteristics, cause, and management of circumferential stress-corrosion cracking," in International Pipeline Conference, ASME (IPC Conference), 2014.

Chapter 5 Pipeline Circumferential Cracking in NNpH Environment Under the Influence of Residual Stress, Part I: Dormancy and Crack Initiation[1]

5. 1 Introduction

Circumferential Near-Neutral pH Corrosion Fatigue (C-NNpH-CF), which is a form of environmentally assisted cracking (EAC), could negatively affect the integrity and safety of pipelines transporting hazardous substances [1]. Cathodic protection and protective coatings are employed for pipeline integrity maintenance to protect the pipe from corrosion caused by soil environments. Although these protective measures are in place, damage to coatings and corrosion cannot entirely be totally avoided, so a minimal amount of crack initiation in a narrow area within the disbonded coating where groundwater is trapped is almost inevitable in large pipelines [2], [3]. This type of external pipeline failure involves the interaction of susceptible pipeline steel in contact with near-neutral pH ground water penetrating the disbonded coating under axial residual and cyclic stresses [4], [5], [6]. The environment responsible for this form of transgranular cracking in the NN pH environment is a dilute carbonic acid solution (pH between 5.5 and 7.5) that forms when CO_2 from decaying organic matter in the soil dissolves in groundwater, providing the necessary conditions for pipe external surface corrosion [1], [7], [8].

[1] A version of this chapter has been submitted: H. Shirazi, Sh. Wang, L, R. Eadie, W. Chen, "Pipeline Circumferential Cracking in NNpH Environment Under the Influence of Residual Stress: Dormancy and Crack Initiation"

It should be noted that crack initiation and propagation mechanisms are thought to be different in NNpH environments [7]. While EAC in near-neutral pH solutions is typically referred to as Near Neutral pH Stress Corrosion Cracking (NNpHSCC), a number of studies [4], [9] have indicated that normal crack growth rates, especially in oil pipelines under monotonic tensile stress, are not high enough to cause concern even when the stress intensity factor (K) is considerable. In other words, significant crack growth has never been observed under static loading conditions except for very low rates in the initiation stage, whereas crack propagation requires cyclic loading [6], [7]. As a result, cyclic loading due to pipeline internal pressure fluctuations [4] and diffusible hydrogen (a by-product of corrosion) [9] are responsible for the corrosion fatigue mechanism of crack growth. The term Near-neutral pH Corrosion Fatigue (NNpH-CF) will be used hereafter to refer to what has been often previously referred to as NNpHSCC.

It is expected that cracks will be perpendicular to the maximum combined tensile stress, including internal pressures, axial stresses, residual stresses from pipe manufacturing and construction, as well as residual stresses from in-service damage [10]. Axial cracking has become a serious and well-known threat to pipeline systems within the past decade [11]. However, external cracking may occur at orientations other than axial, depending on the nature of stresses in the NNpH environment [11]. In fact, when the total axial stress exceeds the total hoop stress, a gas or liquid pipeline can occasionally experience circumferential near-neutral pH corrosion fatigue, causing or contributing to failures [8], [12], [13]. Many hazards and risks are assessed for and mitigated against axial cracks, but circumferential cracks are less well understood, and monitoring and mitigation methods are unclear [13], [14].

The stress caused by internal pressure does not affect circumferential cracks as much as axially oriented cracks [15] at least not in straight pipe sections. Nevertheless, the combination of axial

cyclic stress from pipeline internal pressure fluctuations and other sources of axial stresses can reach a significant value to make the external surface of a pipe susceptible to circumferential crack initiation and propagation in NNpH environments [8]. The following are some potential sources of axial stress [4], [8], [12], [13], [16], [17] [18], [19]:

- Hydrodynamic stress at bends,
- Residual stress: thermal expansion, girth weld, pipe manufacturing and pipeline construction like cold bend,
- Axial stress from internal pressure,
- Axial stress from geohazards: soil movement and settlement, freezing and thawing of soil, permafrost, road/ water crossings,
- Bourdon effect on pipe bends.

Corrosion fatigue of pipeline steels in the near neutral pH environment is often modelled to occur in five stages: stage 0 (incubation stage involving coating deterioration and failure), stage Ia (crack initiation), stage Ib (early-stage crack growth), stage II (sustainable crack growth induced by mechanical driving forces), and stage III (rapid crack propagation to rupture). Note that the sequence has been adopted to maintain the early historical numbering first introduced by R. Parkins. An important part of the pipeline's lifecycle is in stage Ib, this stage is crucial to pipeline integrity management [2], [6], [20]. External corrosion can be caused by various mechanisms, including preferential dissolution at physical or metallurgical discontinuities like scratches, corrosion in stress raisers like pits, and galvanic corrosion related to microstructure or residual stresses. However, there is a decrease in dissolution rate as crack depth increases. This causes most initiated Stage Ia crack-like features to cease growing when they reach a depth of about 1 mm and enter the dormant stage [1], [5], [6], [8]. The majority of cracks in NNpH-CF colonies remain

dormant, and only an estimated five percent can grow deeper [5], [6], [8]. Indeed, reactivating a dormant crack requires certain location-specific conditions. Residual stresses near the crack tip and diffusible hydrogen could determine whether cracks are dormant or reactivated. In other words, it is possible for blunted cracks to be resharpened by the synergistic interaction of cyclic loading and hydrogen-related processes. Wherever these two conditions are met simultaneously, the probability of initiation from a dormant crack is higher [8], [3].

While stress is a crucial parameter for this cracking mechanism, limited research has been dedicated to defining the role of stress type and value in dormancy and crack initiation at the notch (dormant crack) root. This is particularly relevant in cases with a stress gradient in the thickness direction, resulting from specific sources such as bending. This circumferential cracking can be considered a unique mechanism because the stress gradient in the thickness direction, along with other factors like initial notch depth (which influences stress concentration), dictates the cracking mechanism. This stands in contrast to a straight, smooth surface without any sources of in-thickness residual stress distribution.

This paper aims to investigate the stress distributions (derived from the digital image correlation (DIC) method) in the length and depth directions of pipelines under the simultaneous influence of bending residual stress (an appropriate source of residual axial stress) and cyclic loading (simulated pipeline pressure fluctuation). Following this, how stress distribution and depth of the initial dormant notch affect crack initiation will be addressed. The threshold condition for crack initiation will be determined by considering various types and amounts of residual stress and their interactions with axial cyclic loading. A deeper understanding of this mechanism may improve knowledge of Circumferential Near-Neutral pH Corrosion Fatigue (C-NNpH-CF), which plays an important role in pipeline integrity management.

5. 2 Material and experimental methods

This section provides a comprehensive overview of sample preparation and parameter design procedures to rationalize correlations between laboratory experiments and real circumferential near-neutral pH corrosion fatigue (C-NNpH-CF).

5. 2. 1 Material Characterization

The material used in this study was a 16" API-5L Gr. X52 with a wall thickness of 9.2 mm removed from a pipeline with a history of near-neutral pH CF cracking. The chemical composition of this pipe is given in Table 3-1 (chapter 3). Based on the literature review of this study, some information on the presence of C-NNpH-CF in pipelines and conditions for initiation and growth has been obtained by inspecting some pipes removed from slopes [11], [17]. In most of these inspections, C-NNpH-CF happens close to the area where bending is an issue. As bending could be an appropriate source of residual axial stresses causing C-NNpH-CF in the field [13], [14], [15], [21], in this study, bending is considered a significant source of axial residual stresses in the pipe. The actual tensile properties of the pipeline steels used for this study were determined in accordance with ASTM Standard E8 using 9.2 mm thick rectangular sheet-type samples and a crosshead speed of 0.015 mm/mm/min. The test was performed using an INSTRON 8516 machine. Figure 3-1 (chapter 3) shows the result of the tension test. This pipe's yield stress (at 0.2 % offset strain) and ultimate tensile stress were 356 MPa and 561 MPa, respectively.

5. 2. 2 Specimen and cell Preparation

The long samples are machined with the long tensile axis along the axial pipe direction of this pipe using electrical discharge machining (EDM). Figure 3-2 (chapter 3) shows the design and dimensions of the samples.

Three separate reduced gauge sections measuring 80 mm × 20 mm × 9.2 mm with artificial through-thickness notches are explicitly designed to maximize the evaluated parameters. These three specified reduced-width areas in a long sample were bent at different degrees. It should be noted that the samples' inner and outer surfaces must remain intact. Because cold working like machining can change the profile of residual stress distribution, the original curved surfaces were kept before bending.

Residual stress has a self-equilibrating feature, meaning that from Newton's second law, the net force on an object at rest must be zero, so the sum of forces in any cross-section must be zero. As a result, if there is tensile residual stress on the outer surface of the pipeline in contact with the corrosive environment, the inner surface contains equivalent net compressive residual stresses and *vice versa*. Also, different bending angles could make various residual stress changes. Two bending angles of 10 and 20 degrees were designed to simulate cold bending in the field. For instance, Figure 3-3 (chapter 3) illustrates a 20-degree bent pipe (each side is 10 degrees). This figure emphasizes that there are two different kinds of bending regarding the outer surface of the pipeline called inward and outward samples in this study. This feature simulates what happens to an actual bent pipe in the field since any bending that happens to a pipe because of slope or other reasons causes two recognizable bending directions regarding the outer surface of pipes. The distributions of residual stresses in these two conditions are more or less opposites, which will be discussed later.

Cold bending, as one of the causes of this type of cracking (because of pipeline construction or in-service damages related to geohazards, soil moving, *etc.*), creates axial stress in the whole bent area of the pipe which could be added to the cyclic loading from pressure fluctuation results in this type of cracking. It should be noted that there are two different conditions for a bent pipe. Figures

5-1 and 5-2 show the residual stress distribution in a bent section with and without spring back (y is the distance from the bending center on the pipe). As shown in Fig. 5-1, if the pipe is not allowed to spring back, the axial strain would be D/2ρ on the convex side of the bend, where ρ is the bend radius, and D is the pipe diameter. Allowing the pipe to spring back by removing the applied loads would alter the residual stress pattern, with the convex side going into compression and the concave side going into tension [17]. As residual stress self-equilibrates, there is high tensile stress at the concave side to balance the high compressive stress at the convex side. It is possible to approach a material's yield strength when adding this bending axial stress to other sources of stress [8], [17].

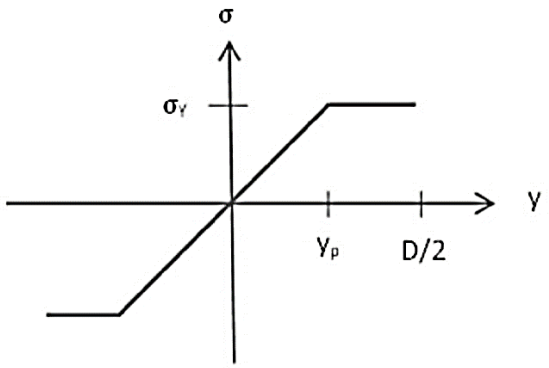

Figure 5-1 Stress profile from the concave to the convex side for the original bend [17]

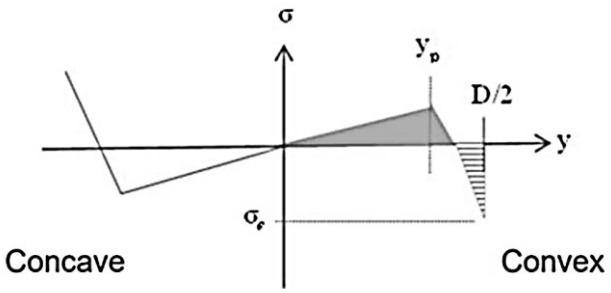

Figure 5-2 Stress distribution after the original bend is allowed to spring back [17]

Another source of axial stress is caused by pressure fluctuation in pipeline steel. Although internal pressure is the source of hoop stress in the pipeline, which expands the pipe circumference, this stress from internal pressure also pushes on the pipe ends and creates axial stress in the pipeline, as a pressurized pipeline transporting fluids usually has ends to press against. Typically, axial stress is about half as high as hoop stress [8], [22]. It is crucial to note that Bourdon and hydrodynamic stresses complicate what would happen in the field where a pipe bend is internally pressurized [8]. The influence of these sources of axial stress on C-NNpH-CF crack initiation and growth should be explored in future research through more experiments and simulations.

According to the research done by J. Beavers *et al*. [10], pipelines operating at stress levels above 60% of the specified minimum yield strength (SMYS) are more susceptible to near-neutral pH corrosion fatigue for longitudinal cracking. Therefore, 35% SMYS (approximately half of the hoop stress) and 50% SMYS (under the condition that some additional cyclic stresses could be added to the hoop stress) were considered for this study. Apart from that, this cyclic axial stress behaves differently in the inward and outward bending directions of the bent pipe, supposing no residual stress from the bend (or the bent section was heat treated and completely stress relieved). To clarify, the axial loading will make tensile stress on the concave side and compressive stress on the convex side of the bend. It would be similar to the residual stress distribution in a bent sample after spring back (without axial loading).

The initial crack/notch depth is another parameter to consider since the residual stress distribution close to the crack tip must be evaluated. An initial 1 mm depth notch was selected since many cracks stop growing after reaching a crack depth of 1 mm; at this point, they enter a state of dormancy [6]. This observation is based on dormant cracks formed in straight pipes, so further investigation is needed for circumferential cracks formed in pipe bends. In addition, an initial notch

with a 0.5 mm depth was added to the study to investigate the effects of initial notch depth on crack initiation. By increasing the initial notch depth to more than 1 mm, the stress intensity factor increases enormously, outside the scope of crack initiation. Therefore, the next step is to make artificial notches on each long sample's bent parts. Figure 3-4 (chapter 3) shows the position of the through-thickness notches on long samples (where X is the number of long samples, and 1-8 is the location of the notches on the long samples). The distance between notches is 20 mm (far enough from each other to inhibit the interaction of crack tip plastic zones close to the crack tip). A milling machine was employed to cut notches with a small width (about 0.2 mm) and various depths, as illustrated in Figure 3-4 (chapter 3). This method provided rectangular-shaped notches to make stress concentrators at two corners. This would make controlling and evaluating crack initiation and growth at those corners easier.

Furthermore, a specific cell (Figure 3-5 (chapter 3)) was designed as a container for C2 solution (synthetic field soil aqueous solution with a pH value of 6.3), which exhibits the greatest corrosion cracking potential, including 0.0274 gr. of $MgSO_4.7H_2O$, 0.034 gr. of $CaCl_2.2H_2O$, 0.0035 gr. of KCl, 0.0195 gr. of $NaHCO_3$ and 0.0606 gr. of $CaCO_3$ in each litre of deionized water) and the solution was sparged with a gas comprised of 5% CO_2 and 95 % N_2. The final pH of the solution was 6.3 ± 0.1, which is consistent with a near-neutral pH environment. Figure 3-5 shows how this particular cell is designed and how a long sample is placed therein. After transferring a long sample to the cell containing C2 solution and before starting cyclic loading, gas sparging with the rate of 1 bubble/second was performed for 12 days in a temperature-controlled laboratory (22°C) to introduce the NNpH environment to the samples (the resulting corrosion leads to hydrogen diffusion into the sample).

5. 2. 3 C-NNpH-CF testing conditions

This 12-day static corrosion test was followed by a C-NNpH-CF test (cyclic loading) with different axial loads, a frequency of 0.001 Hz and a stress ratio (Min stress/Max stress) of 0.1 on an Instron 8516 servo-hydraulic testing machine controlled with Wavemaker Runtime software. Since the stress was offset from the bending position, the applied stress was increased at bends by the bending moment. The test was conducted for 45 days unless a long sample failed during the test. Throughout the entire test, CO_2 was continuously sparged through the solution. According to the reasons that were provided in the previous sections, Table 3-2 shows the test plan to evaluate the effect of the mentioned parameters on the crack initiation mechanism.

Two-digit numbers were used to identify the notches. According to Figure 3-4, the first number indicates the long sample from which the notch originated, while the second number indicates the location of the notch on the long sample (1, 2, 6- 8: inward bending direction, 3-5: outward bending direction). As a complementary test to long sample No. 1, long sample No. 2 was tested to evaluate the consistency of the data acquired. Two additional experiments were conducted on the non-bent sections having 0.5 mm and 1 mm initial notches, subjected to cyclic loading at 35% and 50% SMYS. The purpose of these tests was to evaluate the effect of cyclic loading on reference samples without any other sources of axial stress, such as axial bending stress. All other testing parameters (environment, cyclic loading pattern, *etc.*) were the same as in the previous test on long samples 1 to 8. For simplicity, these notches were designated as follows: A1 (0.5 mm, 35%), A2 (1 mm, 35%), B1 (0.5 mm, step 1: 35% for 45 days, step 2: 50% for 45 days), and B2 (1 mm, step 1: 35% for 45 days, step 2: 50% for 45 days).

5. 2. 4 Post-test Analysis

Upon completion of each test (45 days duration or fracture, whichever happened first), the long sample was rinsed with acetone and dried with hot air to prevent corrosion of the fracture surface, which might occur with water. Next, a precision saw fitted with a diamond-coated wafer blade capable of cutting widths of 0.2 mm was used to cut each unfailed notch into two samples (one half for cross-section analysis and the other half for fractography analysis) to characterize the depth profile of cracks and fractographic morphology.

The first half of each sample was ground to a 1200-grit finish and polished to a mirror finish using 6 μm and 1 μm diamond oil slurry and etched for 5 to 10 seconds using 5 % nital to characterize the crack location, depth, and morphology (cross-section characterization). The other half of each notch was fractured to investigate fractography morphology and crack growth behaviour. The samples were placed in liquid nitrogen for up to four hours, removed, and fractured open by striking the backside notch with a cold chisel. As recommended in ASTM Standard G1-03, the fracture surface was dipped in a solution containing 6N HCl + 3.5 g/L hexamethylene tetramine to remove corrosion products. The fracture surface and cross-sections were imaged using a Zeiss Sigma 300-VP FESEM. A crack growth rate was calculated by dividing the measured crack growth depth by the number of cycles.

5. 2. 5 Stress distribution analysis via Digital Image Correlation (DIC) and the calibration method

Using digital image correlation (DIC), strains are measured through a non-contact procedure from images of a sample under tension in 2D or 3D. This technique can be applied to various materials research and component testing applications to analyze specimen static and dynamic behaviour.

In many cases, strain gauges are replaced by DIC strain maps [23]–[26]. Chapter 4 provides further details on digital image correlation (DIC) and the calibration method.

5. 3 Results

5. 3. 1 Stress distribution analysis based on the DIC method

To determine the stress distribution in the external surface and thickness direction of the bent gauge area from all sources of stresses, two long samples bent at 10 degrees and 20 degrees were loaded to 35% SMYS and 50 % SMYS to develop the strain map in gauge length using the digital image correlation (DIC) method. This method was employed on long samples without notches to simplify the effect of axial stresses on circumferential cracking. However, it is obvious that the presence of notches gives more precise data, which could be the subject of further research.

Figure 5-3a illustrates the final strain distribution in three bent gauges (the center one is in the outward bending direction, and the left and right ones are in the inward bending direction) and two grip regions, which make a distance between the bent gauges. Different regions on this graph show the level of strain: inward bent centrelines have the maximum tensile strain (maximum level of positive strain), though the center of outward bending direction at the middle-bent gauge has the maximum negative/ compressive strain. Also, it could be seen that strain decreases with distance from the bend centerline. Finally, grip regions show the strain/ stress distribution based on the cross-section area under loading.

Figure 5-3b shows an in-thickness directional strain map for the bent grip with an inward bend. Type I residual stresses, which vary continuously over at least several grain diameters, must be self-equilibrated such that they sum to zero in any direction over the total cross-section. Because they sum to zero over the cross-section, it is expected that the highest compressive residual stress gradient in the depth direction accompanies the highest tensile residual stresses on the other side

of the bend [3], [27]. This feature is shown in Figure 5-3b, where the highest tensile strain/stress distribution in an inward 20-degree bending gauge length on the external surface is accompanied by the highest negative strain/stress on the internal surface. Since the thickness of bent samples is the same, maximum stress on the sample results in maximum stress reduction in the thickness direction, too.

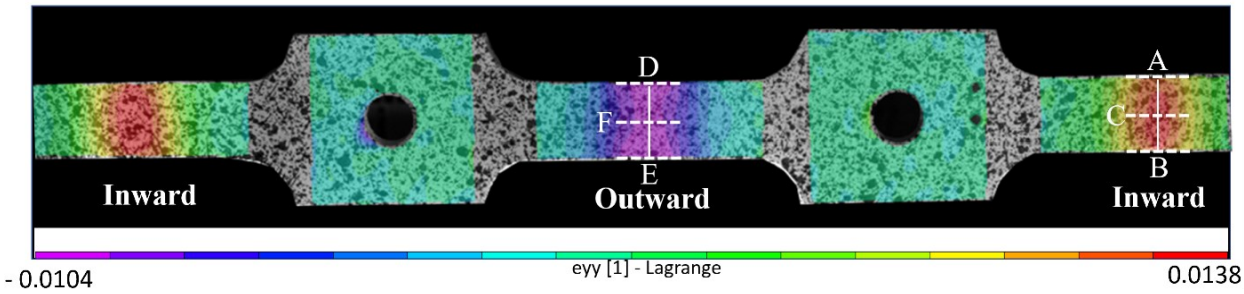

(a)

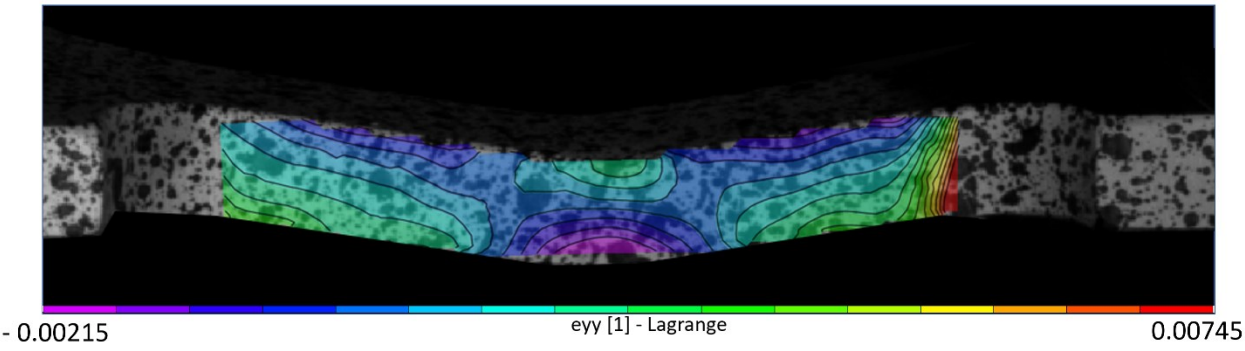

(b)

Figure 5-3 (a) Strain distribution on the long sample external surface under 50% SMYS cyclic loading (20-degree bending), (b) Strain distribution in the thickness direction (inward bending direction: external surface in tension, Internal surface in compression)

- **Level and nature of final tensile stresses in the inward bending direction under the influence of bending and applied stresses**

Figure 5-4a presents the normal stress distribution along the bend centerline (between -20 mm and +20 mm of the bend centerline) at the surface and the notch root (0.5 mm far from the external surface) of long sample No.6 (20-degree bending, 50% SMYS, 0.5 mm initial notch depth). The stress level at the position of the notch root is less than the external surface because of the stress

self-equilibrium feature. It should be mentioned that as a result of the stress magnification of the notch, the actual stress at the notch root is a totally different matter. An additional study examined the effects of maximum cyclic loading on stress distribution and crack growth. Figure 5-4b shows the final stress distributions for different notches (combined residual stress from 10-degree bending and SMYS loading of 35% and 50%: Samples No. 03 and 05).

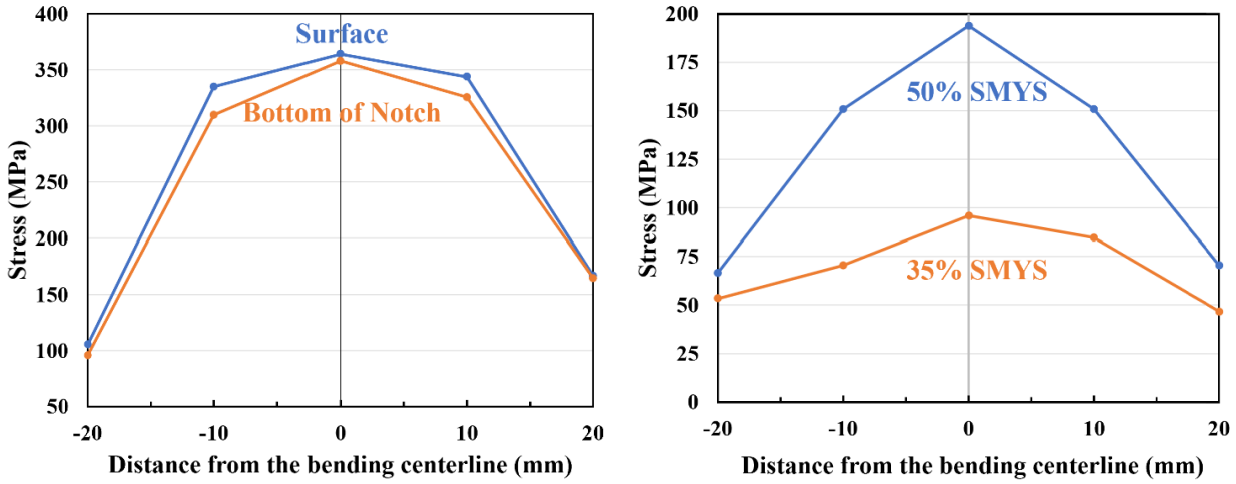

(a) (b)

Figure 5-4 (a) Stress level at the surface and bottom of pits in various initial notch positions (sample No.6: 20-degree bending, 50% SMYS, 0.5 mm initial notch depth), (b) Final stress distribution in 10-degree bending, 50% and 35% SMYS cyclic loading: (samples No. 03 and 05)

The graph in Figure 5-5 depicts stress distribution in the width direction (the width component of the bending stress vector) on the external surface of a 10-degree inward bending direction (line A-B in Figure 5-3a). According to standard ISO 7539-5, there is a stress gradient through the width of the gauge sample, varying from edges to the center, *i.e.*, in the inward bending direction, the tensile stress is lower at the edges than at the center [28]. It is consistent with the stress distribution shown in Figure 5-5 (10-degree bending, 50% SMYS, 0.5 mm initial notch depth), where the maximum stress level at the edges was 235 MPa compared to the 245 MPa at the center.

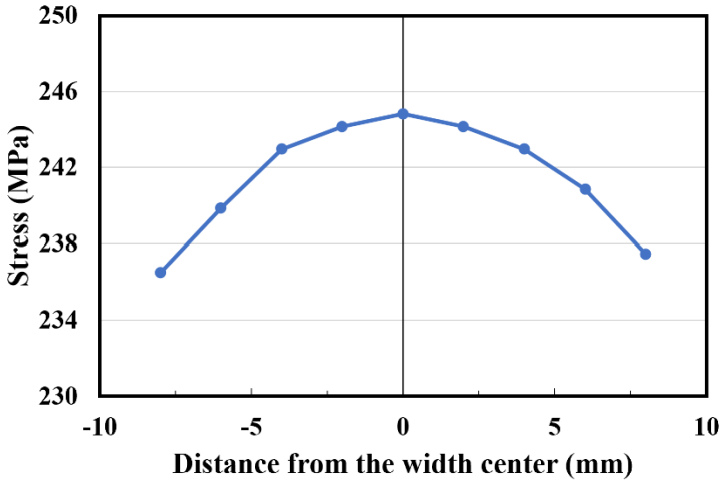

Figure 5-5 Normal stress distribution in the width direction: 10-degree bending, 50% SMYS, 0.5 mm initial notch depth (line A-B in Figure 5-3a)

- **Level and nature of the final stresses in outward/ non-bent sections**

The outward bending direction is affected by two sources of compressive residual stress, one from bending after spring back and the other from axial cyclic loading, as shown in Figure 5-3a's central section of the long sample. The applied axial loading induces a bending moment, a point worth noting due to the offset of the bend from the stress axis. It's essential to highlight that this bending moment reduces as the displacement from the stress axis decreases, particularly when moving away from the center of the bend. These stress distributions can be affected by other testing parameters, such as the bending angle. As an example, Figure 5-6 illustrates the stress distribution in the outward bending direction of long samples No. 6 and 7. In both graphs, compression stress was shown at different values depending on how far the initial notch was from the bend centerline. The bending residual stress generated by 20-degree bending and 10-degree bending is the reason for the huge difference between samples No. 6 and 7 stress distribution. Axial cyclic loading is 50% of SMYS for both mentioned samples.

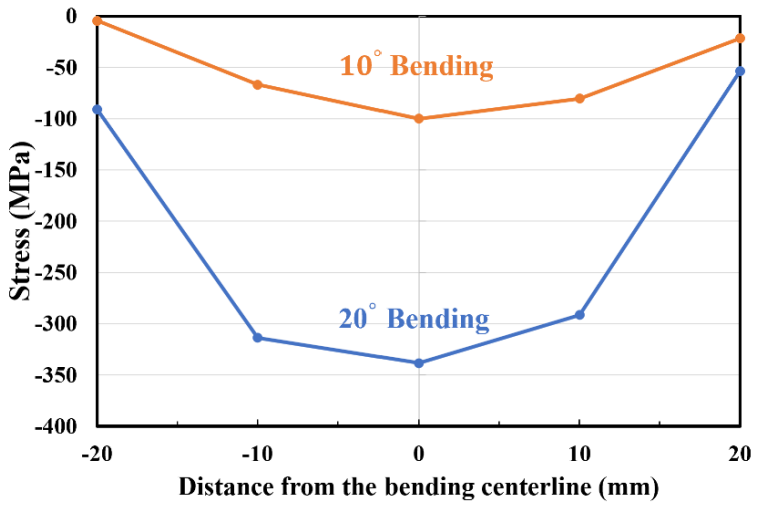

Figure 5-6 Compressive stress level in various initial notch positions under axial cyclic loading of 50% SMYS: (Sample No.6: outward direction/20-degree bending), and (Sample No.7: outward direction/10-degree bending)

Finally, the stress distributions were evaluated for the non-bent sections. These sections did not have any bending, which means the only source of stress was axial cyclic loading, which was a maximum of 50% SMYS (180 MPa), 35% SMYS (126 MPa) at the maximum tensile load, 5% SMYS and 3.5% SMYS at the minimum level, according to the ratio of minimum to maximum load of 0.1 in every corrosion fatigue test cycle.

5. 3. 2 Crack initiation at initial notches under tensile stresses

To examine crack initiation from notches, selected notches were sectioned. For instance, Figure 5-7 shows cross-section and fractography images of crack initiation from the bottom of the artificial notch (No. 61: 20-degree bending, 0.5 mm initial depth, 50% SMYS cyclic loading, 10 mm from bend centerline) at different magnifications. This study assumed that pitting happened at the first stage of the SCC/CF mechanism in the NNpH environment, and these artificial notches simulate the pits or dormant cracks.

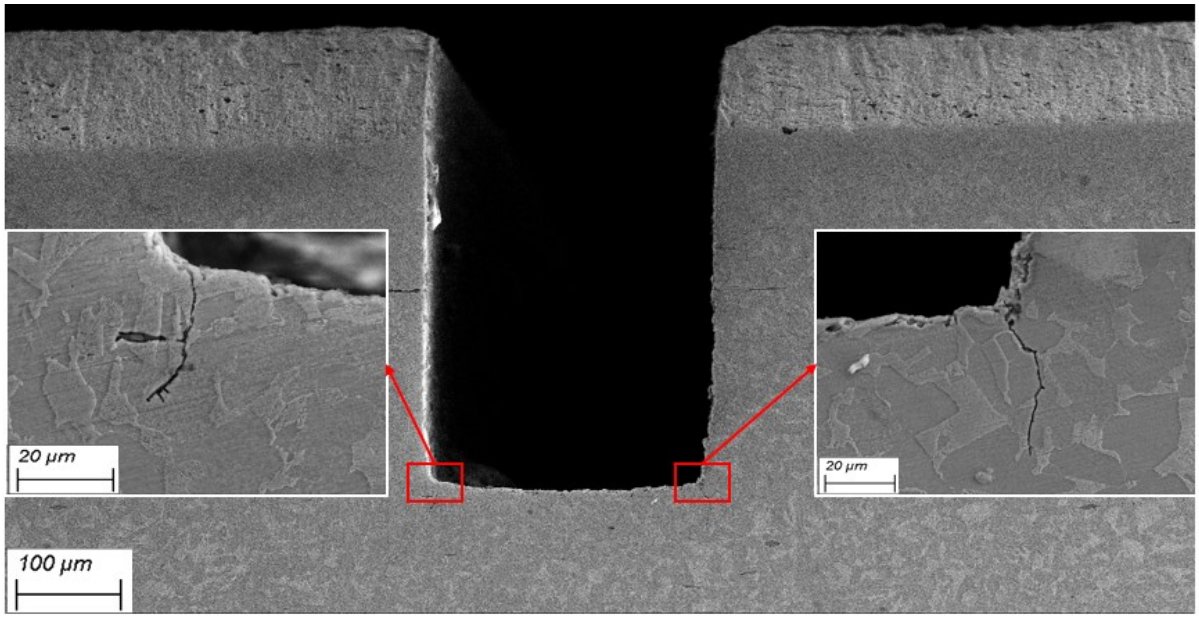

(a)

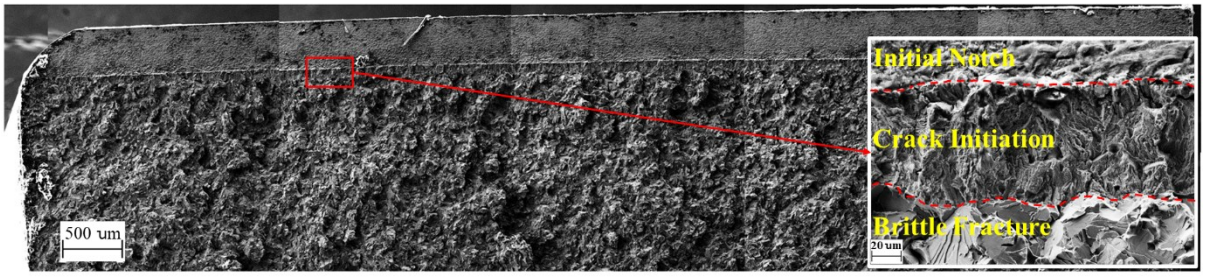

(b)

Figure 5-7 Crack initiation from the bottom of notch No. 61 (20-degree bending, 0.5 mm initial depth, 50% SMYS cyclic loading): (a) Cross-section of the initial notch, (b) Fractography images

As illustrated in Figure 5-7a, in the first stage, crack propagation occurred in a direction approximately 45° inclined to the main crack, the area with the highest shear stress, responsible for plastic deformation [20]. Since the stress intensity factor on the main crack plane is the highest, it is unlikely that the crack will propagate in a direction not perpendicular to the maximum principal stress. Branched cracks may be forced back to the main crack plane, leading to a "zig-zag" pattern on fractured surfaces [29].

The crack initiation was confirmed by fracture of the sample at the notch root site. According to the fractography morphology of notch No. 61 (Figure 5-7b), the fracture surface after placement of the sample in liquid nitrogen is divided into three regions: the initial notch region results from milling (upper part), crack initiation (middle part), and the final fracture regions. The middle part exhibits quasi-cleavage with areas of smooth brittle fracture and ductile dimples [30]. In the bottom part, a complete cleavage region is typical of brittle fracture in liquid nitrogen, similar to cleavage fractures in low-carbon steels under impact below the transition temperature [30].

Table 5-1 provides an overview of average crack growth derived from fractography images over the entire width, specifically in the inward bending direction with tensile residual stress. Consequently, the following section explores how these parameters influence crack initiation at the bottom of an initial notch. It is crucial to note that this study exclusively concentrates on crack initiation and its influencing factors. The analysis of long cracks, where fracture mechanics come into play, will be thoroughly addressed in Chapter 7 of this investigation. This study excludes the failed notches as well.

Table 5-1 The crack growth in various notches under the influence of different testing parameters (inward bending direction)

Long Samples No.	Inward bending angle (degree)	Initial notch depth(mm)	Max. applied stress (% SMYS)	Position (mm)	Notch No.	Net crack growth (mm)	Test duration (hour)
1	20	1.0	50	-10	11	0.95	208
				+10	12	0.5	208
				-20	16	0	208
				+20	18	0	208
2	20	1.0	50	-10	23	1.1	224
3	10	1.0	50	-10	31	0.25	848
				-20	36	0.2	848
				+20	38	0	848
4	20	1.0	35	-10	41	0.65	325
				+10	42	0.6	325
				-20	46	0.045	325
				+20	48	0	325
5	10	1.0	35	-10	51	0.015	1075
				+10	52	0.02	1075
				-20	56	0.008	1075
				+20	58	0.006	1075
				0	57	0.13	1075
6	20	0.5	50	-10	61	0.11	354
				+10	62	0.12	354
				-20	66	0	354
				+20	68	0	354
7	10	0.5	50	-10	71	0.075	997
				+10	72	0.08	997
				-20	76	0.04	997
				+20	78	0.04	997
				0	77	0.2	997
8	20	0.5	35	-10	81	0.2	1283
				+10	82	0.31	1283
				-20	86	0.04	1283
				+20	88	0.04	1283

- **Effect of stress on crack initiation**

Referring to Figure 5-4a (normal stress distribution along the bend centerline (within -20 mm and +20 mm of the bend centerline)), Figure 5-8 illustrates the crack depth observed at notches No. 61, 62, 66 and 68, which were located at -10, +10, -20 and +20 mm from the center in the gauge section with inward bending, respectively. The sample was tested under 50% SMYS for 354 hours/1274 cycles. Notches 61 and 62 (10 mm far from the bend centerline) have a crack depth of around 50 μm (at the edge), although notches 67 and 68 (20 mm from the bend centerline) show less than 10 μm crack depth. This correlation confirms the effect of stress on crack initiation, as more stress results in more crack depth.

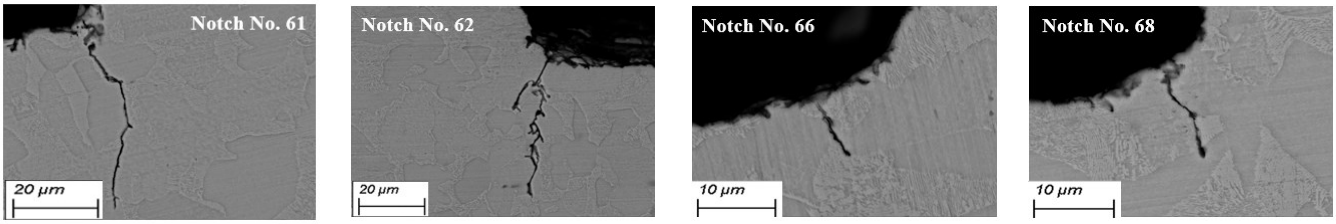

(a) (b) (c) (d)

Figure 5-8 (a) Crack depth in notch No. 61 (-10 mm), (b) Crack depth in notch No. 62 (+10 mm), (c) Crack depth in notch No. 66 (-20 mm), (d) Crack depth in notch No. 68 (+20 mm)

It is important to keep the bend angle and residual stress from bending constant throughout the experimental procedure in order to evaluate the effect of stress from cyclic loading on crack initiation. According to Figure 5-4b, the same 10-degree bend in sample number 3 with 50% SMYS produced a higher stress level than a 35% SMYS loading in sample number 5. Figures 5-9a and b illustrate crack depths caused by these various cyclic loadings (at the same location: -10 mm far from the bend centerline). As a result, the crack depths at the bottom of notch numbers 31 and 51 are 50 μm and 15 μm, respectively. It is consistent with the stress level at the bottom of the pits (notch number 31: 150 MPa, notch number 51: 70 MPa).

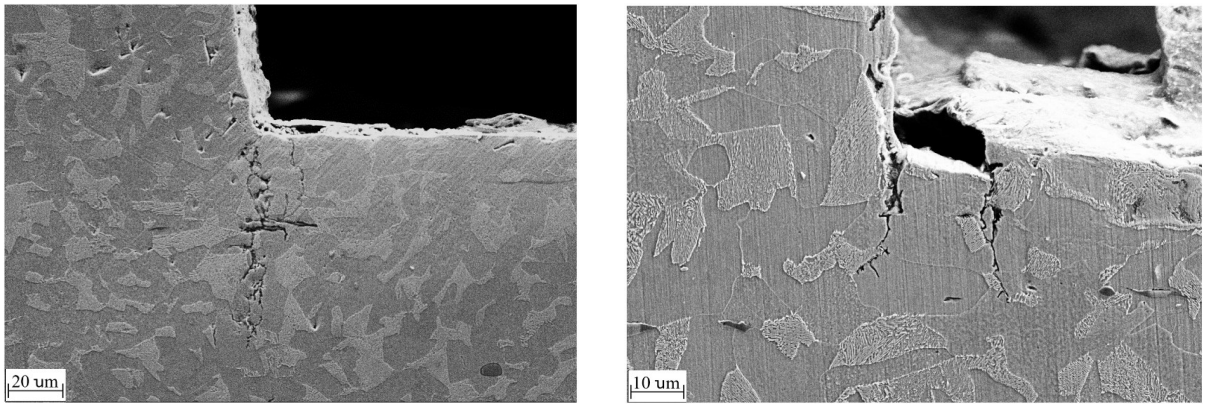

(a) (b)

Figure 5-9 a) Crack initiation in 50% SMYS cyclic loading, b) Crack initiation in 35% SMYS cyclic loading (other parameters kept constant: 10-degree bending, 1 mm initial depth, 10 mm from the bend centerline)

Figure 5-10 illustrates cross-sectional images of notches No. 31 and 71. Both notches are 10 mm from the 10-degree inward bend centerline with 50% SMYS, but initial notch depths for notch numbers 31 and 71 are 1 mm and 0.5 mm, respectively. The duration of both tests is almost the same. Notch No. 71 cross-section shows a crack growth of less than 10 μm, but the crack depth on notch number 31 cross-section is more than 75 μm, so it seems that the effect of crack initiation governed by the dissolution process is less significant than the effect of mechanical processes. However, it is important to note that stress can intensify the impact of dissolution, and this dissolution is more concentrated in the direction with the highest shear stress. The stress concentration factor provides more comprehensive data on crack initiation in the depth direction. Despite a decrease in stress level in the depth direction of a bend section, a higher depth increases the stress concentration factor. As a result, the maximum stress level at the bottom of the 1 mm initial notch is higher than the maximum stress level at the bottom of the 0.5 mm initial notch.

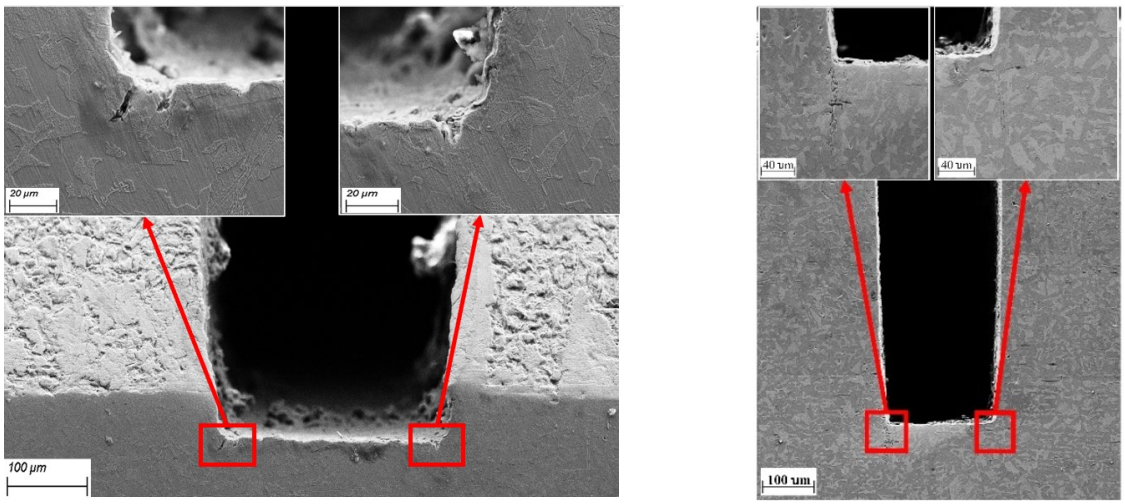

(a) (b)

Figure 5-10 Effect of initial notch depth on the crack initiation (a) Notch No. 71: 0.5 mm initial notch depth, (b) Notch No. 31: 1 mm initial notch depth (other parameters kept constant: 10-degree bending, 50% SMYS, 10 mm from the bend centerline)

- **Crack initiation along specimen width**

Notch 77, listed in Table 5-1 and illustrated in Figure 5-11, could be used to examine the crack initiation behaviour along the specimen width. The gauge section containing Notch 77 was bent by 10 degrees, and the stress distribution in the width direction is shown in Figure 5-5, from which the difference in stress between the edge surface and the mid-width is about 10 MPa. The cross-sectional images 5-11a and 5-11b show the bottom of notch No. 77, which contains the initiation of the crack (sampling location is defined in Figure 5-3a). The crack initiated from the notch root at the edge surface of the specimen is very short but remains relatively sharp, while the crack from the notch root located at the mid-width is long but has a wide crack crevice and blunt crack tip. The latter morphology is typical of a dormant crack often seen in near-neutral pH SCC cracks.

The different crack behaviour and morphologies observed at the edge surface, and the mid-width could be related to the magnitude of stresses in the material surrounding the notch root. Also, the edge surface is in plane stress where the material at the notch root is under biaxial loading and is subject to stress comparable to the yield strength, while the material at the notch root in mid-width

is in plane strain, and the stress in every direction could be as high as 3 times of yield strength because of the presence of triaxial stresses. This high triaxial stress can of course attract hydrogen. Consequently, the risk of initiating a crack from the notch root at mid-width is much higher. However, the triaxial stress zone surrounding the notch root exists over a limited distance to the notch root, leading to limited crack growth, probably within the triaxial zone. Further growth is prohibited because of the sharp reduction of stresses beyond the triaxial stress zone. Under the circumstances, corrosion is continuous on the crack walls and at the crack tip, which blunts the crack tip and increases crack crevice because of the non-passivating nature of near-neutral pH solutions. In contrast, crack initiation from the notch root at the edge surface is limited to a few grain sizes, a typical dimension of a microstructurally short crack. In near-neutral pH solutions, these microstructurally short cracks are formed along grain boundaries and at interfaces between pearlite colony and ferrite phases, which appears consistent with the observations shown in Figure 5-11b. Because of the narrow crack crevice found in Figure 5-11b, the initiation of microstructurally short cracks could occur at a much later testing time. According to this image, initiation occurs at both corners at first, but after a while, one corner grows faster than the other. Indeed, stress shielding prevents the other one from growing, which means crack growth consumes the stress in one corner and there is then not enough stress for the other one to grow.

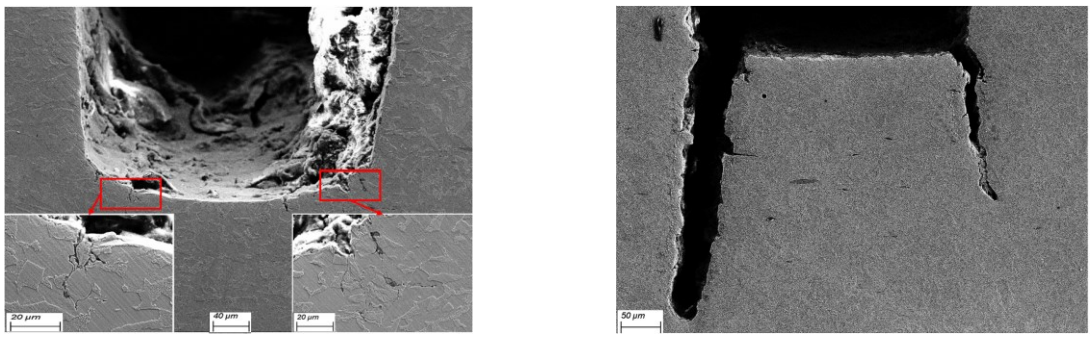

(a) (b)

Figure 5-11 Crack initiation at the edge and center of the width of notch No. 77 (10-degree bending, 50% SMYS, 0.5 mm initial notch depth), (a) Crack initiation at the edge: section A on Figure 5-3a (b) Crack initiation at the center of width: section C on Figure 5-3a

- **Crack initiation in different test durations**

Figure 5-12 illustrates crack depth versus the test duration in different notches with various parameters (notch No. 16: bending angle of 20 degrees, 50% SMYS loading, notch No. 36: bending angle of 10 degrees, 50% SMYS loading, notch No. 46: bending angle of 20 degrees, 35% SMYS loading) at the same location (inwards, 20 mm from the bend centerline). The test durations varied because these long samples (1, 2, 4) failed at different notches. As a matter of fact, these notches could experience a different number of cycles/times in the test. Section 4 will discuss how to consider all relevant factors simultaneously (initial notch depth, axial loading, and bending angle). Nevertheless, only three notches are shown in Figure 5-12 to explain the concept behind the effect of test duration on crack initiation.

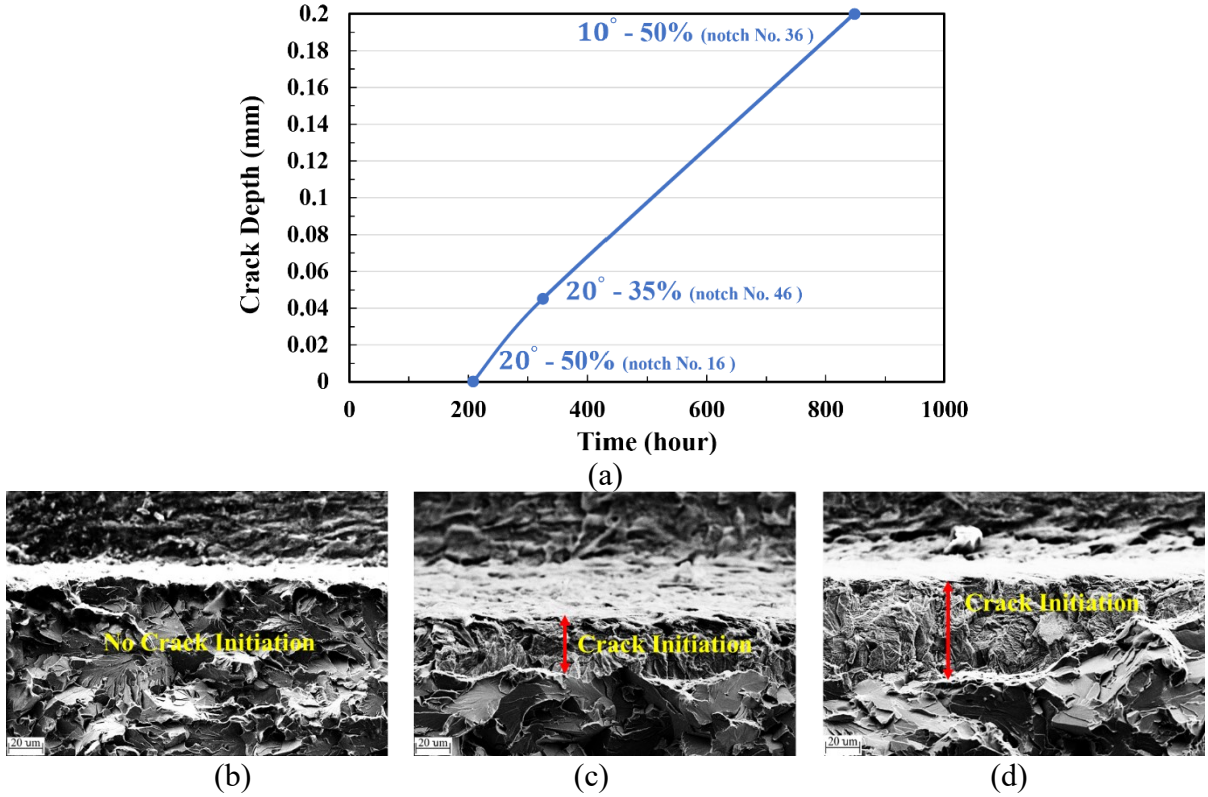

Figure 5-12 Crack initiation as a function of test duration: (a) Crack depth vs. time of test, (b) Crack depth at notch No. 16 (20 degrees, 50% SMYS), (c) Crack depth at notch No. 46 (20 degrees, 35% SMYS), (d) Crack depth at notch No. 36 (10 degrees, 50% SMYS)

As can be seen in this figure, after 750 cycles/208 hours (test duration for long sample No. 1), notch No. 16 does not crack despite having the highest level of stress (95.8 MPa from bending residual stress and axial applied stress). Notch number 46, with a lower stress level (70.4 MPa. because of 35% SMYS loading instead of 50% SMYS in notch number 16), indicates a crack depth of about 30 μm. The maximum crack growth compared with other notches (50 μm) is observed in notch 36 (Figure 5-12d) after 3051 cycles/848 hours with stress of 66.5 MPa, although the average crack depth in the whole width is about 0.2 mm. The figure clearly shows that crack initiation requires a definite time at the bottom of the pit, even though the stress level is high. Accordingly, this supports the hypothesis that different factors affect this time. Despite the presence of severe conditions, such as maximum tensile stress, which results in more hydrogen diffusion to the plastic zone close to the crack tip and more stress concentration at the notch corners (more corrosion in the presence of stress cell), a minimum time is required for hydrogen to diffuse to this plastic zone, and for corrosion to occur at stress concentrators at the bottom of the pit [5].

In Figure 5-13, partial crack initiation is shown as a feature of crack initiation within a limited time (less than the minimum time needed for crack initiation). A full fractography image of notch number 46 (20-degree bending, 35% SMYS, 1 mm initial notch depth) shows regions without crack growth (about 30 percent of the width). It is worth noting that there is a time and location-dependent process for developing microstructural cracks at the notch root [8], [3]. The weakest link sites, such as inclusions near the notch root, can facilitate crack initiation. As discussed, stress distributions in the width direction can also influence partial crack initiation. Under the condition that this notch had been kept in the test longer, *i.e.*, threshold time had completely passed, more uniform crack depth would have been observed (as shown in other crack initiation figures). Therefore, constant crack growth requires passing a minimum time, which is specific for each

condition. In fact, crack initiation in the whole width should be subject to a lower and upper threshold. When the lower threshold is exceeded, microstructural cracks appear somewhere in the width direction, while the upper threshold results in cracks appearing throughout the sample's width.

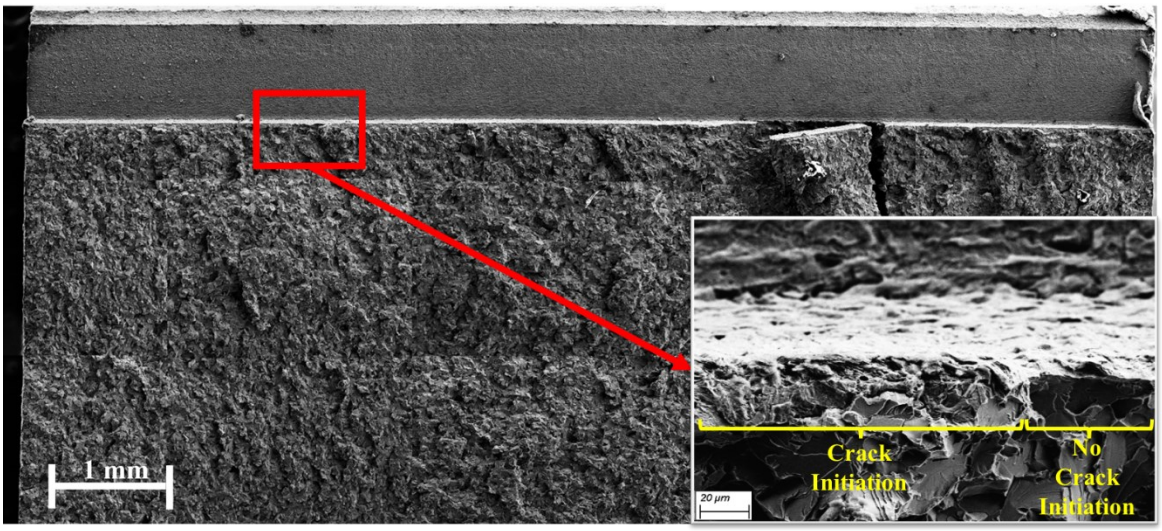

Figure 5-13 Partial crack initiation (Notch No. 46: 20-degree bending, 35% SMYS, 1 mm initial notch depth)

5. 3. 3 Crack initiation at notches in the outward bending direction (compressive stresses) and non-bent sections (no residual stresses)

A summary of average crack growth based on fractography images, specifically in the outward bending direction with compressive residual stress, can be found in Table 5-2. Almost all gauge lengths experiencing compressive stress on the surface (and also at the notch roots), including notches (X3, X4, and X5, where X is the number of long samples 1 to 8), do not show any crack initiation. Indeed, regardless of the bending angle, location of notches with respect to the bend centerline, level of cyclic stress, and initial notch depth, there is almost no crack initiation in the outward bending direction.

Table 5-2 The crack growth in various notches under the influence of different testing parameters (Outward bending direction)

Long Samples No.	Outward bending angle (degree)	Initial notch depth (mm)	Max. applied stress (% SMYS)	Position (mm)	Notch No.	Net crack growth (mm)	Test duration (hour)
1	20	1.0	50	-20	13	0	208
				+20	15	0	208
				0	14	0	208
2	20	1.0	50	-10	21	0	224
				+10	22	0	224
				-20	25	0	224
				+20	27	0	224
				0	26	0	224
3	10	1.0	50	-20	33	0	848
				+20	35	0	848
				0	34	0	848
4	20	1.0	35	-20	43	0	325
				+20	45	0	325
				0	44	0	325
5	10	1.0	35	-20	53	0	1075
				+20	55	0	1075
				0	54	0	1075
6	20	0.5	50	-20	63	0	354
				+20	65	0	354
				0	64	0.005	354
7	10	0.5	50	-20	73	0	997
				+20	75	0	997
				0	74	0	997
8	20	0.5	35	-20	83	0	1283
				+20	85	0	1283
				0	84	0	1283

The general agreement is that compressive residual stress suppresses crack growth while tensile residual stress promotes it [20]. Previously discussed in Figure 5-6 as a sample of compressive residual stress distribution, the outward bending direction is simultaneously affected by two

distinct sources of compressive stress: residual compressive stress from bending (after spring back) and compressive stress from cyclic loading.

There was only one exception for the mentioned explanation: Notch No. 64. Among all notches experiencing compressive stress, this notch had the highest level at the bottom of its notch. This is related to the 20-degree bending angle, bend centerline position and 50% SMYS cyclic loading (Figure 5-6). It is clear from Figure 5-14a that a tiny crack initiation with a depth of 5 μm happened at both corners of this notch at the outer edge of the sample (shown in section D in Figure 5-3a), where the stress concentration is high. The tiny cracks are located at the interface between the ferrite phase and the pearlite colony, reflecting the formation of microstructurally short cracks caused by the galvanic nature of the corrosion, as detailed in Ref [31]. It is also consistent with the study by Van Boven *et al*., emphasizing that surfaces with compressive residual stress can show little pitting. However, there is no chance for this tiny crack-like feature to propagate since a positive high tensile residual stress gradient must be present for mechanically driven crack growth to occur beyond a critical distance [5], [27], [32]. Figure 5-14b is the notch root morphology from the sample's mid-width (shown in section F in Figure 5-3a), indicating that crack initiation under the test conditions is limited and must be microstructurally related if it occurs.

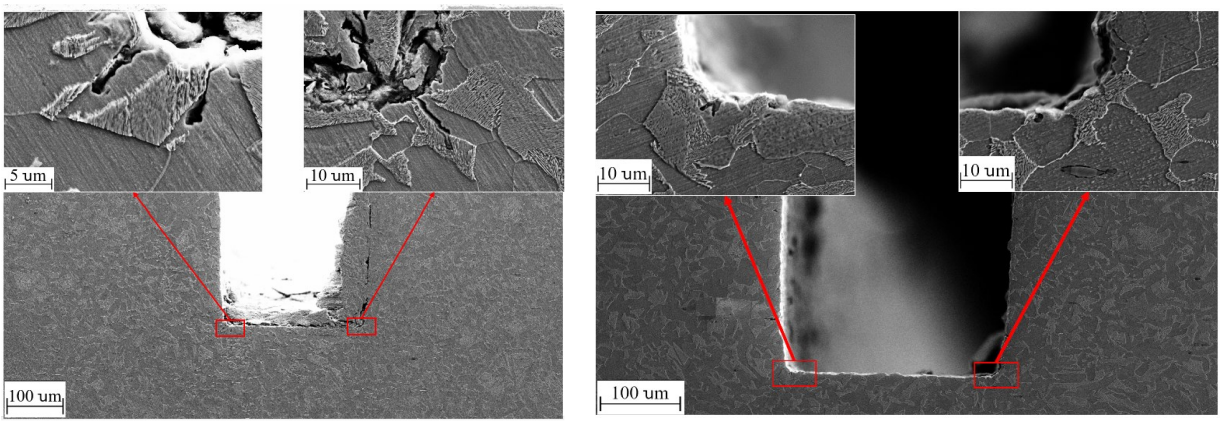

(a) (b)

Figure 5-14 Crack initiation under compressive stress at notch No. 64: 20-degree bending, 50% SMYS, 0.5 mm initial notch depth, outward direction (a) Crack initiation at the outer edge of the sample: section D on Figure 5-3a (b) Crack initiation at the mid-width of the sample: section F on Figure 5-3a

After passing the steps of cycling loading on the non-bent section on notches with different initial depth/cyclic loading (A1, A2, B1, B2), only a short crack around 60 μm was observed on the cross-section of notch B2 (1 mm initial depth, 35 and then 50% SMYS cycling loading), according to Figure 5-15a and Table 5-3. Partial cracking was evident on the fractured surface (Figure 5-15b). In this case, partial crack growth results from axial cyclic loading without other sources of axial stress like bending. Other non-bent section notches provided less stress at the notch root (stress× stress concentration, to be discussed later), so Table 5-3 summarizes the results for the non-bent section.

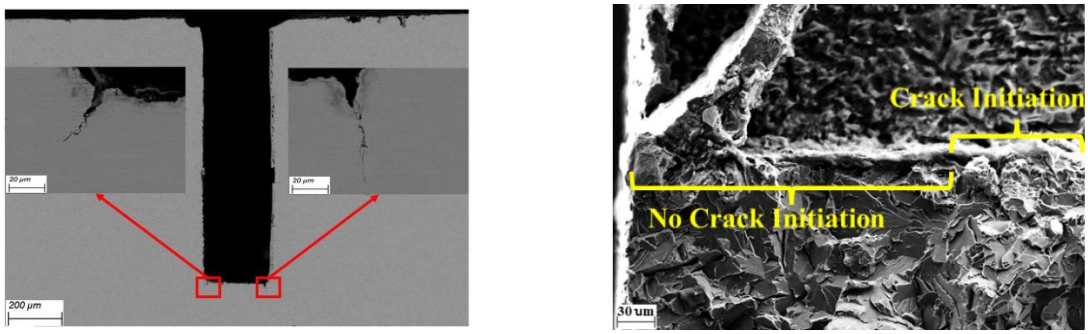

(a) (b)

Figure 5-15 Partial crack initiation (Notch B2: non-bent section (1 mm initial notch depth/ 35 and then 50%SMYS) (a) cross-section analysis (SEM- BSD) (b) Fracture surface

As mentioned before, the non-bent sections have no residual stress gradient in the thickness direction. The stress concentration factor changes as the initial notch depth increases from 0.5 mm to 1 mm. Moreover, the dissolution mechanism cannot cause crack initiation for these notches. As a result, circumferential crack initiation generally cannot occur in a pipeline with only axial loading (from pipe internal pressure fluctuation) and no other sources of axial loading, like bending residual stresses.

Table 5-3 The crack growth in various notches under the influence of different testing parameters (non-bent Section)

Notch No.	Initial notch depth (mm)	Step 1		Step 2		Net crack growth (mm)	Net crack growth rate (mm/s)
		Applied stress, % SMYS	Test time (hour)	Applied stress, % SMYS	Test time (hour)		
A1	0.5	35	1080	N/A		0	0
A2	1.0					0	0
B1	0.5			50	1080	0	0
B2	1.0			50	1080	0.06	7.7×10^{-9}

5. 4 Discussion

Generally, three stages are involved in initiating short cracks: formation of pits, initiation of microstructurally short cracks, and growth of microstructurally short cracks into mechanically short cracks [27], [33].

The same process of crack development at the bottom of a pit could be considered at the stage after dormancy and crack initiation from a dormant crack:

1. Crack initiation and microstructural short cracks depended on galvanic processes, microstructure, and stress concentrators.

2. Growth of mechanically short/ shallow cracks with the dimension from 0.1 to 1 mm, above which fracture mechanic principles can be applied, although crack growth rate for these cracks is more than for long cracks under identical mechanical loading conditions in terms of stress intensity factor [3], [34].

Crack initiation from the bottom of a pit can happen either by dissolution or a mechanical process [5] or the synergistic effect of both. These are microstructurally short cracks of a size equal to the grain size or other microstructure within the material, usually less than 100 μm. Fracture mechanics does not normally adequately describe the growth of these cracks [27], [33]. Note that initiating microstructurally short cracks is also possible under constant stress loading [3].

Dissolution could result in crack initiation if the dissolution rate in the depth direction is at least ten times higher than in the lateral direction [5]. Where crack initiated at the notch root depends on metallurgical factors like the presence of non-metallic inclusions, grain boundaries, specific phases (pearlite/ferrite or mill scale) [1] and mechanical factors like stress raisers and stress cells [33].

In another mechanism of crack initiation at the bottom of the pit, mechanical process, micro-cracks are initiated at the weakest link sites in the hydrostatic zone ahead of a notch tip, not exactly at the corner of the notch. Compared to high pH SCC [35]–[40], this is a completely different case. Accordingly, a micro-crack emerges due to a sharp crack tip propagating back to the bottom of the pit, resulting in a sharp crack forming there. There are two types of weakest link sites: metallurgical discontinuities with low bond strength or regions with high hydrogen segregation [5].

This investigation deals with the initiation of cracks from notch roots of pipeline steels exposed to a typical near-neutral pH environment that can cause pipeline failure through the mechanism of hydrogen-enhanced fatigue. The notch has a depth of either 0.5 mm or 1.0 mm and was made in

the pipe wall with a varied distribution of residual stresses, either compressive, tensile, or free of residual stresses introduced by bending. The width of the notch was controlled within 0.2 mm as the width of cracks found in pipeline steels from field operation can reach 0.5 mm in width [41].

The initiation of cracks in pipeline steels exposed to near-neutral pH environments has been primarily investigated on straight steel surfaces that are either polished, mill-scale covered, or have a varied distribution of residual stresses [20], [31], [33], [42]–[45]. It has been determined that crack initiation on a straight external surface often starts with pit formation, followed by crack initiation from the bottom of the pits [5]. During this stage, coating conditions, soil conditions, and steel metallurgy all play a role. Mechanical driving forces, such as operating pressure fluctuation, are less significant [6].

One of the common characteristics of cracking in pipeline steels exposed to a near-neutral pH environment is the phenomenon of crack dormancy, a situation in which cracks often cease to grow when they reach a depth of about 1.0 mm. While evaluating dormancy, it is critical first to understand why dormancy occurs, which includes but may not be limited to the conditions summarized below [6], [8], [27]:

1. A primary cause of crack dormancy is related to the reduction in dissolution rate at the crack tip. This is due to a complicated process that involves CO_2 gradients and ionic concentration variation in the aqueous solution in the pit.
2. The nature and magnitude of residual stresses at and near pipeline steel's outer surface significantly affect dormancy, specifically when residual stresses dominate a stress distribution in the thickness direction. For instance, decreasing local stresses in the thickness direction as the crack grows may hamper the onset of stage II. Most crack

colonies do not propagate beyond 1 mm because mechanical forces are below the threshold for crack propagation.

3. Hydrogen acts together with residual stresses, and if the hydrogen concentration in the material surrounding the crack tip is low, the crack will be more likely to remain dormant.
4. Crack blunting caused by room-temperature creep may also retard crack growth [8]. The additional deformation from this creep can sometimes increase residual compressive stresses ahead of a crack tip and enhance the retardation effect. In other words, cyclic creep retardation is related to the cyclic hardening effect. Cracks can grow when sustainable strain exists at their tips, so applying pressure slightly higher than operational stress could exhaust this strain and retard crack growth.

A superposition of dissolution growth curves and hydrogen-facilitated fatigue growth curves are shown in Figure 5-16 for crack initiation and growth of near-neutral pH SCC/CF of pipelines [20]. During crack initiation and early-stage crack growth, the former is predominant, while the latter results from fatigue and hydrogen combined dominates in the latter stages. A major role in crack growth in stage Ib should be played by dissolution; hydrogen-facilitated fatigue growth is less evident during this phase because of the benign mechanical driving force. To extend service life, it is crucial to understand how a dormant depth tip becomes active for stage II growth [6], [20].

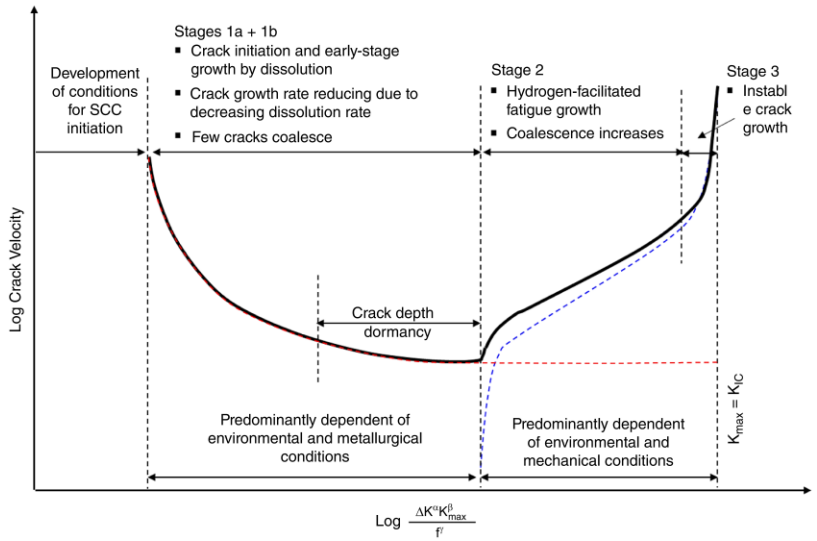

Figure 5-16 Schematic illustration of the effect of $\Delta K^{\alpha} K_{max}^{\beta} / f^{\gamma}$ upon SCC velocity of pipeline steel exposed to near-neutral pH aqueous bicarbonate solution [20]

The initiation of cracks from a dormant crack has been a subject of research over the last decades. To reactivate a dormant crack, certain conditions must be met. The first one is the magnitude and nature of the stresses near the crack tip. The second relates to the amount of diffusible hydrogen reaching the crack tip. There is a connection between these two factors [2], [3], [6], [8]. As mentioned before, sustainable crack growth is possible if two extrinsic sources of crack sharpening, *i.e.,* tensile cyclic loading and the hydrogen enhancement of fatigue, can prevail over crack tip blunting and dormancy.

For crack reactivation, minimum stress must exist ahead of the crack tip. Growth, dormancy, and reactivation of blunted cracks may occur repeatedly in a growing crack. The combination of hydrostatic stresses in the plastic zone, hydrogen segregation, and the presence of weakest link sites, such as inclusions near the crack tip, can cause hydrogen-induced microcracks to form, resharpening the main crack. It is only possible for cracks to grow by this mechanism if they are subjected to cyclic loading. Indeed, hydrogen-related sharpening and cyclic loading can

synergistically resharpen blunted cracks. There is a high probability of growth wherever these two conditions coexist [8], [3], [33]. These factors dominate the crack initiation of blunt notches in this investigation. Crack tip morphology, either sharp or blunt, is another important factor affecting the crack growth rate, which is not considered in this research, so all initial notches were blunted.

With the above introduction, the initiation of cracks from notch roots in the current investigation is much like crack initiation from dormant cracks. Various situations, including the magnitude of externally applied stresses and the residual stresses introduced by bending, and varied depths of notches have been created in the present investigation to understand the mechanisms of crack initiation from the notch roots.

5. 4. 1 Crack initiation from notch roots in the absence of tensile residual stresses

For the notch roots embedded within the pipe wall that were not processed to introduce tensile residual stresses, the initiation of cracks from notch roots appears very difficult compared to the notch roots with tensile residual stresses. This seems surprising, as the actual stresses at the notch roots can be very high, although the applied nominal stresses were low, 35% to 50% SMYS. Based on the stress concentration factors determined by Neuber's Rule [46], the actual stresses at the notch roots are determined to be 415.8 MPa and 458.6 MPa for notches with an initial depth of 0.5 mm and 1.0 mm, respectively, when the applied nominal stress is 50% SMYS.

At both notch depths, the actual stresses at notch roots exceed the yield strength of the pipeline steel. Under this magnitude of stresses, cracks can be readily initiated on smooth surfaces, either freshly polished or covered by mill scales. It has been determined that the rate of crack growth in the stage of crack initiation is well above 10^{-8} mm/s on a straight and smooth surface [33], which is about an order of magnitude higher than the crack growth rate calculated based on the rate of general corrosion of pipeline steel coupons exposed to the same near-neutral pH solution. This

indicates there must exist a galvanic process during crack initiation. On a straight and smooth surface, a galvanic cell is formed between the mill scale and the steel under a cracked mill scale, causing localized corrosion such as pits. Under the circumstances, cracks could be initiated only when such pits are located within the material with high tensile residual stresses and can be extended to a deeper depth if the tensile residual stresses can be maintained in the thickness direction. On a polished surface, galvanic corrosion is found along the interfaces between pearlite bands and ferrites.

The crack growth rate at the root of notch B2 in Table 5-3 is determined to be 7.7×10^{-9} mm/s, which is lower than the crack growth rate during crack initiation on a straight and smooth surface but still much higher than the crack growth rate calculated based on the rate of general corrosion of pipeline steel coupons exposed to the same near-neutral pH solution. It suggests that galvanic corrosion still plays a role in crack initiation at the root of notch B2.

The galvanic cell responsible for crack initiation at notch B2 is obviously a stress cell coupled between the locations with different tensile stresses, such as the corner of the notch root and the wall of the notch. The difference in potential between the anodic surface and the cathodic surface would govern the corrosion rate. Pitting corrosion and pit-induced cracking were not found at the notch root with a depth of 0.5 mm, indicating insufficient potential difference because of the lower stress difference between the anode and cathode. In the case of notch B2 (1 mm depth), pitting corrosion and pit-induced cracking were found in the width section away from the edge surface because of slightly higher stress, as shown in Figure 5-5. As a result, the loading condition applied to notch B2 would represent the threshold condition of crack initiation for the notch root (notch B2) with a notch depth of 1.0 mm.

5. 4. 2 Crack initiation from notch roots/dormant cracks in the presence of residual stresses

The presence of residual stresses changes the magnitude of the difference in potential between the anode and the cathode and their location with respect to notch geometries.

- When notches are made in the specimen with compressive residual stresses, the notch roots are under compressive stress even when a tensile stress of 50% SMYS is applied. This would make the surface of the notch wall that is free of loading an anodic site and the notch root a cathodic site. This is a typical situation of large anode (notch wall) and small cathode (notch root), which would prevent any corrosion and crack initiation from the notch roots.
- When notches are introduced in the specimen with tensile residual stresses, the difference in stress and, therefore, the potential between the anode/notch root and the cathode/notch wall is increased, depending on the magnitude of tensile residual stresses. This is a typical situation of a large cathode (notch wall) and small anode (corner of notch root). Under the circumstances, pit-formation and pit-to-crack initiation at the notch root become possible.

However, by examining cracks found at the notch roots with tensile residual stresses, as shown in Figure 5-17, the typical scenario of pit-formation and pit-to-crack initiation, as seen in the case of crack initiation at the notch root free of residual stresses, is not observed. This may reflect how tensile residual stresses affect the process of crack initiation.

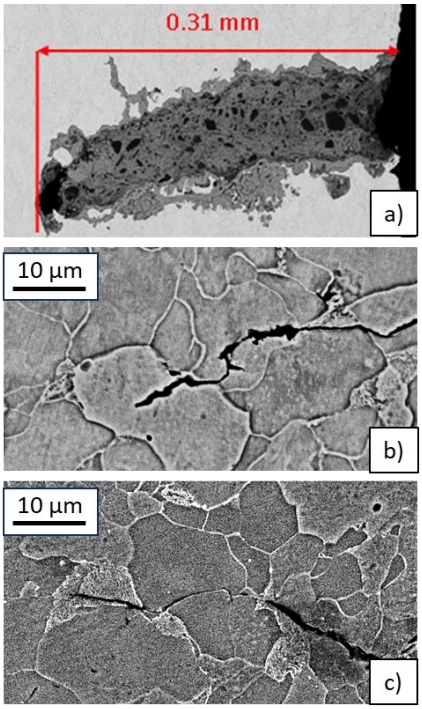

Figure 5-17 (a) a blunt tip resembling a notch root, (b) a blunt tip crack with an indication of corrosion, (c) a sharp crack that is usually advanced by the mechanism of hydrogen-enhanced fatigue [31], [47]

In the case of crack growth in near-neutral pH solutions, three types of crack tip morphologies, as shown in Figure 5-17, are often observed.

a) A blunt tip resembling a notch root, as shown in Figure 5-17a, is a common morphology found in dormant cracks with reasons, as explained previously,

b) A blunt tip crack with an indication of corrosion, as those observed in the current investigation. Under the circumstances, crack walls are separated because of corrosion and crack tips have a radius well larger than 10-100 atoms, which is the radius of a crack defined by fracture mechanics,

c) A sharp crack is usually advanced by the mechanism of hydrogen-enhanced fatigue, in which corrosion plays little role in crack advancement. This often occurs when crack growth is relatively high and/or crack growth is under cathodically protected conditions.

The absence of pitting corrosion at the notch roots with tensile residual stresses is obviously caused by insufficient time of corrosion, very localized anodic sites, or both. For those notch roots with a crack growth rate at the level of 10^{-8} mm/s, the time of corrosion available at the notch roots is an order of magnitude less than that available at the notch root without tensile residual stresses. Upon the initiation of a crack from the notch root, the anodic site shifts to the crack tip and further corrosion of notch roots is prohibited. The anodic site would also be restricted to the direction with the highest shear stress. As soon as the crack is formed, further corrosion of the crack wall would be limited because the anodic site is always associated with the crack tip.

4.1. Threshold of crack initiation under the influence of residual stresses at the notch root

Figure 5-18 summarizes the hypothesis mentioned above regarding the impact of accumulated stress (bending residual stress and applied loading) on the average crack growth rate occurring at the notch root (dormant crack). As previously stated, a minimum stress requirement exists at the notch root for crack initiation, which was determined to be about 85% SMYS. Below this stress threshold, a crack growth rate at a level of 2×10^{-9} mm/s was also observed, as shown in Figure 5-18. This crack growth rate is equivalent to the crack growth rate calculated from the general corrosion rate of flat coupons exposed to the same NNpH solution [48]. Under the circumstances, accelerated crack initiation and growth arising from stress cells would be unlikely if it is existed at all.

To confirm the benign impact of a stress cell, the two data points with a growth rate comparable to the crack growth rate calculated based on the rate of dissolution measured using flat coupons were further examined. They were from notches No. 56 and 58, with a bend angle 10 degrees and notch depth of 1.0 mm under an applied stress of 35% SMYS. The two notches were also located 2 cm from the bend centerline and would have the lowest tensile residual stresses and applied stresses. Only some microstructurally short cracks with dimensions of about 1 grain size were observed, as shown in Figure 5-19.

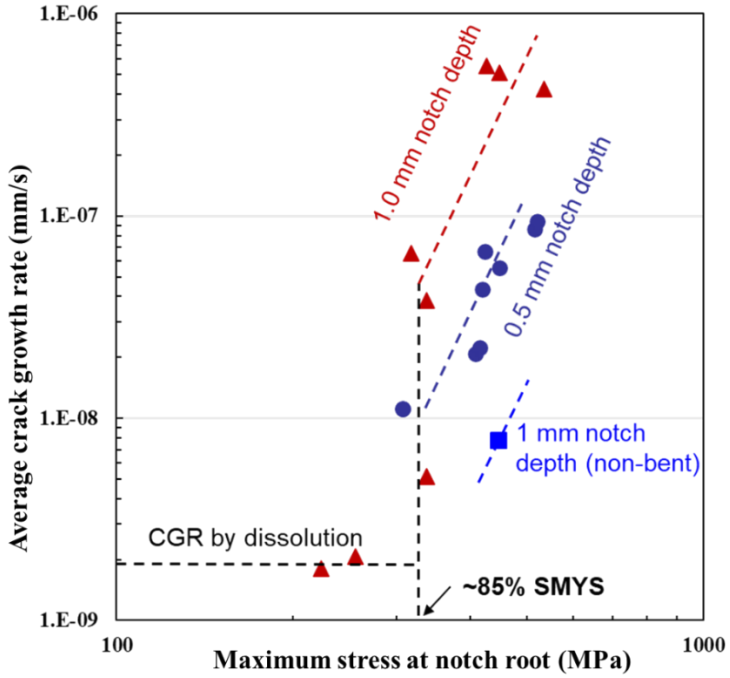

Figure 5-18 Crack growth rate as a function of maximum stress at the notch *root.*

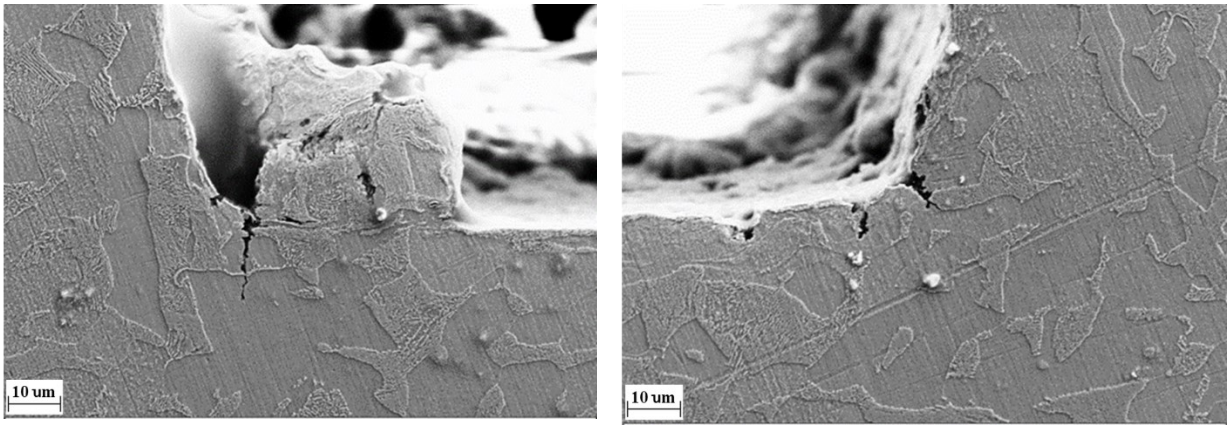

Figure 5-19 SEM images showing microstructurally short cracks initiated from the notch root of notch No. 58

5. 5 Conclusion

This study analyzed circumferential crack initiation at the bottom of dormant cracks/pits in steels exposed to near-neutral pH environments. The following are some key findings of this investigation.

1. The digital image correlation (DIC) method could be considered an appropriate technique for C-NNpH-CF investigations since this method can analyze final stress distribution affected by various sources of residual and applied stresses. In this study, final stress distribution emphasizes that the accumulation of stress from axial loading and residual stress increases the level of stress (compressive/tension) at the bending centerline since the type of axial stress and residual stress in the inward bending direction is tension and in the outward bending direction is compression, regardless of the bending degree and the level of axial loading.

2. The initiation of microstructurally short cracks from the bottom of the pit may result from localized corrosion at the locations with the highest tensile stress levels. Corrosion in the

form of stress cells at the notch corners (stress concentrators) is responsible for this crack initiation mechanism.

3. The presence of a high level of stress at a stress cell would suffice for crack initiation at the notch root by direct dissolution, regardless of the type of stress (compressive/ tensile), emphasizing that a shallow notch with high compressive residual stress can show little crack initiation at stress concentrators. However, these tiny cracks cannot propagate.
4. Stress gradient in the depth direction is a significant feature of circumferential NNpH-CF. Therefore, the stress× stress concentration factor provides more comprehensive data on crack initiation in the depth direction since it considers both effects of stress gradient in the depth direction and notch depth simultaneously.
5. A tensile stress gradient (difference in potential between the anodic surface and the cathodic surface) specifies the first step in the initiation of cracks at the bottom of the pit/dormant cracks. At the crack tip, localized anodic sites inhibit the formation of further corrosion of the notch root, and the crack wall results in blunt tip cracks. It is possible to have a sharp crack when the hydrogen-enhanced fatigue mechanism dominates.

References:

[1] M. Elboujdaini and M. T. Shehata, “Stress corrosion cracking: A Canadian prospective for oil and gas pipeline,” 2005.

[2] J. Zhao, W. Chen, M. Yu, K. Chevil, R. Eadie, J. Been, G. Van Boven, R. Kania & S. Keane, “Crack growth modeling and life prediction of pipeline steels exposed to near-Neutral pH

environments: stage II crack growth and overall life prediction," Metall Mater Trans A Phys Metall Mater Sci, vol. 48, no. 4, pp. 1641–1652, Apr. 2017, https://doi.org/10.1007/s11661-016-3939-z.

[3] W. Chen, R. Kania, R. Worthingham, and G. Van Boven, "Transgranular crack growth in the pipeline steels exposed to near-neutral pH soil aqueous solutions: The role of hydrogen," Acta Mater, vol. 57, no. 20, pp. 6200–6214, Dec. 2009, https://doi.org/10.1016/j.actamat.2009.08.047.

[4] M. J. W. Ilm, "The role of pressure and pressure fluctuation in the growth of Stress Corrosion Cracks in line pipe steels," in Proceedings of the 1998 International Pipeline Conference. Calgary, Alberta, Canada. IPC 1998-2049, 1998. https://doi.org/10.1115/IPC1998-2049.

[5] G. Van Boven, R. Rogge, and W. Chen, "Residual stress and stress corrosion cracking of high pressure hydrocarbon transmission pipelines," in Proceedings of the 2006 International Pipeline Conference. Calgary, Alberta, Canada. IPC2006-10486. https://doi.org/10.1115/IPC2006-10486.

[6] J. Zhao, Weixing Chen, M. Yu, K. Chevil, R. Eadie, G. Van Boven, R. Kania, J. Been & S. Keane, "Crack growth modeling and life prediction of pipeline steels exposed to near-neutral pH environments: dissolution crack growth and occurrence of crack dormancy in stage I," Metall Mater Trans A Phys Metall Mater Sci, vol. 48, no. 4, pp. 1629–1640, Apr. 2017, https://doi.org/10.1007/s11661-016-3951-3.

[7] J. A. Beavers and B. A. Harle, "Mechanisms of high-pH and near-neutral-pH SCC of underground pipelines," Journal of Offshore Mechanics and Arctic Engineering, vol. 123, no. 3, pp. 147–151, Aug. 2001, https://doi.org/10.1115/1.1376716.

[8] H. Shirazi, R. Eadie, and W. Chen, “A review on current understanding of pipeline circumferential stress corrosion cracking in near-neutral PH environment,” Engineering Failure Analysis, vol. 148, Jun. 01, 2023. https://doi.org/10.1016/j.engfailanal.2023.107215.

[9] M. Yu, W. Chen, R. Kania, G. Van Boven, and J. Been, “Crack propagation of pipeline steel exposed to a near-neutral pH environment under variable pressure fluctuations,” Int J Fatigue, vol. 82, pp. 658–666, Jan. 2016, https://doi.org/10.1016/j.ijfatigue.2015.09.024.

[10] J. Beavers and T. A. Bubenik, “Stress corrosion cracking,” in Trends in Oil and Gas Corrosion Research and Technologies: Production and Transmission, 2017, pp. 295–314. https://doi.org/10.1016/B978-0-08-101105-8.00012-7.

[11] M. Brimacombe Senior Advisor, C. Wargacki Key Account Manager, and N. Global Leduc, “Circumferential crack detection: Challenges, solutions and results,” in Proceedings of the 2016 International Pipeline Conference. Calgary, Alberta, Canada. IPC2016-64111. https://doi.org/10.1115/IPC2016-64111.

[12] Ron Thompson, R. Gardner, K. Dwyer, A. Corbett, and M. Marquis Hotel, “A case study in the detection and sizing of circumferential stress corrosion cracking Pipeline Pigging and Integrity Management Conference,” in Pipeline pigging and integrity management conference, Houston, February 2020.

[13] N. Bates, M. Brimacombe, and S. Polasik, “Development and experience of a circumferential stress corrosion crack management program,” in Proceedings of the 2018 International Pipeline Conference. Calgary, Alberta, Canada.IPC2018-78315.

[14] B. Johnson, B Tesfaye, C. Wargacki, T. Hennig, E. Suarez “Complex Circumferential Stress Corrosion Cracking: Identification, Sizing and Consequences for the Integrity Management

Program," in Proceedings of the 2018 International Pipeline Conference. Calgary, Alberta, Canada. IPC2018-78564. https://doi.org/10.1115/IPC2018-78564.

[15] Y. B. Beauregard and C. Edwards, "Analysis of sever circumferential SCC found on an ethane pipeline," in Proceedings of the 2014 International Pipeline Conference. Calgary, Alberta, Canada. , 2014.

[16] S. Jian, Y. Zupei, and M. Yunxin, "Investigation on potential SCC in gas transmission pipeline in China," in Proceedings of the 2004 International Pipeline Conference. Calgary, Alberta, Canada. IPC2014-33059. https://doi.org/10.1115/IPC2004-0709.

[17] R. R. S. M. Fessler, "Characteristics, cause, and management of circumferential stress-corrosion cracking," in International Pipeline Conference, in Proceedings of the 2014 International Pipeline Conference. Calgary, Alberta, Canada. https://doi.org/10.1115/IPC2014-33059.

[18] D. Abdulhameed, S. Adeeb, and R. Cheng, "The influence of the Bourdon effect on pipe elbow" in Proceedings of the 11th International Pipeline Conference, 2016, pp. 1–10. https://doi.org/10.1115/IPC2016-64659.

[19] S. Attia, M. Mohareb, M. Martens, N. Yoosef-Ghodsi, Y. Li, and S. Adeeb, "Numerical assessment of elbow element response under internal pressure," Journal of Pressure Vessel Technology, Transactions of the ASME, vol. 143, no. 5, Oct. 2021, https://doi.org/10.1115/1.4050091.

[20] S. Wang and W. Chen, "Overview of Stage 1b Stress Corrosion Crack Initiation and Growth of Pipeline Steels," Corrosion, vol. 79, no. 3, pp. 284–303, Mar. 2023, https://doi.org/10.5006/4168.

[21] J. Babcock, D. Dewar, and J. Webster, “Deer Mountain case study: integration of pipe and ground monitoring data with historical information o develop landscape management plan,” Proceedings of the 2020 International Pipeline Conference. Calgary, Alberta, Canada. IPC2020-9613. https://doi.org/10.1115/IPC2020-9613.

[22] K. Zhang, R. Chune, R. Wang, and R. Kania, “Role of axial stress in pipeline integrity management,” in Proceedings of the 2022 International Pipeline Conference. Calgary, Alberta, Canada. IPC2022-87327. https://doi.org/10.1115/IPC2022-87327.

[23] K. Manthiramoorthy and A. Krishnaveni, “Fracture Parameter Evaluation Using Digital Image Correlation Technique,” International Journal of Engineering Technology Science and Research, Volume 4, Issue 11, 2017.

[24] B. Tasdemir and B. Taşdemir, “Determination of stress intensity factor using digital image correlation method,” Matter, vol. 2, no. 1, 2015.

[25] R. B. Á. Pradas Cristina, “Stress and strain analysis of a material with Digital Image Correlation method (DIC),” Western Norway University of Applied Sciences, 2020.

[26] L. Shi, X. Zhang, L. Zhang, C. Wang, and J. Wang, “Application of digital image correlation technique in stress and strain measurement. 15th Asia Pacific Conference for Non-Destructive Testing (APCNDT2017), Singapore.

[27] W. Chen, G. Van Boven, and R. Rogge, “The role of residual stress in neutral pH stress corrosion cracking of pipeline steels - Part II: Crack dormancy,” Acta Mater, vol. 55, no. 1, pp. 43–53, Jan. 2007, https://doi.org/10.1016/j.actamat.2006.07.021.

[28] "ISO-7539-5 Corrosion of metals and alloys- Stress Corrosion Cracking- Preparation and use of C-ring specimen." 1989.

[29] R. Sutherby and W. Chen, "Deflected stress corrosion cracks in the pipeline steel," Proceedings of the 2004 International Pipeline Conference. Calgary, Alberta, Canada. https://doi.org/10.1115/IPC2004-0600.

[30] S. L. Asher and P. M. Singh, "Role of stress in transgranular stress corrosion cracking of transmission pipelines in near-neutral pH environments," Corrosion, vol. 65, no. 2, p. 79, 2009. https://doi.org/10.5006/1.3319122.

[31] R. Chu, W. Chen, S.-H. Wang, F. King, T. R. Jack, and R. R. Fessler, "Microstructure Dependence of Stress Corrosion Cracking Initiation in X-65 Pipeline Steel Exposed to a Near-Neutral pH Soil Environment," Corrosion Science , vol. 60, no. 3, 2004. https://doi.org/10.5006/1.3287732.

[32] G. Van Boven, W. Chen, and R. Rogge, "The role of residual stress in neutral pH stress corrosion cracking of pipeline steels. Part I: Pitting and cracking occurrence," Acta Mater, vol. 55, no. 1, pp. 29–42, Jan. 2007, https://doi.org/10.1016/j.actamat.2006.08.037.

[33] W. Chen, "An overview of near-neutral pH stress corrosion cracking in pipelines and mitigation strategies for Its initiation and growth," Corrosion, vol. 72, no. 7, pp. 962–977, Jul. 2016, https://doi.org/10.5006/1967.

[34] J. Toribio, "Residual stress effects in stress-corrosion cracking," J Mater Eng Perform, vol. 7, pp. 173–182, 1998. https://doi.org/10.1361/105994998770347891.

[35] H. Niazi, H. Zhang, and K. Korol, “High pH Crack Growth Sensitivity to Underload-Type of Pressure Fluctuations,” 2018. Proceedings of the 2018 International Pipeline Conference. Calgary, Alberta, Canada. https://doi.org/10.1115/IPC2018-78394.

[36] H. Niazi, H. Zhang, L. Lamborn, and W. Chen, “The impact of pressure fluctuation on the early onset of stage II growth of high pH stress corrosion cracking,” Proceedings of the 2020 13th International Pipeline Conference, IPC2020-9511. https://doi.org/10.1115/IPC2020-9511.

[37] H. Niazi, R. Eadie, W. Chen, and H. Zhang, “High pH stress corrosion cracking initiation and crack evolution in buried steel pipelines: A review,” Engineering Failure Analysis, vol. 120. Elsevier Ltd, Feb. 01, 2021. https://doi.org/10.1016/j.engfailanal.2020.105013.

[38] H. Niazi, K. Chevil, E. Gamboa, L. Lamborn, W. Chen, and H. Zhang, “Effects of Loading Spectra on High pH Crack Growth Behavior of X65 Pipeline Steel,” Corrosion, vol. 76, no. 6, pp. 601–615, Jun. 2020, https://doi.org/10.5006/3472.

[39] H. Niazi, G. Nelson, L. Lamborn, R. Eadie, W. Chen, and H. Zhang, “Crack Growth Sensitivity to the Magnitude and Frequency of Load Fluctuation in Stage 1b of High-pH Stress Corrosion Cracking,” Corrosion, vol. 77, no. 6, pp. 618–631, Jun. 2021, https://doi.org/10.5006/3711.

[40] H. Niazi, S. Wang, L. Lamborn, R. Eadie, W. Chen, and H. Zhang, “Effects of load interactions on the onset of stage two of high pH stress corrosion cracking,” Journal of Pipeline Science and Engineering, vol. 1, no. 1, pp. 122–136, Mar. 2021, https://doi.org/10.1016/j.jpse.2021.01.003.

[41] W. Chen, F. King, and E. Vokes, “Characteristics of Near-Neutral-pH Stress Corrosion Cracks in an X-65 Pipeline,” Corrosion Science , vol. 58, no. 3, 2002.

[42] Y.-Z. Wang, R. W. Revie, and R. N. Parkins, “Mechanistic aspects of stress corrosion crack initiation and early propagation,” in NACE International Conference, Paper No.: 143., 1999.

[43] A. Eslami, *M. Marvasti, W. Chen, R. Eadie, R. Kania, R. Worthingham, G. Van Boven* “The role of electrochemical condition in near neutral pH SCC initiation mechanism(s),” in Proceedings of the 2010 International Pipeline Conference. Calgary, Alberta, Canada.IPC2010-31190. https://doi.org/10.1115/IPC2010-31190.

[44] S. Wang, L. Lamborn, and W. Chen, “Stress corrosion crack initiation and propagation before proceeding to Stage 2 for hydrostatically tested pipeline steels,” J Mater Sci, 2022, https://doi.org/10.1007/s10853-022-07606-w.

[45] S. Wang, L. Lamborn, and W. Chen, “Near-neutral pH corrosion and stress corrosion crack initiation of a mill-scaled pipeline steel under the combined effect of oxygen and paint primer,” Corrosion Sci, vol. 187, Jul. 2021, https://doi.org/10.1016/j.corsci.2021.109511.

[46] W. D. Pilkey, Formulas for stress, strain, and structural matrices. John Wiley & Sons, 2005.

[47] W. Chen and R. Sutherby, “Environmental effect of crack growth rate of pipeline steel in near neutral pH soil environments,” in International Pipeline Conference, 2004.

[48] W. Chen and R. L. Sutherby, “Crack growth behavior of pipeline steel in near-neutral pH soil environments,” Metall Mater Trans A Phys Metall Mater Sci, vol. 38, no. 6, pp. 1260–1268, Jun. 2007, https://doi.org/10.1007/s11661-007-9184-8.

Chapter 6 Pipeline Circumferential Cracking in NNpH Environment Under the Influence of Residual Stress, Part II: Crack Growth[1]

6. 1 Introduction

The safety and integrity of buried pipelines transporting crude oil and natural gas are of utmost importance, considering the hazardous nature of the substances they transport. Environmentally assisted cracking (EAC), including Stress Corrosion Cracking (SCC) and corrosion fatigue, can threaten pipeline safety and integrity. Under pipe disbonded coatings, transgranular corrosion fatigue cracking is generally initiated from the bottom of corrosion pits on the outer surface of the pipe in a dilute carbonic acid solution (near-neutral pH environment, pH: 5.5-7.5) [1]–[3].

When tensile axial (also called longitudinal) stresses exceed hoop stresses in an operational gas or liquid pipeline, circumferentially oriented cracking can occur. Corrosion fatigue was found to be responsible for cracking in near-neutral pH environments since crack growth does not occur without significant stress variations (cyclic loading related to pressure fluctuations during pipeline operations). Henceforth, the term "Circumferential Near-neutral pH Corrosion Fatigue (C-NNpH-CF)" will describe this particular form of cracking [1], [4]–[7].

Additional stresses in the axial or flow direction above the normal stresses from pressurization are mainly introduced to the pipeline by the movement of the pipeline due to landslides, rock dents or road/water crossings. They also can be caused by thermal expansion, residual stresses from pipe

[1] A version of this chapter has been submitted: H. Shirazi, Sh. Wang, W. Chen, R. Eadie, “Pipeline Circumferential Cracking in NNpH Environment Under the Influence of Residual Stress, Crack Growth.

manufacturing and pipeline construction (cold bend/ girth weld), hydrodynamic stress at bends and the Bourdon effect on pipe bends [8]. These sources of axial stress will be added to the axial cyclic stress from internal pressure, making pipelines prone to C-NNpH-CF [5], [8]–[16].

There are four main stages in the life cycle of pipeline steel experiencing NNpH-CF: incubation stage, Stage I (crack initiation and early-stage crack growth), Stage II (sustainable crack growth driven by mechanical forces), and stage III (rapid crack propagation to rupture) [17]. Studies [2], [18], [19] have revealed that cracks in stage 1 often enter a state of dormancy once they reach 1 mm in depth.

It has been found, using long-term and extensive laboratory crack growth simulations, that crack growth rate in Stage II can be correlated with both mechanical and environmental driving forces under constant amplitude cyclic loading in near-neutral pH environments by this combined factor: $\Delta K^{\alpha} K_{max}^{\beta} / f^{\gamma} +$ h, where A, n, α, β, and γ are all constants and α + β = 1. In Stage II crack growth, h represents the rate of dissolution at the crack tip, which is about one order of magnitude lower than the first term and can usually be ignored [7], [17].

Integrity management measures should be implemented before Stage III. These techniques focus primarily on Stage II because Stage III crack growth is extremely rapid, whereas Stage II crack growth is steady. A periodic inspection can detect cracking and control crack growth when cracks are detected with depths above threshold conditions [2], [17]. Some time and location dependence factors should be considered to predict the time taken for a crack to grow to a critical size, such as stress level and hydrogen diffusion near the crack tip [20]–[23].

There has been limited research on the role of stress type and value in stage II crack growth, particularly when there is a stress gradient in the thickness direction caused by specific sources

such as bending. Circumferential cracking can be considered a unique mechanism since this stress gradient in the thickness direction can define the cracking mechanism at Stage II. This contrasts with a straight, smooth surface that does not have any residual stress variation within its thickness.

Pipeline operators have enhanced their understanding of longitudinally oriented corrosion fatigue cracking, leading to the implementation of effective mitigation measures. There is; however, a limited understanding of Circumferential Near Neutral Ph Corrosion Fatigue (C-NNpH-CF), and monitoring and mitigation techniques are limited as well [12]. In addition, current in-line inspection (ILI) tools have difficulty detecting circumferentially oriented cracks [13]. It should be noted that this cracking mechanism has been found to contribute to or cause failures in some cases [12]. This investigation is intended to evaluate the impact of the combination of bending residual stress (an appropriate source of residual axial stress) and cyclic loading (simulated pipeline pressure fluctuation) on crack growth at Stage II. The final stress distribution in length and thickness direction derived from the digital image correlation (DIC) method will be employed to analyze crack growth in different test parameters, including applied loading, initial notch depth/position, and bending angle/direction. Finally, the crack growth rates obtained from different combined factors will be compared to previous works on longitudinally oriented NNpH-CF to uncover the crack growth mechanism in C-NNpH-CF. Undoubtedly, a better understanding of C-NNpH-CF crack propagation would greatly reduce rupture rates and pipeline companies' costs.

6. 2 Material and experimental methods

This study used a 16" API-5L Gr. X-52 pipe with a wall thickness of 9.2 mm, which was taken from a pipeline that had experienced near-neutral pH CF in the past. It was observed that C-NNpH-CF mainly occurred near areas where bending was an issue [10]–[12], [24], so bending was considered a significant factor in causing axial residual stresses, which contributed to C-NNpH-

CF in the field. As shown in Figure 3-1 (chapter 3), the tensile properties of the pipeline steels used in the study were determined according to ASTM Standard E8. The yield stress (at 0.2% offset strain) and ultimate tensile stress of this pipe were measured to be 356 MPa and 561 MPa, respectively.

Long samples were extracted from the pipe using electrical discharge machining (EDM). Three reduced gauge sections (80 mm × 20 mm × 9.2 mm) with artificial through-thickness notches were designed to evaluate different parameters. The sections were bent at different degrees in a manner that ensured both the inner and outer surfaces remained intact since cold working, such as machining, can change residual stress distribution. Two bending angles of 10 and 20 degrees were designed to simulate cold bending in the field. Cold bending, a factor contributing to this type of cracking, often arises during pipeline construction or due to in-service issues associated with geohazards or soil movement. This bending process introduces axial stress throughout the entire bent section of the pipe. Combined with cyclic loading caused by pressure fluctuations (an internal pressure pushes on the pipe ends and creates axial stress), it can lead to this type of cracking. It's essential to recognize that there are two distinct conditions for a bent pipe. Residual stress, which naturally self-equilibrates, results in high tensile stress on the concave side to counterbalance the substantial compressive stress on the convex side once the pipe undergoes spring back [15]. The addition of this bending axial stress to other stress sources can potentially approach or even exceed a material's yield strength [19], [15]. Research by J. Beavers *et al.* [6] highlighted that those pipelines with hoop stress levels surpassing 60% of the specified minimum yield strength (SMYS) are prone to near-neutral pH corrosion fatigue. Consequently, this study considered axial stress levels of 35% SMYS (about half the hoop stress) and 50% SMYS, with the potential addition of extra cyclic stresses to the hoop stress.

Artificial notches (of different depths) were then created on the bent parts of the samples using a milling machine to evaluate crack growth, as illustrated in Figure 3-4 (chapter 3). In order to investigate the effect of initial notch depth on crack growth, a 1 mm notch was selected since most cracks become dormant when they reach this depth [2]. An initial notch with a 0.5 mm depth was also included in the study to examine the impact of varying notch depth on crack growth. Figure 3-4 also illustrates two types of bending, inward and outward, on the outer surface of the pipeline, which will be further explored later (X is the number of the long sample, 1, 2, 6-8: position of notches in inward direction, 3-5: position of notches in outward direction).

A specific cell containing C2 solution (synthetic field soil solution) was prepared for testing with gas sparging (5% CO_2, 95 % N_2). The final pH of the solution is 6.3 ± 0.1, which is consistent with a near-neutral pH environment. After a 12-day static corrosion test (introducing and stabilizing the NNpH environment in the samples), cyclic loading with various axial loads was conducted on an Instron 8516 servo-hydraulic testing machine controlled with Wavemaker Runtime software for 45 days or until there was a cracking failure. All experiments maintained a frequency of 0.001 Hz and a stress ratio R (Min stress/Max stress) of 0.1. The effect of the mentioned parameters on the crack growth mechanism was evaluated according to a plan outlined in Table 3-2 (chapter 3). Long sample No. 2 was employed as an additional test to verify the data's consistency, complementing long sample No. 1. Cyclic loading was also applied to the non-bent sections with 0.5 mm and 1 mm initial notches at 35% and 50% SMYS. During these tests, cyclic loading was applied to reference samples without any other sources of axial stress, such as axial bending stress. All other test parameters (environment, cyclic loading pattern, *etc.*) were the same as for the previous test on long samples 1 to 8. These notches were designated as follows: A1 (0.5

mm, 35%), A2 (1 mm, 35%), B1 (0.5 mm, step 1: 35%, step 2: 50%), and B2 (1 mm, step 1: 35%, step 2: 50%).

After each cyclic loading test (45 days or fracture, whichever occurred first), the long sample was rinsed with acetone and dried with hot air to prevent further corrosion. A precision saw with a diamond-coated wafer blade cut each notch into two samples. One-half was analyzed for cross-sectional characterization, including crack location, depth, and morphology. The other half was fractured to examine fractographic morphology and crack growth behaviour. The fracture surface was treated with a solution containing 6N HCl + 3.5 g/L hexamethylene tetramine to remove corrosion products. Images of the fracture surface and cross-sections were taken using a Zeiss Sigma 300-VP FESEM. The crack growth rate was calculated based on the crack growth depth and the number of cycles.

The same long samples were used for the digital image correlation (DIC) technique, which involved bending at 10- and 20-degree angles. The samples were prepared for this technique by applying a white layer and a black speckle pattern. Then, the specimens were loaded on an MTS tensile testing machine to a maximum force equivalent to 35% and 50% SMYS of X52, and force and displacement were recorded during the test. Sequential images were captured at specific force increments (100 N) for DIC measurements. Vic-3D 9, a commercial DIC software, was used to analyze the images. Strain maps were derived, and based on the stress-strain curve, stress values were correlated with the strain map to obtain the stress distribution.

- **Stress intensity factor analysis/ crack growth rate calculation method**

Residual stress fields (depending on their tensile or compressive nature) can accelerate or delay the environmentally assisted cracking process [25]. According to the Paris fatigue equation, crack growth under cyclic loading generally relates to the stress intensity factor range, so the growth rate

of a crack can be related simply to the maximum stress intensity factor at the crack tip for a given stress ratio [26]. This stress intensity factor is affected by residual stress fields in the material [25]. For the calculation of the stress intensity factor of longitudinally oriented corrosion fatigue cracks in near-neutral pH environments, the single-edge notched tension (SENT) [27] methodology for through thickness initial notch/ dormant crack can be used since there is no stress gradient in the depth direction of the sample. Having a stress gradient in the depth direction makes finding stress intensity factors at different positions challenging in C-NNpH-CF. As shown in Figure 6-1a, the average crack growth rate can be determined by dividing the crack depth (from the bottom of the pit to the end of the quasi-cleavage region (Stage II) in fractography images. Through the depth direction, stress would change dramatically, resulting in a considerable change in the stress intensity factor. Therefore, a new method has to be introduced to find the stress intensity factor in circumferentially oriented cracks. C-NNpH-CF fracture surface of notch No. 42 is shown in Figure 6-1a. This Figure shows the initial notch, crack growth, and final brittle fracture. Using SENT methodology, crack depth (a) is measured from the external surface to the middle of the crack growth region. In this case, the equivalent stress value should be the average stress level from the bottom of the notch (crack initiation point) to the end of the crack growth. In this way, crack depth and stress level can be considered when calculating the stress intensity factor. According to Figure 6-1b, the average stress in the depth direction can be derived from a digital image correlation strain map.

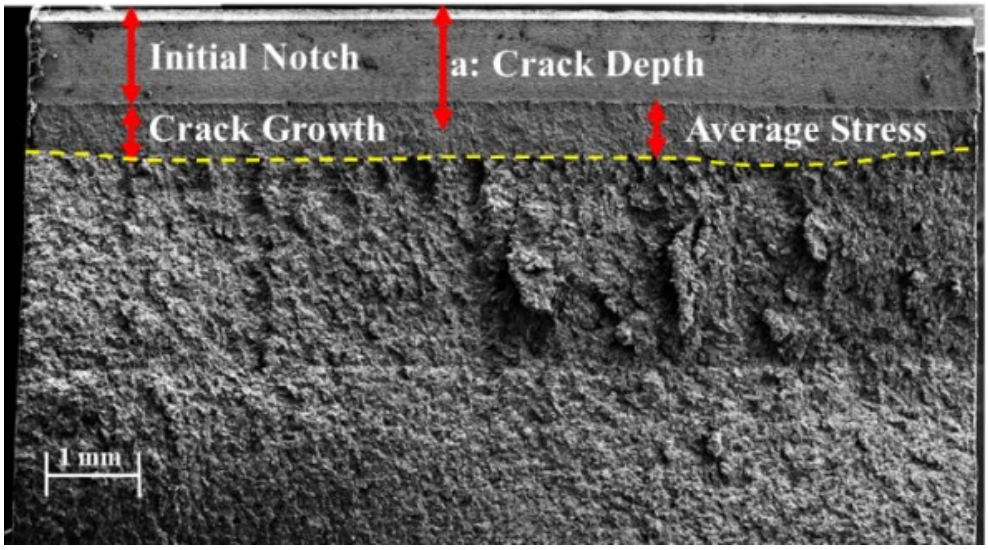

(a)

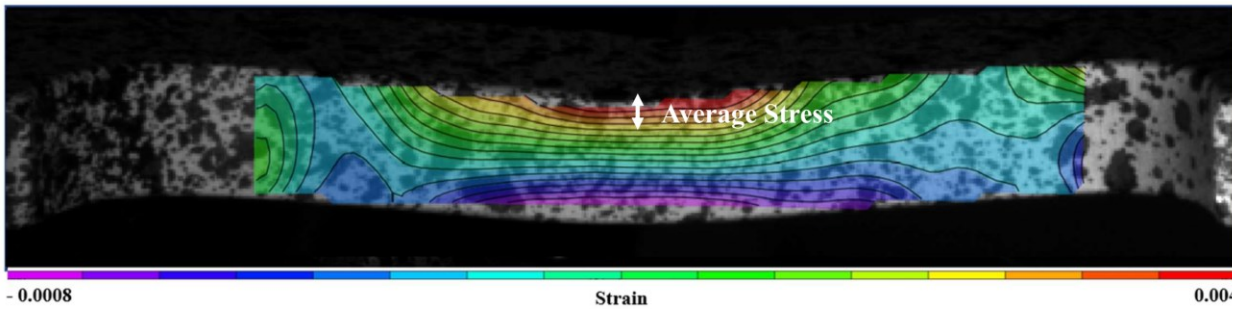

(b)

Figure 6-1 Stress intensity factor analysis based on the fractography images (a) fracture surface of notch No. 42, (b) strain map of notch No. 42

6. 3 Results

6. 3. 1 Stress distribution analysis based on the DIC method

Identifying the final stress distribution across the external surface and thickness direction of the bent gauge area from all sources of stress is the first step in evaluating corrosion fatigue in the NNpH environment. The DIC method can, therefore, be used to represent the final stress distribution of longitudinal samples. Chapter 4 explains how to use the DIC method to derive strain maps (to find stress) for bent pipelines. Using the strain map to convert strain to stress involves

defining a desired point, reading strain values from DIC export data, and then finding the stress equivalent to that strain based on the stress-strain curve (detailed data of Figure 3-1).

According to Figure 6-2, the final stress distribution in the inward (Figure 6-2a) and outward (Figure 6-2b) direction of a bend from -20 mm to +20 mm of bend centerline on an external surface of a pipeline is shown. Since crack growth depends on tensile stress distribution in the inward direction, Figure 6-2 should be considered more carefully. According to the Figure, the stress distribution is symmetrical around the bend centerline. The artificial bending process would cause a small change. Additionally, bending residual stress has a greater impact on final stress distribution than cyclic loading changes of 35% to 50% SMYS, as the final stress distribution graph resulting from a 20-degree bend angle with 35% SMYS is significantly higher than a 10-degree bend with 50% SMYS. These figures again emphasized that the bend centerline is under maximum stress (tension or compressive) as stress level at the bend centerline of gauge length with 20 degree bending angle and 50% SMYS is twice the applied loading (50 % SMYS: 180 MPa) and close to API 5L- X52 actual yield strength (356 MPa).

The stress level decreases with the distance from the bend centerline (±10 mm). By increasing this distance to ±20 mm from the bend centerline, stress levels drop dramatically. For the bent gauges to return to the straight direction, any bends at the center of the gauge length are accompanied by two bends in the opposite direction. Since the ±20 mm notch positions are closer to these bendings than the main bending at the bend centerline, their effects are considerable. Due to this, these positions experience lower stress levels than applied stress. For example, notches at the position ±20 mm far from the bend centerline in the inward direction are under the influence of tensile residual stress (20-degree bending at the centerline) and compressive residual stress (10-degree bending), which reorient the sample into the straight direction. Since it is closer to the straightening

bend with compressive residual stress, the final stress at this point is less than the applied load. It is worth mentioning that crack growth is affected by stress at the bottom of the notch, which is lower than stress on the external surface. Also, a notch can modify the residual stress pattern and allow stresses to relax, so the stresses may be less than expected without this relaxation.

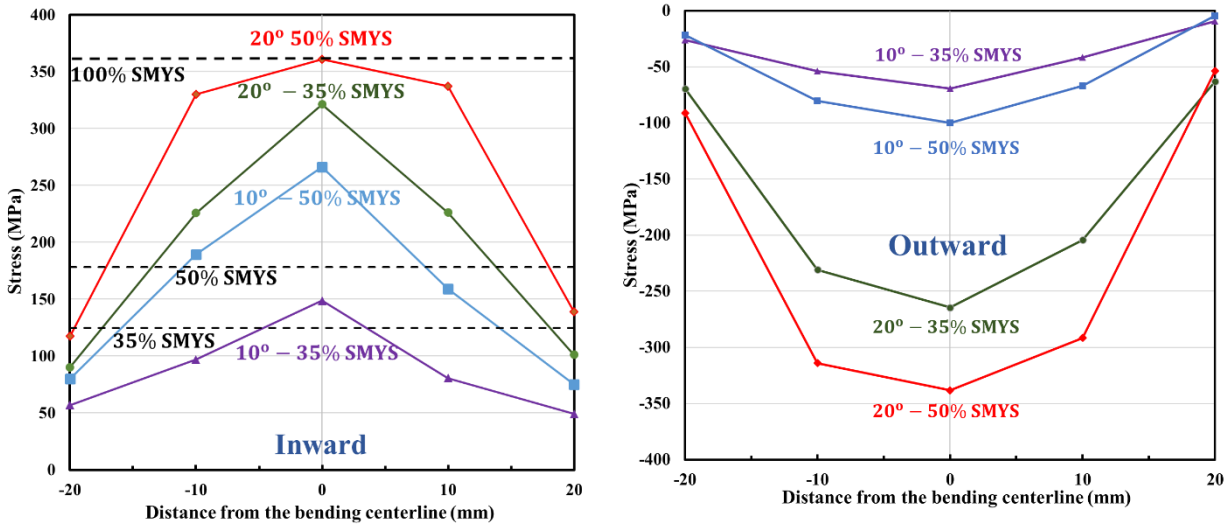

(a) (b)

Figure 6-2 Final stress distribution along gauge length (under the influence of bending residual stress and axial loading) (a) inward direction/ tensile stress, (b) outward direction/ compressive stress

The cross-sectional strain pattern of sample No.7 (10-degree bending) after 50% SMYS loading is shown in Figure 6-3a. Clearly, the pipe's external surface is under tensile stress, while the internal surface is under compressive stress. Figure 6-3b illustrates how strain on the external and internal surfaces changes with applied loading. On the gauge, there is no strain in the whole material before applying load, but as the load increases, the strain in these two surfaces turns in opposite directions.

Figure 6-3c shows the stress distribution in the thickness direction following 35% and 50% SMYS loading of the 10-degree bend gauge length at the bend centerline. In the absence of cold work residual stress, there should be no stress distribution in the thickness direction because the entire

material carries the same load at each point. Cold work bending, however, creates a stress distribution across all bending directions (width, length, and thickness). Type I residual stresses, which vary continuously over at least several grain diameters, must be self-equilibrated so that they sum to zero in any direction over the area of the cross-section, *i.e.,* the net force on a free-standing stationary object must be zero unless it is being accelerated (Newton's first law). Therefore, tensile residual stresses on the external surface are associated with the negative residual stress on the internal surface [22].

By comparing the stress distribution profiles of 50% SMYS and 35% SMYS on graph 6-3c, it is possible to see how cyclic loading affects crack growth. Firstly, 50% SMYS cyclic loading results in higher tensile stress levels on the external surface. To achieve a sufficient level of compressive stress on the internal side of the sample, 50% SMYS has a higher stress reduction rate in the thickness direction, *i.e.,* the highest tensile residual stresses are accompanied by the highest negative residual stress gradient in the depth direction [18]. As a result of equilibration in the thickness direction, the neutral plane under 50% SMYS is closer to the internal surface than under 35% SMYS. Since the crack growth direction is perpendicular to the loading direction [28], stress distribution in the thickness direction and its effects on the stress intensity factor will be discussed in more detail in the next sections.

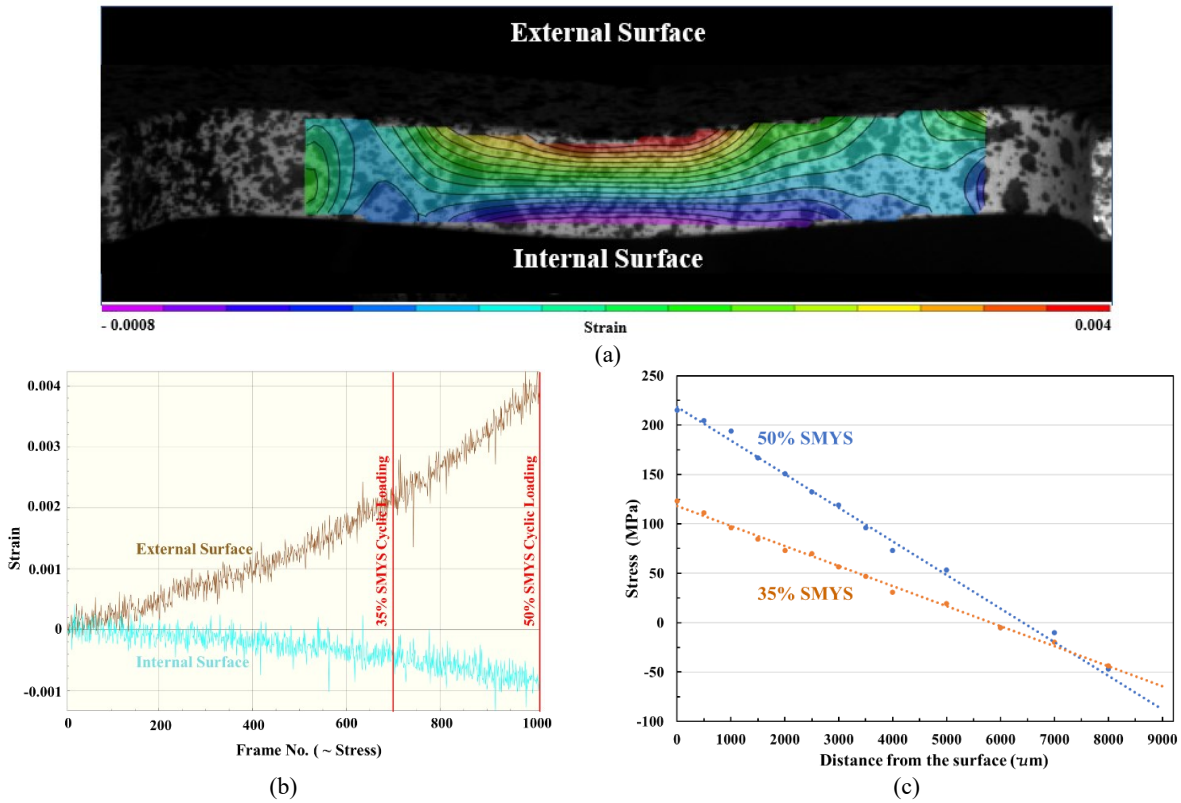

Figure 6-3 (a) Cross-sectional strain pattern of sample No.7 (10-degree bending) after 50% SMYS loading, (b) Strain changes on the external and internal surfaces with increasing applied loading, (c) Stress distribution in the thickness direction (10-degree bending)

6. 3. 2 Crack initiation and growth under the influence of different stress conditions (compressive residual stress, tensile residual stress, no residual stress)

- **Crack initiation and growth of the outwardly bent specimen**

Based on the fractography images, Table 6-1 summarizes net crack growth, specifically in the outward bending direction (X3, X4, and X5, where X is the number of the longitudinal samples from 1 to 8). According to Figure 6-2b, all notches positioned in the outwardly bent gauge lengths experience compression residual stress on the surface (and at the bottom of the notch) due to two distinct sources of compressive stress: residual compressive stress from bending (after spring back) and compressive stress from cyclic loading. Crack growth is generally suppressed by compressive residual stress, while it is promoted by tensile residual stress. Therefore, almost all notches in these

gauge lengths do not exhibit crack initiation. Notch 64 was the only exception to the mentioned expectation where the maximum level of compressive stress exists at the bottom of the notch due to 20-degree bending angle, bending centerline position and 50% SMYS cyclic loading. The tiny initiated crack reflects the formation of microstructurally short cracks caused by galvanic corrosion, as detailed in Ref [29]. Despite this, mechanically driven crack growth cannot occur beyond a critical distance in the absence of a positive high tensile residual stress gradient [18], [26], [30]. Therefore, circumferential corrosion fatigue cracks are not a concern in the outward direction of bent pipelines in any realistic set of testing parameters of normal pipe operation, including bending angle, applied loading, and notch depth.

Table 6-1 The crack growth in various notches under the influence of different testing parameters (Outward bending direction)

Long Samples No.	Outward bending angle (degree)	Initial notch depth (mm)	Max. applied stress (% SMYS)	Position (mm)	Notch No.	Net crack growth (mm)	Test duration (hour)
1	20	1.0	50	-20	13	0	208
				+20	15	0	208
				0	14	0	208
2	20	1.0	50	-10	26	0	224
				+10	28	0	224
				-20	23	0	224
				+20	25	0	224
				0	24	0	224
3	10	1.0	50	-20	33	0	848
				+20	35	0	848
				0	34	0	848
4	20	1.0	35	-20	43	0	325
				+20	45	0	325
				0	44	0	325
5	10	1.0	35	-20	53	0	1075
				+20	55	0	1075
				0	54	0	1075
6	20	0.5	50	-20	63	0	354
				+20	65	0	354
				0	64	0.005	354
7	10	0.5	50	-20	73	0	997
				+20	75	0	997
				0	74	0	997
8	20	0.5	35	-20	83	0	1283
				+20	85	0	1283
				0	84	0	1283

- **Crack initiation and growth of non-bent specimen**

Table 6-2 shows crack initiation would not have occurred if the only source of stress in the non-bend Section was 35% or 50% SMYS axial cyclic loading on notches A1, A2, B1, and B2. Although only a short crack around 60 μm was observed on the cross-section of notch B1 (1 mm initial depth, 35 and 50% SMYS cycling loadings), this microstructurally initiated crack is associated with pitting. This indicates substantial dissolution/corrosion, resulting in dormancy and inadequate driving forces to advance crack growth by other mechanisms, such as fatigue or hydrogen-enhanced fatigue. Since it is designed to operate under pressures to achieve a hoop stress below 80% SMYS, corresponding to an axial stress of 40% SMYS, an axial stress arising from internal operating pressure alone would not be able to cause circumferential corrosion fatigue cracking. This confirms the observation of the necessity of other sources of axial tensile stress besides operating stress (such as residual axial stress from girth welding, bending, geohazards, *etc*.) to cause C-NNpH-CF cracking.

Table 6-2 The crack growth in various notches under the influence of different testing parameters (non-bent section)

Notch No.	Initial notch depth (mm)	Step 1		Step 2		Net crack growth (mm)
		Applied stress, % SMYS	Test time (hour)	Applied stress, % SMYS	Test time (hour)	
A1	0.5	35	1080	N/A		0
A2	1.0					0
B1	0.5			50	1080	0
B2	1.0			50	1080	0.06

- **Crack initiation and growth of the inwardly bent specimen**

A breakdown of net crack growth is provided in Table 6-3 based on fractographic images, specifically in the inward bending direction with tensile residual stress. In order to better understand these parameters, the following section explores how they influence crack growth.

Table 6-3 The crack growth in various notches under the influence of different testing parameters (inward bending direction)

Long Samples No.	Inward bending angle (degree)	Initial notch depth(mm)	Max. applied stress (% SMYS)	Position (mm)	Notch No.	Net crack growth (mm)	Test duration (hour)
1	20	1.0	50	-10	11	0.95	208
				+10	12	0.5	208
				-20	16	0	208
				+20	18	0	208
				0	17	2.6	208
2	20	1.0	50	-10	21	1.1	224
				+10	22	2.4	224
3	10	1.0	50	-10	31	0.25	848
				+10	32	2.8	848
				-20	36	0.2	848
				+20	38	0	848
				0	37	2.2	848
4	20	1.0	35	-10	41	0.65	325
				+10	42	0.6	325
				-20	46	0.045	325
				+20	48	0	325
				0	47	2.7	325
5	10	1.0	35	-10	51	0.015	1075
				+10	52	0.02	1075
				-20	56	0.008	1075
				+20	58	0.006	1075
				0	57	0.13	1075
6	20	0.5	50	-10	61	0.11	354
				+10	62	0.12	354
				-20	66	0	354
				+20	68	0	354
				0	67	2.1	354
7	10	0.5	50	-10	71	0.075	997
				+10	72	0.08	997
				-20	76	0.04	997
				+20	78	0.04	997
				0	77	0.2	997
8	20	0.5	35	-10	81	0.2	1283
				+10	82	0.31	1283
				-20	86	0.04	1283
				+20	88	0.04	1283
				0	87	2.6	1283

The crack growth rate (inward direction) is shown in Figure 6-4a for all notches with a 1 mm initial depth under various parameters, while in Figure 6-4b, the same graph is shown for all notches with a 0.5 mm initial depth. The first feature this Figure provides is the impact of stress distribution in the length direction, *i.e.*, the maximum crack growth is at the bend centerline of any sample, regardless of other parameters, like bending angle, cyclic loading, and initial notch depth. The maximum crack growth rate is meaningful since the bend centerline is influenced by the highest tensile residual stress (on the surface). As the distance from the bend centerline increases, the residual stress decreases, resulting in less crack growth, where notches 20 mm from the bend centerline show approximately the minimum crack growth. Two sole dark orange points in Figure 6-4a represent the crack growth rate for notches of ±10 mm far from the bend centerline of sample No. 2. This sample was designed with the same parameters as sample No. 1 (20°, 50% SMYS, 1 mm) to ensure test consistency. This figure shows that the crack growth rate in these two notches is close to those at sample No. 1 with the same position and testing parameters.

On the other hand, some of these notches 20 mm far from the bend centerline show no crack growth. In general, samples No. 1 (20°, 50% SMYS, 1mm), 4 (20°, 35% SMYS, 1 mm), 6 (20°, 50% SMYS, 0.5 mm) and 8 (20°, 35% SMYS, 0.5 mm) do not show any crack growth at notches positioned 20 mm away from the bend centerline due to the stress level (Figure 6-2a), which emphasizes that these notches are closer to straightening bends, so they have less stress than applied cyclic loading. Notches No. 36 (10°, 50% SMYS, 1 mm, -20 mm) and 46 (20°, 35% SMYS, 1 mm, -20 mm) exhibit small crack growth rate, though notches No. 38 (10°, 50% SMYS, 1mm, +20 mm) and 48 (20°, 35% SMYS, 1 mm, +20 mm) do not show the same pattern (there is no sign of crack initiation or growth). This would be related to the shape and depth of the handmade notches.

It should be mentioned that notches at the bend centerline of samples 1 (20°, 50% SMYS, 1 mm), 4 (20°, 35% SMYS, 1 mm), 6 (20°, 50% SMYS, 1 mm) and 8 (20°, 35% SMYS, 0.5 mm) failed before the end of the test period (45 days). Therefore, these notches show higher crack growth rates than others. Just one inconsistency is found in notch No. 32, located 10 mm from the bend centerline of long sample No. 3 (10°, 50% SMYS, 1 mm). This notch failed during the test despite having a lower stress level than notch No. 37 at the bend centerline. In Figure 6-2a, notches 32 and 37 have 116 MPa and 152 MPa stress levels on their external surfaces. Because sample bending and notch-making were manual processes, this inconsistency could be acceptable since small changes in the bending angle and initial notch depth can impact the stress and stress intensity factors at the bottom of the notch. For instance, R. Fessler *et al.* [15] reported that a bend angle as small as 1 or 2 degrees can produce stresses of about 70 to 140 MPa. Apart from notch No. 32, all other notches show a consistent relationship to the stress distribution in the length direction of the gauge sample under bending. The present paper avoids discussions of rapid crack growth in Stage III and plastic collapse on failed notches (17, 47, 67, and 87: notches at the bend centerline of samples 1, 4, 6 and 8). Since other notches were in Stage II (steady crack growth), that part of crack growth in failed notches related to steady crack growth in Stage II was evaluated and compared.

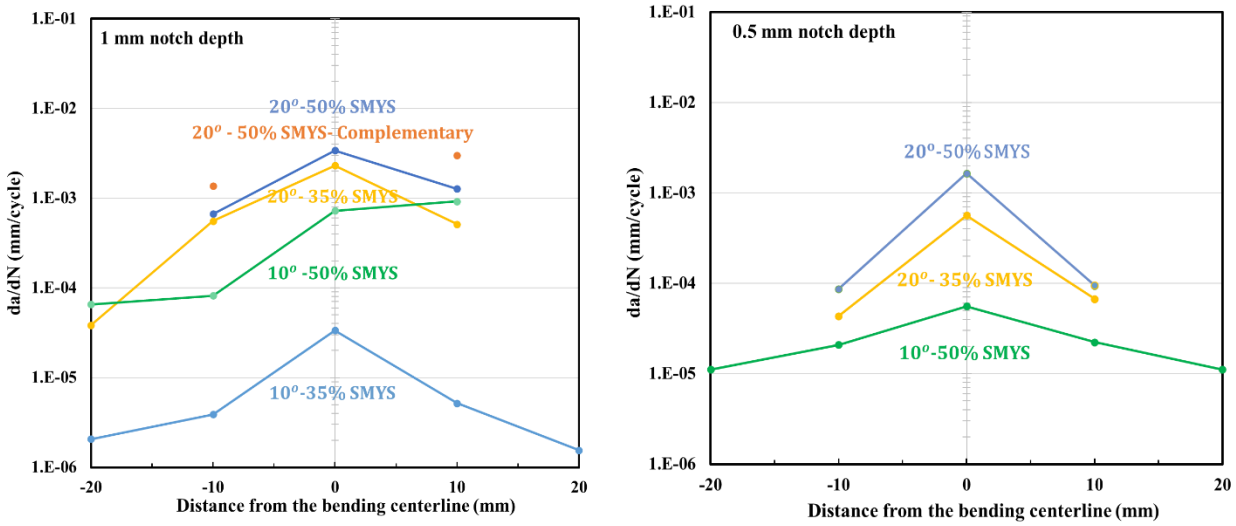

(a) (b)

Figure 6-4 Crack growth rate for various test parameters (a) 1 mm initial depth (b) 0.5 mm initial depth

According to Figure 6-4, bending angle has a greater effect on final stress distribution and crack growth rate than cyclic loading. For example, samples No. 1 and 4 (20-degree bending, 35/50% SMYS) show more crack growth in all positions (bend centerline, ±10 mm, ±20 mm) rather than samples No. 3 and 5 (10-degree bending, 35/50% SMYS).

- **Crack growth characteristics of the inwardly bent specimen**

As shown in Figure 6-5, crack growth at both corners (points A and B) of initial notch No. 41 (20-degree bending, 35% SMYS, 1 mm initial depth, -10 mm from bend centerline) is seen in cross-section images at higher magnifications. Sample No. 4 (20°, 35% SMYS, 1mm) failed after approximately 14 days (1173 cycles) in notch No. 47, which has the highest tensile stress. As a result, the test was stopped, and long samples, including all notches, were extracted. Hence, this paper focuses on crack growth for notches with long cracks where fracture mechanics may apply. Due to the presence of stress cells between corners with higher levels of tensile stress in comparison with another area with lower tensile stress levels, crack initiation has occurred at notch corners (stress concentrators). Even though crack initiation happened at both corners, the first one

achieving the desired depth/ stress intensity factor would have this chance to grow more, while the second one has stopped growing. Therefore, Zone A in Figure 6-5 shows deeper crack growth than Zone B. It is likely that notch No. 41 crack would have grown more and cracked to failure in zone A if notch No. 47 had not failed beforehand. In contrast to high pH SCC with intergranular microcracks in narrow crevices [31]–[35], near-neutral pH CFs have transgranular microcracks with wider crack crevices based on crack growth path in Figure 6-5 [17].

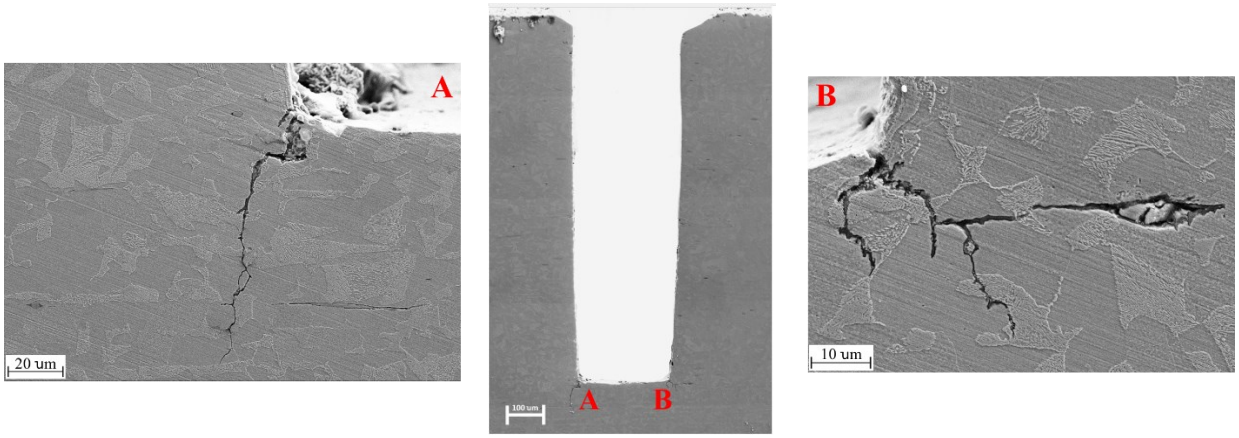

Figure 6-5 Cross-section analysis of notch No. 41 (20-degree bending, 35% SMYS, 1 mm initial depth, -10 mm from bend centerline)

The fractography image of notch No. 23 (20°, 50% SMYS, 1 mm, -10 mm from bend centerline) after fracturing in liquid nitrogen is shown in Figure 6-6a. There are three main regions in the fractography image. A milling machine created a notch in the upper region resembling a dormant crack of 1 mm depth. A quasi-cleavage fracture morphology dominates the fracture surface in the middle regions of Figure 6-6a. A faceted, transgranular plane (quasi-cleavage) strongly indicates hydrogen embrittlement during crack growth. In Figure 6-6b, the striations were the direct physical evidence of crack growth caused by corrosion fatigue [36], [37]. These striations ran perpendicular to the growth direction of macroscopic fatigue cracks [37]. By measuring the striations' inter-spatial distances along fracture surfaces using a line intercept method and dividing the total

distance by the number of visible striations, the average crack growth can be determined in the quasi-cleavage region at any point in depth. Finding pockets of ductile dimples [37] was also possible, especially closer to the boundary between the quasi-cleavage region and the final brittle fracture at liquid nitrogen (Figure 6-6c). This is related to the short time for general corrosion to occur in this last region, so the surface is less corroded.

In Figure 6-6c, the bottom section shows characteristic features of a brittle fracture, including cleavage, transgranular fracture, and secondary cracks [38]. Dynamic loading or loading at low temperatures usually causes this transgranular brittle fracture. A cleavage crack propagates transgranularly along well-defined low-index crystallographic planes. Cleavage, which is characterized by faceted crack paths and river line patterns, occurs primarily along the <100> cubic planes in iron and ferritic steels. The transgranular crack changes its propagation direction through grain boundaries to comply with a new crystal orientation [39]. The fractographic images were used to determine the crack growth rate in the corrosion fatigue region based on the crack depth and the number of cycles during the test.

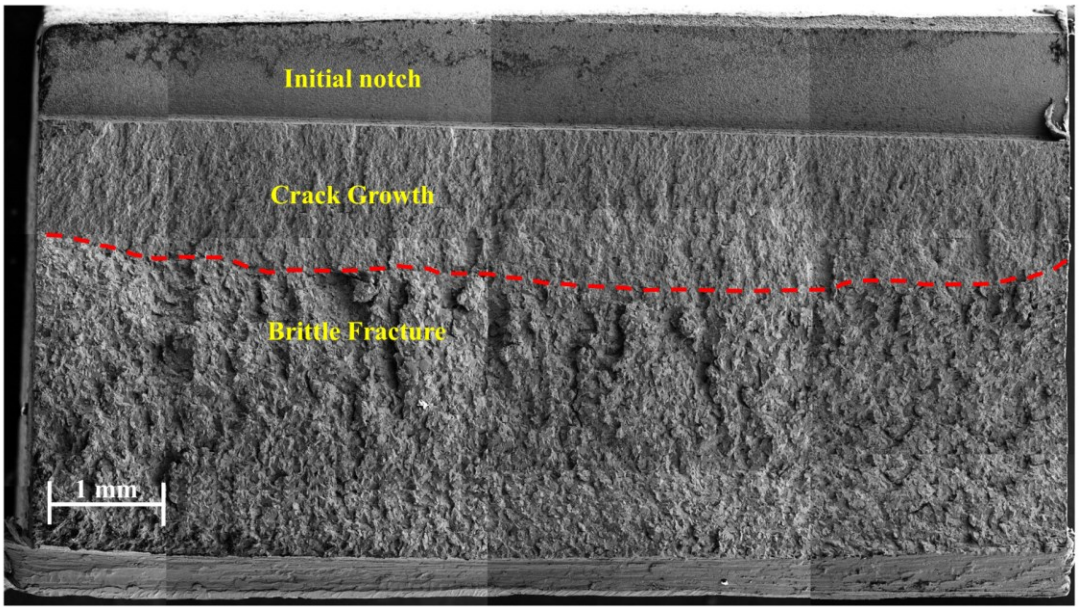

(a)

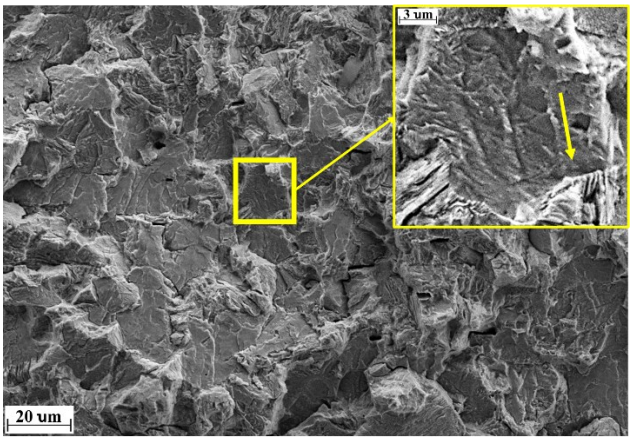

(b)

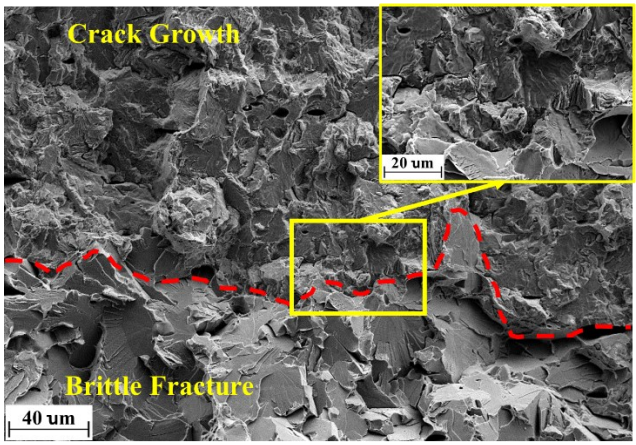

(c)

Figure 6-6 Fractography analysis of notch No. 23 (20-degree bending, 50% SMYS, 1 mm initial depth, 10 mm from bend centerline) (a) fracture surface including an initial notch, crack growth region, and final fracture (b) quasi-cleavage region (c) boundary between quasi-cleavage and brittle fracture regions

Figure 6-7a shows the fractography image of notches No. 47 (20°, 35% SMYS, 1.0 mm initial depth notch, bend centerline) fractured during the test and after 325 hours. Figure 6-7b depicts fractography morphologies at various positions along the crack growth path marked in Figure 6-7a. In the presence of hydrogen, the fracture surface exhibited quasi-cleavage, characterized by stepped surfaces and river patterns, along with striations. While quasi-cleavage is technically

defined as fractography resembling cleavage, it is acknowledged that the fracture plane may not necessarily align with the known cleavage plane. A possible explanation for the formation of such planar and wide striations is offered by a model based on hydrogen-enhanced localized plasticity (HELP) [40], [41]. Crack growth, as indicated by river lines, progresses from top to bottom [42]. In the depth direction, brittle fracture zones were associated with localized regions of ductile failure, *i.e.*, void coalescence, during Stage III (rapid crack growth) and preceding the final fracture (plastic collapse). It is postulated that these regions of ductile failure originated due to high localized strain rates, connecting non-planar regions of brittle fracture, unlike Stage II. Specifically, the localized strain rate at a propagating crack front is sufficiently high to impede diffusion-controlled hydrogen embrittlement mechanisms [43]. A band of tearing, characterized by well-defined dimples, between striated areas is also possible under high loads [44]. Despite extensive areas of flat fracture surface (Stage II and the initial part of Stage III, quasi-cleavage), some ductile fractures exhibited shear lips at the specimen's bottom. Ductile fractures involve significant plastic deformation, with the fracture mechanism primarily driven by micro void coalescence originating at metallic or non-metallic inclusions [43]. Nevertheless, certain studies [45] suggested that hydrogen might expedite this final stage of failure by accelerating extreme plastic processes.

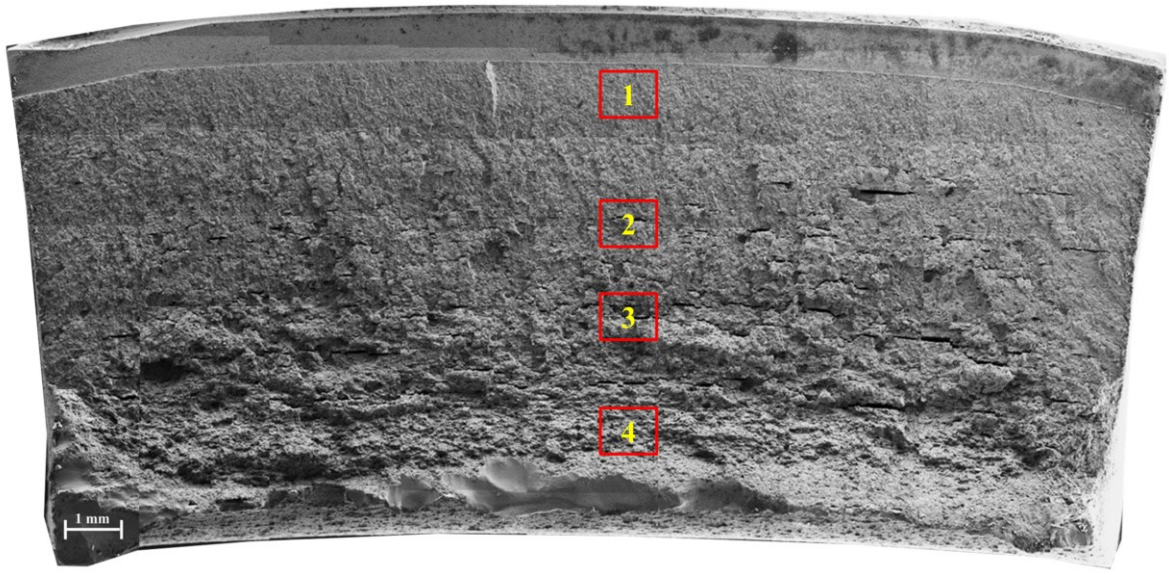

(a)

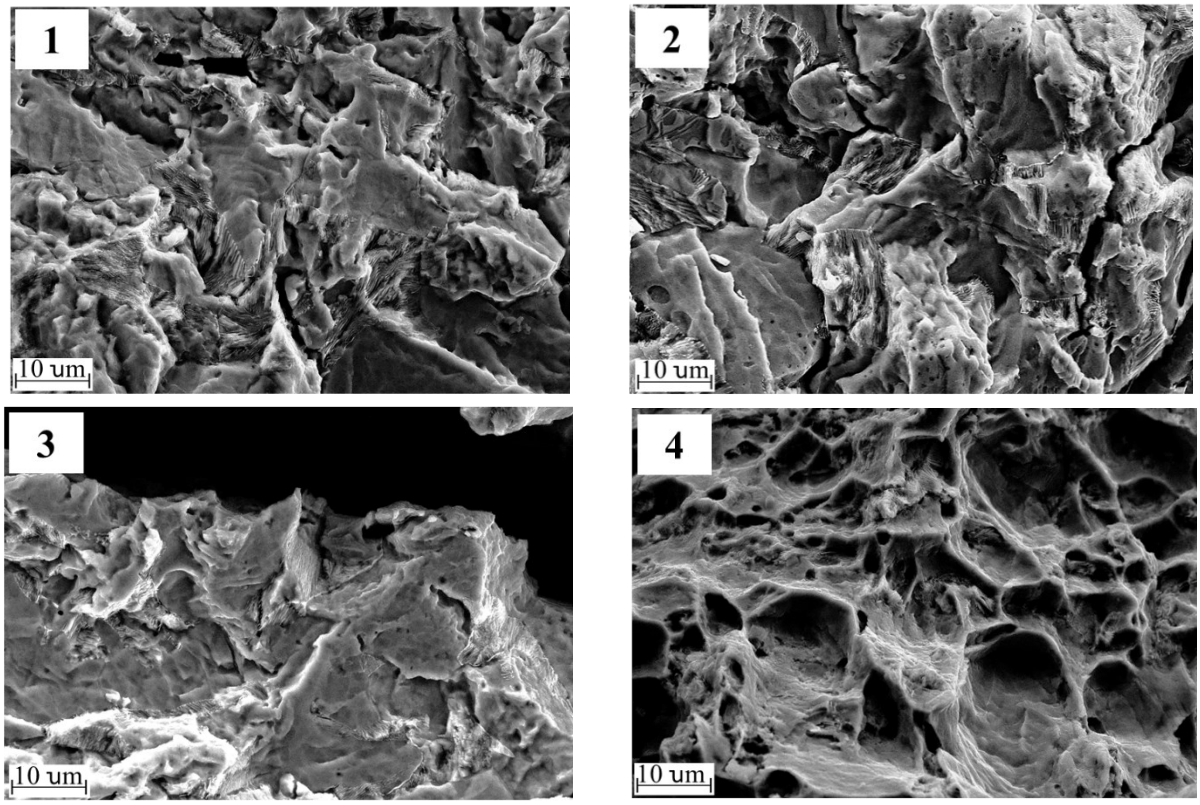

(b)

Figure 6-7 SEM images showing morphologies from various positions along the crack growth path, (a) fractography image of notch No. 47 fractured during the test, (b) fractography images from various positions marked in (a)

6. 4 Discussion

6. 4. 1 Circumferential crack growth mechanism at the bottom of the notch

Various models have been developed to predict crack growth in pipeline steels in near-neutral pH environments. Many research studies [23], [46] have developed crack tip strain rate models based on the assumption of SCC, but now, the dependence of crack growth on mechanical cyclic loading has become the more accepted theory. In fact, the growth of cracks in pipeline steel exposed to a near-neutral pH environment has not been observed under monotonic loading, even though crack initiation is possible [46]. If loading is switched to a static hold, even an active crack will stop growing [23]. In addition, the original superposition model, which considers the combined effect of SCC and fatigue cracking, does not fit the data reported from the field due to its inadequate consideration of environmental conditions [23], [46].

In general, crack growth in Stage II is strongly influenced by mechanical driving forces and environmental conditions, and crack growth is more likely to occur at locations with higher residual tensile stresses and more diffusible hydrogen in the material surrounding the crack tip [23], [47]. In fact, crack sharpening and growth may be caused by the segregation of atomic hydrogen in the hydrostatic zone (the highly deformed areas ahead of the crack tip). Hydrogen-induced microcracks (HICs) can initiate when the plastic zone is subjected to high hydrostatic stresses. These microcracks can connect with the main crack, extending the crack and sharpening the blunt tip [18], [22]. It is common for the above events to repeat, especially when there is a large fluctuation in pressure. It should be mentioned that the stress fields at the bottom of pits/ dormant cracks at the time of cracking determine whether cracking can occur, not the residual stress state at the location before testing [30]. J. Toribio [25] reported that these stress fields can enhance or delay the environmentally assisted degradation process (dependent upon their tensile or

compressive nature) since they alter the stress state near the element surface and influence hydrogen entry and diffusion toward the fracture zone. As shown in Figures 6-6 and 6-7, hydrogen-enhanced localized plasticity (HELP) may be responsible for cracking behaviour in near-neutral pH environments. In regions of high hydrogen concentration, dislocation motion is less restrained, and flow stress is lower, so dislocations move at stress levels below those normally required for plastic deformation. The crack propagates along the slip plane as a result of the localized slip. In addition, hydrogen and cyclic loadings interact synergistically in HELP mechanism [48]. Y. Ogawa [41] reported that the quasi-cleavage fracture surface was formed near the crack initiation site, as crack growth accelerated even in low-stress intensity factor ranges.

According to the results presented in the previous section, circumferential near-neutral pH corrosion fatigue crack growth follows the same parameters as longitudinal corrosion fatigue crack growth. However, circumferential cracking is characterized by axial tensile stresses that exceed normal hoop stress due to diverse sources of axial stress, including in-service damage/ geohazards [6], or residual stresses from pipe manufacturing and construction (e.g., bends), the subject of this study. Furthermore, according to Figure 6-3, circumferential cracking under axial bending is marked by a stress gradient in the thickness direction. Contrary to longitudinal corrosion fatigue cracking, where hoop stress creates uniform stress across the pipe's thickness, circumferential cracking involves residual tensile stresses on the outside surface accompanied by compressive stresses on the inside (Figure 6-3a in the inward direction). Based on Figure 6-3c, a higher stress level on the external surface increases the stress reduction rate in the depth direction. Therefore, the stress state at the bottom of the pit/ dormant crack during the crack growth phenomenon is governed by the final stress distribution under the influence of bending residual stress (bending angle, bending radius) and the axial cyclic loading from internal pressure fluctuation and the

bending stress occurring in these tests. Of course, with crack propagation, there is redistribution and relaxation of the residual stresses.

Moreover, in contrast to longitudinal cracking, which can potentially occur anywhere along the length of the pipeline, circumferential cracking tends to only occur in areas where additional sources of axial loading exist, such as bending or girth welds. In addition to prioritizing inspections in these regions, inspectors should recognize that certain sources of axial loading, like bending, can generate stress distributions that span both the pipe's length and diameter. Identifying critical points with the highest susceptibility to circumferential cracking is essential and will be a focal point of discussion in the upcoming section.

6. 4. 2 Effect of residual stress on crack growth

It is essential to characterize the mechanical loading conditions during pipeline operation in detail to develop appropriate crack growth rate and service life prediction models [6], [17]. In the case of circumferential cracking, the source, type, and value of axial loading from various sources should be considered, too [23].

As discussed before, the following conditions must be met for continuous growth beyond Stage I, causing steel pipelines to fail prematurely [23]: sufficient mechanical driving force, tensile residual stress, and diffusible hydrogen, which can synergistically interact to lower the threshold for Stage II crack growth while enhancing Stage II crack growth rates. When a pipe surface has high tensile residual stresses, crack colonies can develop, but if there is high diffusible hydrogen at particular locations in a crack colony, repeated crack growth is believed to be possible [21], [22]. Compared to hydrogen generated by general corrosion or cathodic reaction on the pipeline surface, hydrogen produced by corrosion at the crack tip is secondary in terms of crack growth. The crack tip's dissolution rate in Stage II growth is extremely slow [22], [23]. According to X. Xing *et al*.,

hydrogen atoms diffuse to the crack tip during loading and unloading and form hydrogen-rich regions. Indeed, a region at the tip of sharp cracks experiences high hydrostatic tensile stress, and hydrogen migrates to this region and affects the material's properties. Due to the brittle nature of the steel in regions of hydrogen accumulation, cracks can propagate once hydrogen-rich regions form [49], [50] since a sufficient quantity of hydrogen in the high hydrogen region can modify mechanical behavior based on the HELP mechanism. The crack tip becomes blunted after passing through hydrogen-rich regions and then restarts to accumulate hydrogen atoms [50]. While many mechanisms have been proposed for explaining hydrogen-induced steel ductility loss (hydrogen embrittlement), it is generally assumed that atomic hydrogen in steel will increase crack propagation because hydrogen atoms will lower the strain energy threshold for unstable de-bonding [22], [50]. Therefore, as steel is tensioned, hydrogen diffusion to the region increases, and higher stress is better for hydrogen charge [50].

Figure 6-2 presents the stress distribution along the gauge length under different testing conditions, encompassing bending angle, cyclic loading, and initial notch depth. Additionally, Figure 6-4 illustrates the crack growth rate across various test parameters. A comprehensive technique encompassing all these parameters is required to establish correlations between these factors and the crack growth rate. For instance, depending on the residual stress field, the maximum stress intensity factor and, consequently, crack growth rate may increase or decrease with crack depth [30]. In the context of longitudinal corrosion fatigue, as a crack grows, the mechanical driving forces, represented by the stress intensity factor, tend to increase, which would logically lead to an acceleration in the crack growth rate [2]. However, circumferential corrosion fatigue introduces a more intricate scenario. In Stage II, two opposing factors affect the stress intensity factor as the crack progresses through the depth direction. While greater depth does indeed result in higher

stress intensity factors, it is important to note that there is a reduction in residual tensile stress as depth increases. However, the axial stress will increase because of the reduced cross-section. In fact, it is critical to have considerable residual tensile stress as the crack to bring about initiation, and if this residual stress is relaxed by cracking additional tensile stress is needed to reach a critical stress intensity factor for corrosion fatigue. But as the crack gets longer, even though the residual stress is relieved by the cracking, this is balanced in stress intensity because the crack is longer. Therefore, expressing the growth rate in terms of da/dN as a function of ΔK in Figure 6-8 could serve as a suitable approach for discussing the impact of the various mentioned parameters on circumferential crack growth [46].

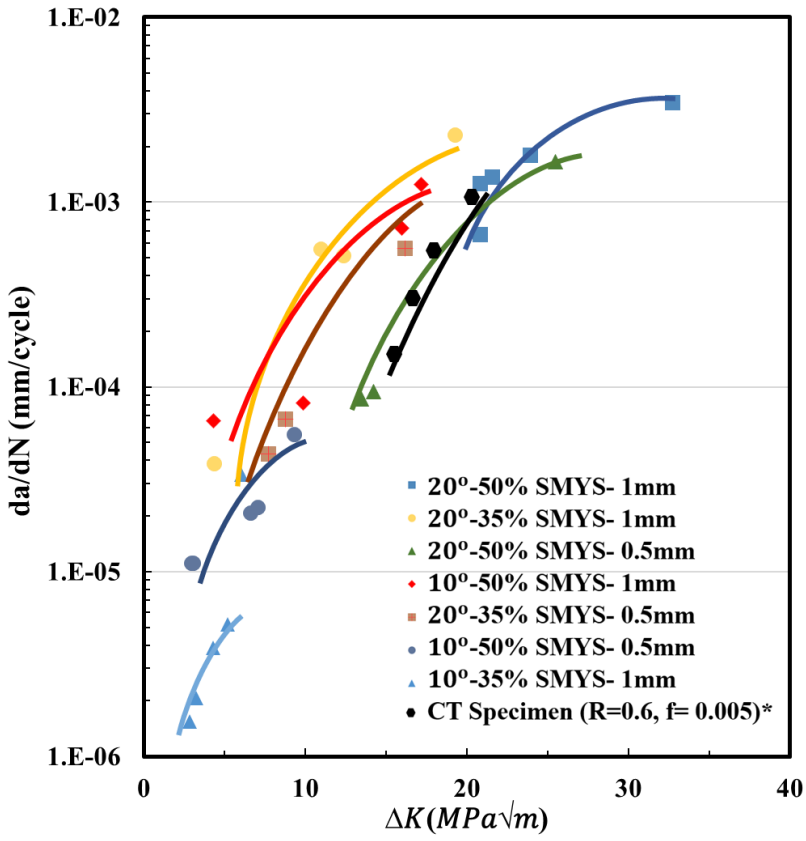

Figure 6-8 Circumferential crack growth rate da/dN as a function of ΔK obtained from corrosion fatigue testing in various experimental parameters, in comparison with Compact Tension (CT) specimen derived from Ref. [46]

Figure 6-8 reveals a general trend where the crack growth rate increases with an escalation in the stress intensity factor range. As mentioned earlier, a higher stress intensity factor range signifies greater hydrogen diffusion to the crack tip during the load cycle, creating hydrogen-rich regions that make the material more susceptible to corrosion fatigue. Despite parameter variations such as bending angle, notch position, initial notch depth, and axial cyclic loading, this trend holds true across all graphs. One notable observation is that a 20-degree angle leads to a higher crack growth rate, regardless of axial loading and the initial notch position or depth. Also, notch No. 17, characterized by a 1 mm initial notch depth and a 20-degree bend at the centerline under 50% cyclic loading (located in sample No. 1), exhibits both the maximum crack growth rate and the highest stress intensity factor range.

In contrast, all notches associated with sample No. 5, featuring a 10-degree bend and 35% SMYS with an initial notch depth of 1 mm, exhibited the lowest stress intensity factor range and crack growth rate. This represents the least severe condition, with the crack growth rate for this sample approaching the direct dissolution rate of iron at the crack tip, which is approximately 10^{-6} mm/cycle [17], [30].

The results of longitudinal NNpH-CF tests, as outlined in [46], are depicted in Figure 6-8 as a basis for comparing longitudinal and circumferential cracking. Despite variations in frequency and stress ratio between these longitudinal cracks and those investigated in this study, other fundamental characteristics of circumferential cracking outweigh these minor differences in frequency and stress ratio. In conventional laboratory tests, longitudinal crack growth rates (da/dN) are attributed to the stress intensity factor range, especially when Compact Tension (CT) specimens are used with sharp crack tips. At first glance, it is apparent that all the circumferential

crack growth rate data obtained in this investigation are situated to the left of the longitudinal crack data (higher velocity at the same ΔK).

In CT specimens, general corrosion is believed to be the primary source of lattice hydrogen, which diffuses toward the center of the specimen over a certain period and reaches equilibrium in a manner dependent on the diffusivity of hydrogen, the test temperature, and the thickness of the specimen [22]. To establish a high hydrogen concentration in the plastic zone that affects crack growth, hydrogen must be generated on the surface of the CT specimen in order to reach the equilibrium lattice hydrogen concentration in the specimen. Equilibrium requires a critical diffusion time. The hydrogen diffusion rate in steels is about 2×10^{-7} cm^2/s [22]. In contrast to CT specimens, this study employed elongated samples extracted directly from real pipes, where the initial crack depth is closer to the pipe's external surface. This proximity means that the source of hydrogen is more readily accessible to the bottoms of cracks with initial depths of 1 and 0.5 millimetres. Consequently, crack initiation becomes possible even at lower stress intensity factor ranges.

On the other hand, CT specimens start with sharp cracks, *i.e.*, there is no need for crack initiation. However, this investigation employed actual pipe samples with blunt notches (dormant cracks). Consequently, the time required for crack initiation at the base of these notches was factored into the crack growth rate calculation. As a result, when compared to sharp cracks, there was a considerable decrease in the crack growth rate.

Based on our understanding, the primary reason for circumferential cracking in a near-neutral pH (NNpH) environment occurring at lower stress intensity factor ranges is the presence of residual stress. When the loaded notched steel samples were held in the C2 solution, hydrogen was produced in a corrosive bicarbonate NNpH environment, and that hydrogen accumulated ahead of

the notch and caused embrittlement [36]. Hydrogen intake may increase further with increased applied load or stress concentration. Stress concentrations ahead of defects or cracks can cause hydrogen to accumulate at lattice defect interfaces [36]. The process of cold bending notably elevates the levels of residual tensile stress throughout the entire bend area, particularly at the bottom of the initial notch. A 12-day static corrosion test conducted before commencing cyclic loading provides sufficient time for hydrogen diffusion and accumulation at this point.

Consequently, after undergoing cyclic loading, hydrogen sources are more readily available at the bottom of the notch, and hydrogen levels are higher at lower stress intensity factors. This phenomenon represents a distinctive characteristic of circumferential crack growth mechanisms, particularly when compared to longitudinal cracking. It can be attributed to the presence of stress concentration resulting from the cold bending process that precedes crack growth.

Once more, Figure 6-8 exclusively presents the relationship between crack growth rate and stress intensity factor range in the inward direction. This is due to the absence of crack growth in the outward direction and the non-bend section under 35/ 50% SMYS axial cyclic loading.

6. 4. 3 Crack growth probability at a lower combined factor in the presence of residual stresses

To effectively analyze the experimental findings, it's essential to account for the collective influences of the maximum stress intensity factor, stress intensity factor range (the primary driving force for crack growth) and loading frequency (f), which is an environmentally sensitive factor. By incorporating these into the combined factor, it becomes feasible to create a model for circumferential crack growth that encompasses all contributing elements: crack dimensions, pressure fluctuations, axial stresses, material properties, and environmental conditions [7], [23], [46].

The combined factor $\Delta K^{\alpha} K_{max}^{\beta} / f^{\gamma} + \mathrm{h}$ is related to the critical threshold for measurable crack growth of Compact Tension (CT) specimens in environmentally assisted cracking of pipeline steel exposed to near-neutral pH environments, where A, α, β, and γ are all constants, α + β = 1, and h denotes the rate of dissolution at the crack tip. Crack growth by dissolution in Stage II is one order of magnitude smaller than crack growth by dissolution in Stage I. A factor representing the influence of corrosion on crack growth was found to be γ, which is 0.1 in the C2 solution. The effect of diffusible hydrogen in the cracking process is greatly influenced by f, the frequency of the pressure fluctuation cycle. The combined factor of 8,000 to 8,500 $(MPa\sqrt{m})^3/f^{0.1}$ has been determined as the threshold value for stage II longitudinal crack growth. This threshold value was determined using CT specimens with long, through-thickness sharp cracks [17], [23], [46] and it is known that these values vary with different geometries. The threshold should be much lower for small surface cracks that are initiated in the pipeline steels in the field, for instance, around 1,000 $(MPa\sqrt{m})^3/f^{0.1}$ [17].

Figure 6-9 shows the crack growth rates based on the combined factor for circumferential crack growth in this study compared to the longitudinal crack growth rates derived from Ref. [46]. During cyclic loading, hydrogen-rich regions form, resulting in lower stress intensity required to initiate crack propagation. Hydrogen atoms should move at a rate related to the hydrogen concentration gradient and hydrostatic stress distribution. It takes several loading cycles to accumulate enough hydrogen atoms to restart crack cleavage after a crack propagates through the hydrogen-rich region [21], [22], [50]. The initial notch depth of 1 mm shows a high crack growth rate at the same combined factor. This is due to higher stress concentrations at the bottom of 1 mm initial notches than 0.5 mm initial notches. Therefore, stress concentration at the bottom of the notch has a greater impact despite the reduced access to hydrogen sources diffused from the

external surface at the 1 mm initial notch compared to the 0.5 mm initial notch. In addition, since the combined factor takes into account max stress, stress range and frequency, a higher actual stress intensity factor range in the depth direction as a result of increasing crack depth results in more crack growth in a 1mm initial depth notch as compared to a 0.5mm initial depth notch.

Accordingly, circumferential cracking has occurred with a lower combined factor than longitudinal cracking. Several factors can contribute to this: The sharpness/bluntness of the crack tip, which would affect the threshold of the combined factor. A higher threshold value is reached when the crack tip becomes blunt. The longitudinal crack growth rate in this graph did not consider the time required to pass dormancy (Stage 1b) since CT specimens contain a sharp crack ready for growth following ASTM E647-23, so incubation time is eliminated by the test conditions. However, in real pits or dormant cracks in this study, the first stage is crack initiation, requiring a few cycles to prepare appropriate conditions for microstructurally initiating cracks. M. Yu *et al*. [7] also confirmed that a higher threshold value of the combined factor is needed for a blunt crack tip.

It is essential to emphasize that circumferential cracks demonstrate higher crack growth rates than longitudinal cracks at the same stress/combined factor level, particularly under bending stresses. However, achieving such elevated crack growth rates in real pipeline conditions typically requires substantial axial stresses. These significant axial stresses result from factors like bending, geohazards, etc., and need to increase to a level equivalent to the stress/ combined factor required for axial cracking. This, however, is not a common condition in field pipeline bending.

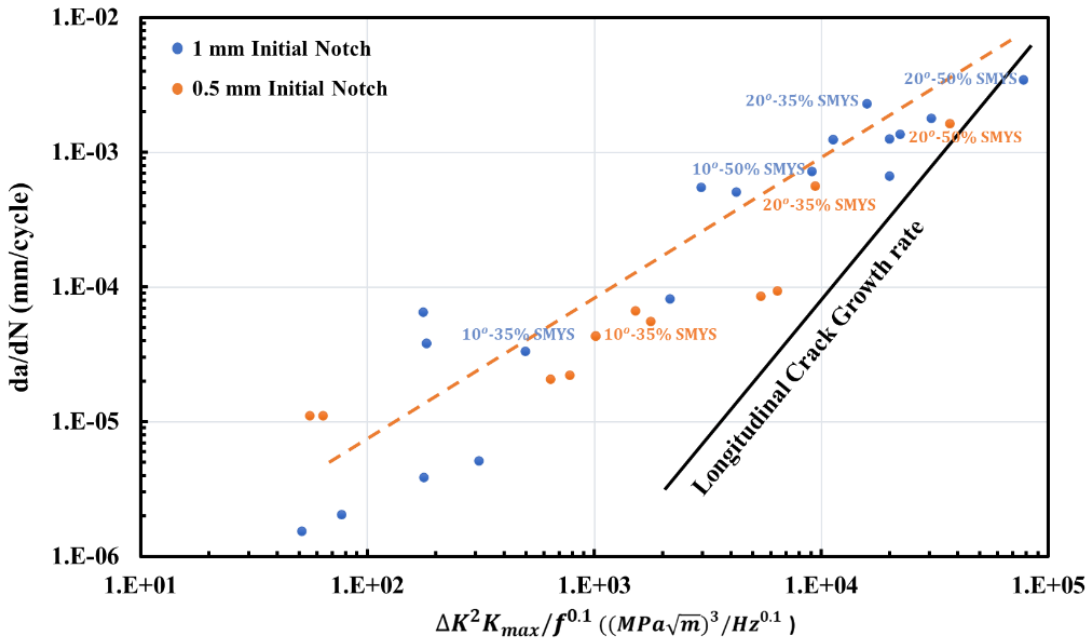

Figure 6-9 Comparison of circumferential crack growth rate as a result of bending with longitudinal crack growth rate da/dN as a function of combined factor

It is also possible to compare circumferential cracking in longitudinal samples and longitudinal cracking in CT specimens based on the previous scenario for the differences between 0.5 mm and 1 mm initial notches regarding access to hydrogen sources. In CT specimens, the deeper crack position means less access to the hydrogen source on the external surface. According to the comprehensive explanation in section 6.4.2, the main cause of this difference is residual stress in the cold work bent sample. Based on the DIC method, Figure 6-10 illustrates the typical distributions of final stresses measured in inwardly bent samples (bend centerline), including axial loading (35% and 50% SMYS) and residual stresses. Because of the curvature and momentum around the bent centerline, applied loading in a bent pipe makes another source of stress distribution in the thickness direction. After deducting applied loading from the total stress, the remaining part would be the net residual stresses in a given free body. These stresses must integrate to zero over any cross-sectional area, so regions with compressive stresses must balance regions

with high tensile residual stresses. Because the external surface of the inward bend section is subject to two sources of tensile stress (applied and residual), external surfaces undergo higher stress levels. This high tensile stress on the external surface is consistent with the higher crack growth rate, as shown in Figure 6-9. For example, a 20-degree bending angle sample under 50% SMYS applied loading produces the maximum stress level on the external surface and, therefore, the maximum crack growth rate. In contrast, a 10-degree bending sample under 35% SMYS applied loading shows the minimum crack growth rate (at the same initial notch depth of 1 mm). It is possible to apply the same scenario once circumferential and longitudinal cracks are compared. In this regard, a cumulative higher level of tensile stress exactly on the external surface of the inwardly bent section is the characteristic which causes more driving force for crack growth at the same combined factor compared to longitudinal crack growth. It can be concluded that a higher crack growth rate in circumferential cracks compared with longitudinal cracks at the same combined factor may result in a shorter service life. According to Figure 6-9, both circumferential and longitudinal crack growth rate graphs converge as combined factors increase, which means that the differences discussed earlier cannot affect the crack growth rate at higher combined factors.

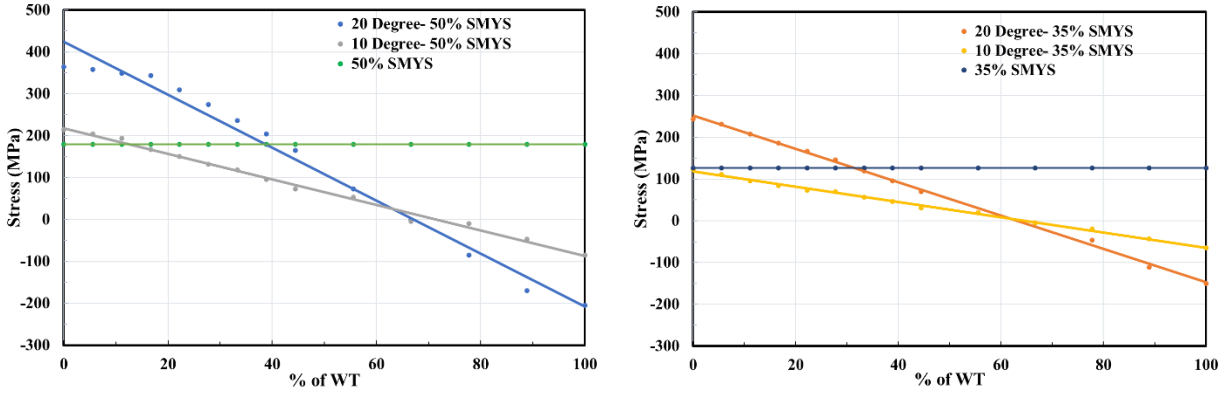

(a) (b)

Figure 6-10 Comparison of stress distribution in the thickness direction of bent samples (a) 50% SMYS loading (b) 35% SMYS loading

6. 5 Conclusion

This study analyzed circumferential corrosion fatigue crack growth at the bottom of dormant cracks/pits on the external surface of a steel pipeline exposed to near-neutral pH environments. These are some of the most significant results of this study:

1. For investigations of C-NNpH-CF crack growth, the digital image correlation (DIC) method is an appropriate technique since it can analyze the final stress distribution of bent pipelines influenced by various residual and applied stresses in the inward and outward directions of bent pipelines.
2. The crack depth and the stress gradient in the depth direction should be considered when calculating the stress intensity factor in circumferential corrosion fatigue crack growth. This gradient is also a pump that brings hydrogen from the corrosion on the nearby surface to the crack tip.
3. The expected pressure fluctuation from normal pipeline operation alone cannot cause circumferential corrosion fatigue cracking in the pipeline. Hence, other sources of axial stress are needed (residual axial stress from girth weld, bending, geohazards, *etc.*) for the occurrence of C-NNpH-CF on the external surface of the pipeline.
4. In the field, corrosion fatigue cracks are not a concern in the outward direction of bent pipelines (under compressive residual stress), so integrity management activities should focus on evaluating the bend centerline in the inward direction (after spring back).
5. Circumferential corrosion fatigue cracking in near-neutral pH (NNpH) environments occurs at lower stress intensity factor ranges/ combined factors due to the presence of residual stress. Cold bending increases residual tensile stress throughout the entire bend

area, especially at the bottom of the initial notch, increasing hydrogen diffusion and causing more embrittlement and crack growth.

References

[1] Canadian Energy Pipeline Association (CEPA), Stress Corrosion Cracking Recommended Practices, 2nd Edition, an industry leading document detailing the management of transgranular SCC, December 2007.

[2] J. Zhao, W. Chen, M. Yu, K. Chevil, R. Eadie, J. Been, G. Van Boven, R. Kania & S. Keane, "Crack growth modeling and life prediction of pipeline steels exposed to near-Neutral pH environments: stage II crack growth and overall life prediction," Metall Mater Trans A Phys Metall Mater Sci, vol. 48, no. 4, pp. 1641–1652, Apr. 2017, https://doi.org/10.1007/s11661-016-3939-z.

[3] J. A. Beavers and B. A. Harle, "Mechanisms of high-pH and near-neutral-pH SCC of underground pipelines," Journal of Offshore Mechanics and Arctic Engineering, vol. 123, no. 3, pp. 147–151, Aug. 2001, https://doi.org/10.1115/1.1376716.

[4] Ron Thompson, R. Gardner, K. Dwyer, A. Corbett, and M. Marquis Hotel, "A case study in the detection and sizing of circumferential stress corrosion cracking Pipeline Pigging and Integrity Management Conference," in Pipeline pigging and integrity management conference, Houston, February 2020.

[5] M. Brimacombe, C. Wargacki, and N. Global Leduc, "Circumferential crack detection: Challenges, solutions and results," in Proceedings of the 2016 International Pipeline Conference. Calgary, Alberta, Canada. IPC2016-64111. https://doi.org/10.1115/IPC2016-64111.

[6] J. Beavers and T. A. Bubenik, “Stress corrosion cracking,” in Trends in Oil and Gas Corrosion Research and Technologies: Production and Transmission, 2017, pp. 295–314. https://doi.org/10.1016/B978-0-08-101105-8.00012-7.

[7] M. Yu, W. Chen, R. Kania, G. Van Boven, and J. Been, “Crack propagation of pipeline steel exposed to a near-neutral pH environment under variable pressure fluctuations,” Int J Fatigue, vol. 82, pp. 658–666, Jan. 2016, https://doi.org/10.1016/j.ijfatigue.2015.09.024.

[8] D. Abdulhameed, S. Adeeb, and R. Cheng, “The influence of the Bourdon effect on pipe elbow” in Proceedings of the 11th International Pipeline Conference, 2016, pp. 1–10. https://doi.org/10.1115/IPC2016-64659.

[9] M. J. W. Ilm, “The role of pressure and pressure fluctuation in the growth of Stress Corrosion Cracks in line pipe steels,” in Proceedings of the 1998 International Pipeline Conference. Calgary, Alberta, Canada. IPC 1998-2049, 1998. https://doi.org/10.1115/IPC1998-2049.

[10] Y. B. Beauregard and C. Edwards, “Analysis of sever circumferential SCC found on an ethane pipeline,” in Proceedings of the 2014 International Pipeline Conference. Calgary, Alberta, Canada. , 2014.

[11] J. Babcock, D. Dewar, and J. Webster, “Deer Mountain case study: integration of pipe and ground monitoring data with historical information o develop landscape management plan,” Proceedings of the 2020 International Pipeline Conference. Calgary, Alberta, Canada. IPC2020-9613. https://doi.org/10.1115/IPC2020-9613.

[12] N. Bates, M. Brimacombe, and S. Polasik, “Development and experience of a circumferential stress corrosion crack management program,” in Proceedings of the 2018 International Pipeline Conference. Calgary, Alberta, Canada.IPC2018-78315.

[13] K. Zhang, R. Chune, R. Wang, and R. Kania, “Role of axial stress in pipeline integrity management,” in Proceedings of the 2022 International Pipeline Conference. Calgary, Alberta, Canada. IPC2022-87327. https://doi.org/10.1115/IPC2022-87327.

[14] S. Attia, M. Mohareb, M. Martens, N. Yoosef-Ghodsi, Y. Li, and S. Adeeb, “Numerical assessment of elbow element response under internal pressure,” Journal of Pressure Vessel Technology, Transactions of the ASME, vol. 143, no. 5, Oct. 2021, https://doi.org/10.1115/1.4050091.

[15] R. R. S. M. Fessler, “Characteristics, cause, and management of circumferential stress-corrosion cracking,” in International Pipeline Conference, in Proceedings of the 2014 International Pipeline Conference. Calgary, Alberta, Canada. https://doi.org/10.1115/IPC2014-33059.

[16] M. Pope*, C. S. Camerini, J. C. G. Teixeira, M. T. Piza, W. Baptista, B. G. de Souza, H. L. Oliver*, “Circumferential SCC in pipeline due to land creeping,” in Proceedings of the 2002 International Pipeline Conference. Calgary, Alberta, https://doi.org/10.1115/IPC2002-27192

[17] S. Wang and W. Chen, “Overview of Stage 1b Stress Corrosion Crack Initiation and Growth of Pipeline Steels,” Corrosion, vol. 79, no. 3, pp. 284–303, Mar. 2023, https://doi.org/10.5006/4168.

[18] W. Chen, G. Van Boven, and R. Rogge, “The role of residual stress in neutral pH stress corrosion cracking of pipeline steels - Part II: Crack dormancy,” Acta Mater, vol. 55, no. 1, pp. 43–53, Jan. 2007, https://doi.org/10.1016/j.actamat.2006.07.021.

[19] H. Shirazi, R. Eadie, and W. Chen, “A review on current understanding of pipeline circumferential stress corrosion cracking in near-neutral PH environment,” Engineering Failure Analysis, vol. 148, Jun. 01, 2023. https://doi.org/10.1016/j.engfailanal.2023.107215.

[20] M. Hilvert, T. Penney, M. Enginering Ltd, I. Richardson, and A. Russell, “Integrity management of Stress Corrosion Cracking in pipeline a case study,” in 26th World Gas conference Paris, France, 2015.

[21] W. Chen, “An overview of near-neutral pH stress corrosion cracking in pipelines and mitigation strategies for Its initiation and growth,” Corrosion, vol. 72, no. 7, pp. 962–977, Jul. 2016, https://doi.org/10.5006/1967.

[22] W. Chen, R. Kania, R. Worthingham, and G. Van Boven, “Transgranular crack growth in the pipeline steels exposed to near-neutral pH soil aqueous solutions: The role of hydrogen,” Acta Mater, vol. 57, no. 20, pp. 6200–6214, Dec. 2009, https://doi.org/10.1016/j.actamat.2009.08.047.

[23] J. Zhao, W. Chen, M. Yu, K. Chevil, R. Eadie, J. Been, G. Van Boven, R. Kania & S. Keane, “Crack growth modeling and life prediction of pipeline steels exposed to near-Neutral pH environments: stage II crack growth and overall life prediction,” Metall Mater Trans A Phys Metall Mater Sci, vol. 48, no. 4, pp. 1641–1652, Apr. 2017, https://doi.org/10.1007/s11661-016-3939-z.

[24] B. Johnson, B Tesfaye, C. Wargacki, T. Hennig, E. Suarez “Complex Circumferential Stress Corrosion Cracking: Identification, Sizing and Consequences for the Integrity Management Program,” in Proceedings of the 2018 International Pipeline Conference. Calgary, Alberta, Canada. IPC2018-78564. https://doi.org/10.1115/IPC2018-78564.

[25] J. Toribio, “Residual stress effects in stress-corrosion cracking,” J Mater Eng Perform, vol. 7, pp. 173–182, 1998. https://doi.org/10.1361/105994998770347891.

[26] G. Van Boven, W. Chen, and R. Rogge, “The role of residual stress in neutral pH stress corrosion cracking of pipeline steels. Part I: Pitting and cracking occurrence,” Acta Mater, vol. 55, no. 1, pp. 29–42, Jan. 2007, https://doi.org/10.1016/j.actamat.2006.08.037.

[27] T.L. Anderson, Fracture Mechanics Fundamentals and Applications, vol. 3. Taylor & Francis, 2005.

[28] R. Sutherby and W. Chen, “Deflected stress corrosion cracks in the pipeline steel,” Proceedings of the 2004 International Pipeline Conference. Calgary, Alberta, Canada. https://doi.org/10.1115/IPC2004-0600.

[29] R. Chu, W. Chen, S.-H. Wang, F. King, T. R. Jack, and R. R. Fessler, “Microstructure Dependence of Stress Corrosion Cracking Initiation in X-65 Pipeline Steel Exposed to a Near-Neutral pH Soil Environment,” Corrosion Science , vol. 60, no. 3, 2004. https://doi.org/10.5006/1.3287732.

[30] G. Van Boven, R. Rogge, and W. Chen, “Residual stress and stress corrosion cracking of high pressure hydrocarbon transmission pipelines,” in Proceedings of the 2006 International Pipeline Conference. Calgary, Alberta, Canada. IPC2006-10486. https://doi.org/10.1115/IPC2006-10486.

[31] H. Niazi, G. Nelson, L. Lamborn, R. Eadie, W. Chen, and H. Zhang, “Crack Growth Sensitivity to the Magnitude and Frequency of Load Fluctuation in Stage 1b of High-pH Stress Corrosion Cracking,” Corrosion, vol. 77, no. 6, pp. 618–631, Jun. 2021, https://doi.org/10.5006/3711.

[32] H. Niazi, K. Chevil, E. Gamboa, L. Lamborn, W. Chen, and H. Zhang, "Effects of Loading Spectra on High pH Crack Growth Behavior of X65 Pipeline Steel," Corrosion, vol. 76, no. 6, pp. 601–615, Jun. 2020, https://doi.org/10.5006/3472.

[33] H. Niazi, S. Wang, L. Lamborn, R. Eadie, W. Chen, and H. Zhang, "Effects of load interactions on the onset of stage two of high pH stress corrosion cracking," Journal of Pipeline Science and Engineering, vol. 1, no. 1, pp. 122–136, Mar. 2021, https://doi.org/10.1016/j.jpse.2021.01.003.

[34] H. Niazi, H. Zhang, L. Lamborn, and W. Chen, "The impact of pressure fluctuation on the early onset of stage II growth of high pH stress corrosion cracking," Proceedings of the 2020 13th International Pipeline Conference, IPC2020-9511. https://doi.org/10.1115/IPC2020-9511.

[35] H. Niazi, H. Zhang, and K. Korol, "High pH Crack Growth Sensitivity to Underload-Type of Pressure Fluctuations," 2018. Proceedings of the 2018 International Pipeline Conference. Calgary, Alberta, Canada. https://doi.org/10.1115/IPC2018-78394.

[36] S. L. Asher and P. M. Singh, "Role of stress in transgranular stress corrosion cracking of transmission pipelines in near-neutral pH environments," Corrosion, vol. 65, no. 2, p. 79, 2009. https://doi.org/10.5006/1.3319122.

[37] Y. Ogawa*, D. Birenis , H. Matsunaga, A. Thøgersen, O. Takakuwa , J. Yamabe*, "Multi-scale observation of hydrogen-induced, localized plastic deformation in fatigue-crack propagation in a pure iron," Scr Mater, vol. 140, pp. 13–17, Nov. 2017, https://doi.org/10.1016/j.scriptamat.2017.06.037.

[38] Y. Torres, J. M. Gallardo, J. Domínguez, and F. J. Jiménez E, "Brittle fracture of a crane hook," Eng Fail Anal, vol. 17, no. 1, pp. 38–47, Jan. 2010, https://doi.org/10.1016/j.engfailanal.2008.11.011.

[39] E. Merson, A. V. Kudrya, V. A. Trachenko, D. Merson, V. Danilov, and A. Vinogradov, "Quantitative characterization of cleavage and hydrogen-assisted quasi-cleavage fracture surfaces with the use of confocal laser scanning microscopy," Materials Science and Engineering: A, vol. 665, pp. 35–46, May 2016, https://doi.org/10.1016/j.msea.2016.04.023.

[40] D. Birenis, Y. Ogawa, H. Matsunaga, O. Takakuwa. Yamabe, Prytz, A. Thøgersen, "Interpretation of hydrogen-assisted fatigue crack propagation in BCC iron based on dislocation structure evolution around the crack wake," Acta Mater, vol. 156, pp. 245–253, Sep. 2018, https://doi.org/10.1016/j.actamat.2018.06.041.

[41] Y. Ogawa, H. Matsunaga, J. Yamabe, M. Yoshikawa, and S. Matsuoka, "Unified evaluation of hydrogen-induced crack growth in fatigue tests and fracture toughness tests of a carbon steel," Int J Fatigue, vol. 103, pp. 223–233, Oct. 2017, https://doi.org/10.1016/j.ijfatigue.2017.06.006.

[42] B. A. Kim, W. Zheng, G. Williams, M. Laronde, J. A. Gianetto, G. Shen, W. R. Tyson, N. Oguchi, Y. Hosokawa, "Experimental study on SCC susceptibility of X60 using full pipe section in near-neutral pH environment," Proceedings of the 2004 International Pipeline Conference. Calgary, Alberta, Canada. https://doi.org/10.1115/IPC2004-0280.

[43] J. A. R. G. K. and D. K. M. Seok-Jae LEE, "Hydrogen Embrittlement of Hardened Low-carbon Sheet Steel," ISIJ International, vol. 50, pp. 294–301, 2010.

[44] S. Lynch and S. Lynch, “Some fractographic contributions to understanding fatigue crack growth,” Int J Fatigue, vol. 104, pp. 12–26, Nov. 2017, doi: 10.1016/j.ijfatigue.2017.06.036.

[45] M. L. Martin, J. A. Fenske, G. S. Liu, P. Sofronis, and I. M. Robertson, “On the formation and nature of quasi-cleavage fracture surfaces in hydrogen embrittled steels,” Acta Mater, vol. 59, no. 4, pp. 1601–1606, Feb. 2011, https://doi.org/10.1016/j.actamat.2010.11.024.

[46] W. Chen and R. L. Sutherby, “Crack growth behavior of pipeline steel in near-neutral pH soil environments,” Metall Mater Trans A Phys Metall Mater Sci, vol. 38, no. 6, pp. 1260–1268, Jun. 2007, https://doi.org/10.1007/s11661-007-9184-8.

[47] R. N. Parkins, “A review of stress corrosion cracking of high pressure gas pipelines,” in NACE International Conference, Paper No.: 00363., 2000.

[48] H. K. Birnbaum and P. Sofronis, “Hydrogen-enhanced localized plasticity-a mechanism for hydrogen-related fracture,” Materials Science and Engineering: A. Volume 176, Issues 1–2, 31 March 1994, Pages 191-202 https://doi.org/10.1016/0921-5093(94)90975-X.

[49] W. Chen and R. Sutherby, “Environmental effect of crack growth rate of pipeline steel in near neutral pH soil environments,” in International Pipeline Conference, 2004.

[50] X. Xing, W. Chen, and H. Zhang, “Atomistic study of hydrogen embrittlement during cyclic loading: Quantitative model of hydrogen accumulation effects,” Int J Hydrogen Energy, vol. 42, no. 7, pp. 4571–4578, Feb. 2017, https://doi.org/10.1016/j.ijhydene.2016.12.127.

[51] K. Manthiramoorthy and A. Krishnaveni, “Fracture Parameter Evaluation Using Digital Image Correlation Technique,” International Journal of Engineering Technology Science and Research, Volume 4, Issue 11, 2017.

[52] B. Tasdemir and B. Taşdemir, “Determination of stress intensity factor using digital image correlation method,” Matter, vol. 2, no. 1, 2015.

[53] R. B. Á. Pradas Cristina, “Stress and strain analysis of a material with Digital Image Correlation method (DIC),” Western Norway University of Applied Sciences, 2020.

[54] L. Shi, X. Zhang, L. Zhang, C. Wang, and J. Wang, “Application of digital image correlation technique in stress and strain measurement. 15th Asia Pacific Conference for Non-Destructive Testing (APCNDT2017), Singapore.

Chapter 7 Pipeline Circumferential Corrosion Fatigue Failure Under the Influence of Bending Residual Stress in the Near-Neutral pH Environment[1]

7. 1 Introduction

Near-neutral-pH Corrosion Fatigue (NNpH-CF) is a form of Environmentally Assisted Cracking (EAC) that is linked to the presence of a dilute carbonic acid solution (pH: 5.5-7.5) formed at the pipe's external surface when CO_2 in the soil dissolves in groundwater which penetrates through a holiday in the coating and in the absence of cathodic protection penetrating through the coating [1]–[4]. This corrosion fatigue poses a significant threat to buried oil and gas pipelines, challenging their reliability and safety, even with protective measures like coatings and cathodic protection [2], [5], [6]. This specific form of EAC, traditionally referred to as Stress Corrosion Cracking (SCC), is increasingly recognized as a type of "corrosion fatigue". This distinction is made because crack growth cannot occur without significant changes in stress (pressure fluctuations), which are characteristic of fatigue [2], [6]–[8].

NNpH-CF is classified into two categories based on the direction of crack propagation: axially oriented corrosion fatigue, which is better understood and actively mitigated by pipeline operators, and Circumferential Near-neutral-pH Corrosion Fatigue (C-NNpH-CF), where monitoring and mitigation techniques are less established [9]–[12]. C-NNpH-CF can occur when the tensile axial

[1] A version of this chapter has been submitted: H. Shirazi, Sh. Wang, R. Eadie, W. Chen, “Pipeline Circumferential Corrosion Fatigue Failure Under the Influence of Bending Residual Stress in the Near-Neutral pH Environment”,

or longitudinal stress exceeds hoop stress (cyclic stresses due to pressure fluctuations within the pipe) in an operational pipeline. There are many possible sources of axial stress, including but not limited to residual axial stresses developed during pipe manufacturing and pipeline construction (*e.g.,* field bends (and related stresses in the bent section, such as hydrodynamic and Bourdon stresses)), girth welds, as well as geotechnical stresses caused by soil and pipeline movement, landslides, and residual stresses opposite rock dents [9]–[17].

C-NNpH-CF failure progresses through several stages: incubation stage, Stage I (crack initiation and early-stage crack growth), Stage II (sustainable crack growth under sufficient mechanical driving forces), and Stage III (rapid crack propagation leading to rupture when the fracture toughness of the pipe is exceeded) [6], [18]. The predominant driving force for crack propagation during the early stages of crack life might be environmental; however, as cracks deepen, the dominant driving force might be mechanical [9]. Laboratory crack growth simulations demonstrated that the crack growth rate could be correlated with a combined factor that included both mechanical and environmental driving forces [19]: $\Delta K^{\alpha} K_{max}^{\beta} / f^{\gamma} +$ h, where A, n, α, β, and γ are all constants, α + β = 1, ΔK is the stress intensity factor range at the crack tip due to cyclic loading, K_{max} is the maximum stress intensity factor at the crack tip, and γ is a factor representing the influence of the corrosion environment on the crack growth rate. In extensive research, it has been shown that continuous growth beyond Stage I is possible if the following conditions are met [1]: Having sufficient mechanical driving forces, residual stresses, and diffusible hydrogen (a by-product of corrosion) that can interact synergistically with the mechanical driving forces.

C-NNpH-CF was observed to mostly occur near areas where bending was present [10], [11], [20], [21], so bending was considered a significant factor in causing axial residual stresses in the field that led to C-NNpH-CF. The stresses in a bent section are characterized by the presence of residual

stress gradients in the thickness direction of the pipe, which contribute to the presence of the mentioned stages before rupture. Indeed, in pipelines subjected to cyclic loading, residual stress plays a key role in crack evolution by either accelerating (tensile stresses) or retarding (compressive stresses) crack initiation and growth [22]. Engineering-fracture-mechanics-based assessments of energy pipelines require identifying the fracture stages and expected fracture behaviour. Physical fracture features like striations on quasi-cleavage fracture surfaces should be correlated with experimental fracture results to provide reliable predictions [23], [24]. Hydrogen-enhanced fracture surface morphology in NNpH environments can, for example, remain unchanged or change from ductile microvoid coalescence to quasi-cleavage or even cleavage under the combined effects of stress and hydrogen [24].

This study aims to assess the combined impact of bending residual stress (an appropriate source of residual axial stress and cyclic loading (simulated pipeline pressure fluctuation) on C-NNpH-CF failure. Digital image correlation (DIC) will be used to analyze stress distribution, and fractographic images will provide insights into crack propagation stages before failure under the influence of varying test parameters, including applied loading, initial notch depth/position, and bending angle/direction. For a deeper understanding of the C-NNpH-CF failure mechanism, striation analysis, Crack Mouth Opening Displacement (CMOD), and Electron Backscatter Diffraction (EBSD) investigation will also be employed. This will improve the accuracy of C-NNpH-CF modelling and enable operators to reduce the risk, costs, and environmental consequences of these failures.

7. 2 Material and experimental methods

In this study, a 16" API-5L Gr X52 pipe with a wall thickness of 9.2 mm was taken from a pipeline that had shown NNpH-CF in the past. In the field, pipeline bending has a significant role in causing

C-NNpH-CF since it creates axial residual stresses [10], [11], [20], [21]. Figure 3-1 (chapter 3) shows the tensile properties of the pipeline steels used in the study. These values were determined using testing according to ASTM Standard E8. This pipe's yield stress (at 0.2% offset strain) and ultimate tensile stress were found to be 356 MPa and 561 MPa, respectively.

Electrical discharge machining (EDM) was used to produce longitudinal long samples from the pipes. Three reduced gauge sections (80 mm x 20 mm x 9.2 mm) with artificial through-thickness notches were designed to evaluate different parameters. Since cold working, such as machining, can alter residual stress distribution, the sections were bent at different degrees so that both the inner and outer surfaces remained intact. Two bending angles of 10 and 20 degrees were designed to simulate cold bending in the field. As a result of this bending process, the entire bent section of the pipe is subjected to axial stress. It can lead to this type of cracking when combined with cyclic loading caused by pressure fluctuations (internal pressure pushes on the pipe ends and creates axial stress). Bending a pipe involves two distinct conditions. After springback, residual stresses, which self-equilibrate naturally, create high tensile stress on the concave side to counterbalance the substantial compressive stress on the convex side [14]. The combined effect of bending axial stress and other stress sources can potentially exceed a material's yield strength [25], [14]. Research by J. Beavers *et al.* [8] showed that pipelines with hoop stress levels exceeding 60% of specified minimum yield strength (SMYS) are susceptible to near-neutral pH corrosion fatigue. Therefore, this study considered axial stress levels of 35% SMYS (roughly half the hoop stress) and 50% SMYS, with potential additions of axial stresses. A milling machine was used to create artificial notches on the bent parts of the samples to assess crack growth. The study also included a 1- and 0.5-mm depth initial notch to examine the effect of notch depth on failure. As shown in Figure 3-4 (chapter 3), there are two types of bending on the outer surface of the pipeline, inward and

outward on the outer surface of the pipeline, (X is the number of the long samples, 1, 2, 6-8: inward notches, 3-5: outward notches).

Cyclic loading tests were conducted in a water-tight cell containing C2 solution (synthetic field soil solution) with gas sparging (5% CO_2, 95% N_2). The solution pH was 6.3 ± 0.1, consistent with a near-neutral pH environment. After a 12-day static corrosion test (introducing the NNpH environment to samples), cyclic loading with varying axial loads was conducted on an Instron 8516 servo-hydraulic testing machine controlled by Wavemaker Runtime software for 45 days as long as no failures occurred during the test of long samples. Since the stress was offset from the bending position, the applied stress was increased at bends by the bending moment. A frequency of 0.001 Hz and a stress ratio of 0.1 were maintained in all experiments. Table 3-2 (chapter 3) outlines a method for evaluating the effects of the mentioned parameters on crack growth mechanisms. To verify the consistency of the data, long sample No. 2 (excluding the notch located at the inwardly bent gauge centerline: notch No. 27) was employed in addition to long sample No. 1. Non-bent sections with 0.5 mm and 1 mm initial notches were also subjected to cyclic loading at 35% and 50% SMYS.

Among all long samples, including various parameters, just 5 long samples failed during the test in different test durations, summarized in Table 3-3 (chapter 3) . Long sample No. 8 was fixed in an Instron 8516 servo-hydraulic testing machine equipped with a virtual extensometer available in Wavemaker Runtime software and then subjected to a cyclic load to investigate crack mouth opening displacement (CMOD) on notch No. 87. When subjected to load, the specimen will deform as a function of time, t, as well as a function of load cycles, N. This will result in elastic and plastic CMOD (δe and δp) and crack growth [26]–[29]. Each parameter was recorded during

testing and subsequently used to calculate relevant data, such as CMOD. Photos were taken during notch No. 87 crack propagation to determine the actual crack growth rate.

Following ASTM Standard G1-03, the fracture surface of these failed notches was dipped in a solution containing 6N HCl + 3.5 g/L hexamethylene tetramine to remove corrosion products. The fracture surfaces were then imaged using a Zeiss Sigma 300-VP FESEM. The crack growth rate was calculated by dividing the measured crack growth depth (at the end of Stage II) by the number of cycles.

Electron backscatter diffraction (EBSD) analysis was used to analyze crystallographic orientations along fracture paths. EBSD specimens were ground to 1200 grit and then mechanically polished using a diamond suspension with 6μm and 1μm abrasive particle sizes. Afterwards, an alumina suspension with a particle size of 0.05μm was applied to polish the surface. Zeiss Sigma FESEM equipped with an Oxford Instruments Nordlys Nano detector (at a step size of 1.5 μm, an accelerating voltage of 20 kV and a tilt of 70°) and Oxford Instruments AZtec software version 2.4 was used to acquire and perform a preliminary analysis on EBSD maps. Oxford Instruments HKL Channel 5 was selected for post-processing and data analysis. In addition to the inverse pole figure (IPF) maps, the strain contouring method was used to analyze the plastic deformation around the fracture path. This component estimates the extent of deformation, or strain, in individual grains on a map. The strain contouring component measures the maximum misorientation between any 2 points in the grain and then weights this grain according to this misorientation value. Because these maps are related to orientation gradients in the material, they can be used to assess small local strain gradients qualitatively [30]–[36].

A similar set of long samples bent at 10- and 20-degree angles was used to evaluate stress distribution by the digital image correlation (DIC) method [37]–[40]. A white layer was applied to

prepare the samples for this technique, followed by a black speckle pattern. On an MTS tensile testing machine, the specimens were loaded to a maximum force equivalent to 35% and 50% SMYS of X52, and force and displacement were recorded. Sequential images were captured at specific force increments (100 N) to obtain DIC results. The images were analyzed using Vic-3D 9, a commercial DIC software. Based on the stress-strain curve, stress values were correlated with the strain map derived from the DIC method to obtain stress distributions.

7. 3 Results

7. 3. 1 Stress distribution analysis based on the DIC method

An initial step towards evaluating corrosion fatigue in the NNpH environment is to determine the final stress distribution across the external surface and thickness direction of the bent gauge area. Figure 7-1a shows the digital image correlation pattern of a long sample with 20-degree bending after applying load to 50% SMYS. Based on these results, a comprehensive analysis of accumulated stresses from residual bending and axial cyclic stresses was performed to investigate the mechanism of C-NNpH-CF failure. As a result of applying cyclic loading, a new stress state must be established fairly quickly, allowing a significant portion of the corrosion fatigue testing to occur under the new stress distribution [3], [41].

Based on Figure 7-1a, the inward directions are under maximum tensile stress (positive strain). Moving away from the bend centerline reduces the tensile stress. Furthermore, maximum compressive stress (negative strain) adversely affects the outward bend centerline and decreases as it moves away from the bend centerline. The inward direction is subjected to two types of tensile stress: residual stress from bending (following the springback effect) and applied loading. Field tests have shown that when the pipe is not allowed to spring back (as in roping), the axial strain on the concave side of the bend is equal to $D/2\rho$, where D is the pipe diameter, and ρ is the bend

radius. It has been confirmed that when the pipe springs back, the concave side will be in tension, and the convex side will be in compression [14]. Note that the final stress increases in both directions since the sources of stress are the same (inward is under tension, outward is under compression) from two sources (bending and axial cyclic loading). Figure 7-1b shows an in-thickness directional strain map for an inwardly bent gauge. Type I residual stresses, which vary continuously over at least several grain diameters, must be self-equilibrated such that they sum to zero in any direction over the entire cross-section [42], [43]. Figure 7-1b illustrates this phenomenon, where the highest tensile stress/positive strain on the external surface of an inward 20-degree bending gauge length is accompanied by the highest compressive stress/negative strain on the internal surface. Since bent samples have the same thickness, maximum stress on the external surface of the sample also results in maximum stress reduction in the thickness direction.

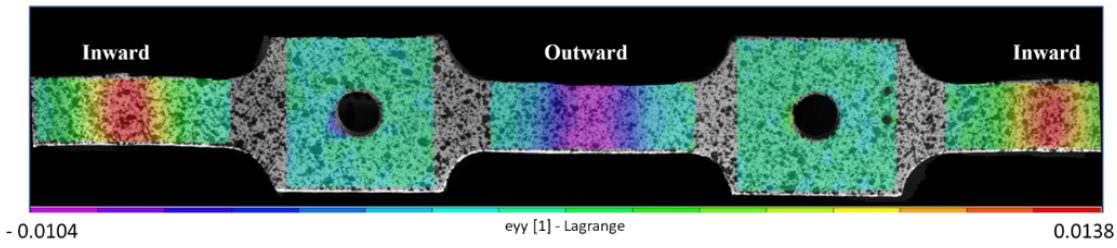

(a)

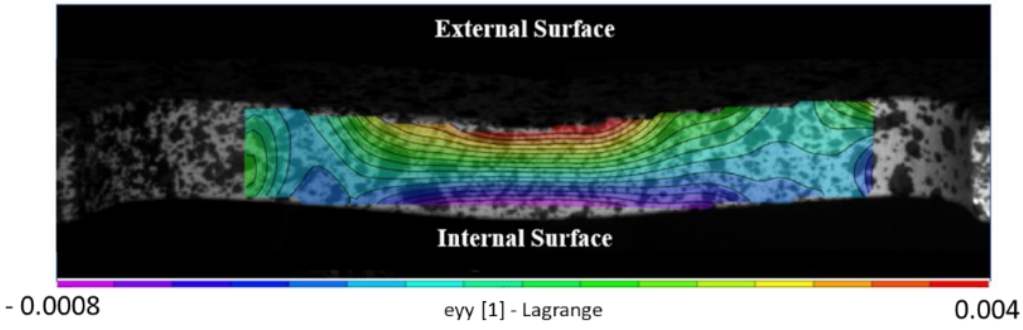

(b)

Figure 7-1 (a) Digital image correlation pattern of 20-degree bent section (b) In-thickness directional strain map for the 20-degree bent gauge with an inward bend

As mentioned, C-NNpH-CF crack growth in bent pipelines is characterized by stress variation in the thickness direction. Figure 7-2a shows the original stress distribution in the thickness direction of notch No. 22 (20-degree bending, 1 mm initial notch depth and 50% SMYS cyclic loading) and 87 (20-degree bending, 0.5 mm initial notch depth and 35% SMYS cyclic loading) which were derived using the digital image correlation (DIC) method before notching and crack initiation at the notch root. Cold work bending creates stress distribution across all bending directions (width, length, and thickness). The net force on a free-standing stationary object must be zero unless it is being accelerated (Newton's first law), so residual stress self-equilibrates in length and depth directions. Therefore, tensile residual stress on the external surface corresponds to a compressive residual stress on the internal surface.

Figure 7-2b shows the initial stress intensity factor in the depth direction before crack growth begins. The residual stress fields in the material clearly affect this stress-intensity factor [44]. Single-edge notched tension (SENT) [45] methodology for through-thickness initial notch/crack can be used to calculate the stress intensity factor. The stress intensity factor can be calculated based on the stress value at any depth point. Two opposite factors affect the stress intensity factor in the depth direction. The stress would change dramatically from maximum tensile stress on the external surface to maximum compressive stress on the internal surface (inwardly bent gauge). In addition, increasing depth has a significant effect on increasing the stress intensity factor. In response to these two competing factors, the stress intensity factor rises to the maximum point (the effect of crack depth dominates the intensity factor) and then falls (the effect of stress reduction dominates the intensity factor) as the maximum stress intensity factor reaches zero at a certain depth (based on stress distribution). It should be noted that this graph represents the stress intensity

factor changes in the thickness direction before crack initiation. Cracking will of course redistribute these stresses.

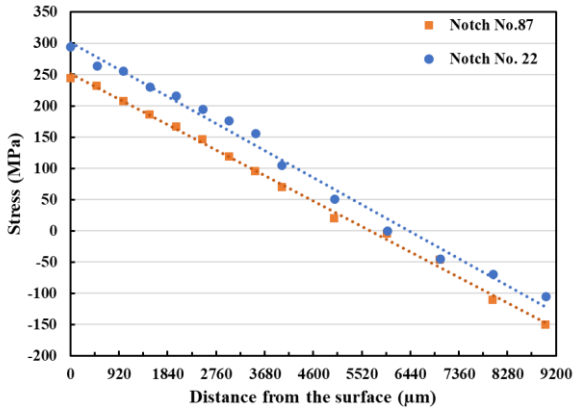

(a)

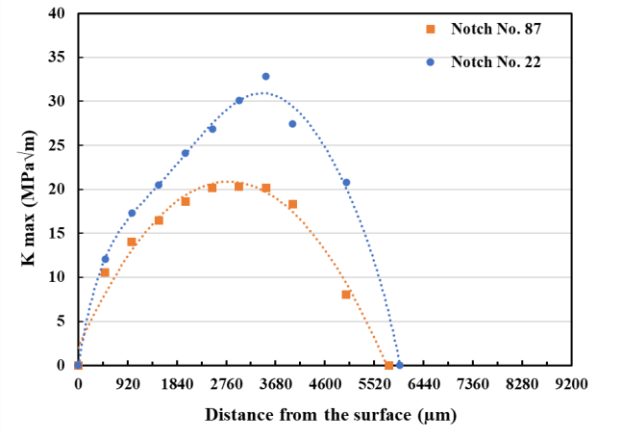

(b)

Figure 7-2 (a) Initial stress distribution in the depth direction before crack initiation: notches No. 22 and 87 (b) Maximum stress intensity factor in the depth direction before crack initiation: notches No. 22 and 87

7. 3. 2 Fracture surface morphology

Figure 7-3 shows low-magnification SEM fractographic images of all the notch failures at various times during testing under different parameters from the crack initiation site to the final fracture (from top to bottom). Despite the presence of various morphologies in these images, the first insight is the similarity in crack growth stages in the depth direction of failed notches. Even though various testing parameters can affect crack growth rates at different stages, the boundary between

regions remains pretty much at a similar location regardless of factors that influence stress distribution in the thickness direction, such as bending angle and applied loading. However, more sophisticated methods must be applied to find more precise boundaries between stages, which will be discussed in more detail in the next section. Overall, Stage II crack growth appears smoother and more reflective than Stage III crack growth. The increase in stress intensity factors could result in more crack deflections and changes in roughness over an extended distance during Stage III until the crack passes through the 'overload' plastic zone at the bottom of the notch [46]. The higher roughness in Stage III could be attributed to tearing (well-defined dimples) between striated areas due to high loads [46], which will be explained later. Based on various testing parameters (bending angle, initial notch depth, and applied cyclic loading), Table 7-1 summarizes crack growth in Stage II.

Table 7-1 Stage II crack growth rate in failed notches under various testing parameters

Long Sample	Notch No.	Radius of Bending (Degree)	Initial Notch Depth (mm)	Maximum Applied Stress (% SMYS)	Test duration (hour)	Crack growth rate at Stage II (mm/cycle)
1	**17**	20	1	50	208	0.0034
2	**22**	20	1	50	224	0.0018
4	**47**	20	1	35	325	0.0023
6	**67**	20	0.5	50	354	0.0016
8	**87**	20	0.5	35	1283	0.00056

For a better understanding of various stages in the depth direction, the approximate boundary between stages for one of the fractured notches (notch No. 47: 20-degree bending, 35% SMYS, and 1 mm initial notch depth) is shown in Figure 7-3e. First, cracks develop in some crystalline grains at the notch root (Stage I). The second stage (Stage II) involves stably propagating cracks on a cycle-by-cycle basis, with crack growth directions macroscopically perpendicular to loading directions. Stage III occurs when the material undergoes rapid crack growth and then sudden

fracture during which ductile tearing and shear detachment produce a tilted fracture surface called the shear lip [47].

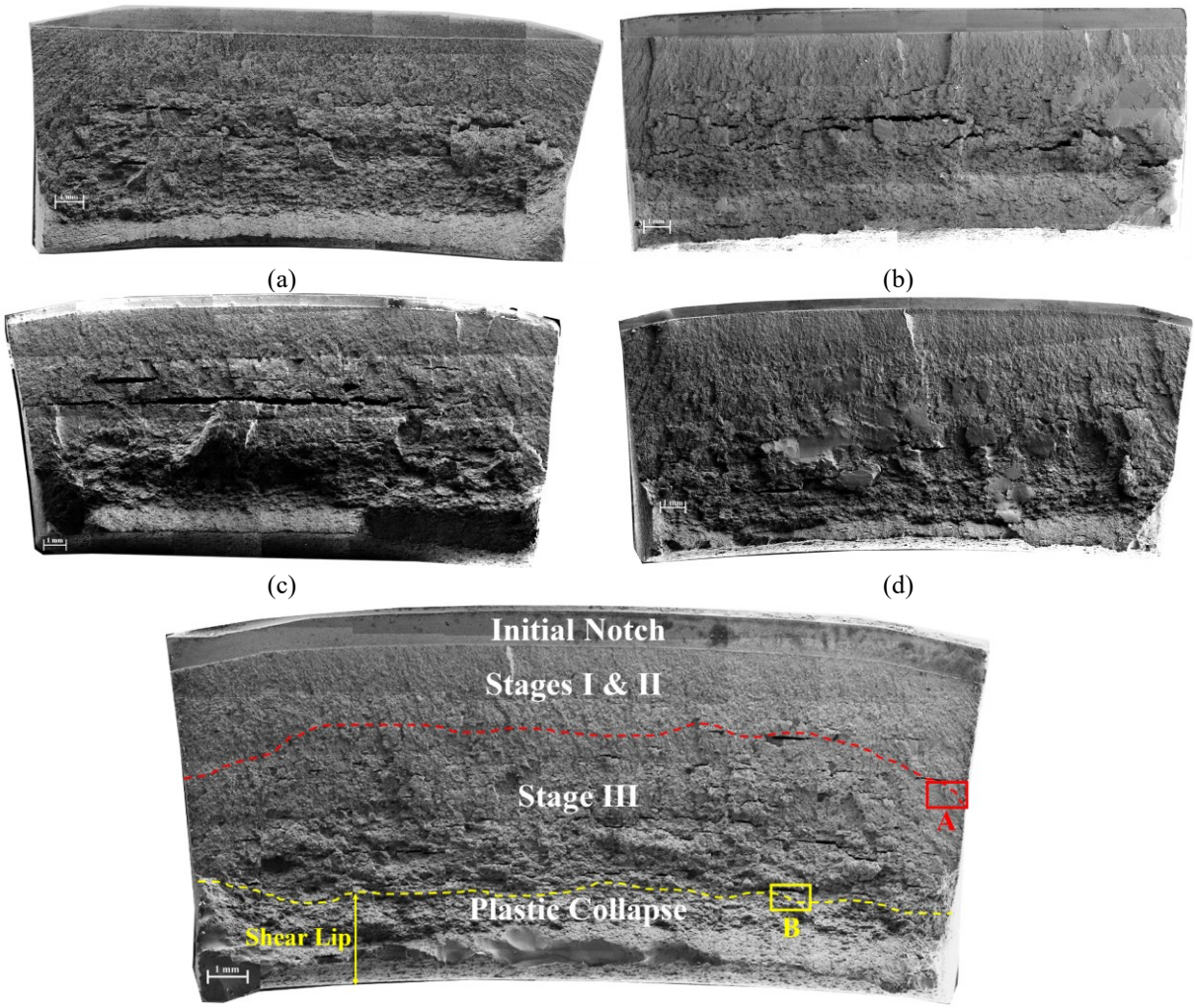

Figure 7-3 Fractography images (a) Notch No. 17, (b) Notch No. 22, (c) Notch No. 67, (d) Notch No. 87, (e) Notch No. 47. The crack growth directions are from top to bottom.

Based on the fractography images of notch No. 47 (20-degree bending, 35% SMYS, and 1 mm initial notch depth) shown in Figure 7-3e, Figure 7-4 depicts their various morphologies and boundaries. Also, Figure 7-5 provides images of different stages at higher magnifications to compare the morphologies. In the presence of hydrogen, the fracture surface was covered with quasi-cleavage morphology (Figures 7-4a and 7-5a), characterized by stepped surfaces decorated with river patterns. There were also wider and more planar striations observed. Although quasi-

cleavage is technically defined as fractography that looks like cleavage, it is generally accepted that the fracture plane does not necessarily follow the known cleavage plane. An explanation for the formation of such planar and wide striations can be provided by a model based on hydrogen-enhanced localized plasticity (HELP) [31], [47]. The observed surface morphology can be explained by the initiation of voids and/or microcracks at the intersection between slip bands, dislocation-cell walls, and vacancy clusters. Widening of these voids via dislocation processes ultimately produces the characteristics of the observed fracture surface. Hydrogen helps to develop intense slip bands, lower the stress needed to create the initial voids and speed up the expansion of those voids. It is suggested that fracture surfaces with river markings and relatively flat areas between them are not formed by cleavage-like processes but by plastic processes that are enhanced and accelerated by hydrogen [24], [46]. Section 7.3.3 discusses the mechanism for striation formation in more detail. As indicated by the river lines in the figure, crack growth occurs from top to bottom [48].

Figures 7-4a, 7-4b and 7-5b show that some brittle fracture zones were separated from other brittle fracture zones by localized regions of ductile failure, i.e., void coalescence, during Stage III (rapid crack growth) and before final fracture (plastic collapse). It is believed that these regions of ductile failure developed because of high localized strain rates that were joining non-planar regions of brittle fracture (as opposed to Stage II). In particular, the localized strain rate at a propagating crack front is sufficiently high to prevent diffusion-controlled hydrogen embrittlement mechanisms from operating [49]. A band of tearing (well-defined dimples) between striated areas is also possible when a high load is applied [46].

Despite large areas of flat fracture surface (Stage II and the first part of Stage III, which are quasi-cleavage), some ductile fractures were associated with shear lips at the bottom of the specimen, as

shown in Figure 7-3 (low-magnification SEM fractographic image of different failed notches). A ductile fracture exhibits substantial plastic deformation, and the fracture mechanism is mainly driven by micro void coalescence, which begins at metallic or non-metallic inclusions [49], [50]. Nevertheless, some research [24] suggested that hydrogen may accelerate this final stage of failure by accelerating extreme plastic processes.

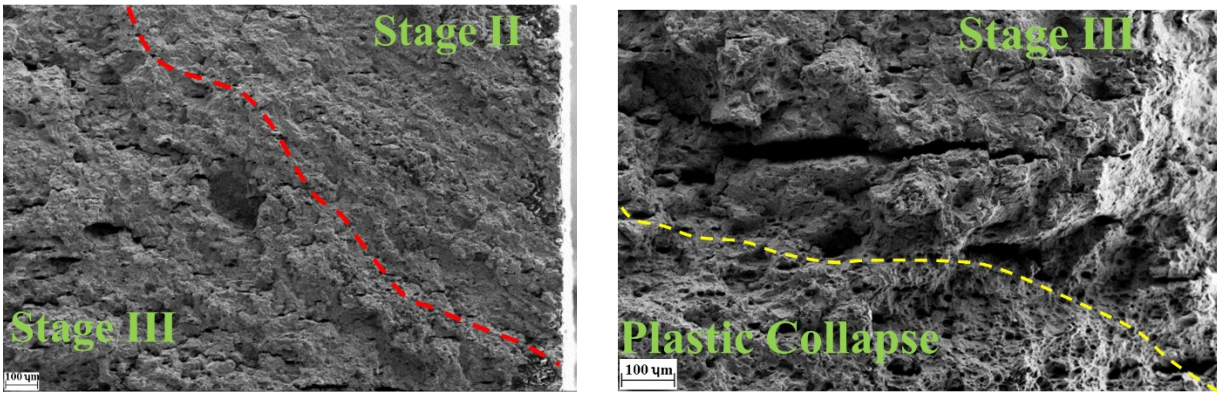

(a) (b)

Figure 7-4 Crack growth stages in the fractographic image of failed notch No. 47 (20-degree bending, 1 mm initial depth, 35% SMYS) (a) boundary between Stages II and III crack growth (A in Figure 7-3e), (b) boundary between Stages III crack growth and plastic collapse (B in Figure 7-3e)

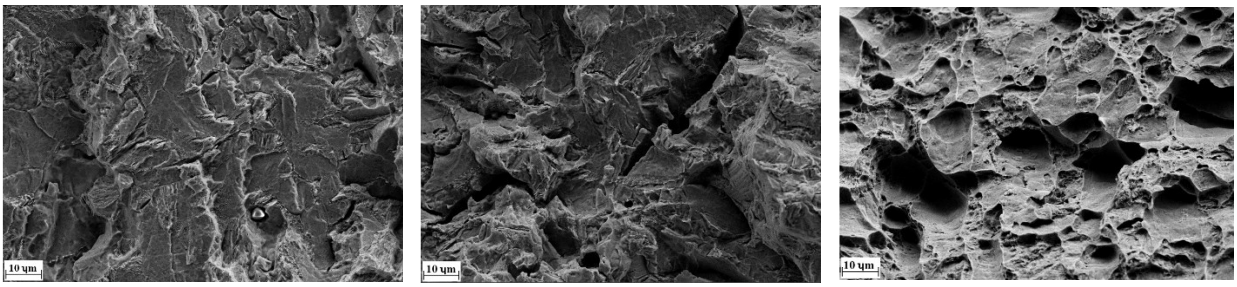

(a) (b) (c)

Figure 7-5 Fractographic details of crack propagation in the depth direction (a) Stage II, (b) Stage III, (c) Plastic collapse

7. 3. 3 Striation Analysis

In a near-neutral pH environment, hydrogen-assisted fatigue crack growth is exemplified by quasi-cleavage fractures along with striations. These striations are formed by crack advance and blunting

by slip during loading, and resharpening of the crack tip by slip just behind crack tips during unloading [46], [51]. In a near-neutral pH environment, hydrogen concentrates ahead of the crack tip, resulting from penetration from the crack surface and/or stress-induced diffusion. Hydrogen enhances slip deformation according to the HELP mechanism. Consequently, slip deformation is localized near crack tips in hydrogen-rich areas. The crack continues to grow with minimal blunting since reverse slip under unloading hardly occurs. This is because there is little crack blunting under the influence of hydrogen, resulting in flat and blurred striations. At this stage, these striations are useful for determining crack growth history because they delineate successive positions of the crack tip, and their spacing represents crack growth for each stress cycle. For example, Figure 7-6a shows the striations in Stage II crack growth (2000 μm from the bottom of the notch) of notch No. 87 (20-degree bending, 0.5 mm initial notch depth and 35% SMYS cyclic loading). A definite length divided by the number of striations can be used to calculate the crack growth rate. Figure 7-7 shows that an increase in striation spacing results in an increase in fatigue crack growth [47].

In Figure 7-7, the striation spacing, and derived crack growth rate were in reasonable agreement with the macroscopic crack growth rate (Figure 7-3), which indicates that these striations were formed cycle by cycle [31], [34], [52], [53]. Based on the striation, the average crack growth rate is 0.57 μm/cycle (orange point on the graph), close to the average macroscopic crack growth (2.6 mm of Stage II crack depth divided by the number of cycles in that Stage (4533 cycles), resulting in 0.58 μm/cycle). It should be noticed that Figure 7-7 only shows the crack growth rate derived from striation interspace in Stage II.

Figure 7-6b illustrates a striation at a depth of 4500 μm (Stage III). Striations with shallower profiles result in smoother, more reflective fracture surfaces (Figure 7-6a: Stage II) when stress intensity factor ranges (ΔK) are lower. Over significant distances, a high load can cause crack deflections and roughness changes [46]. Regarding the Stage III crack growth striation, it is interesting that the macroscopic crack growth rate differs from that derived from striation. Despite the higher crack growth rate in Stage III than in Stage II (which will be discussed later), the striation interspacing does not reflect this difference in Figure 7-6b. In fact, the crack growth rate increases in the depth direction due to complicated stress conditions at the crack tip as a result of two main sources of stress: applied loading in a bent sample, residual stress distribution from the bending source, and stress intensity factors related to the interaction of these stresses. This is more evidence that the crack growth mechanism in Stage III differs from Stage II.

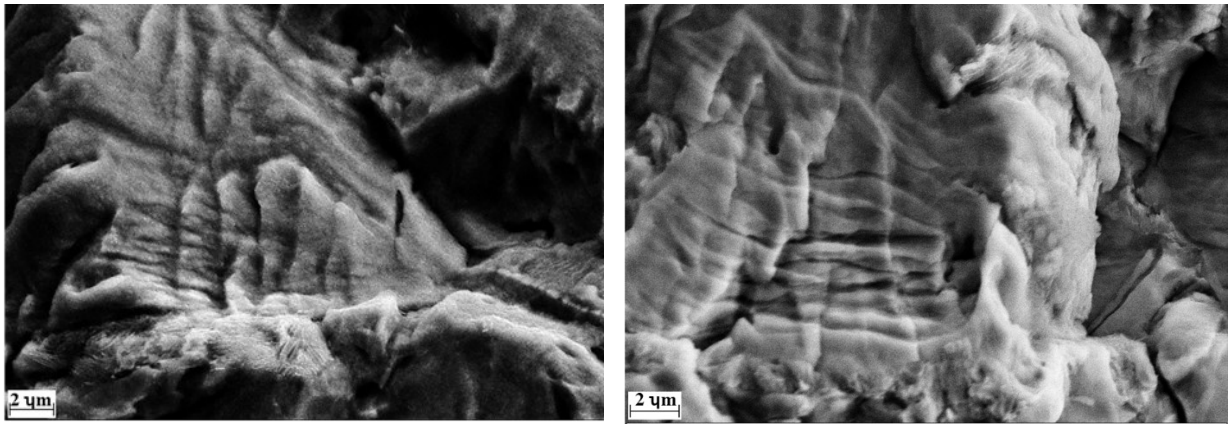

(a) (b)

Figure 7-6 Striation in (a) crack depth= 2000 μm (b) crack depth= 4500 μm

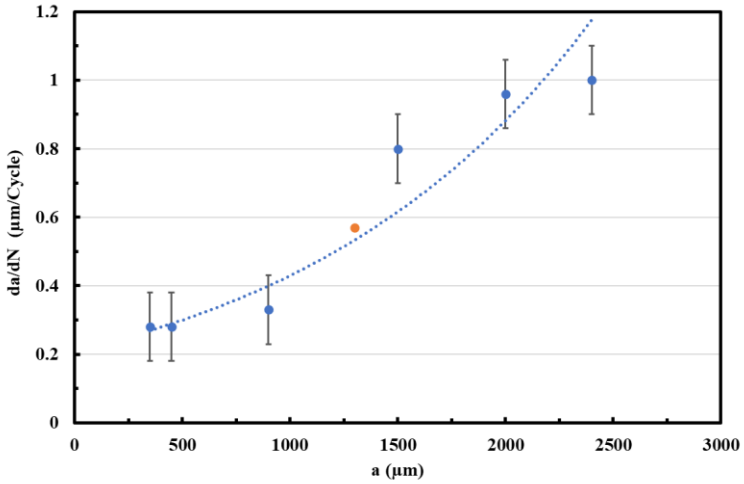

Figure 7-7 Crack growth rate derived from striation in the depth direction in Stage II (notch No. 87)

7. 3. 4 Crack Mouth Opening Displacement (CMOD) and actual crack growth rate in the depth direction investigation

The fracture mechanics parameter can be determined using numerous techniques, but accurate determination still faces several challenges. Crack Mouth Opening Displacement (CMOD) measurement could be used to characterize crack growth and fracture behaviour of pipeline steels in NNpH corrosive environments [28], [54]. CMOD results during crack propagation at notch No. 87 (20-degree bending, 0.5 mm initial notch depth and 35% SMYS cyclic loading) are shown in Figure 7-8. Throughout the testing process, the CMOD displayed distinctive behaviour [26], [55]. CMOD did not change before Stage III crack growth, which means crack growth occurred with the sharp tip without any change in CMOD (or a change less than the software accuracy). The permanent change in CMOD could be a way to find the boundary between Stage II and Stage III, which happened exactly at a crack depth of 2.6 mm (from the bottom of the initial notch) after around 4500 cycles. It can be seen from this Figure that CMOD increased rapidly with increasing test duration in Stage III. In the final stages leading to failure after 4620 cycles, the CMOD experienced a rapid and pronounced escalation, eventually resulting in plastic collapse.

Figure 7-9 shows the actual crack growth rate in the depth direction of notch No. 87 during crack propagation. The first crack appeared on the external edge of notch No. 87 exactly after the permanent change in CMOD at a depth of 2.6 mm from the bottom of the initial notch, which was considered the transition boundary between stages II and III. The crack growth rate for Stage II can be determined before reaching this depth from crack depth (2.6 mm) and number of cycles (4533), which is 0.57 μm/cycle. Accordingly, this average crack growth rate would be considered equivalent to crack growth at a depth of 1.3 mm (from the bottom of the notch) or 1.8 mm from the external surface. A significant increase in crack growth rate was seen after starting Stage III, reaching the maximum of 0.65 mm/cycle (considerable crack growth rate) till the depth of 4.5 mm, after which the crack growth rate decreased to 0.01 mm/cycle. The crack growth rate, however, increased again until the final fracture at 6.5 mm from the pipe's external surface. Section 7.4 will explain this complicated behaviour in detail.

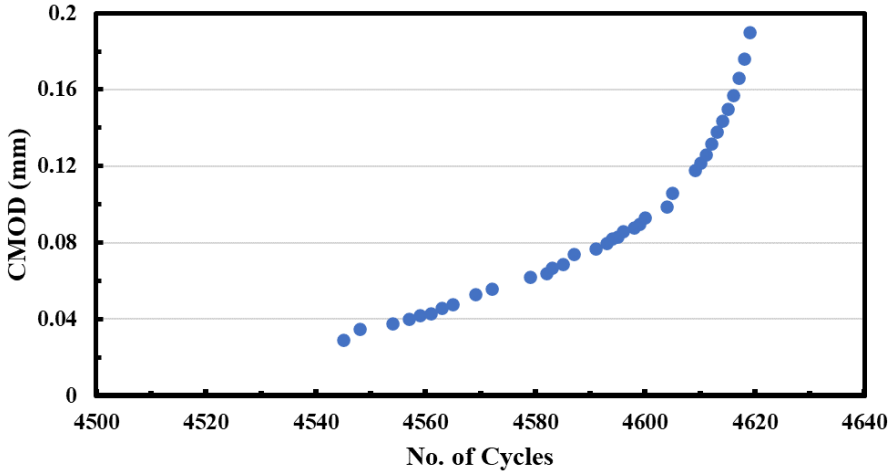

Figure 7-8 CMOD at Stage III (notch No. 87)

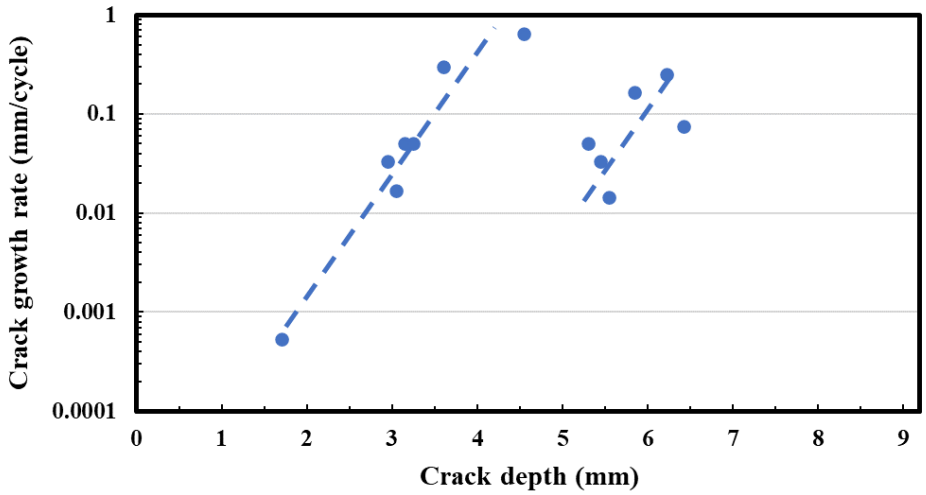

Figure 7-9 Actual crack growth rate in the depth direction (notch No. 87)

7. 3. 5 EBSD failure analysis

Figure 7-10 shows the cross-sectional fracture surfaces used for the EBSD investigations of notch No. 22 (20-degree bending, 1 mm initial notch depth, 50% SMYS cyclic loading) and 87 (20-degree bending, 0.5 mm initial notch depth, 35% SMYS cyclic loading). There is a similar pattern of crack propagation in both notches. Despite the difference in initial notch depth (1 mm in notch No. 22 (Figure 7-10a) and 0.5 mm in notch No. 87 (Figure 7-10b), crack paths at Stage II are relatively smooth, but at Stage III they are coarsely dented. The dentation was more obvious in notch No. 22 (Figure 7-10a), which is under higher stress levels. At the bottom of both failed notches, 45° slants and shear lips are associated with plastic collapse. It is possible to see a small depression in the internal surface of the failed sample due to complicated stress parameters at the time of fracture, including shear and bending stresses [50].

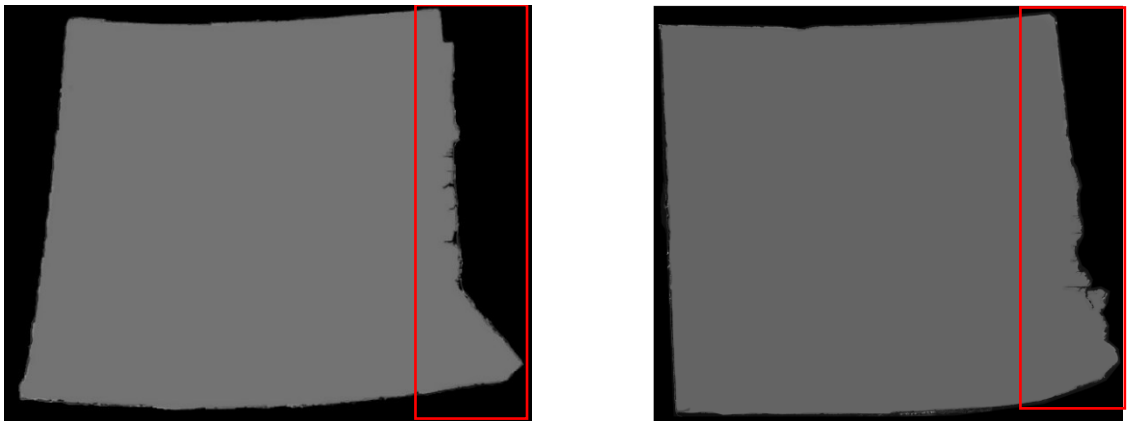

(a) (b)

Figure 7-10 Cross-sectional fracture surface used for EBSD investigations (crack growth direction from top to bottom) (a) notch No. 22 (b) notch No. 87

The crystallographic characteristics of the specimens were examined using the Electron Backscatter Diffraction method. This technique provides a more efficient and effective way to analyze crack growth and failure than traditional scanning electron microscopy (SEM) [56]. Figure 7-11 shows EBSD crystal orientation maps and Inverse Pole Figures (IPF) for the above-mentioned failed notches. High-angle grain boundary (HAGB) refers to grain boundaries that are misoriented more than 15° [35]. Every point in the Figure represents a specific crystal orientation; the corners represent <001>, <101> and <111> directions. The colour of each point indicates the density or concentration of that particular crystallographic orientation. These Figures demonstrate the corrosion fatigue mechanism in the NNpH environment by the transgranular crack paths in both failed notches (in contrast to high pH SCC with intergranular crack growth [57]–[62]). IPF images acquired in this study indicate that crack propagates independently of grain orientation, according to research [30]. Although the pipeline steel used in this study was normalized (API 5L-X52N), hot rolling and subsequent processing can affect grain orientation [63].

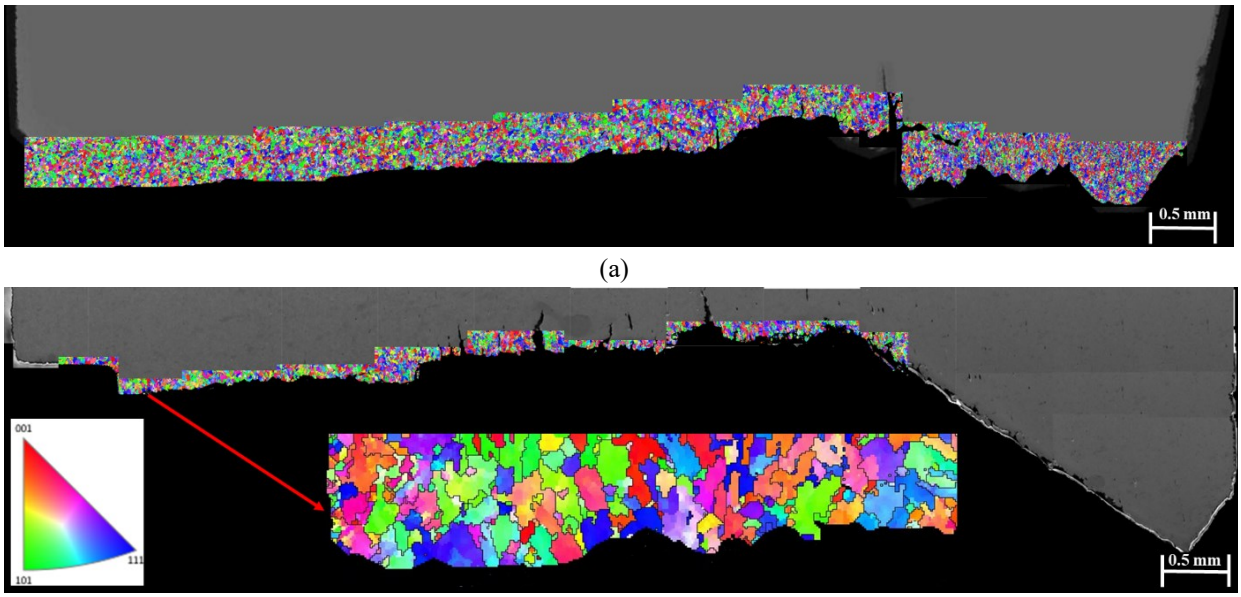

(a)

(b)

Figure 7-11 Inverse polar Figure (IPF) of the fracture surface edge (red rectangle in Figure 7-10): crack growth direction from left to right (a) notch No. 22 (b) notch No. 87

By providing information on local crystal misorientations, EBSD maps can also be used to show how the pipe is deformed near the cracks (degree of deformation around cracks). Small rotations are called misorientations. These rotations may result from dislocation movement within the material [30], [64]. There is a small amount of misorientation between adjacent microregions under small deformations. As a result, the misorientation of the regions can be applied to identify local zones (regions) that have undergone plastic deformation [33]. Figure 7-12 shows strain contour maps used in this study to analyze plastic deformation around fracture paths. As mentioned, this component estimates the extent of deformation, or strain, in individual grains on a map. The strain contouring component measures the maximum misorientation between any two points in the grain and then weights this grain according to this misorientation value. They can be used to qualitatively assess small local strain gradients (as a measure of local deformation severity).

Figures 7-12c and 7-12d show that the maximum misorientation values within grains are much lower in Stage II than in Stage III crack growth, emphasizing that plastic deformation is suppressed

in Stage II. It is known that misorientation analyses via EBSD, such as strain contouring, qualitatively reflect the plastic strain within the plastic zone surrounding the crack tip and the corresponding density of the geometrically necessary dislocations (GNDs) [31], [34]. Because of this, a lower plastic strain amplitude is required in Stage II when the hydrogen-related mechanism (HELP) is the main cause of crack propagation. This indicates that the crack propagated in a brittle manner without extensive plasticity. In fact, this map indicated heavily suppressed plastic deformation around the crack path [31], [34]. D. Birenis *et al.* [31] found similar plasticity suppression and cleavage fracture during a fatigue crack growth rate test using pure Fe under 90 MPa hydrogen, interpreted as a hydrogen-enhanced decohesion mechanism.

On the other hand, evidence of plastic deformation was apparent along the crack path in Stage III (rapid crack growth) and the final collapse (Figures 7-12e and 7-12f). During Stage III, grain orientations near fracture paths were heavily distorted and clear contrast changes were observed, suggesting the formation of sub-grains or dislocation cell structures. Also, it is obvious that plastic deformation was uniformly distributed along the crack path at this Stage [31], [34], [51], [52]. A high dislocation density around the crack path allows misorientations to accumulate inside grains and distortion to occur between neighbouring lattices [63].

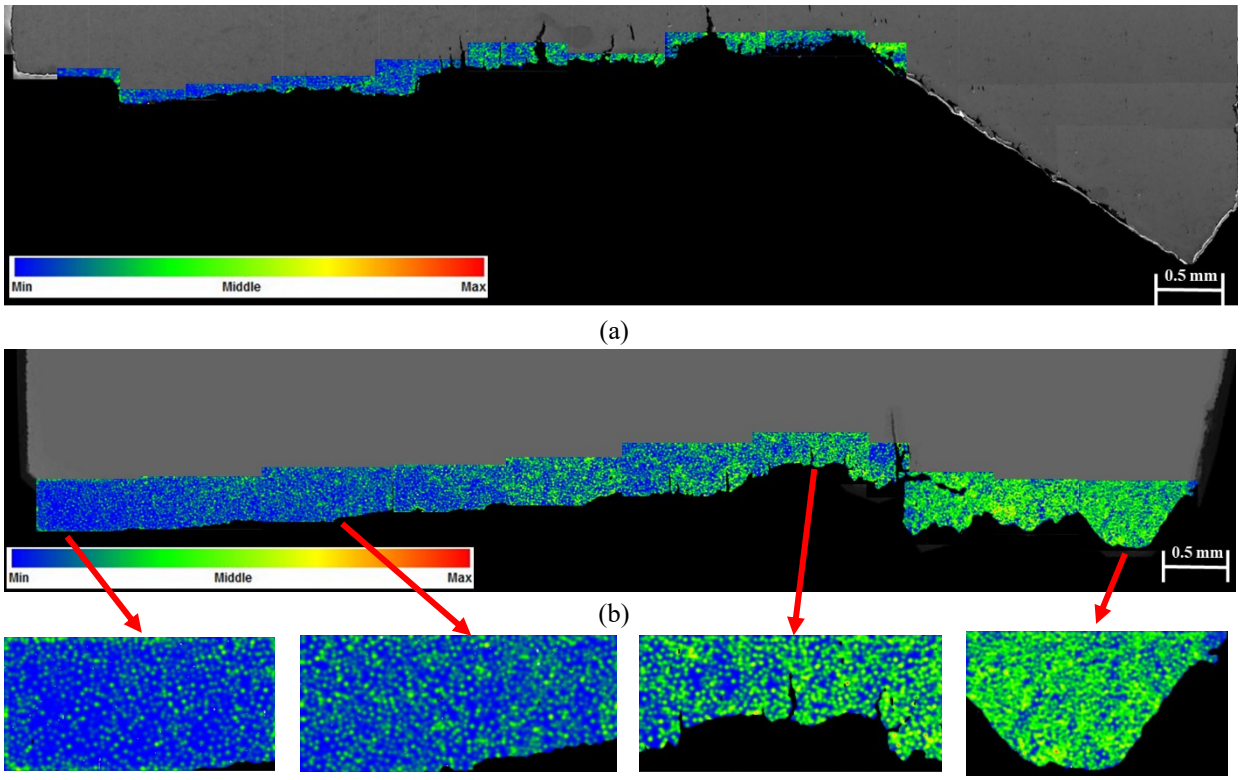

Figure 7-12 EBSD strain contouring of the fracture surface edge (red rectangle in Figure 7-10) (crack growth direction from left to right): (a) notch No. 22 (b) notch No. 87 including crack growth stages in the depth direction: (c) initial notch (d) crack growth Stage II (e) crack growth Stage III (f) plastic collapse

Figure 7-13 shows the distribution of the scanned points in strain contouring maps according to the misorientation angles they correspond to, allowing a quantitative analysis of plastic deformation. Plastic deformation was greatly reduced in the Stage II regime. Thus, the lower magnitude plastic strain occurred in Stage II, and much less plasticity was involved [31]. Stage III, however, shows a significantly higher misorientation than Stage II [31], [36]. A. Laureys *et al.* [36] reported that stress fields would be so large that slip planes inside the grains originated from shear deformation between the two cracks. Therefore, the crack growth mechanism in Stage III is influenced by stress fields, which are more significant than hydrogen-related mechanisms. The maximum misorientation observed was approximately 10 degrees in the plastic collapse region.

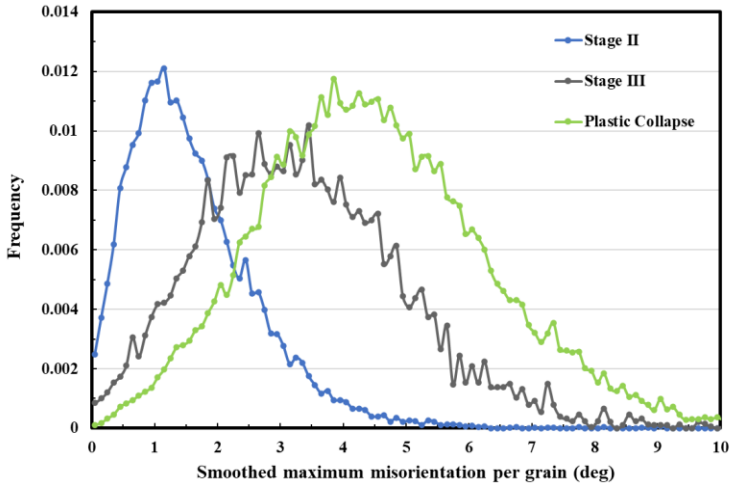

Figure 7-13 Frequency distribution of scanned points in strain contouring maps for different misorientation angles: Notch No. 87

7. 4 Discussion

7. 4. 1 Circumferential corrosion fatigue failure mechanism

This investigation deals with the final fracture from the growth of simulated dormant cracks of pipeline steels exposed to a typical near-neutral pH solution through the mechanism of hydrogen-enhanced fatigue. A notch with a 0.5 mm or 1.0 mm depth was made in the pipe wall with a varied distribution of residual stresses, either compressive, tensile, or free of residual stresses introduced by bending. As cracks can reach 0.5 mm in width in pipeline steels during field operations [65], the width of the notch was controlled within 0.2 mm.

Researchers have primarily investigated crack initiation in pipeline steel exposed to near-neutral pH environments on straight steel surfaces that are either polished, mill-scale covered, or with varied residual stresses. The initiation of cracks on a straight external surface often begins with pit formation and then crack initiation from the bottom of the pits. The artificial notches placed on the pipe's external surface in this study resemble pits/dormant notches. As this investigation assumes that crack initiation at Stage I occurred after passing dormancy, it is necessary to analyze crack

growth behaviour in the depth direction of failed notches, considering the effects of significant parameters and mechanisms, including stress distribution in the bent pipeline as a result of bending residual stress and cyclic loading.

Among all samples bent in inward and outward directions at various bending angles, just inward notches at the bend centerline showed failure before the end of the test (45 days) because of a higher crack growth rate as a result of higher residual tensile stress levels on the surface and consequently in the depth direction. However, the time to failure was different because of the stress distribution in the thickness direction and, consequently, various crack growth rates at different stages (which will be discussed in the next section). Based on the results of the cyclic loading test on the non-bent section that did not crack, it is clear that cyclic loading solely cannot cause failure at these levels with this depth of starter crack, so circumferential crack growth cannot be considered a threat for normal loading when there are no other sources of axial stresses, like the tensile residual stresses introduced by bending, *etc.*, which could add to the axial cyclic loading (pressure fluctuation). Similarly, the same approach can be applied to initial notches placed in the outward direction of the external pipe surface, showing no failure due to compressive residual stresses. The general agreement is that compressive residual stress suppresses crack growth while tensile residual stress promotes it [18]. Also, one of the three notches along the inward direction, located in the middle of the gauge length, failed the test because of higher tensile stress. Only five samples failed during the test, which were investigated in detail to better understand circumferential crack growth and failure at the bends in pipelines.

According to Figure 7-3, lower magnification fractography images can give a general idea of different stages. Finding the boundary between these stages, understanding the mechanism behind these stages, and understanding the crack growth rate exclusively in Stage II must be emphasized

in detail. Along with all other methods used in this investigation, the results of the CMOD test confirmed again that pipeline integrity management should focus on crack growth before reaching Stage III. For instance, notch No. 87 failed after 4620 cycles, of which 4533 cycles occurred before Stage III began, which means that only about 2% of its lifetime was associated with crack growth in Stage III. There was a transition from Stage II to Stage III in one-third of the pipeline steel's thickness in this notch. The importance of determining the crack growth rate at Stage II can be seen in this example. Determining the fracture mechanism using fractography images alone is difficult, so other supplementary tools have been used.

Although numerous researchers [6], [18], [46] have worked on the NNpH-CF crack growth mechanism, it seems that the presence of two sources of stress distribution in the depth direction of bent pipe in circumferential cracking makes the theory of failure through several stages more difficult. However, this type of failure consists of three main stages, similar to longitudinal NNpH-CF. These three stages and transition boundaries are influenced by hydrogen interaction with the steel and the level of stress/stress intensity factor in the depth direction [31]. It is imperative to remember that in this study, all bent samples were exposed to the same corrosive environment (C2 solution sparged with 5% CO_2). Since the diffusion of available hydrogen decreases in the thickness direction, the boundary between Stage II and III should be related to other factors, not hydrogen level. For example, L. Amaro *et al.* [66] demonstrated that experimental fatigue crack growth rate curves converge at high stress intensity ranges, indicating a decrease in hydrogen level dependence at the Stage II/III boundary. However, hydrogen concentration within a material is very difficult to measure accurately, especially within highly stressed fatigue zones [66].

As mentioned before, Figure 7-2a illustrates the initial stress distribution in the depth direction before crack initiation. However, this graph can not explain the actual situation during crack

propagation as it overlooks the significance of traction stress. Traction stress, defined as the through-thickness linear distribution stress meeting equivalent equilibrium conditions, becomes crucial during crack growth. As the remaining area carrying the load decreases during crack growth, this force shifts to the remaining area, causing an increase in stress across the entire remaining section. Figure 7-14 displays the initial stress distribution from the DIC method (orange line) and the traction stress (grey line), which escalates during crack propagation in the depth direction. Consequently, the actual stress distribution should consider both the DIC result and traction stress simultaneously. It is evident that the actual stress during crack growth (blue line) experiences a slight decrease followed by a sharp increase. Another curve illustrates the plastic collapse stress (green line) in the depth direction derived from the CSA-Z662 code (Canadian standard for oil and gas pipeline systems), depicting the collapse stress distribution with an increase in crack depth in the thickness direction. The point of intersection between plastic collapse stress and the actual stress distribution signifies the real plastic collapse occurring at a depth of approximately 6.5 mm, in complete alignment with data obtained from other methods discussed previously, such as EBSD strain countering and CMOD investigation. The DIC result and the traction stress were accumulated precisely at the location of the slanting, so the actual stress could be verified.

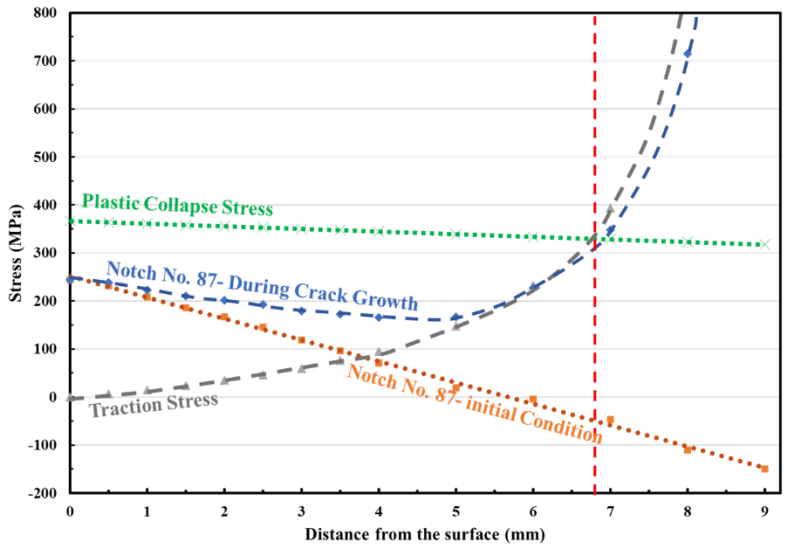

Figure 7-14 Stress distribution in the thickness direction: notch No. 87

As a result of these many complementary methods were used in this study (fractography images, striation, CMOD, and EBSD analysis) to determine the crack growth behaviour at failed notches, Figure 7-15 illustrates crack growth stages for a failed notch (notch No. 87: 20-degree bending, 0.5 mm initial notch depth and 35% SMYS cyclic loading) as an example. This image utilized diverse tools, including the actual crack growth rate (depicted in Figure 7-15a), changes in maximum stress intensity factor in the depth direction (illustrated in Figure 7-15b), and EBSD strain counting (shown in Figure 7-15c). These tools were employed to identify the boundary between different regions (red lines) and understand cracking behaviors. Figure 7-15b comprises two distinct graphs: the initial maximum stress intensity factor changes in the depth direction before notching and crack initiation, obtained from the DIC method, and the actual maximum stress intensity factor changes in the depth direction during crack growth. While the analysis of initial stress intensity factor range changes was extensively discussed in Section 7.3.1 and Figure 7-2, the primary determinant of crack growth behavior appears to be related to the actual stress intensity factor change. This value can be derived from the traction stress, which shifts to the remaining ligament during crack growth, in addition to the stress derived from the DIC method

(including residual stress and applied loading). As a result of a detailed discussion of the various stages of C-NNpH-CF failure provided here, Figure 7-15d suggests different crack growth stages.

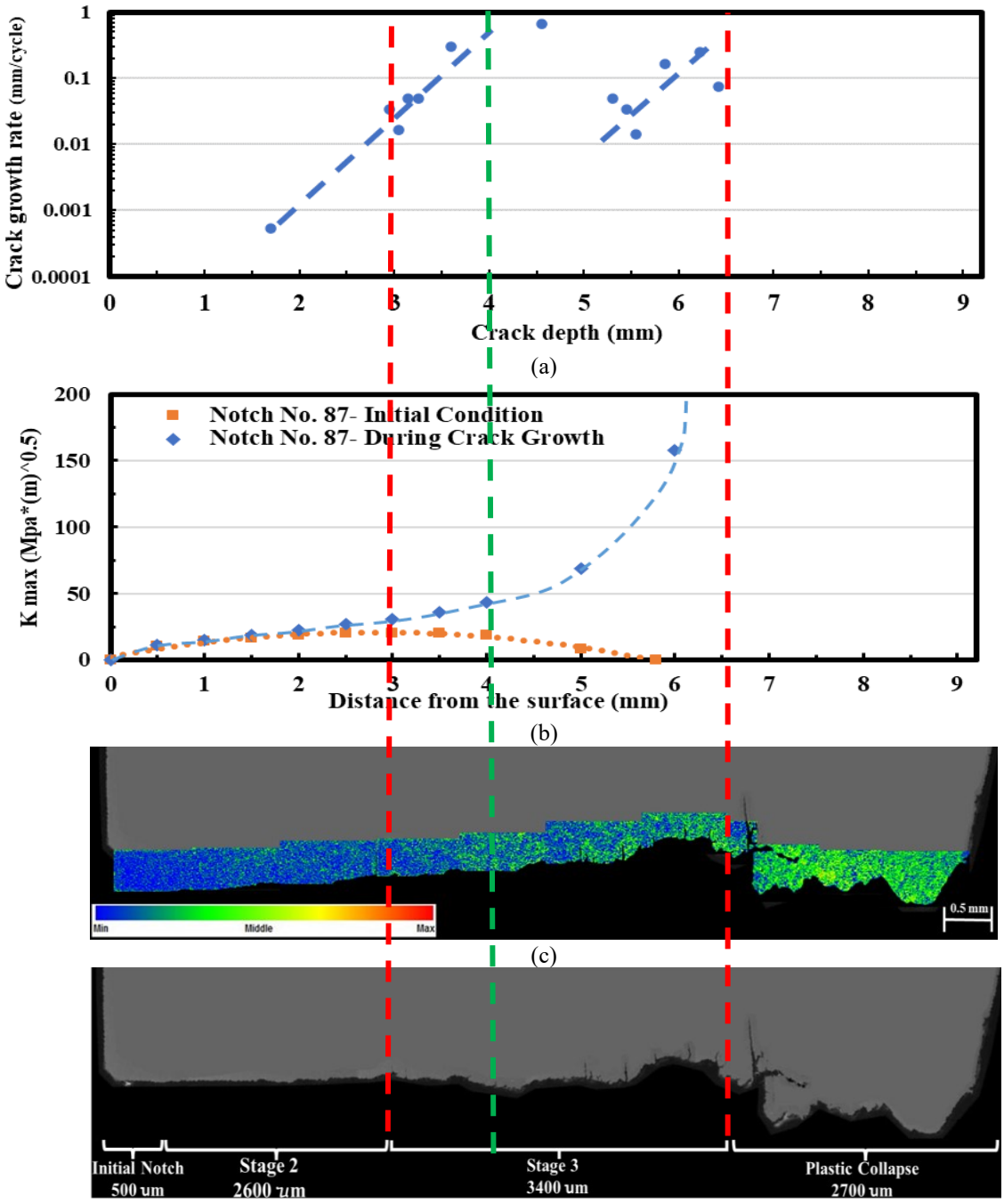

Figure 7-15 Circumferential corrosion fatigue failure mechanism (notch No. 87: 20-degree bending, 0.5 mm initial notch depth and 35% SMYS cyclic loading): a) actual crack growth rate, b) maximum stress intensity factor changes in the depth direction, (c) EBSD strain countering, (d) crack growth stages

- **Stage I: crack re-initiation and dormancy**

In recent decades, researchers have studied the initiation of active cracks from dormant cracks (the initial notch in this study). Certain conditions must be met to reactivate a dormant crack. One is the magnitude and nature of the stresses near the crack tip. A second factor is the amount of diffusible hydrogen reaching the crack tip. These two factors are interconnected [1], [6], [25], [43]. In order to have a sustained crack growth, tensile cyclic loading and hydrogen-enhanced fatigue must prevail over crack tip blunting and dormancy. Hydrostatic stresses in the plastic zone, hydrogen segregation, and weakest links near the crack tip can cause hydrogen-induced microcracks to form, resharpening the main crack. Indeed, hydrogen-related sharpening and cyclic loading can synergistically resharpen blunted cracks. The likelihood of growth is high wherever these two conditions coexist for a prolonged period [25], [43], [67]. These factors also dominate the crack initiation of blunt notches in this investigation. As crack depth increases, the dissolution rate decreases, so corrosion from the NNpH environment has a negligible effect after Stage I (crack initiation from the bottom of the notch).

Crack re-initiation from the bottom of artificial notch/dormant cracks is not the topic of this paper. However, it should be noted that the crack growth rate acquired in Stage II includes the time/number of cycles needed for crack re-initiation from the notch root.

- **Stage II: stable crack growth**

Stage II crack growth includes specific features of the crack growth mechanism under the influence of hydrogen-enhanced fatigue. However, determining the crack growth mechanism in the NNpH environment is difficult because hydrogen cannot be directly observed in the fracture process [68]. SEM images and EBSD IPF maps show brittle transgranular quasi-cleavage fracture as the first characteristic of crack growth in NNpH environments accompanied by striations on fracture

surfaces [31], [49]. Cracking behaviour in this region may be caused by hydrogen-enhanced localized plasticity (HELP). As hydrogen concentration increases, dislocation motion is less resistant, and flow stress is lower, so dislocations move at lower stress levels. The crack propagates along the slip plane in response to localized shear stress. As a result, it appears that hydrogen has a significant effect on crack growth at this stage.

A study conducted by D. Birenis *et al.* [31] demonstrated that hydrogen can harden pure Fe by affecting screw dislocation motion. However, at higher hydrogen concentrations, hydrogen may form pairs or clusters or interact with interstitial carbon atoms and pin edge dislocations. By slowing down the kinked edge components of the screws, this can significantly reduce the screw dislocation mobility. Due to a combination of high stress and hydrogen concentrations, quasi-cleavage fracture occurs in the Stage II regime by inhibiting plastic relaxation [31]. In the crack tip zone, tensile stress is not only responsible for triggering fracture but also for dilation of the lattice, which results in a higher concentration of hydrogen in the vicinity of the crack tip, which operates dislocation locking and weakens matrix bonding [31], [47].

The combination of critical tensile stress and critical hydrogen concentration causes suppressed plastic deformation and primary cleavage micro crack formation ahead of the crack tip. The main crack and the primary cleavage microcrack coalesce and advance the main crack forward, resulting in striation formation cycle-by-cycle in Stage II [31], [69]. This feature is completely consistent with the strain contouring maps and shows the minimum strain and deformation at the fracture surface edge. The stress intensity factor increases with increasing depth, and the striation interspace and crack growth rate subsequently increase. It should be noted, however, that the average crack growth rate derived from striation during Stage II is similar to the actual crack growth rate derived from the actual crack growth depth at Stage II and the total number of cycles.

The minor differences are likely due to ignorance regarding the number of cycles required for crack re-initiation from the notch root.

- **Stage III: rapid crack growth and final fracture**

Based on fractographic images, it is difficult to determine the exact boundary between stages II and III. Furthermore, the striation interspace (and related crack growth rate) shown in Figure 7-6b is inconsistent with the actual crack growth rate in Figure 7-9. In addition to the EBSD strain contouring method (Figure 7-12), it would seem that a plastic CMOD starting point (Figure 7-8 and Figure 7-15) might be an appropriate way to determine this precise boundary. A failure root analysis of pipeline fractures in service requires finding this boundary, as this crack depth can provide a stable crack growth rate in Stage II, which is needed for pipeline integrity management regarding C-NNpH-CF susceptibility. Fortunately, these failures commonly leak only, which is usually less destructive than fast fracture in the axial direction.

The type and proportion of dislocation structures depend on Stage III's applied plastic strain amplitude. Plastic strain is sufficiently high at this stage due to a higher stress intensity factor to form dislocation cell structures [34]. Figure 7-15 provides a comprehensive information for distinguishing between stages II and III. The obvious difference between the EBSD map in stages II and III demonstrated a significant plasticity increase in Stage III. As shown in Figure 7-15c, the EBSD strain countering map in Stage III confirms that much plasticity was involved, and the lower magnitude plastic strain was needed for the material to fail when having a higher stress level in the presence of hydrogen [31].

It seems that a high stress intensity factor governs Stage III crack growth compared to Stage II, which is governed by a medium stress intensity factor and hydrogen-enhanced fatigue. Since crack growth is limited to only a few cycles at Stage III, hydrogen-enhanced fatigue cannot occur [52].

However, hydrogen can diffuse from the external surface to the remaining ligament during the test, which results in a weak iron structure. According to the research by T. Michler *et al.* [70], the HELP mechanism can result in micro void coalescence (MVC), which is supported by high-magnification SEM images (Figure 7-5b) [70]. These voids become elongated and often have equiaxed morphologies.

The transition from Stage II (stable crack growth) to Stage III (rapid crack growth) usually occurs when the stress intensity factor is high enough. EBSD strain contouring map (Figure 7-12 and Figure 7-15c) confirms that the crack growth rate increases continuously after passing the Stage II region (Figure 7-8). However, it is inconsistent with the initial accumulated stress distribution (from applied loading and residual stress) in the depth direction, which reaches zero at a depth of 5.5 to 6 mm, as well as the maximum stress intensity factor, which decreases as depth increases. In general, the stress intensity factor (range) is the driving force for corrosion fatigue crack growth in the NNpH environment [71], so having no stress intensity factor when the initial stress reaches zero should have prevented crack growth. It must be noted, however, that cracking mechanisms cannot be explained by the initial stress or stress intensity factor distribution in the depth direction due to substantial crack growth at this depth. In fact, according to Figure 7-14 and Figure 7-15c, although crack growth can release residual stress, all different methods used in this study emphasize that crack growth in the depth direction modifies stress level (and consequent stress intensity factor so that a higher crack growth rate happens. Figure 7-15b indicates the actual changes in maximum stress intensity factor in the depth direction results from the increase in actual tensile stress levels (Figure 7-14) when considering the shift of applied stress to the remaining ligament of the gauge thickness (traction stress). The combination of increasing actual stress during crack growth and the influence of growing crack depth leads to a sharp elevation in the

stress intensity factor range during Stage III, as depicted in Figure 7-15b. Therefore, the physical morphology, changes in stress intensity factor range, actual crack growth, and the extent of plastic deformation (EBSD strain counting) collectively define Stages II and III.

The crack growth rate in Stage III ranges from 0.01 to 0.6 mm/cycle, which is about 1000 times faster than in Stage II (0.00057 mm/cycle). That's why just 2% of the pipeline's lifetime was spent in Stage III. Figure 7-15a also shows a drop in the actual crack growth rate (at a depth of about 4 mm). The reduction in the actual crack growth rate could be associated with the transition from a region governed by linear elastic fracture mechanics (LEFM) to one governed by elastic-plastic fracture (EPFM) mechanics. In fact, the vertical green line in Figure 7-15 delineates the boundary between the LEFM and EPFM regions. Beyond this boundary, a rapid increase in the maximum stress intensity factor occurs due to the presence of traction stress, which is added to the initial stress obtained from the DIC method. This substantial rise in the actual stress level is depicted in Figure 7.14. As the stress level increases dramatically, the plastic zone becomes very large, making LEFM no longer applicable. In the case of EPFM, the stress in the region ahead of the crack is reduced. Consequently, this stress level and stress intensity factor allow for the establishment of another growth rate, which could be governed by EPFM. As indicated by EBSD strain countering in Figure 7-15c, the degree of plastic deformation exhibits a significant increase immediately after crossing the boundary between LEFM and EPFM (green line). As the crack continues to propagate, the crack growth rate increases again, ultimately reaching the final depth just before instantaneous fracture at the depth of around 6.5 mm. Further study is needed to determine the precise stress distribution in the depth direction after each level of crack propagation.

The specimen eventually fails due to plastic collapse or tearing instability. Fracture toughness can explain the transition from quasi-cleavage to final fracture [47]. At the final stage, after voids have

formed, further plastic strains and hydrostatic stresses cause them to grow and eventually coalesce. Local instabilities develop when plastic strain is concentrated along a sheet of voids. In the larger particles, the remaining ligament produces a triaxial stress state that promotes the nucleation and growth of voids. Due to the closely spaced particles, instability occurs soon after these smaller voids form, resulting in the specimen's total fracture. The 45° angle between the fracture plane and the applied stress results in combined Mode I/Mode II loading for this type of fracture [45].

7. 4. 2 Influence of bending residual stress and other variables on circumferential corrosion fatigue failure

This section focuses on how various bending parameters and stress distribution affect crack growth stages in the depth direction. After 45 days of cyclic loading in an NNpH environment, all three long samples with 10-degree bending showed no signs of failure. Thus, 20-degree bending residual stress has significantly more effect on crack growth and failure. According to Table 7-1, the crack growth rate is generally highest for notch No.17 because it has a 20-degree bent centerline and 50% SMYS, with maximum stress on its external surface. The higher the initial stress on the external surface, the higher the stress at the bottom of the notch (considering the stress concentration factor), increasing the likelihood of crack initiation at a shorter incubation time. Due to 35% SMYS loading and 0.5 mm initial depth, notch No. 87 shows the minimum crack growth rate.

Since the mentioned parameters also strongly impact crack initiation from the bottom of artificial notches (as well as increasing the incubation time required for crack initiation), it is not feasible to conduct a comprehensive study on the effects of various parameters on crack growth as a whole. However, in fractography images, all failed notches share a similar pattern, as shown in Figure 7-3. In this investigation, two failed notches, No. 22 (20-degree bending, 1 mm initial notch depth

and 50% SMYS cyclic loading) and 87 (20-degree bending, 0.5 mm initial notch depth and 35% SMYS cyclic loading), were selected for further study using EBSD images and making a correlation between the stress distribution and stress intensity factor changes in the thickness direction and crack growth mechanism. Because long sample No. 2 was designed as a repeat test for long sample No. 1 to ensure test consistency, it failed in a notch located 10 mm from the bend centerline. On this long sample, notch 27 was not made. On the external surface of notch No. 22, the tensile stress level is higher than notch No. 87 due to the higher applied loading (50% SMYS compared with 35% SMYS). Figure 7-2a shows the initial stress distribution in the thickness direction. It should be emphasized again that both bending and applied loading contribute to stress distribution in the thickness direction, so any depth in notch No. 22 is under more tensile stress. A higher stress intensity factor (higher peak in Figure 7-2b) results from combining this higher tensile residual stress with crack depth. EBSD strain contouring of the fracture surface edge in Figure 7-12 also shows a similar pattern of increasing plastic deformation from Stage II (affected by hydrogen-assisted fatigue) to Stage III (affected by higher stress intensity factors associated with rapid crack propagation). The boundary between stages II and III appears at a similar depth regardless of the stress level in the depth direction. This concept is depicted in Figure 7-12, where the boundary between the two stages is about 3 mm from the pipe's external surface (about 30% of the pipe's wall thickness). Due to higher stress at each depth, notch No. 22 has a more dentate edge in stages II and III than notch No. 87. It is the crack growth rate in Stage II that matters to pipeline integrity specialists since uncontrolled and fast crack growth in Stage III leads to pipeline failure (leakage/ rupture).

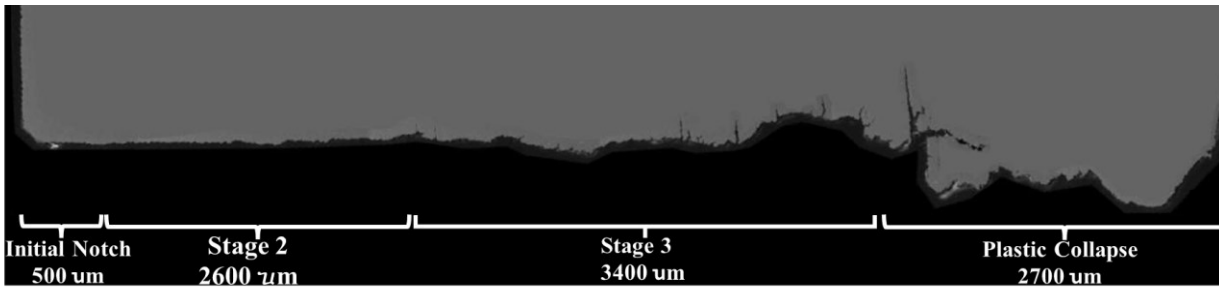

(a)

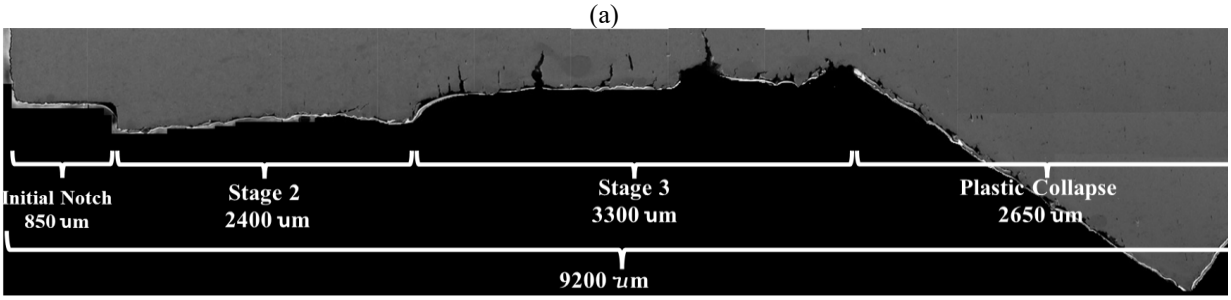

(b)

Figure 7-16 Crack growth stages (a) notch No. 87 (b) notch No. 22

7. 5 Conclusion

This study analyzed circumferential corrosion fatigue crack failure at the bottom of dormant cracks/pits in steels exposed to near-neutral pH environments. The following are some key findings of this investigation:

1. For C-NNpH-CF investigations, the digital image correlation (DIC) method could be considered an appropriate technique since it can analyze stress distributions impacted by various residual and applied stresses. Based on the final stress distribution in this study, it is evident that the accumulation of axial loading and residual stress results in an increase in the level of stress (compressive/tension) at the bending centerline since the type of axial cyclic stress and bending residual stress in the inward bending direction is tension and in the outward bending direction is compression, regardless of the degree of bending and axial loading level.

2. Among all samples bent inward and outward at various bending angles, just artificial notches at the centerline of inwardly bent sections showed failure during the test (45 days). Due to different stress distributions in the thickness direction and various crack growth rates, the test duration varied. As a result of the corrosion fatigue test performed on the non-bent section (no residual stress), it is evident that cyclic loading alone at this level cannot cause failure; therefore, circumferential crack growth cannot be considered a threat when there are no other sources of axial stresses, such as bending. In the same scenario, outwardly bent sections show no failure due to compressive residual stress.

3. Pipeline integrity management can rely on Stage II's stable crack growth rate to predict pipeline lifetime. Determining the crack growth rate for a failed pipeline is possible by simultaneously using fractography images, CMOD results, and EBSD strain countering.

4. A high stress intensity factor governs Stage III crack growth compared to Stage II, which is governed by a medium stress intensity factor and hydrogen-enhanced fatigue.

5. Despite crack growth releasing residual stress, crack growth in the depth direction modifies stress level (and consequently stress intensity factor) so that a higher crack growth rate occurs.

6. Stress gradient in the depth direction is a significant feature of circumferential NNpH-CF. Different stress distributions in the thickness direction (as a result of applied cyclic loading and bending residual stress) define the C-NNpH-CF behaviour.

References

[1] J. Zhao, W. Chen, M. Yu, K. Chevil, R. Eadie, J. Been, G. Van Boven, R. Kania & S. Keane, “Crack growth modelling and life prediction of pipeline steels exposed to near-Neutral pH

environments: stage II crack growth and overall life prediction," Metall Mater Trans A Phys Metall Mater Sci, vol. 48, no. 4, pp. 1641–1652, Apr. 2017, https://doi.org/10.1007/s11661-016-3939-z.

[2] M. Elboujdaini and M. T. Shehata, "Stress corrosion cracking: A Canadian prospective for oil and gas pipeline," 2005.

[3] G. Van Boven, R. Rogge, and W. Chen, "Residual stress and stress corrosion cracking of high pressure hydrocarbon transmission pipelines," in Proceedings of the 2006 International Pipeline Conference. Calgary, Alberta, Canada. IPC2006-10486. https://doi.org/10.1115/IPC2006-10486.

[4] J. A. Beavers and B. A. Harle, "Mechanisms of high-pH and near-neutral-pH SCC of underground pipelines," Journal of Offshore Mechanics and Arctic Engineering, vol. 123, no. 3, pp. 147–151, Aug. 2001, https://doi.org/10.1115/1.1376716.

[5] S. Jian, Y. Zupei, and M. Yunxin, "Investigation on potential SCC in gas transmission pipeline in China," in Proceedings of the 2004 International Pipeline Conference. Calgary, Alberta, Canada. IPC2014-33059. https://doi.org/10.1115/IPC2004-0709.

[6] J. Zhao, Weixing Chen, M. Yu, K. Chevil, R. Eadie, G. Van Boven, R. Kania, J. Been & S. Keane, "Crack growth modeling and life prediction of pipeline steels exposed to near-neutral pH environments: dissolution crack growth and occurrence of crack dormancy in stage I," Metall Mater Trans A Phys Metall Mater Sci, vol. 48, no. 4, pp. 1629–1640, Apr. 2017, https://doi.org/10.1007/s11661-016-3951-3.

[7] Y.-Z. Wang, R. W. Revie, and R. N. Parkins, "Mechanistic aspects of stress corrosion crack initiation and early propagation," in NACE International Conference, Paper No.: 143., 1999.

[8] J. Beavers and T. A. Bubenik, “Stress corrosion cracking,” in Trends in Oil and Gas Corrosion Research and Technologies: Production and Transmission, 2017, pp. 295–314. https://doi.org/10.1016/B978-0-08-101105-8.00012-7.

[9] M. J. W. Ilm, “The role of pressure and pressure fluctuation in the growth of Stress Corrosion Cracks in line pipe steels,” in Proceedings of the 1998 International Pipeline Conference. Calgary, Alberta, Canada. IPC 1998-2049, 1998. https://doi.org/10.1115/IPC1998-2049.

[10] B. Johnson, B Tesfaye, C. Wargacki, T. Hennig, E. Suarez “Complex Circumferential Stress Corrosion Cracking: Identification, Sizing and Consequences for the Integrity Management Program,” in Proceedings of the 2018 International Pipeline Conference. Calgary, Alberta, Canada. IPC2018-78564. https://doi.org/10.1115/IPC2018-78564.

[11] N. Bates, M. Brimacombe, and S. Polasik, “Development and experience of a circumferential stress corrosion crack management program,” in Proceedings of the 2018 International Pipeline Conference. Calgary, Alberta, Canada.IPC2018-78315.

[12] M. Brimacombe, C. Wargacki, and N. Global Leduc, “Circumferential crack detection: Challenges, solutions and results,” in Proceedings of the 2016 International Pipeline Conference. Calgary, Alberta, Canada. IPC2016-64111. https://doi.org/10.1115/IPC2016-64111.

[13] Ron Thompson, R. Gardner, K. Dwyer, A. Corbett, and M. Marquis Hotel, “A case study in the detection and sizing of circumferential stress corrosion cracking Pipeline Pigging and Integrity Management Conference,” in Pipeline pigging and integrity management conference, Houston, February 2020.

[14] R. R. S. M. Fessler, “Characteristics, cause, and management of circumferential stress-corrosion cracking,” in Proceedings of the 2014 International Pipeline Conference. Calgary, Alberta, Canada. https://doi.org/10.1115/IPC2014-33059.

[15] M. Pope, *C. S. Camerini, J. C. G. Teixeira, M. T. Piza, W. Baptista, B. G. de Souza, H. L. Oliver*, "Circumferential SCC in pipeline due to land creeping," in Proceedings of the 2002 International Pipeline Conference. Calgary, Alberta, Canada. https://doi.org/10.1115/IPC2002-27192.

[16] D. Abdulhameed, S. Adeeb, and R. Cheng, “The influence of the Bourdon effect on pipe elbow” in Proceedings of the 11th International Pipeline Conference, 2016, pp. 1–10. https://doi.org/10.1115/IPC2016-64659.

[17] S. Attia, M. Mohareb, M. Martens, N. Yoosef-Ghodsi, Y. Li, and S. Adeeb, “Numerical assessment of elbow element response under internal pressure,” Journal of Pressure Vessel Technology, Transactions of the ASME, vol. 143, no. 5, Oct. 2021, https://doi.org/10.1115/1.4050091.

[18] S. Wang and W. Chen, “Overview of Stage 1b Stress Corrosion Crack Initiation and Growth of Pipeline Steels,” Corrosion, vol. 79, no. 3, pp. 284–303, Mar. 2023, https://doi.org/10.5006/4168.

[19] Weixing Chen, "The Effect of Pressure Fluctuations on the Growth Rate of Near-Neutral pH SCC," 2020.

[20] Y. B. Beauregard and C. Edwards, “Analysis of sever circumferential SCC found on an ethane pipeline,” in Proceedings of the 2014 International Pipeline Conference. Calgary, Alberta, Canada. , 2014.

[21] J. Babcock, D. Dewar, and J. Webster, “Deer Mountain case study: integration of pipe and ground monitoring data with historical information o develop landscape management plan,” Proceedings of the 2020 International Pipeline Conference. Calgary, Alberta, Canada. IPC2020-9613. https://doi.org/10.1115/IPC2020-9613.

[22] A. Contreras, L. Quej-Ake, R. Galvan-Martinez, O. Vega, L. Cárdenas Norte, and C. San Bartolo Atepehuacan, "Residual stress assessment and its effect on SCC of pipelines steel in acidic soil environment," in MRS Online Proceedings Library 1616, 122 (2014). https://doi.org/10.1557/opl.2014.235.

[23] S. Limon, P. Martin, M. Barnum, and R. Pilarczyk, "Fracture toughness testing and its implications to engineering fracture mechanics analysis of energy pipelines," in Proceedings of the 2018 International Pipeline Conference. Calgary, Alberta, Canada. https://doi.org/10.1115/IPC2018-78723.

[24] M. L. Martin, J. A. Fenske, G. S. Liu, P. Sofronis, and I. M. Robertson, "On the formation and nature of quasi-cleavage fracture surfaces in hydrogen embrittled steels," Acta Mater, vol. 59, no. 4, pp. 1601–1606, Feb. 2011, https://doi.org/10.1016/j.actamat.2010.11.024.

[25] H. Shirazi, R. Eadie, and W. Chen, “A review on current understanding of pipeline circumferential stress corrosion cracking in near-neutral PH environment,” Engineering Failure Analysis, vol. 148, Jun. 01, 2023. https://doi.org/10.1016/j.engfailanal.2023.107215.

[26] P. Malmqvist, "Monitoring of crack growth and crack mouth opening displacement in compact tension specimens at high temperatures Development and implementation of the Direct Current Potential Drop (DCPD) method."

[27] Y. Song, P. Yang, T. Xia, Z. Peng, and J. Zhang, "The crack growth rate and crack opening displacement of EH-36 steel under low-cycle fatigue loading," Ocean Engineering, vol. 280, Jul. 2023, https://doi.org/10.1016/j.oceaneng.2023.114734.

[28] N. Walker and C. J. Beevers, "A fatigue crack closure mechanism in titanium," Fatigue Fract Eng Mater Struct, vol. 1, no. 1, pp. 135–148, 1979, https://doi.org/10.1111/j.1460-2695.1979.tb00372.x.

[29] S. Hu, Z. Mi, and J. Lu, "Effect of crack-depth ratio on double-K fracture parameter of reinforced concrete," in Applied Mechanics and Materials, 2012, pp. 937–941. https://doi.org/10.4028/www.scientific.net/AMM.226-228.937.

[30] E. Entezari, J. L. Velázquez, M.A. Mohtadi-Bonab, D. Rivas López, M. Alejandro Beltrán Zúñiga, R. Khatib Zadeh Davani, J. Szpunar, "Experimental observations of nucleation and crack growth paths of hydrogen-induced cracking in pipeline steel," Eng Fail Anal, vol. 154, Dec. 2023, https://doi.org/10.1016/j.engfailanal.2023.107650.

[31] D. Birenis, Y. Ogawa, H. Matsunaga, O. Takakuwa. Yamabe, Prytz, A. Thøgersen, "Interpretation of hydrogen-assisted fatigue crack propagation in BCC iron based on dislocation structure evolution around the crack wake," Acta Mater, vol. 156, pp. 245–253, Sep. 2018, https://doi.org/10.1016/j.actamat.2018.06.041.

[32] J. B. Wiskel, J. Ma, J. Valloton, D. G. Ivey, and H. Henein, "Strain aging on the yield strength to tensile strength ratio of UOE pipe," Materials Science and Technology, vol. 33, no. 11, pp. 1319–1332, Jul. 2017, https://doi.org/10.1080/02670836.2017.1288776.

[33] A. Smirnov, E. Smirnova, and S. Alexandrov, "A new experimental method for determining the thickness of thin surface layers of intensive plastic deformation using electron

backscatter diffraction data," Symmetry (Basel), vol. 12, no. 4, Apr. 2020, https://doi.org/10.3390/SYM12040677.

[34] Y. Ogawa*, D. Birenis , H. Matsunaga, A. Thøgersen, O. Takakuwa , J. Yamabe*, "Multi-scale observation of hydrogen-induced, localized plastic deformation in fatigue-crack propagation in a pure iron," Scr Mater, vol. 140, pp. 13–17, Nov. 2017, https://doi.org/10.1016/j.scriptamat.2017.06.037.

[35] S. Nafisi, M. Arafin, R. Glodowski, L. Collins, and J. Szpunar, "Impact of vanadium addition on API X100 steel," ISIJ International, vol. 54, no. 10, pp. 2404–2410, 2014, https://doi.org/10.2355/isijinternational.54.2404.

[36] A. Laureys, M. Pinson, T. Depover, R. Petrov, and K. Verbeken, "EBSD characterization of hydrogen induced blisters and internal cracks in TRIP-assisted steel," Mater Charact, vol. 159, Jan. 2020, https://doi.org/10.1016/j.matchar.2019.110029.

[37] K. Manthiramoorthy and A. Krishnaveni, "Fracture Parameter Evaluation Using Digital Image Correlation Technique," 2017.

[38] B. Tasdemir and B. Taşdemir, “Determination of stress intensity factor using digital image correlation method,” Matter, vol. 2, no. 1, 2015.

[39] R. B. Á. Pradas Cristina, "Stress and strain analysis of a material with Digital Image Correlation method (DIC)," Western Norway University of Applied Sciences, 2020.

[40] L. Shi, X. Zhang, L. Zhang, C. Wang, and J. Wang, "Application of digital image correlation technique in stress and strain measurement," Materials (Basel) https://doi.org/10.3390/ma12152349.

[41] G. Van Boven, W. Chen, and R. Rogge, "The role of residual stress in neutral pH stress corrosion cracking of pipeline steels. Part I: Pitting and cracking occurrence," Acta Mater, vol. 55, no. 1, pp. 29–42, Jan. 2007, https://doi.org/10.1016/j.actamat.2006.08.037.

[42] W. Chen, G. Van Boven, and R. Rogge, "The role of residual stress in neutral pH stress corrosion cracking of pipeline steels - Part II: Crack dormancy," Acta Mater, vol. 55, no. 1, pp. 43–53, Jan. 2007, https://doi.org/10.1016/j.actamat.2006.07.021.

[43] W. Chen, R. Kania, R. Worthingham, and G. Van Boven, "Transgranular crack growth in the pipeline steels exposed to near-neutral pH soil aqueous solutions: The role of hydrogen," Acta Mater, vol. 57, no. 20, pp. 6200–6214, Dec. 2009, https://doi.org/10.1016/j.actamat.2009.08.047.

[44] J. Toribio, "Residual stress effects in stress-corrosion cracking," J Mater Eng Perform, vol. 7, pp. 173–182, 1998. https://doi.org/10.1361/105994998770347891.

[45] T.L. Anderson, Fracture Mechanics Fundamentals and Applications, vol. 3. Taylor & Francis, 2005.

[46] S. Lynch and S. Lynch, "Some fractographic contributions to understanding fatigue crack growth," Int J Fatigue, vol. 104, pp. 12–26, Nov. 2017, https://doi.org/10.1016/j.ijfatigue.2017.06.036.

[47] Y. Ogawa, H. Matsunaga, J. Yamabe, M. Yoshikawa, and S. Matsuoka, "Unified evaluation of hydrogen-induced crack growth in fatigue tests and fracture toughness tests of a carbon steel," Int J Fatigue, vol. 103, pp. 223–233, Oct. 2017, https://doi.org/10.1016/j.ijfatigue.2017.06.006.

[48] B. A. Kim, W. Zheng, G. Williams, M. Laronde, J. A. Gianetto, G. Shen, W. R. Tyson, N. Oguchi, Y. Hosokawa., "Experimental study on SCC susceptibility of X60 using full pipe section in near-neutral pH environment," Proceedings of the 2004 International Pipeline Conference, https://doi.org/10.1115/IPC2004-0280.

[49] J. A. R. G. K. and D. K. M. Seok-Jae LEE, "Hydrogen Embrittlement of Hardened Low-carbon Sheet Steel," ISIJ International, vol. 50, pp. 294–301, 2010.

[50] M. O. Lai and W. G. Ferguson, "Relationship between the Shear Lip Size and the Fracture Toughness," Materials Science and Engineering, Volume 45, Issue 2, Sep. 1980. https://doi.org/10.1016/0025-5416(80)90224-4.

[51] Y. Takahashi, H. Nishikawa, Y. Oda, and H. Noguchi, "Microscopic characterization of hydrogen-induced quasi-brittle fatigue fracture in low-strength carbon steel," Mater Lett, vol. 64, no. 22, pp. 2416–2419, Nov. 2010, https://doi.org/10.1016/j.matlet.2010.08.019.

[52] J. Shang W. Chen, J. Zheng, Z. Hua, L. Zhang, C.Zhou, C. Gu, "Enhanced hydrogen embrittlement of low-carbon steel to natural gas/hydrogen mixtures," Scr Mater, vol. 189, pp. 67–71, Dec. 2020, https://doi.org/10.1016/j.scriptamat.2020.08.011.

[53] J. Yamabe, M. Yoshikawa, H. Matsunaga, and S. Matsuoka, "Hydrogen trapping and fatigue crack growth property of low-carbon steel in hydrogen-gas environment," Int J Fatigue, vol. 102, pp. 202–213, Sep. 2017, https://doi.org/10.1016/j.ijfatigue.2017.04.010.

[54] A. B. Patil, S. P. Toppo, and R. K. P. Singh, "Digital Image Correlation (DIC) Technique for Fracture Toughness Calculation of Microalloyed Steel (38MnVS6)," in IOP Conference Series: Materials Science and Engineering, Institute of Physics Publishing, Nov. 2018. https://doi.org/10.1088/1757-899X/422/1/012016.

[55] J. Karimi, H. Reza Nejati, and M. Ahmadi, "Application of digital image correlation to derive Paris' law constants in granite specimens," Theoretical and Applied Fracture Mechanics, vol. 128, Dec. 2023, https://doi.org/10.1016/j.tafmec.2023.104166.

[56] Almojil, M. Patil, and S. Alshahrani, “Microstructures and textures comparison of conventional and high Niobium API 5l x 80-line pipe steel using EBSD,” La Metallurgia Italiana, vol. 1, 2014.

[57] H. Niazi, H. Zhang, and K. Korol, “High pH Crack Growth Sensitivity to Underload-Type of Pressure Fluctuations,” 2018. Proceedings of the 2018 International Pipeline Conference. Calgary, Alberta, Canada. https://doi.org/10.1115/IPC2018-78394.

[58] H. Niazi, H. Zhang, L. Lamborn, and W. Chen, “The impact of pressure fluctuation on the early onset of stage II growth of high pH stress corrosion cracking,” Proceedings of the 2020 13th International Pipeline Conference, IPC2020-9511. https://doi.org/10.1115/IPC2020-9511.

[59] H. Niazi, R. Eadie, W. Chen, and H. Zhang, “High pH stress corrosion cracking initiation and crack evolution in buried steel pipelines: A review,” Engineering Failure Analysis, vol. 120. Elsevier Ltd, Feb. 01, 2021. https://doi.org/10.1016/j.engfailanal.2020.105013.

[60] H. Niazi, K. Chevil, E. Gamboa, L. Lamborn, W. Chen, and H. Zhang, “Effects of Loading Spectra on High pH Crack Growth Behavior of X65 Pipeline Steel,” Corrosion, vol. 76, no. 6, pp. 601–615, Jun. 2020, https://doi.org/10.5006/3472.

[61] H. Niazi, G. Nelson, L. Lamborn, R. Eadie, W. Chen, and H. Zhang, “Crack Growth Sensitivity to the Magnitude and Frequency of Load Fluctuation in Stage 1b of High-pH Stress Corrosion Cracking,” Corrosion, vol. 77, no. 6, pp. 618–631, Jun. 2021, https://doi.org/10.5006/3711.

[62] H. Niazi, S. Wang, L. Lamborn, R. Eadie, W. Chen, and H. Zhang, “Effects of load interactions on the onset of stage two of high pH stress corrosion cracking,” Journal of Pipeline Science and Engineering, vol. 1, no. 1, pp. 122–136, Mar. 2021, https://doi.org/10.1016/j.jpse.2021.01.003.

[63] M. Masoumi, C. C. Silva, and H. F. G. de Abreu, “Effect of crystallographic orientations on the hydrogen-induced cracking resistance improvement of API 5L X70 pipeline steel under various thermomechanical processing,” Corrosion Sci, vol. 111, pp. 121–131, Oct. 2016, https://doi.org/10.1016/j.corsci.2016.05.003.

[64] J. Konrad, “Characterisation of the Microstructure of X80 Heavy Plate for Pipeline Applications using the EBSD Method,” in 3rd international conference on thermomechanical processing of steels, 2008.

[65] W. Chen, F. King, and E. Vokes, "Characteristics of Near-Neutral-pH Stress Corrosion Cracks in an X-65 Pipeline," Corrosion Science , vol. 58, no. 3, 2002.

[66] R. L. Amaro, N. Rustagi, K. O. Findley, E. S. Drexler, and A. J. Slifka, "Modeling the fatigue crack growth of X100 pipeline steel in gaseous hydrogen," Int J Fatigue, vol. 59, pp. 262–271, 2014, https://doi.org/10.1016/j.ijfatigue.2013.08.010.

[67] W. Chen, "An overview of near-neutral pH stress corrosion cracking in pipelines and mitigation strategies for Its initiation and growth," Corrosion, vol. 72, no. 7, pp. 962–977, Jul. 2016, https://doi.org/10.5006/1967.

[68] M. Nagumo, "Function of Hydrogen in Embrittlement of High-strength Steels," ISIJ International, vol. 41, pp. 590–598, 2001.

[69] H. Nishikawa, Y. Oda, and H. Noguchi, “Investigation of the Mechanism for Brittle-Striation Formation in Low Carbon Steel Fatigued in Hydrogen Gas (Fractographic Observation on Fracture Processes Visualized by Controlling Load Sequence and Testing Environment),” Journal of Solid Mechanics and Materials Engineering, vol. 5, no. 8, pp. 370–385, 2011, https://doi.org/10.1299/jmmp.5.370.

[70] T. Michler and J. Naumann, “Microstructural aspects upon hydrogen environment embrittlement of various bcc steels,” Int J Hydrogen Energy, vol. 35, no. 2, pp. 821–832, Jan. 2010, https://doi.org/10.1016/j.ijhydene.2009.10.092.

[71] W. Chen and R. L. Sutherby, "Crack growth behavior of pipeline steel in near-neutral pH soil environments," Metall Mater Trans A Phys Metall Mater Sci, vol. 38, no. 6, pp. 1260–1268, Jun. 2007, https://doi.org/10.1007/s11661-007-9184-8.

Chapter 8 Conclusion and Recommendations

8. 1 Concluding Remarks

This study analyzed circumferential corrosion fatigue crack initiation, growth, and failure mechanisms at the bottom of dormant cracks/pits on the external surface of a steel pipeline exposed to a near-neutral pH environment. Circumferential NNpH-CF is characterized by a stress gradient in the depth direction, while different stress distributions in the thickness direction, resulting from applied cyclic loading and bending residual stress, define C-NNpH-CF behaviour. The main findings are summarized as follows:

1. The digital image correlation (DIC) method is an appropriate technique for investigating C-NNpH-CF crack growth. It can analyze the final stress distribution of bent pipelines that are influenced by various residual and applied stresses in both inward and outward directions. This study emphasizes that the accumulation of stress from axial loading and residual stress increases the level of stress (compressive/tension) at the bending centerline. The axial stress and residual stress in the inward bending direction are tension, while in the outward bending direction, it is compression, irrespective of the bending degree and the level of axial loading. It is recognized that the application of a tensile straightening force (axial bending stress) to the samples in this study may not replicate actual pipeline conditions. Nevertheless, equivalent stresses are expected to exist in the real field such as hydrodynamic and Bourdon stress. Importantly, the final stress determined through the DIC method remains accurate.
2. Circumferential corrosion fatigue cracking in a pipeline cannot be caused by pressure fluctuations alone. Therefore, other sources of axial stress, such as residual axial stress

from girth welding, bending, geohazards, *etc.,* are necessary for C-NNpH-CF to occur on the pipeline's external surface. Corrosion fatigue cracks are not a concern in the outward direction of bent pipelines (under compressive stress) in the field. For this reason, integrity management activities should focus on evaluating the bend centerline in the inward direction (after springing back).

3. Corrosion in the form of stress cells at the notch corners (stress concentrators) is responsible for this crack initiation mechanism. The presence of a high stress level at a stress cell is enough for a crack to form at the bottom of the notch due to direct dissolution, regardless of whether the stress is compressive or tensile. The stress × stress concentration factor, which takes into account both the stress gradient in the depth direction and the notch depth, provides more detailed information about crack initiation in the depth direction.
4. The initiation of cracks at the bottom of the pit/dormant cracks begins with a tensile stress gradient, signifying a difference in potential between the anodic surface and the cathodic surface. At the crack tip, localized anodic sites hinder the further corrosion of the notch root, leading to blunt-tip cracks. The presence of a sharp crack is possible when the hydrogen-enhanced fatigue mechanism prevails.
5. In near-neutral pH environments, circumferential corrosion fatigue cracking occurs in lower stress intensity factor ranges/ combined factors, mainly due to the presence of residual stress. When pipes are cold bent, residual tensile stress increases throughout the entire bend area, especially at the bottom of the initial notch. This leads to more hydrogen diffusion, making the material more susceptible to corrosion fatigue and causing the crack to grow further.

6. During the test, various samples were bent inward and outward at different angles. However, only the artificial notches located at the centerline of the inwardly bent sections showed failure within the 45-day period. The lifetime was different due to different stress distributions in the thickness direction and varying crack growth rates.
7. Despite crack growth releasing residual stress, crack growth in the depth direction modifies stress level (and consequently stress intensity factor) so that a higher crack growth rate occurs. A high stress intensity factor governs Stage III crack growth compared to Stage II, which is governed by a medium stress intensity factor and hydrogen-enhanced fatigue.
8. Pipeline integrity management can predict pipeline lifetime by relying on Stage II's stable crack growth rate. It is possible to determine the crack growth rate for a failed pipeline by simultaneously using fractography images, CMOD results, and EBSD strain countering.

8. 2 Recommendations for Future Studies

To the best of our knowledge, this study is the first systematic study on "Circumferential Near-Neutral pH Corrosion Fatigue of Bent Pipelines." After conducting a comprehensive literature review and examining the influence of various parameters on this cracking mechanism, suggestions for future work are as follows:

1. Conducting the digital image correlation (DIC) method on the notched samples is recommended to characterize the effect of stress removal during creating notches with different depths on the external surface of the pipe.
2. Employing Finite Element Analysis (FEA) is recommended to simulate:
    - Bending residual stress distribution (considering the effect of spring back)
    - Stress distribution in a bent pipe under the influence of axial cyclic loading

- Interaction of above-mentioned sources of stresses (comparing with the DIC results)
- How the residual tensile stress is changed by crack growth
- The effect of hydrostatic stresses and Bourdon effect on stress distribution in a bent pipeline
- The total stresses in this experiment, including the bending moment, residual stress, and axial loading, as well as the stresses in the field, including hydrodynamic stress, Bourdon stress, residual stresses, axial loading from pressure fluctuations, *etc.*

3. Creating artificial sharp cracks is recommended to find the exact crack growth rate in stage II through removing the effect of incubation time on crack initiation from the bottom of a dormant crack (artificial notch).
4. Since the initial stress distribution in the bent section is completely changed during the crack propagation, finding new stress distribution in any crack depth under the influence of various stress sources is recommended. In this way, finding the exact amount of stress intensity factor value can be helpful to make a correlation with an accurate actual crack growth rate (exclusively in stage III (rapid crack growth)), which could be found through a potential drop system.

Bibliography

- A. Beavers and B. A. Harle, "Mechanisms of high-pH and near-neutral-pH SCC of underground pipelines," *Journal of Offshore Mechanics and Arctic Engineering*, vol. 123, no. 3, pp. 147–151, Aug. 2001, https://doi.org/10.1115/1.1376716.
- A. Beavers, "Integrity management of natural gas and petroleum pipelines subject to stress corrosion cracking," *Corrosion*, vol. 70, no. 1, pp. 3–18, Jan. 2014, https://doi.org/10.5006/0998.
- A. Beavers, J. T. Johnson, and R. L. Sutherby, "Materials factor influencing the Initiation of Near- neutral pH SCC on Underground pipelines," in *International Pipeline Conference*, 2000. http://asmedigitalcollection.asme.org/IPC/proceedings-pdf/IPC2000/40252/V002T06A041/2507801/v002t06a041-ipc2000-221.pdf
- A. Kim, *W. Zheng, G. William, M. Laronde,* "Experimental study on SCC susceptibility of X60 using full pipe section in near-neutral pH environment," in *International Pipeline Conference 2004-280*, http://asmedigitalcollection.asme.org/IPC/proceedings-pdf/IPC2004/41766/133/4563529/133_1.pdf
- A. R. G. K. and D. K. M. Seok-Jae LEE, "Hydrogen Embrittlement of Hardened Low-carbon Sheet Steel," *ISIJ International*, vol. 50, pp. 294–301, 2010.
- D. Abdulhameed, S. Adeeb, and R. Cheng, "The influence of the Bourdon effect on pipe elbow" in Proceedings of the 11th International Pipeline Conference, 2016, pp. 1–10. https://doi.org/10.1115/IPC2016-64659.
- Almojil, M. Patil, and S. Alshahrani, "Microstructures and textures comparison of conventional and high Niobium API 5l x 80-line pipe steel using EBSD," *La Metallurgia Italiana*, vol. 1, 2014.

- ASTM B909- 17 Standard Guide for Plane Strain Fracture Toughness Testing of Non-Stress Relieved Aluminum Products", https://doi.org/10.1520/B0909-17.
- Attia, M. Mohareb, M. Martens, N. Yoosef-Ghodsi, Y. Li, and S. Adeeb, "Numerical assessment of elbow element response under internal pressure," *Journal of Pressure Vessel Technology, Transactions of the ASME*, vol. 143, no. 5, Oct. 2021, https://doi.org/10.1115/1.4050091.
- B. Á. Pradas Cristina, "Stress and strain analysis of a material with Digital Image Correlation method (DIC)," Western Norway University of Applied Sciences, 2020.
- B. Beuregard and C. Edwards, "Analysis of sever circumferential SCC found on ab ethane pipeline," in *Proceedings of the 2014 International Pipeline Conference. Calgary, Alberta, Canada.* , 2014.
- B. Lambert, J. A. Beavers, B. Delanty, R. Sutherby, and A. Plumtree, "Mechanical factors affecting stress corrosion crack growth rates in buried pipelines," in *International Pipeline Conference*, 2000. http://asmedigitalcollection.asme.org/IPC/proceedings-pdf/IPC2000/40252/V002T06A039/2507684/v002t06a039-ipc2000-219.pdf
- B. Patil, S. P. Toppo, and R. K. P. Singh, "Digital Image Correlation (DIC) Technique for Fracture Toughness Calculation of Micro alloyed Steel (38MnVS6)," in *IOP Conference Series: Materials Science and Engineering*, Institute of Physics Publishing, Nov. 2018. https://doi.org/10.1088/1757-899X/422/1/012016.
- Bates, M. Brimacombe, and S. Polasik, "Development and experiences of a circumferential stress corrosion crack management," in *12th International Pipeline Conference-78315*, 2018. http://asmedigitalcollection.asme.org/IPC/proceedings-pdf/IPC2018/51869/V001T03A062/2510991/v001t03a062-ipc2018-78315.pdf

- D. Birenis, Y. Ogawa, H. Matsunaga, O. Takakuwa. Yamabe, Prytz, A. Thøgersen, "Interpretation of hydrogen-assisted fatigue crack propagation in BCC iron based on dislocation structure evolution around the crack wake," *Acta Mater*, vol. 156, pp. 245–253, Sep. 2018, https://doi.org/10.1016/j.actamat.2018.06.041.
- Brimacombe Senior Advisor, C. Wargacki Key Account Manager, and N. Global Leduc, "Circumferential crack detection: Challenges, solutions and results," in *Proceedings of the 2016International Pipeline Conference. Calgary, Alberta, Canada. IPC2016-64111.*, 2016. http://asmedigitalcollection.asme.org/IPC/proceedings-pdf/IPC2016/50251/V001T03A056/2510160/v001t03a056-ipc2016-64111.pdf
- Canadian Energy Pipeline Association (CEPA), Stress Corrosion Cracking Recommended Practices, 2nd Edition, an industry leading document detailing the management of transgranular SCC, December 2007. https://www.academia.edu/36586872/Stress_Corrosion_Cracking_Recommended_Practices_2nd_Edition_An_industry_leading_document_detailing_the_management_of_transgranular_SCC
- Chen and R. L. Sutherby, "Crack growth behavior of pipeline steel in near-neutral pH soil environments," *Metall Mater Trans A Phys Metall Mater Sci*, vol. 38, no. 6, pp. 1260–1268, Jun. 2007, https://doi.org/10.1007/s11661-007-9184-8.
- Chen and R. Sutherby, "Environmental effect of crack growth rate of pipeline steel in near neutral pH soil environments," in *International Pipeline Conference*, 2004
- Chen and S.-H. Wang, "Room temperature creep behavior of pipeline steels and its influence on stress corrosion cracking," in *International Pipeline Conference*, 2002.

- Chen, “An overview of near-neutral pH stress corrosion cracking in pipelines and mitigation strategies for Its initiation and growth,” *Corrosion*, vol. 72, no. 7, pp. 962–977, Jul. 2016, https://doi.org/10.5006/1967.
- W. Chen, F. King, and E. Vokes, “Characteristics of Near-Neutral-pH Stress Corrosion Cracks in an X-65 Pipeline,” Corrosion Science , vol. 58, no. 3, 2002.
- Choi Byoung-Ho and Chudnovsky Alexander, “Stress corrosion crack growth in pipe grade steels in near-neutral pH environment,” *Int J Fract*, vol. 116, pp. 43–48, 2002. https://doi.org/10.1023/A:1022665831622.
- R. Chu, W. Chen, S.-H. Wang, F. King, T. R. Jack, and R. R. Fessler, “Microstructure Dependence of Stress Corrosion Cracking Initiation in X-65 Pipeline Steel Exposed to a Near-Neutral pH Soil Environment,” Corrosion Science, vol. 60, no. 3, 2004. https://doi.org/10.5006/1.3287732.
- Contreras, L. Quej-Ake, R. Galvan-Martinez, O. Vega, L. Cárdenas Norte, and C. San Bartolo Atepehuacan, “Residual stress assessment and its effect on SCC of pipelines steel in acidic soil environment,” in *Materials Research Society Symposium Proceedings*, 2014.
- E. Entezari, J. L. Velázquez, M.A. Mohtadi-Bonab, D. Rivas López, M. Alejandro Beltrán Zúñiga, R. Khatib Zadeh Davani, J. Szpunar, “Experimental observations of nucleation and crack growth paths of hydrogen-induced cracking in pipeline steel,” *Eng Fail Anal*, vol. 154, Dec. 2023, https://doi.org/10.1016/j.engfailanal.2023.107650.
- A. Eslami*, M. Marvasti, W. Chen, R. Eadie, R. Kania, R. Worthingham, G. Van Boven* “The role of electrochemical condition in near neutral pH SCC initiation mechanism(s),” in *Proceedings of the 2010 International Pipeline Conference. Calgary, Alberta,*

Canada.IPC2010-31190, 2010. http://asmedigitalcollection.asme.org/IPC/proceedings-pdf/IPC2010/44205/315/2703559/315_1.pdf

- Eslami, W. Chen, R. Worthingham, R. Kania, and J. Been, "Effect of CO2 on Near-Neutral pH Stress Corrosion Cracking Initiation of Pipeline Steel," in *NACE International Conference, Paper No.: 10300.*, 2010. http://onepetro.org/NACECORR/proceedings-pdf/CORR10/All-CORR10/NACE-10300/1718239/nace-10300.pdf/1
- F. Cheng and L. Niu, "Mechanism for hydrogen evolution reaction on pipeline steel in near-neutral pH solution," *Electrochem commun*, vol. 9, no. 4, pp. 558–562, Apr. 2007, https://doi.org/10.1016/j.elecom.2006.10.035.
- H. Niazi, H. Zhang, and K. Korol, "High pH Crack Growth Sensitivity to Underload-Type of Pressure Fluctuations," 2018. http://asmedigitalcollection.asme.org/IPC/proceedings-pdf/IPC2018/51869/V001T03A064/2511039/v001t03a064-ipc2018-78394.pdf
- H. Niazi, H. Zhang, L. Lamborn, and W. Chen, "The impact of pressure fluctuation on the early onset of stage II growth of high pH stress corrosion cracking," Proceedings of the 2020 13th International Pipeline Conference, IPC2020-9511, 2020. https://doi.org/10.1115/IPC2020-9511.
- H. Niazi, K. Chevil, E. Gamboa, L. Lamborn, W. Chen, and H. Zhang, "Effects of Loading Spectra on High pH Crack Growth Behavior of X65 Pipeline Steel," *Corrosion*, vol. 76, no. 6, pp. 601–615, Jun. 2020, https://doi.org/10.5006/3472.
- H. Niazi, R. Eadie, W. Chen, and H. Zhang, "High pH stress corrosion cracking initiation and crack evolution in buried steel pipelines: A review," *Engineering Failure Analysis*, vol. 120. Elsevier Ltd, Feb. 01, 2021. https://doi.org/10.1016/j.engfailanal.2020.105013.

- H. Niazi, S. Wang, L. Lamborn, R. Eadie, W. Chen, and H. Zhang, "Effects of load interactions on the onset of stage two of high pH stress corrosion cracking," *Journal of Pipeline Science and Engineering*, vol. 1, no. 1, pp. 122–136, Mar. 2021, https://doi.org/10.1016/j.jpse.2021.01.003.
- H. Nishikawa, Y. Oda, and H. Noguchi, "Investigation of the Mechanism for Brittle-Striation Formation in Low Carbon Steel Fatigued in Hydrogen Gas (Fractographic Observation on Fracture Processes Visualized by Controlling Load Sequence and Testing Environment)," *Journal of Solid Mechanics and Materials Engineering*, vol. 5, no. 8, pp. 370–385, 2011, https://doi.org/10.1299/jmmp.5.370.
- H. Shirazi, R. Eadie, and W. Chen, "A review on current understanding of pipeline circumferential stress corrosion cracking in near-neutral PH environment," *Engineering Failure Analysis*, vol. 148., Jun. 01, 2023. https://doi.org/10.1016/j.engfailanal.2023.107215.
- Hasegawa, B. Strnadel, D. Dvořák, and V. Mareš, "Failure bending stresses for pressurized pipes with circumferentially part-through cracks," *International Journal of Pressure Vessels and Piping*, vol. 186, Sep. 2020, https://doi.org/10.1016/j.ijpvp.2020.104146.
- *ISO 7539-5: Corrosion of Metals and Alloys- Stress Corrosion Cracking- Part 5: Preparation and use of C- ring specimen*. International Organization for Standardization, 1989.
- ISO-7539-5 Corrosion of metals and alloys- Stress Corrosion Cracking- Preparation and use of C-ring specimen." 1989.
- J. B. Wiskel, J. Ma, J. Valloton, D. G. Ivey, and H. Henein, "Strain aging on the yield strength to tensile strength ratio of UOE pipe," *Materials Science and Technology (United*

Kingdom), vol. 33, no. 11, pp. 1319–1332, Jul. 2017, https://doi.org/10.1080/02670836.2017.1288776.

- J. Babcock, D. Dewar, and J. Webster, "Deer Mountain case study: integration of pipe and ground monitoring data with historical information o develop landscape management plan," *Proceedings of the 2020 International Pipeline Conference. Calgary, Alberta, Canada. IPC2020-9613*, 2020, http://asmedigitalcollection.asme.org/IPC/proceedings-pdf/IPC2020/84461/V003T04A021/6620292/v003t04a021-ipc2020-9613.pdf
- J. Beavers and T. A. Bubenik, "Stress corrosion cracking," in *Trends in Oil and Gas Corrosion Research and Technologies: Production and Transmission*, Elsevier Inc., 2017, pp. 295–314. https://doi.org/10.1016/B978-0-08-101105-8.00012-7.
- J. Bestautte, S. Kalácska, D. Béchet, Z. Obadia, and F. Christien, "Investigation of quasi-cleavage in a hydrogen charged maraging stainless steel," *Corrosion Science*, vol. 218, Jul. 2023, https://doi.org/10.1016/j.corsci.2023.111163.
- J. Karimi, H. Reza Nejati, and M. Ahmadi, "Application of digital image correlation to derive Paris' law constants in granite specimens," *Theoretical and Applied Fracture Mechanics*, vol. 128, Dec. 2023, https://doi.org/10.1016/j.tafmec.2023.104166.
- J. Konrad, "Characterisation of the Microstructure of X80 Heavy Plate for Pipeline Applications using the EBSD Method," in *3rd international conference on thermomechanical processing of steels*, 2008.
- J. Shang W. Chen, J. Zheng, Z. Hua, L. Zhang, C.Zhou, C. Gu, "Enhanced hydrogen embrittlement of low-carbon steel to natural gas/hydrogen mixtures," *Scr Mater*, vol. 189, pp. 67–71, Dec. 2020, https://doi.org/10.1016/j.scriptamat.2020.08.011.

- J. Toribio, “Residual stress effects in stress-corrosion cracking,” J Mater Eng Perform, vol. 7, pp. 173–182, 1998. https://doi.org/10.1361/105994998770347891.
- P. J. Withers, H. K. D. H. Bhadeshia, Residual stress Part 1-Measurement techniques, Materials Science and Technology 17 (2001) 355–365. https://doi.org/10.1179/026708301101509980
- J. Yamabe, M. Yoshikawa, H. Matsunaga, and S. Matsuoka, “Hydrogen trapping and fatigue crack growth property of low-carbon steel in hydrogen-gas environment,” *Int J Fatigue*, vol. 102, pp. 202–213, Sep. 2017, https://doi.org/10.1016/j.ijfatigue.2017.04.010.
- J. Zhao, W. Chen, M. Yu, K. Chevil, R. Eadie, J. Been, G. Van Boven, R. Kania & S. Keane, “Crack growth modeling and life prediction of pipeline steels exposed to near-Neutral pH environments: stage II crack growth and overall life prediction,” *Metall Mater Trans A Phys Metall Mater Sci*, vol. 48, no. 4, pp. 1641–1652, Apr. 2017, https://doi.org/10.1007/s11661-016-3939-z.
- J. Zhao, Weixing Chen, M. Yu, K. Chevil, R. Eadie, G. Van Boven, R. Kania, J. Been & S. Keane, “Crack growth modeling and life prediction of pipeline steels exposed to near-neutral pH environments: dissolution crack growth and occurrence of crack dormancy in stage I,” *Metall Mater Trans A Phys Metall Mater Sci*, vol. 48, no. 4, pp. 1629–1640, Apr. 2017, https://doi.org/10.1007/s11661-016-3951-3.
- J. Zhao, T. Mo, D. F. Nie, M. F. Ren, X. L. Guo, and W. X. Chen, “Acceleration and retardation of fatigue crack growth rate due to room temperature creep at crack tip in a 304 stainless steel,” *J Mater Sci*, vol. 41, no. 19, pp. 6431–6434, Oct. 2006, https://doi.org/10.1007/s10853-006-0502-0.
- Jaap Schijve, *Fatigue of Structures and Materials*, Second Edition. Springer, 2009.

- B. Johnson, B Tesfaye, C. Wargacki, T. Hennig, E. Suarez "Complex Circumferential Stress Corrosion Cracking: Identification, Sizing and Consequences for the Integrity Management Program," in Proceedings of the 2018 International Pipeline Conference. Calgary, Alberta, Canada. IPC2018-78564. https://doi.org/10.1115/IPC2018-78564.
- K. Zhang, R. Chune, R. Wang, and R. Kania, "Role of axial stress in pipeline integrity management," in *Proceedings of the 2022 International Pipeline Conference. Calgary, Alberta, Canada. IPC2022-87327*, 2022. http://asmedigitalcollection.asme.org/IPC/proceedings-pdf/IPC2022/86571/V002T03A053/6965592/v002t03a053-ipc2022-87327.pdf
- L. Shi, X. Zhang, L. Zhang, C. Wang, and J. Wang, "Application of digital image correlation technique in stress and strain measurement," http://www.ndt.net/?id=22154
- L. Y. Xu and Y. F. Cheng, "An experimental investigation of corrosion of X100 pipeline steel under uniaxial elastic stress in a near-neutral pH solution," *Corrosion Sci*, vol. 59, pp. 103–109, Jun. 2012, https://doi.org/10.1016/j.corsci.2012.02.022.
- Laureys, M. Pinson, T. Depover, R. Petrov, and K. Verbeken, "EBSD characterization of hydrogen induced blisters and internal cracks in TRIP-assisted steel," *Mater Charact*, vol. 159, Jan. 2020, https://doi.org/10.1016/j.matchar.2019.110029.
- Laureys, T. Depover, R. Petrov, and K. Verbeken, "Microstructural characterization of hydrogen induced cracking in TRIP-assisted steel by EBSD," *Mater Charact*, vol. 112, pp. 169–179, Feb. 2016, https://doi.org/10.1016/j.matchar.2015.12.017.
- M. Calcagnotto, D. Ponge, E. Demir, and D. Raabe, "Orientation gradients and geometrically necessary dislocations in ultrafine grained dual-phase steels studied by 2D

and 3D EBSD," *Materials Science and Engineering: A*, vol. 527, no. 10–11, pp. 2738–2746, Apr. 2010, https://doi.org/10.1016/j.msea.2010.01.004.

- M. D. Roach, S. I. Wright, J. E. Lemons, and L. D. Zardiackas, "An EBSD based comparison of the fatigue crack initiation mechanisms of nickel and nitrogen-stabilized cold-worked austenitic stainless steels," *Materials Science and Engineering: A*, vol. 586, pp. 382–391, Dec. 2013, https://doi.org/10.1016/j.msea.2013.08.027.
- M. Hilvert, T. Penney, M. Enginering Ltd, I. Richardson, and A. Russell, "Integrity management of Stress Corrosion Cracking in pipeline a case study," in *26th World Gas conference Paris, France*, 2015.
- M. J. W. Ilm, "The role of pressure and pressure fluctuation in the growth of Stress Corrosion Cracks in line pipe steels," in *Proceedings of the 1998 International Pipeline Conference. Calgary, Alberta, Canada. IPC1998-2049*, 1998. http://asmedigitalcollection.asme.org/IPC/proceedings-pdf/IPC1998/40221/409/2507331/409_1.pdf
- M. Javidi and S. Bahalaou Horeh, "Investigating the mechanism of stress corrosion cracking in near-neutral and high pH environments for API 5L X52 steel," *Corrosion Sci*, vol. 80, pp. 213–220, Mar. 2014, https://doi.org/10.1016/j.corsci.2013.11.031.
- M. L. Lobanov Vladislav A. Khotinov, V. N. Urtsev 3,S. V. Danilov,N. V. Urtsev ,S. I. Platov, Stepan I. Stepanov, "Tensile Deformation and Fracture Behavior of API-5L X70 Line Pipe Steel," *Materials*, vol. 15, no. 2, Jan. 2022, https://doi.org/10.3390/ma15020501.
- M. L. Martin, J. A. Fenske, G. S. Liu, P. Sofronis, and I. M. Robertson, "On the formation and nature of quasi-cleavage fracture surfaces in hydrogen embrittled steels," *Acta Mater*, vol. 59, no. 4, pp. 1601–1606, Feb. 2011, https://doi.org/10.1016/j.actamat.2010.11.024.

- M. Lin, “Characterization of Tensile and Fracture Properties of X52 Steel Pipes and Their Girth Welds,” University of Alberta, 2015.
- M. Masoumi, C. C. Silva, and H. F. G. de Abreu, “Effect of crystallographic orientations on the hydrogen-induced cracking resistance improvement of API 5L X70 pipeline steel under various thermomechanical processing,” *Corros Sci*, vol. 111, pp. 121–131, Oct. 2016, https://doi.org/10.1016/j.corsci.2016.05.003.
- M. Masoumi, L. F. G. Herculano, and H. F. G. de Abreu, “Study of texture and microstructure evaluation of steel API 5L X70 under various thermomechanical cycles,” *Materials Science and Engineering: A*, vol. 639, pp. 550–558, 2015, https://doi.org/10.1016/j.msea.2015.05.020.
- M. Nagumo, “Function of Hydrogen in Embrittlement of High-strength Steels,” *ISIJ International*, vol. 41, pp. 590–598, 2001.
- M. O. Lai and W. G. Ferguson, “Relationship between the Shear Lip Size and the Fracture Toughness,” Materials Science and Engineering, Volume 45, Issue 2, Sep. 1980. https://doi.org/10.1016/0025-5416(80)90224-4.
- M. Pope, *C. S. Camerini, J. C. G. Teixeira, M. T. Piza, W. Baptista, B. G. de Souza, H. L. Oliver*, “Circumferential SCC in pipeline due to land creeping,” in *International Pipeline Conference*, International Pipeline Conference , 2002. https://doi.org/10.1115/IPC2002-27192.
- M. Sabokrouh and M. Farahani, “Experimental study of the residual stresses in girth weld of natural gas transmission pipeline,” *Journal of Applied and Computational Mechanics*, vol. 5, no. 2, pp. 199–206, 2019, https://doi.org/10.22055/JACM.2018.25756.1294.

- M. Yu, W. Chen, R. Kania, G. Van Boven, and J. Been, "Crack propagation of pipeline steel exposed to a near-neutral pH environment under variable pressure fluctuations," *Int J Fatigue*, vol. 82, pp. 658–666, Jan. 2016, https://doi.org/10.1016/j.ijfatigue.2015.09.024.
- Manthiramoorthy and A. Krishnaveni, "Fracture Parameter Evaluation Using Digital Image Correlation Technique," 2017. www.ijetsr.com
- Merson, A. V. Kudrya, V. A. Trachenko, D. Merson, V. Danilov, and A. Vinogradov, "Quantitative characterization of cleavage and hydrogen-assisted quasi-cleavage fracture surfaces with the use of confocal laser scanning microscopy," *Materials Science and Engineering: A*, vol. 665, pp. 35–46, May 2016, https://doi.org/10.1016/j.msea.2016.04.023.
- N. Bates, M. Brimacombe, and S. Polasik, "Development and experience of a circumferential stress corrosion crack management program," in *Proceedings of the 2018 International Pipeline Conference. Calgary, Alberta, Canada.IPC2018-78315*, 2018. http://asmedigitalcollection.asme.org/IPC/proceedings-pdf/IPC2018/51869/V001T03A062/2510991/v001t03a062-ipc2018-78315.pdf
- N. E. Anderson, "Influence of the Post-Weld Heat Treatment on the Low-Temperature Toughness of ERW API X70 Line Pipe."
- N. Hempel, J. R. Bunn, T. Nitschke-Pagel, E. A. Payzant, and K. Dilger, "Study on the residual stress relaxation in girth-welded steel pipes under bending load using diffraction methods," *Materials Science and Engineering A*, vol. 688, pp. 289–300, Mar. 2017, https://doi.org/10.1016/j.msea.2017.02.005.

- N. Leis and R. J. Eiber, “Stress Corrosion Cracking on gas-transmission pipelines: History, causes, and mitigation,” in *First International Business Conference on Onshore Pipelines, Berlin, December 1997*, 1997. https://www.researchgate.net/publication/265031582
- N. Sridhar, “Transgranular stress corrosion cracking of high-pressure pipelines in contact with solutions of near neutral pH,” *Corrosion*, vol. 50, no. 5, pp. 394–408, 1994.
- N. WALKER and C. J. BEEVERS, “A fatigue crack closure mechanism in titanium,” *Fatigue Fract Eng Mater Struct*, vol. 1, no. 1, pp. 135–148, 1979, https://doi.org/10.1111/j.1460-2695.1979.tb00372.x.
- National Energy Board (NEB), Report of the Inquiry concerning Stress Corrosion Cracking on Canadian Oil and Gas Pipelines, NEB MH-2-95, December 1996. https://publications.gc.ca/collections/Collection/NE23-58-1996E.pdf
- Niazi, G. Nelson, L. Lamborn, R. Eadie, W. Chen, and H. Zhang, “Crack Growth Sensitivity to the Magnitude and Frequency of Load Fluctuation in Stage 1b of High-pH Stress Corrosion Cracking,” *Corrosion*, vol. 77, no. 6, pp. 618–631, Jun. 2021, https://doi.org/10.5006/3711.
- Niu and Y. F. Cheng, “Corrosion behavior of X-70 pipe steel in near-neutral pH solution,” *Appl Surf Sci*, vol. 253, no. 21, pp. 8626–8631, Aug. 2007, https://doi.org/10.1016/j.apsusc.2007.04.066.
- Norouzi, R. Miresmaeili, H. R. Shahverdi, M. Askari-Paykani, and L. M. Vergani, “Hydrogen embrittlement behavior in FeCCrNiBSi TRIP steel,” *Journal of Materials Research and Technology*, vol. 23, pp. 859–868, Mar. 2023, https://doi.org/10.1016/j.jmrt.2023.01.052.

- D. O. Harris, Stress Corrosion Crack Growth in the Presence of residual Stresses, in: Eric Kula, Volker Weiss, Residual Stress and Stress Relaxation (1982), Springer, New York, pp. 273–295. https://doi.org/10.1007/978-1-4899-1884-0_15
- P. K. H. Underwood, "Fracture Toughness Testing Using the C-Shaped Specimen," in *ASTM STP 632 Developments in fracture mechanic test method standardization*, 1976, pp. 25–38.
- P. Kendall and M. A. Hussain, "A New Fracture-toughness Test Method Thick-walled Cylinder Material for," in *SESA Spring Meeting*, 1971.
- R. L. Amaro, N. Rustagi, K. O. Findley, E. S. Drexler, and A. J. Slifka, "Modeling the fatigue crack growth of X100 pipeline steel in gaseous hydrogen," *Int J Fatigue*, vol. 59, pp. 262–271, 2014, https://doi.org/10.1016/j.ijfatigue.2013.08.010.
- R. L. Champoux, J. H. Underwood, J. A. Kapp, ASTM Committee E-9 on Fatigue., and Ariz.) Symposium on Analytical and Experimental Methods for Residual Stress Effects in Fatigue (1986 : Phoenix, *Analytical and experimental methods for residual stress effects in fatigue*. ASTM, 1988.
- R. L. Sutherby and P. Eng, "The CEPA Report on Circumferential Stress Corrosion Cracking," in *International Pipeline Conference* , ASME, 1998. http://asmedigitalcollection.asme.org/IPC/proceedings-pdf/IPC1998/40221/493/2507128/493_1.pdf
- R. N. Parkins, "A review of stress corrosion cracking of high-pressure gas pipelines," in *NACE International Conference, Paper No.: 00363.*, 2000. http://onepetro.org/NACECORR/proceedings-pdf/CORR00/All-CORR00/NACE-00363/1915567/nace-00363.pdf/1

- R. N. Parkins, “Factors influencing stress corrosion crack growth kinetics,” 1987.
- R. Palmer-Jones, A. Young, B. Kerrigan, J. Soltis, and T. Beuker, “A practical process for managing the threat of circumferential stress corrosion cracking,” in *Rio Pipeline Conference & Exhibition*, 2017.
- R. R. Fessler, M. Sen, Characteristics, cause, and management of circumferential stress-corrosion cracking, Proceedings of the 2004 International Pipeline Conference. Calgary, Alberta, Canada. IPC2014-33059. https://doi.org/10.1115/IPC2014-33059.
- R. Sutherby, W. Chen, Deflected stress corrosion cracks in the pipeline steel, Proceedings of the 2004 International Pipeline Conference. Calgary, Alberta, Canada. IPC2004-0600. https://doi.org/10.1115/IPC2004-0600
- Ron Thompson, R. Gardner, K. Dwyer, A. Corbett, and M. Marquis Hotel, “A case study in the detection and sizing of circumferential stress corrosion cracking Pipeline Pigging and Integrity Management Conference,” in *Pipeline pigging and integrity management conference, Houston, February 2020*, 2020.
- S. Hu, Z. Mi, and J. Lu, “Effect of crack-depth ratio on double-K fracture parameter of reinforced concrete,” in *Applied Mechanics and Materials*, 2012, pp. 937–941. https://doi.org/10.4028/www.scientific.net/AMM.226-228.937.
- S. Jian, Y. Zupei, and M. Yunxin, “Investigation on potential SCC in gas transmission pipeline in China,” in *Proceedings of the 2004 International Pipeline Conference. Calgary, Alberta, Canada. IPC2014-33059.*, http://asmedigitalcollection.asme.org/IPC/proceedings-pdf/IPC2004/41766/151/4563160/151_1.pdf

- S. Kortovich and E. A. Steigerwald, “A comparison of hydrogen embrittlement and stress corrosion cracking in high strength steels,” *Eng Fract Mech*, vol. 4, pp. 637–651, 1972.
- S. L. Asher and P. M. Singh, Role of stress in transgranular stress corrosion cracking of transmission pipelines in near-neutral pH environments, Corrosion Science Section 65 (2009) 79. https://doi.org/10.5006/1.3319122
- S. Limon, P. Martin, M. Barnum, and R. Pilarczyk, “Fracture toughness testing and its implications to engineering fracture mechanics analysis of energy pipelines,” in *12th International Pipeline Conference--78723*, 2018. http://asmedigitalcollection.asme.org/IPC/proceedings-pdf/IPC2018/51869/V001T03A077/2510911/v001t03a077-ipc2018-78723.pdf
- S. Lynch and S. Lynch, “Some fractographic contributions to understanding fatigue crack growth,” *Int J Fatigue*, vol. 104, pp. 12–26, Nov. 2017, https://doi.org/10.1016/j.ijfatigue.2017.06.036.
- S. Lynn Asher, P. M. Singh, and R. Neu, “Investigating the Mechanism of Transgranular Stress Corrosion Cracking in Near-Neutral pH Environments on Buried Fuel Transmission Pipelines,” 2007.
- S. Nafisi, M. Arafin, R. Glodowski, L. Collins, and J. Szpunar, “Impact of vanadium addition on API X100 steel,” *ISIJ International*, vol. 54, no. 10, pp. 2404–2410, 2014, https://doi.org/10.2355/isijinternational.54.2404.
- S. Wang and W. Chen, “Overview of Stage 1b Stress Corrosion Crack Initiation and Growth of Pipeline Steels,” *Corrosion*, vol. 79, no. 3, pp. 284–303, Mar. 2023, https://doi.org/10.5006/4168.

- S. Wang, L. Lamborn, and W. Chen, “Near-neutral pH corrosion and stress corrosion crack initiation of a mill-scaled pipeline steel under the combined effect of oxygen and paint primer,” *Corros Sci*, vol. 187, Jul. 2021, https://doi.org/10.1016/j.corsci.2021.109511.
- S. Wang, L. Lamborn, and W. Chen, “Stress corrosion crack initiation and propagation before proceeding to Stage 2 for hydrostatically tested pipeline steels,” *J Mater Sci*, 2022, https://doi.org/10.1007/s10853-022-07606-w.
- S. Wang, L. Lamborn, K. Chevil, E. Gamboa, and W. Chen, “Near-neutral pH corrosion of mill-scaled X-65 pipeline steel with paint primer,” *J Mater Sci Technol*, vol. 49, pp. 166–178, Jul. 2020, https://doi.org/10.1016/j.jmst.2020.01.016.
- Smirnov, E. Smirnova, and S. Alexandrov, “A new experimental method for determining the thickness of thin surface layers of intensive plastic deformation using electron backscatter diffraction data,” *Symmetry (Basel)*, vol. 12, no. 4, Apr. 2020, https://doi.org/10.3390/SYM12040677.
- Standard ASTM E399-12 Test Method for Linear-Elastic Plane-Strain Fracture Toughness KIc of Metallic Materials.” https://doi.org/10.1520/E0399-12E02.
- Standard ISO 7539-9 Corrosion of metals and alloys - Stress corrosion testing- Part 9: Preparation and use of pre-cracked specimens for tests under rising load or rising displacement.” 2003.
- Sutcliffe J.M., Fessler R.R., Boyd W.K., and Parkins R.N, “Stress corrosion cracking of carbon steel in carbonate solutions,” *Corrosion*, vol. 28, pp. 313–320, 1972. https://doi.org/10.1016/B978-0-08-034804-9.50176-5.
- T. Lu, J. L. Luo, P. R. Norton, and H. Y. Ma, “Effects of dissolved hydrogen and elastic and plastic deformation on active dissolution of pipeline steel in anaerobic groundwater of

near-neutral pH," *Acta Mater*, vol. 57, no. 1, pp. 41–49, Jan. 2009, https://doi.org/10.1016/j.actamat.2008.08.035.

- T. Michler and J. Naumann, "Microstructural aspects upon hydrogen environment embrittlement of various bcc steels," *Int J Hydrogen Energy*, vol. 35, no. 2, pp. 821–832, Jan. 2010, https://doi.org/10.1016/j.ijhydene.2009.10.092.
- T. Neeraj, T. Gnäupel-Herold, H. J. Prask, and R. Ayer, "Residual stresses in girth welds of carbon steel pipes: Neutron diffraction analysis," *Science and Technology of Welding and Joining*, vol. 16, no. 3, pp. 249–253, Apr. 2011, https://doi.org/10.1179/1362171810Y.0000000028.
- T.L. Anderson, *Fracture Mechanics Fundamentals and Applications*, vol. 3. Taylor & Francis, 2005.
- Tang and Y. F. Cheng, "Quantitative characterization by micro-electrochemical measurements of the synergism of hydrogen, stress and dissolution on near-neutral pH stress corrosion cracking of pipelines," *Corrosion Sci*, vol. 53, no. 9, pp. 2927–2933, Sep. 2011, https://doi.org/10.1016/j.corsci.2011.05.032.
- Tasdemir and B. Taşdemir, "Determination of stress intensity factor using digital image correlation method," *Matter*, vol. 2, no. 1, 2015, https://www.researchgate.net/publication/297375840
- Van Boven, R. Rogge, and W. Chen, "Residual stress and stress corrosion cracking of high-pressure hydrocarbon transmission pipelines," in *Proceedings of the 2006 International Pipeline Conference. Calgary, Alberta, Canada. IPC2006-10486*, 2006. http://asmedigitalcollection.asme.org/IPC/proceedings-pdf/IPC2006/42622/725/2653667/725_1.pdf

- Van Boven, W. Chen, and R. Rogge, "The role of residual stress in neutral pH stress corrosion cracking of pipeline steels. Part I: Pitting and cracking occurrence," *Acta Mater*, vol. 55, no. 1, pp. 29–42, Jan. 2007, https://doi.org/10.1016/j.actamat.2006.08.037.
- W. Chen, G. Van Boven, and R. Rogge, "The role of residual stress in neutral pH stress corrosion cracking of pipeline steels - Part II: Crack dormancy," *Acta Mater*, vol. 55, no. 1, pp. 43–53, Jan. 2007, https://doi.org/10.1016/j.actamat.2006.07.021.
- W. Chen, J. Zhao, J. Been, G. Van Boven, S. Keane, and K. Chevil, "Update of understanding of near-neutral pH SCC crack growth mechanisms and development of pipe-online software for pipeline integrity management," in *International Pipeline Conference*, 2016. http://asmedigitalcollection.asme.org/IPC/proceedings-pdf/IPC2016/50251/V001T03A076/2510196/v001t03a076-ipc2016-64626.pdf
- W. Chen, R. Kania, R. Worthingham, and G. Van Boven, "Transgranular crack growth in the pipeline steels exposed to near-neutral pH soil aqueous solutions: The role of hydrogen," *Acta Mater*, vol. 57, no. 20, pp. 6200–6214, Dec. 2009, https://doi.org/10.1016/j.actamat.2009.08.047.
- W. Chen, S.-H. Wang, R. Chu, F. King, T. R. Jack, and R. R. Fessler, "Effect of Pericyclic Loading on Stress-Corrosion-Cracking Initiation in an X-65 Pipeline Steel Exposed to Near-Neutral pH Soil Environment," *Metallurgical and Materials Transactions A*, vol. 34A, no. 2601, 2003. https://ui.adsabs.harvard.edu/link_gateway/2003MMTA...34.2601C/doi:10.1007/s11661-003-0019-y
- W. D. Pilkey and R. E. Peterson, *Peterson's stress concentration factors*. Wiley, 1997.

- W. D. Pilkey, *Formulas for stress, strain, and structural matrices*. John Wiley & Sons, 2005.
- X. Xing, W. Chen, and H. Zhang, "Atomistic study of hydrogen embrittlement during cyclic loading: Quantitative model of hydrogen accumulation effects," *Int J Hydrogen Energy*, vol. 42, no. 7, pp. 4571–4578, Feb. 2017, https://doi.org/10.1016/j.ijhydene.2016.12.127.
- X.-K. Zhu, "Evaluation of normalization method with crack mouth opening displacement for developing J-R curves," in *Pressure Vessels & Piping Conference PVP2021-60755*, http://asmedigitalcollection.asme.org/PVP/proceedings-pdf/PVP2021/85345/V004T06A057/6781635/v004t06a057-pvp2021-60755.pdf
- X.-Y. Zhang, S. B. Lambert, R. Sutherby, and A. Plumtree, "Transgranular stress corrosion cracking of X-60 pipeline steel in simulated ground water," *Corrosion*, vol. 55, no. 3, 1999. https://doi.org/10.5006/1.3283991.
- Y. Fang, E. H. Han, J. Q. Wang, and W. Ke, "Stress corrosion cracking of X-70 pipeline steel in near neutral pH solution subjected to constant load and cyclic load testing," *Corrosion Engineering Science and Technology*, vol. 42, no. 2, pp. 123–129, Jun. 2007, https://doi.org/10.1179/174327807X196843.
- Y. Ogawa*, D. Birenis , H. Matsunaga, A. Thøgersen, O. Takakuwa , J. Yamabe*, "multi-scale observation of hydrogen-induced, localized plastic deformation in fatigue-crack propagation in a pure iron," *Scripta Materialia*, vol. 140, pp. 13–17, Nov. 2017, https://doi.org/10.1016/j.scriptamat.2017.06.037.
- Y. Ogawa, H. Matsunaga, J. Yamabe, M. Yoshikawa, and S. Matsuoka, "Unified evaluation of hydrogen-induced crack growth in fatigue tests and fracture toughness tests of a carbon

steel," *Int J Fatigue*, vol. 103, pp. 223–233, Oct. 2017, https://doi.org/10.1016/j.ijfatigue.2017.06.006.

- Y. Onishi, M. Koyama, D. Sasaki, and H. Noguchi, "Characteristic fatigue crack growth behavior of low carbon steel under low-pressure hydrogen gas atmosphere in an ultralow frequency," *ISIJ International*, vol. 56, no. 5, pp. 855–860, 2016, https://doi.org/10.2355/isijinternational.ISIJINT-2015-647.
- Y. Song, P. Yang, T. Xia, Z. Peng, and J. Zhang, "The crack growth rate and crack opening displacement of EH-36 steel under low-cycle fatigue loading," *Ocean Engineering*, vol. 280, Jul. 2023, https://doi.org/10.1016/j.oceaneng.2023.114734.
- Y. Takahashi, H. Nishikawa, Y. Oda, and H. Noguchi, "Microscopic characterization of hydrogen-induced quasi-brittle fatigue fracture in low-strength carbon steel," *Mater Lett*, vol. 64, no. 22, pp. 2416–2419, Nov. 2010, https://doi.org/10.1016/j.matlet.2010.08.019.
- Y. Torres, J. M. Gallardo, J. Domínguez, and F. J. Jiménez E, "Brittle fracture of a crane hook," *Eng Fail Anal*, vol. 17, no. 1, pp. 38–47, Jan. 2010, https://doi.org/10.1016/j.engfailanal.2008.11.011.
- Y.-Z. Wang, R. W. Revie, and R. N. Parkins, "Mechanistic aspects of stress corrosion crack initiation and early propagation," in *NACE International Conference, Paper No.: 143.*, 1999.